Assessment of Paleo-Landscape Features using Advanced Remote Sensing Techniques, Modelling and GIS Methods in the Lake Manyara Basin, Northern Tanzania

Dissertation

der Mathematisch-Naturwissenschaftlichen Fakultät
der Eberhard Karls Universität Tübingen
zur Erlangung des Grades eines
Doktors der Naturwissenschaften
(Dr. rer. nat.)

vorgelegt von
Felix Bachofer
aus Filderstadt

Tübingen
2015

Gedruckt mit Genehmigung der Mathematisch-Naturwissenschaftlichen Fakultät der Eberhard Karls Universität Tübingen.

Tag der mündlichen Qualifikation:	08.02.2016
Dekan:	Prof. Dr. Wolfgang Rosenstiel
1. Berichterstatter:	Prof. Dr. Volker Hochschild
2. Berichterstatter:	Jun.-Prof. Dr. Annett Junginger
3. Berichterstatter	Ass.-Prof. Dr. Karsten Lambers

DISSERTATION

Assessment of Paleo-Landscape Features using Advanced Remote Sensing Techniques, Modelling and GIS Methods in the Lake Manyara Basin, Northern Tanzania

Felix Bachofer

Department of Geography, Eberhard-Karls University of Tuebingen

ACKNOWLEDGEMENTS

This study would not have been possible without many people to whom I want to deliver my sincere thanks. At this point, I want to express my gratitude to all the people who contributed to this work. This includes of course also all friends and colleagues who I do not mention here, yet who did support me during the time of processing, travelling and writing.

I kindly thank the *Heidelberg Academy for Sciences and Humanities* for supporting this research by funding the field visits within the research project "*The Role of Culture in Early Expansions of Humans* - ROCEEH". Without this support, this thesis would not have been possible. I would like to take this chance to express my thanks to several earth-observation data providers, which provided free access to remote sensing data. These institutions and companies are: the *European Space Agency* (ESA), the *National Aeronautics and Space Administration* (NASA), the *German Aerospace Center* (DLR), the *United States Geological Survey* (USGS) and the *DigitalGlobe Foundation*. I also want to thank the *Tanzanian Commission for Science and Technology* (COSTECH) for making this research possible.

I want to express my sincere gratitude to Professor Dr. Volker Hochschild, who always supported my work, for his advice and for the freedom to develop my own ideas. I would particularly like to thank Dr. Michael Märker and Geraldine Quènèhervè, with whom I worked closely together, in conducting field work in Tanzania and spending uncountable hours discussing our research in the Manyara basin and other research projects. I would also like to thank Dr. Christine Hertler for her introduction into the paleontology of the study area during my first visit in Makuyuni. My special thanks also to our driver and friend Lameck Mariki, who drove me to the most remote places without any complaints (most of the time). I want to thank Jun.-Professor Dr. Annett Junginger, who agreed to supervise my thesis. I would like to extend my sincere thanks to my actual and former colleagues Alice, Andy, Bernd, Christian, Gebhard, Hans-Joachim, Jan, Markus and Niklas from the Geoinformatics Group at the University of Tübingen. I also want to thank Dr. Michael Hagenlocher, with whom I had the most fruitful discussions on and off-topic.

Finally, I would like to express my gratitude to my family. My father Hanspeter Bachofer, my mother Ute Mayländer and her husband Klaus Mayländer, as well as my sister Steffi Bachofer, for their unconditional support and encouragement. I would like to thank Saskia Rens for accompanying me during a large part of this difficult time. Last, but not least, I want to express my sincere thanks to my all friends and my tennis team, who managed to take my mind off the thesis from time to time.

TABLE OF CONTENTS

List of Figures

LIST OF TABLES

List of Abbreviations

^{14}C yr BP	conventional ^{14}C age in years before 1950
a.s.l.	Above Sea Level (based on the EGM96 geoid)
AHP	African Humid Period
ALOS	Advanced Land Observing Satellite
ASTER	Advanced Spaceborne Thermal Emission and Reflection Radiometer
BRT	Boosted Regression Trees
cal. yr BP	calibrated ^{14}C age in years before 1950
CNES	French Space Agency (Centre national d'études spatiales)
DEM	Digital Elevation Model
DGPS	Differential Global Positioning System
DLR	German Space Agency (Deutsches Luft- und Raumfahrtzentrum)
EARS	East African Rift System
EGM96	Earth Gravitational Model 1996
EMR	Electromagnetic Radiation
ENSO	El Niño Southern Oscillation
ESA	European Space Agency
Ga	Billion Years Ago (date)
GHz	Gigahertz (frequency)
GIS	Geographic Information System
GLAS	Geoscience Laser Altimeter System
GPS	Global Positioning System
GSD	Ground Sampling Distance (alternatively Image Resolution)
ICESat	Ice Cloud and Elevation Satellite
ITCZ	Inter-tropical Convergence Zone
ka	Thousand Years Ago (date)
kyr	Thousand Years (period)
LEM	Landscape Evolution Model
LMB	Lower Manyara Beds
LSA	Later Stone Age
Ma	Million Years Ago (date)
METI	Ministry of Economy, Trade, and Industry (Japan)
MPR	Mid-Pleistocene Revolution
MSA	Middle Stone Age
Myr	Million Years (period)
NASA	United States National Aeronautics and Space Administration
NTD	North Tanzanian Divergence Zone
OA	Overall Classification Accuracy
PALSAR	Phased Array type L-band Synthetic Aperture Radar
SAR	Synthetic Aperture Radar
SPOT	Satellite Pour l'observation De La Terre
SRTM	Shuttle Radar Topography Mission
SST	Sea Surface Temperatures
SVM	Support Vector Machines
SWIR	Shortwave Infrared
TIR	Thermal Infrared
TRMM	Tropical Rainfall Measurement Mission
UMB	Upper Manyara Beds
USGS	United States Geological Survey
VNIR	Visible- and Near-Infrared
WGS84	World Geodetic System 1984

SUMMARY

In researching the evolution of hominids, the East African Rift System acts as a vital region. The rift valleys enabled some of the most sensational hominid findings to date. Various hypotheses have been developed in the last decades, which try to explain the influence of changes in paleo-climate, paleo-landscape and paleo-environment on hominin evolution in the Quaternary. Additionally, the sediments and the morphology of the East African Rift System provide excellent terrestrial archives for paleo-environmental reconstruction.

Lake Manyara is located in an endorheic basin in the eastern arm of the East African Rift System in northern Tanzania. The surroundings of the Lake Manyara are in the focus of paleontological and archaeological investigations. For instance, two hominin bearing sites were found within the catchment of the Makuyuni River, as well as artefacts and fossils are periodically uncovered. The study area, which is located east of the present-day lake, provides an insight into relevant geological and geomorphological drivers of paleo-landscape evolution of the whole region.

This thesis aims at contributing to the understanding of landscape evolution in the Lake Manyara region. Compared to other regions in the East African rift system, few landscape evolution studies took place for the Lake Manyara basin. As such, an integrative scientific investigation of the spatial situation of paleo-landscape features and of paleo-lake level fluctuations is missing. The proposed study utilizes state-of-the-art remote sensing based research methods in evaluating the landscape, and in concluding from present-day landforms and processes, how the landscape developed during the Pleistocene and Holocene. In striving to accomplish this goal, this cumulative dissertation comprises eight central research questions, which are introduced in a conceptual framework. The research questions have been considered in seven scientific publications, which describe the applied methodologies and results in detail. The framework of the thesis provides a coherent and detailed interpretation and discussion of the scientific findings. The research questions and outcomes of the analyses are listed below.

Key drivers of landscape development in the East African Rift System are tectonic and tectonically induced processes. Drainage network, stream longitudinal profiles and basin analysis based on topographic analyses, as well as lineaments extracted from remote sensing images, were successfully used as methods in identifying tectonic activity and related features in rift areas. The application of a gully erosion model suggests that the gully channel systems in the study area are relatively stable and that they had developed prior to the last significant lake regression.

The paleo-landscape and the paleo-environment are closely connected to lake level changes of the paleo-Lake Manyara. Hence, a key question concerns the extent of the Manyara Beds, which are lacustrine deposits that indicate the maximum extent of the paleo-Lake Manyara. A combined analysis, utilizing ASTER multispectral indices and topographic parameters from a digital elevation model, led to the spatial delineation of lacustrine sediments. Their extent indicates a relation to lacustrine sediments in the southern part of the basin, and reveals lacustrine / palustrine deposits further east. A methodological comparison of Support Vector Machines and Boosted Regression Trees, which served as classification methods to identify the lacustrine sediments, exhibited high accuracies for both approaches, with minor advantages for Support Vector Machines.

Closely related to the previous research question is the question on the spatial distribution of surface substrates. By incorporating a WorldView-2 scene and Synthetic Aperture Radar data to the previously mentioned datasets, it was possible to distinguish between nine topsoil and lithological target classes in the study area. The surface substrates indicate the underlying lithologies, sediments and soils, as well as soil formation processes.

Between the village of Makuyuni and the present-day Lake Manyara, paleo-shorelines and terraces were formed by various paleo-lake levels. Questions arise, at which elevation these features occur and what is the maximum elevation, which was reached. ALOS PALSAR and TerraSAR-X backscatter intensity information provided the possibility of an area-wide mapping of those morphological features. Some radiometric dates exist for stromatolites from a distinct paleo-shoreline level, which support the interpretation of the lake fluctuations. The paleo-shoreline, which was identified with the highest elevation, coincides with the elevation of the lowest possible outlet of the closed Manyara basin. It can be assumed that the paleo-Lake Manyara over-spilled into the neighboring Engaruka and Natron-Magadi basins.

The question of the location of sites with a high probability of artefact and/or fossil presence is important for future archaeological and paleontological research. ASTER remote sensing data and topographic indices contributed likewise to the predictive modelling of probabilities of archaeological and paleontological sites in the study area. Generally, paleontological sites are found on a higher elevation, compared to Stone Age sites. In addition, fossil sites seem to be related to stable paleo-landscape features according to this study's findings.

The results of this dissertation provide new insights in the landscape development of the Lake Manyara basin. The scientific findings contribute to the understanding of the landscape evolution for the study area, as well as for the neighboring basins in the East African Rift System. The applied geospatial methodologies can be transferred to other study areas with similar research needs.

KURZFASSUNG

Bei der Erforschung der Evolutionsgeschichte von Hominiden nimmt das Ostafrikanische Grabensystem eine zentrale Rolle ein. In dem Grabensystem konnten einige sensationelle hominide Funde zu Tage gebracht werden. Im Zuge dessen wurden in den letzten Jahrzehnten verschiedene Hypothesen entwickelt, um den Einfluss von Veränderungen des Paläo-Klimas, der Paläo-Landschaft und der Paläo-Umwelt auf die Entwicklung der Hominiden im Quartär zu erklären. Zudem bieten die Morphologie und die Sedimente des Grabensystems hervorragende terrestrische Archive für die Rekonstruktion der Paläo-Umweltbedingungen.

Der Lake Manyara liegt in einem abflusslosen Becken im östlichen Arm des Ostafrikanischen Grabensystems im nördlichen Tansania. Das Lake Manyara Becken und die angrenzenden Regionen befinden sich im Fokus von paläontologischen und archäologischen Untersuchungen. Im Einzugsgebiet des Makuyuni Flusses wurden beispielsweise hominide Überreste gefunden und es werden zahlreiche Artefakte und Fossilien in regelmäßigen Abständen wissenschaftlich erfasst. Das Untersuchungsgebiet dieser Arbeit liegt östlich des heutigen Sees und bietet einen umfassenden Einblick in die relevanten geologischen und geomorphologischen Prozesse der Paläo-Landschaftsentwicklung in der gesamten Region.

Ziel dieser Arbeit ist zu einem besseren Verständnis der Landschaftsentwicklung des Lake Manyara Beckens beizutragen. Verglichen mit anderen Regionen des Ostafrikanischen Grabensystems, fanden in der Region des Lake Manyara nur wenige Studien zur Landschaftsentwicklung statt. Daher steht bisher eine integrative, wissenschaftliche Untersuchung der räumlichen Zusammenhänge zwischen Landschaftsformen und den Seespiegelschwankungen des Paläo-Sees Manyara aus. Die vorliegende Studie nutzt Fernerkundungsanalysen auf dem aktuellen Stand der Forschung, um von den heutigen morphologischen Prozessen und Landschaftsformen auf die Landschaftsentwicklung im Pleistozän und Holozän zu schließen. Um dieses Ziel zu erreichen wurden acht Forschungsfragen entwickelt, welche im konzeptuellen Rahmen dieser kumulativen Dissertation vorgestellt werden. Die Fragestellungen werden in sieben wissenschaftlichen Publikationen untersucht, in denen die verwendeten Methoden und die gewonnenen Ergebnisse genauestens erörtert werden. Der konzeptuelle Rahmen dieser Dissertation schließt mit einer vollständigen und detaillierten Interpretation und Diskussion der wissenschaftlichen Ergebnisse ab. Der folgende Überblick zeigt zentralen Forschungsfragen auf und stellt die Ergebnisse der Analysen dar.

Wesentliche Faktoren der Landschaftsentwicklung im Ostafrikanischen Grabensystem sind tektonische und tektonisch induzierte Prozesse. Aus topographischen Analysen abgeleitete Abflussnetzwerke, Längsprofile von Flüssen und Einzugsgebiete, ebenso wie aus Satellitendaten extrahierte geologische Lineamente, wurden erfolgreich eingesetzt um tektonische Aktivitäten und damit verbundene Landschaftsformen zu identifizieren. Die Anwendung eines Gully-Erosionsmodells ergab, dass die Gully Systeme der Region relativ stabil sind und dass sie sich einige bereits vor dem letzten signifikanten Seespiegelrückgang gebildet haben.

Die Paläo-Landschaft und die Paläo-Umwelt sind eng mit den Seespiegelschwankungen des Paläosees Manyara verknüpft. Von daher betrifft eine zentrale Frage das Auftreten der Lower Manyara Beds. Dabei handelt es sich um lakustrine Sedimenten, welche die maximale Ausdehnung

des Paläo-Sees Manyara anzeigen. Eine kombinierte Analyse, von auf ASTER Satellitendaten basierenden multispektralen Indizes und topographischen Parametern eines digitalen Geländemodells, führte zur räumlichen Abgrenzung der Seesedimente. Deren Ausdehnung lässt einen Zusammenhang mit Seesedimenten im südlichen Teil des Manyara Beckens annehmen und weist auch auf Seesedimente oder in Feuchtgebieten abgelagerte Sedimente weiter östlich der bisher identifizierten Sedimente hin. Ein methodischer Vergleich der Klassifikationsmethoden Support Vector Machines und Boosted Regression Trees, welche zur Klassifikation der Seesedimente verwendet wurden, führte zu hohen Klassifikationsgenauigkeiten mit beiden Methoden, mit leichten Vorteilen bei den Support Vector Machines.

Eng verbunden mit der vorherigen Forschungsfrage ist die Frage nach der räumlichen Verteilung von Oberflächensubstraten im Untersuchungsgebiet. Unter Einbeziehung einer World-View-2 Szene und Radaraufnahmen zu den bereits erwähnten Datensätzen, konnte zwischen neun Oberflächensubstraten und Lithologien unterschieden werden. Die Oberflächensubstrate ermöglichen es auf ihre Ausgangsgesteine, sowie auf Sedimente, Böden und Bodenbildungsprozesse zu schließen.

Zwischen dem Dorf Makuyuni und dem heutigen Lake Manyara haben sich Paläo-Uferlinien und Paläo-Seeterrassen durch unterschiedliche Paläo-Seespiegel gebildet. Dies führt zu den Fragen, auf welchen Höhen diese Landschaftsformen anzutreffen sind und welches Niveau die maximale Höhe einnimmt, die sich mit den ehemaligen Uferlinien nachweisen lässt. ALOS PALSAR und TerraSAR-X Radar-Intensitätsinformationen ermöglichten eine flächendeckende Kartierung der morphologischen Formen. Einige radiometrische Datierungen von Stromatolithen eines bestimmten Seespiegelniveaus liegen bereits vor und tragen zur Interpretation der Paläo-Seespiegelschwankungen bei. Die höchstgelegene Paläo-Uferlinie stimmt mit der Höhe des tiefst gelegenen Überlaufs des Manyara Beckens überein. Daher kann davon ausgegangen werden, dass der Paläo-See Manyara zumindest zeitweise in die benachbarten Engaruka und Natron-Magadi Becken entwässert hat.

Die Frage nach der Lage von Standorten mit einer hohen Wahrscheinlichkeit des Vorhandenseins von Artefakten und/oder Fossilien, ist für die zukünftige archäologische und paläontologische Forschung in der Region wesentlich. ASTER Satellitendaten und topographische Indizes haben zu der prädikativen Modellierung der Wahrscheinlichkeiten von steinzeitlichen und paläontologischen Fundstellen im Untersuchungsgebiet beigetragen. Dabei konnte festgestellt werden, dass paläontologischen Fundstätten, im Vergleich zu steinzeitlichen Fundstellen, auf einem höher gelegenen Niveau auftreten. Darüber hinaus ließ sich feststellen, dass fossile Fundstellen auf morphologisch stabilen Positionen in der Landschaft vorkommen.

Die Ergebnisse dieser Dissertation liefern neue Einblicke in die Landschaftsentwicklung des Manyara Beckens. Die wissenschaftlichen Erkenntnisse tragen zum Verständnis der Landschaftsentwicklung im Untersuchungsgebiet, wie auch der benachbarten Einzugsgebiete im Ostafrikanischen Grabensystem bei. Die angewandten räumlichen Methoden können auf andere Untersuchungsgebiete mit ähnlichem Forschungsbedarf übertragen werden.

CHAPTER 1 - INTRODUCTION

1.1 BACKGROUND

The African rift valleys are complex geosystems, with geomorphological landforms and processes that are shaped by Quaternary tectonic events and an intricate climatic system [Nicholson 1996, Dawson 2008]. They enabled some sensational hominid findings and are giving insight into geological and geomorphological records, which allow the determination of former environments. For multiple reasons, the surroundings of Lake Manyara Basin in Tanzania are in the focus of paleontological and archaeological investigations. The location is close to the famous Olduvai Gorge where paleo-anthropological findings can be traced back to the *Homo Habilis*. Within the catchment of Lake Manyara, hominin bearing sites (0.78 to 0.633 Ma), Acheuléen artefacts and fossils are found [Ring *et al.* 2005, Kaiser *et al.* 2010, Frost *et al.* 2012, Giemsch 2015]. The findings contribute to the knowledge of human evolution and expansion. For an improved integration of these discoveries, a better understanding of the paleo-landscape and the paleo-environment in the region is necessary. As such is the case, the paleo-hydrology is, besides tectonics and volcanism, the most crucial aspect for the development of paleo-landscapes during the Quaternary. For the Lake Manyara basin, the maximum water extent, as well as phases of transgression and regression, are still under debate [Keller *et al.* 1975, Holdship 1976, Casanova & Hillaire-Marcel 1992, Somi 1993, Ring *et al.* 2005, Schwartz *et al.* 2012] and require further investigations.

For the evolution of hominids and especially hominins, the East African Rift System (EARS) seems to be a crucial region. Yet, the scenarios of the relationship between the evolution of landscape and humankind are hypothetical [Chorowicz 2005]. Potts [1998] provides a comprehensive overview and discussion of theories of adaptions and trends in human evolution. The Savanna hypothesis [Smith 1924, Dart 1925], as an example, proposes an adaption to a drier open land environment, including the development of bipedalism, but is largely disapproved today [Trauth *et al.* 2010]. The Turnover Pulse hypothesis [Vrba 1980] explains evolution by the gradual shift to drier environmental conditions by climatic events (linked to the northern hemisphere glaciation), which led to a concentration of specification and extinction in a relatively short period of time. The Riparian-Woodland-Scavenging model [Blumenschine 1986] proposes closed habitats in a wooded environment in the vicinity of water to early humans, where they found scavenging opportunities. The Variability hypothesis [Potts 1998] is split into a short-term and a long-term variant. The short-term variant states that variabilities during the lifetime of individuals, like climatic seasonality and year-to-year changes, forced the evolution of humans. The long-term variant, which is called Variability Selection hypothesis, is favored by Potts [1998]. It suggests that long-term changes favor genetic settings, which allow an adaptive versatility over several generations. Because individuals cannot predict the environmental changes, as in short-term setting, but have to find innovative strategies. The paleo-lake evidence in the EARS correlates

with the important global orbitally forced climatic changes, and with junctures in human evolution [deMenocal 1995, Trauth *et al.* 2005, Trauth *et al.* 2007]. The available evidence indicates a high variability, which supports the Variability hypothesis [Trauth *et al.* 2009]. The tectonic influence on the local climate is an important aspect, since the mountain ranges of the EARS act as barriers for moisture transport [Bergner *et al.* 2009]. High precipitation in the elevated areas of the EARS, combined with high evaporation rates in the basins resulted into climate sensitive environments and lake systems, which again agrees with the Variability hypothesis [Trauth *et al.* 2010]. Because episodes of extreme variability between humidity and aridity in short periods were determined, a modification of the Variability hypothesis was developed - the Pulsed Climate Variability hypothesis [Maslin & Trauth 2009, Maslin *et al.* 2014]. King & Bailey [2006] suggest that the hilly environment of the EARS provided possibilities for hunting, hiding and migration, not only topographical barriers. Trauth *et al.* [2010] developed the hypothesis of amplifier lakes, based on the work by Street [1980], Street-Perrott & Haarison [1985]. It assumes that the specific geometry of many rift valley lakes makes them sensitive to climate changes. The hypothesis of Trauth *et al.* [2010] states that such amplifier lakes functioned as dynamical barriers during wet phases with high lake level and during extremely dry episodes with no water supply in open plains. Thus, the rift lakes contributed to habitat fragmentation of early hominins. This overview about theories of human evolution attests the relevance of the paleo-landscape, without attempting to validate their individual assumptions. It can be concluded, that the relations between human evolution, the paleo-environment and the geomorphic landscape can be described as determinant, causal and systemic [Waters 1992].

Besides the paleontological and archaeological relevance of paleo-landscape interpretation, the terrestrial sediment archives and paleo-lake level indicators provide an important contribution to the understanding of the paleo-climate and present day climate change parameters [deMenocal 1995, Gasse 2000, Gasse *et al.* 2008, Foerster *et al.* 2012]. Even though this thesis is investigating paleo-landscape features, various results regarding paleo-lake fluctuations may contribute to a deeper understanding of climate change effects. This is of particular importance, since East Africa is highly vulnerable to climate change. The Intergovernmental Panel on Climate Change (IPCC) report an increase in temperature and precipitation for East Africa, but with a high spatial variability [Niang *et al.* 2014]. This may result in an increased risk of droughts and floods, and the change of precipitation patterns and rise in temperatures may lead to an increased incidence of Malaria in the highlands of East Africa.

This study contributes to the reconstruction of the paleo-landscape in the Lake Manyara basin. The presented research is based on geographical methods with a strong spatial component, and is not to be considered as purely supporting discipline for archaeology and paleontology. In this thesis, the term landscape is referred to as the interface between lithosphere, atmosphere and hydrosphere, and is shaped by endogenic and exogenic processes [Sharp 1982]. As an alternative term for paleo-landscape, paleo-geography of landscapes is used [Irving 2005]. Whereas, the often applied terminus “paleo-environmental reconstruction” is a hypernym, which is mostly used to describe the paleo-climate and the paleo-ecology in the context of hominid living conditions

[Bishop & Pickford 1975, Verstraeten 2013, Barr in press]. The term "landscape archaeology" on the contrary, focuses on the cultural landscape [Layton & Ucko 1999, Branton 2009]. The study has a geoarchaeological context, since it applies concepts and methods from different parts of geoscience. It investigates the morphology of the noncultural paleo-landscape and its formation processes to contribute in answering archaeological and paleontological questions [Rapp & Hill 2006, Ghilardi & Desruelles 2008, Verstraeten 2013].

Remote sensing data, in combination with geospatial analyses, offer a variety of possibilities to obtain information about the present land cover. Many surface substrates and landforms are relicts from paleo-landscapes and thereby can contribute to the understanding of complex geosystems and paleo-environments. Arid and semiarid regions offer the most promising conditions for spectral remote sensing applications, because of their relatively low vegetation cover of soils, lithologies and landforms.

1.2 Remote Sensing in Archaeology and Landscape Reconstruction

Although aerial photographs were used to prospect and survey archaeological structures since the beginning of the nineteenth century [Lasaponara & Masini 2011], new satellite sensors and advanced digital image processing techniques make it not only possible to find archaeological evidence, but also help to better understand paleo-landscapes and paleo-environments. In recent years, various books have been published, which focus on remote sensing and spatial analysis in archaeology [Johnson 2006, Mehrer & Wescott 2006, Robertson *et al.* 2006, Wiseman & El-Baz 2007, Parcak 2009, Lasaponara & Masini 2012]. In scientific journals, such as the *Journal of Archaeological Science* (ISSN: 0305-4403), *Geoarchaeology* (ISSN: 1520-6548) and *Archaeological Prospection* (ISSN: 1099-0763), remote sensing analyses are well established. Most remote sensing related publications in these journals focus on a local scale and supplement research on anthropogenic archaeological features and cultural paleo-landscape [Montufo 1997, Altaweel 2005, De Laet *et al.* 2007, Siart *et al.* 2008, Campana *et al.* 2009, Gallo *et al.* 2009, Trier *et al.* 2009, Prinz *et al.* 2010, Pryce & Abrams 2010, Kennedy 2011, Cigna *et al.* 2013, Dore *et al.* 2013, Gaber *et al.* 2013, Linck *et al.* 2013, Patruno *et al.* 2013, Stewart *et al.* 2013, Tapete *et al.* 2013, Chen *et al.* 2014b, Hritz 2014, Stewart *et al.* 2014, De Laet *et al.* 2015]. An overview of SAR remote sensing in a geoarchaeological / paleo-landscape context is provided by Holcomb & Shingiray [2007] and by Lasaponara & Masini [2013]. In addition to paleo-landscape approaches and relevant for this thesis are studies, which utilized remote sensing data and topographic parameters from remote sensing based digital elevation models (DEM) for the probabilistic modelling of archaeological sites [Espa *et al.* 2006, Danese *et al.* 2014, Menze & Ur 2014, Schmaltz *et al.* 2014].

Geomorphological research, and thereby remote sensing based geomorphological studies, is related to past processes and landforms. This introductory chapter focuses on studies with distinct paleo-landscape research questions that have a methodological or thematic relation to the foci of this thesis. The seven scientific publications, which are part of this thesis, elaborate on the state of each topic in detail (Appendices I – VII). Methodological research articles and scientific

reviews, which represent the methodological state-of-the art concerning the research questions of this thesis, are provided by following publications. Extensive overviews about soil mapping are given by Anderson & Croft [2009], Dewitte *et al.* [2012] and Mulder *et al.* [2011]. A detailed analysis of the mineral components in tropical soils was conducted by Vicente & de Souza Filho [2011], who used Advanced Spaceborne Thermal Emission and Reflection Radiometer (ASTER) multispectral images. Various studies use the backscatter information of Synthetic Aperture Radar (SAR) data for the physical characterization of surface sediments [Gaber *et al.* 2009b, Aubert *et al.* 2011, Zribi *et al.* 2012, Gaber *et al.* 2015]. Pour & Hashim [2011] provide a review of lithological mapping using ASTER spectral information. Outstanding research in this field is introduced by Hewson *et al.* [2001], Rowan & Mars [2003], Hewson *et al.* [2005], Ninomiya *et al.* [2005], Rowan *et al.* [2005], Mars & Rowan [2010] and Hewson & Cudahy [2011]. The quantitative analysis of the topography is necessary for an understanding of the landscape evolution. A non-complete overview is provided by Zevenbergen & Thorne [1987], Dikau [1988], Moore *et al.* [1991, 1997], Mulder *et al.* [2011] and Wilson [2012]. Closely related to topographic analyses, and partly to this thesis, are physical and numerical "landscape evolution models" (LEMs). LEMs simulate changing terrain over time, predominantly by considering erosion, transport and deposition processes on hillslopes [Sharp 1982, Tucker & Hancock 2010, Chen *et al.* 2014a].

The mapping of subsurface structures like paleo-drainage networks buried by sediments using SAR is a well-known example of paleo-landscape reconstruction - mostly applied in northern Africa and Arabia. Depending on the SAR wavelength, signals are able to penetrate dry surface sediments in arid environments and thereby reveal the paleo-surface [Stern & Abdelsalam 1996, Dabbagh *et al.* 1997, Schaber *et al.* 1997, Paillou *et al.* 2003, Robinson *et al.* 2006, Ghoneim & El-Baz 2007, Paillou *et al.* 2009, Ghoneim *et al.* 2012]. Gaber *et al.* [2009a] have successfully applied IKONOS high-resolution satellite imagery in combination with topographic analysis for the delineation and characterization of paleo-lakes on the Sinai Peninsula, Egypt. Elmahdy [2012] used ASTER and high resolution QuickBird satellite information, as well as topographic parameters, Geographical Information Systems (GIS) and geophysical methods to delineate a paleo-lake in northern Darfur. Khan *et al.* [2014] delineated paleo-drainages and tectonic lineaments of the paleo-Lake Moghra in Egypt. Breeze *et al.* [in press] delineated a paleo-drainage network and mapped paleo-lakes in Arabia, using Landsat multispectral data and a SRTM DEM. AbuBakr *et al.* [2013] identified lineaments and a paleo-drainage system with a Shuttle Radar Topography Mission (SRTM) and derived DEM and RADARSAT-1 SAR data on the Sinai Peninsula, Egypt. They exploited the surface penetration capabilities of the Phased Array type L-band Synthetic Aperture Radar (PALSAR) L-band sensor on the Advanced Land Observing Satellite (ALOS), as well as geophysical approaches. Gharibreza [in press] delineated coastal paleo-shorelines with spectral remote sensing image and radiocarbon dated these in Southeast Iran. Schmid *et al.* [2008] applied spectral information derived from IKONOS and ASTER satellite images for the identification of soil surface properties in order to compare them with the location of archaeological sites of Aksum in Ethiopia. Vining & Wiseman [2006] utilized RADARSAT-1

SAR data, ASTER based DEM, Landsat Enhanced Thematic Mapper and SPOT IV High Resolution Visible multispectral information to delineate the Holocene coastline development in the Ambracian Gulf, Greece. Ciminale *et al.* [2009] used QuickBird imagery and the results of a magnetic survey for the reconstruction of natural and cultural landscape in northern Apulia, Italy. For the reconstruction of the paleo-landscape in the vicinity of Mount Vesuvius in Italy, topographic parameters and stratigraphic analysis were adopted to estimate the paleo-surface and the evolution of the landscape [Vogel & Märker 2010, Vogel *et al.* in press].

So far, the presented studies focused primarily on one specific paleo-landscape feature. Multiple landscape elements are however necessary to understand complex causal relations. In his thesis, Berking [2011] reconstructed the paleo-environment of the site of Naga in Central Sudan. Within the study, ASTER and IKONOS multispectral data were utilized for geomorphological mapping and interpretation [Berking & Schütt 2011b]. Geophysical methods were applied to delineate lacustrine sediments, radiometric dating methods were applied to gain age estimates and the hydrological situation was modelled using DEMs [Berking *et al.* 2010, Berking *et al.* 2011, Berking & Schütt 2011a, 2011b]. Alexakis *et al.* [2011] reconstructed the Neolithic landscape for Thessaly, Greece. They took into account the coastline change caused by sea level fluctuations, as well as different paleo-lake levels for a lake. They utilized different spaceborne remote sensing data sources for the detection of ancient settlements and, in combination with topographic parameters, for the reconstruction of the topography. Bailey *et al.* [2011] used satellite data and topographic information to reconstruct the landscape of tectonically active regions with complex topographies in Africa. They contribute with their research to the understanding of hominin habitats and human evolution.

The presented studies show, that a wide range of remote sensing sensors, including DEM products, can be used to determine paleo-landscape elements. Besides SAR data, which can characterize surface substrates, subsurface features and landforms, the wide use of the multispectral ASTER sensor is evident. This can be explained by its good global coverage and relatively high spectral resolution, which was designed for soil and mineral mapping [Fujisada 1995, Yamaguchi *et al.* 1998, Zhang & Pazner 2007, Pour & Hashim 2014].

1.3 Research in the Manyara Basin and Research Gaps

The previous research in the Lake Manyara basin comprises of studies, which focus on distinct research topics. The following studies are a non-exhaustive overview of the research activities, which are presented in detail in the second chapter of this thesis framework. In general, geological and tectonic research investigates a larger region of the EARS [Dawson 1992, Nyblade & Brazier 2002, Dawson 2008]. Nevertheless, some studies focus on the Tanzanian sector of the EARS [Macintyre *et al.* 1974, Ebinger *et al.* 1997, Foster *et al.* 1997, Mulibo & Nyblade 2010]. Keller *et al.* [1975], Dixit [1984], Casanova & Hillaire-Marcel [1992] and Somi [1993] studied and radiometrically dated paleo-shorelines and paleo-terraces in the East of the present-day Lake Manyara. Holdship [1976] and Barker [1992] analyzed two different lake-sediment cores. Schlüter

[1987], Schlüter *et al.* [1992], Ring *et al.* [2005] and Schwartz *et al.* [2012] investigated lacustrine sediments of the paleo-Lake Manyara. Archaeological and paleontological research is published by Seitsonen [2006a, 2006b], Wolf *et al.* [2010], Kaiser *et al.* [2010], Frost *et al.* [2012], Prendergast *et al.* [2013] and Giemsch [2015]. A general overview of the geomorphology and sedimentology of the Manyara basin is provided by Vaidyanadhan *et al.* [1993].

Despite these studies, various research questions are still un-answered, respectively have not been investigated thus far. This particularly concerns the spatial distribution and the spatial relation of lacustrine sediments and other surface substrates. Likewise, an in-depth spatial consideration of paleo-shorelines is missing that far. The fluctuation of the paleo-lake level, as well as the maximum lake level, is intensively debated in the previously mentioned studies. Changes in the base level of the basin, resulting from the lake level fluctuations in the Quaternary, have a strong impact on the hydro-erosive processes and hence, on sediment dynamics and landscape evolution on the long term. These topics have not been investigated so far. In particular, integrative approaches combining geospatial analyses with various techniques of the fields of geomorphology, hydrology, climatology, archaeology, paleontology, sedimentology, stratigraphy and radiometric dating as well as numeric modelling techniques have not been applied in the study area. Generally, as showed in chapter 1.2, the use of satellite based remote sensing data and methods is rather confined specific research questions, and not as part of an assessment of paleo-landscape pattern and features.

1.4 Objectives and Research Questions

The main objective of this dissertation is to contribute to the understanding of the process dynamics and the paleo-landscape of the Lake Manyara basin during different climatic periods throughout the Quaternary. This comprises the the identification and interpretation of quaternary geology, geomorphology, as well as sediments and soils. The objective is achieved by providing answers to a set of distinct research questions. Special attention is paid to the vicinity of the town Makuyuni, lying within the Makuyuni River catchment east of the present day Lake Manyara, as it provides insight into the relevant drivers of paleo-landscape evolution. The proposed study utilizes state-of-the-art remote sensing based research methods to evaluate the landscape and to derive from today's landforms and processes to how the landscape developed during the Pleistocene and Holocene. The focus is set on the capabilities of remote sensing data and remote sensing based methods. The archaeology and palaeontology in the region serve as thematic frame for this research. The study implements integrative landscape reconstruction approaches, combining remote sensing with stratigraphy, sedimentology, radiocarbon dating, hydro-geomorphological process analyses and field work. In order to fulfil the objective of the thesis, following eight concrete research questions (Q) were developed:

Research questions

The understanding of geomorphological forms and processes is immanent for the interpretation of the landscape evolution. Tectonic processes are an important contributor to the landscape formation in the EARS and are indicated by lineaments. Soil erosion and especially gully erosion are highly dynamic processes, which occur in the study area.

Q1: Can remote sensing contribute to the detection of lineaments?

Q2: What conclusions on the landscape development can be drawn from the evolutionary stages of gully erosion features for the study area?

The area of focus in the vicinity of Makuyuni has a heterogeneous and complex geology and geomorphology. Because of the conjuncture of the Precambrian Masai Plain, Younger Extrusives and tectonics, accompanying soils, paleo-lake sediments (Manyara Beds) and various landforms and surface processes, the focus area possesses dynamic features. However, it allows an in-depth look into the development of the basins and therefore is exceptionally suitable as a focus area. Following questions arise from the local setting:

Q3: What is the spatial extent of the Manyara Beds?

Q4: Is it possible to delineate multiple surface substrate types and does the spatial distribution of the surface substrates give indication on landscape evolution?

Various studies identified the existence of paleo-shorelines and terraces in the east of Lake Manyara [Keller *et al.* 1975, Casanova 1986, Casanova & Hillaire-Marcel 1992, Somi 1993]. Yet, the linear shorelines still have yet to be mapped, except for selected parts close to the Arusha - Dodoma Road (A 104) mapped by Keller *et al.* [1975]. In addition, the paleo-lake highstand related to the shorelines is under discussion [Keller *et al.* 1975, Holdship 1976, Casanova 1986, Barker 1990, Casanova & Hillaire-Marcel 1992, Somi 1993].

Q5: What are the elevations of paleo-shorelines and paleo-lake terraces and how does this information contribute to the understanding of the paleo-history of Lake Manyara?

Q6: What was the maximum water level for the time period of the formation of the identified paleo-shorelines?

Remote sensing data and associated analysis technologies represent the central methodological approaches for this thesis. Various studies identified Support Vector Machines (SVM) and Boosted Regression Trees (BRT) as powerful classification approaches for analyses with multiple input datasets [Foody & Mathur 2004, Esch *et al.* 2009, Pal & Foody 2010, Gessner *et al.* 2013].

Q7: Does either SVM or BRT perform significantly better with multiple (spectral, microwave and topographical) input parameters?

The vicinity of Makuyuni is rich with archaeological and paleontological sites, as indicated by various studies [Kaiser *et al.* 2010, Frost *et al.* 2012, Giemsch 2015]. To increase the scientific significance of the archaeological and paleontological research, it is necessary to gain information from spatially well-distributed sites, to reduce the effect of spatial autocorrelation. Additional results from archaeological and paleontological research in the study area may help to transfer the results from the paleo-landscape analysis to a paleo-environmental reconstruction.

Q8: What is the distribution of sites with a high probability of artefact and/or fossil presence?

1.5 Structure of the Thesis

This dissertation is a paper-based (cumulative) thesis, consisting of a framework text and seven publications (Tab. 1), which can be found in the Appendix. The published articles P2, P3 and P4 are the core papers of this thesis, since they primarily address remote sensing analyses (Tab. 2). The publications P1, P6 and P7 describe the contribution of remote sensing technology to specific methodologies. P5 is a purely methodological paper, while P2 addresses a thematical research question, as well as a methodological. The content of the publications addresses the research questions stated in chapter 1.4 and/or focuses on applied methodologies. The framework of this dissertation formulates the overall objective of the thesis, and provides background information on the study area and the applied research methods, which are discussed in more detail in the respective publications.

Chapter 1 gives a comprehensive review on the use of remote sensing data and methods in archaeological and paleo-environmental research. The chapter also defines the research questions of this thesis.

Chapter 2 discusses the present and past setting of the study area in more detail and gives an overview of relevant literature. The topics that are addressed are the geological and tectonic development of the North Tanzanian Divergence Zone, the paleo-Lake Manyara in the context of other East African paleo-lakes, the paleo-climate of East Africa and the archaeological and paleontological evidence in the study area.

Chapter 3 introduces the basics of remote sensing, which helps to understand the data and methods applied in the publications. It also entails the field data collection for this thesis.

Chapter 4 summarizes the results from the publications by addressing the research questions and provides an integrative discussion of the outcomes.

Chapter 5 concludes the thesis and provides an outlook on future research and research needs.

Appendices: All peer-reviewed publications, which are related to this PhD thesis, are attached in the appendices (I – VII). Additional supplementary material is attached to the thesis.

Tab. 1: Overview of publications included in this dissertation and the respective author contributions of Felix Bachofer.

ID	Publication	Status	Publication Type	Peer Review	Impact Factor*
P1	FLORES-PRIETO, E., QUÉNÉHERVÉ, G., BACHOFER, F., SHAHZAD, F. & MAERKER, M., 2015 - *Morphotectonic Interpretation of the Makuyuni Catchment in Northern Tanzania using DEM and SAR data*. Geomorphology 248: 427-439 (doi: 10.1016/j.geomorph.2015.07.049).	Published	Journal Article. ISSN: 0169-555X	Yes	2.785
	Author contributions: Processing of ALOS PALSAR, ENVISAT ASAR and TerraSAR-X scenes; Extraction and interpretation of lineaments from SAR images; Contributing to writing and interpretation of results.				
P2	BACHOFER, F., QUÉNÉHERVÉ, G., MÄRKER, M. & HOCHSCHILD, V., 2015 - *Comparison of SVM and Boosted Regression Trees for the Delineation of Lacustrine Sediments using Multispectral ASTER Data and Topographic Indices in the Lake Manyara Basin*. Photogrammetrie, Fernerkundung, Geoinformation (PFG) 1(2015): 81-94 (doi: 10.1127/pfg/2015/0251).	Published	Journal Article. ISSN: 1432-8364	Yes	0.733
	Author contributions: Responsible for research design; Processing of remote sensing data; Collection of ground reference data; Interpretation and discussion of results; Writing of the initial manuscript and handling of the review process.				
P3	BACHOFER, F., QUÉNÉHERVÉ, G., HOCHSCHILD, V. & MAERKER, M., 2015 - *Multisensoral Topsoil Mapping in the Semiarid Lake Manyara Region, Northern Tanzania*. Remote Sensing 7 (8): 9563-9586 (doi:10.3390/rs70809563).	Published	Journal Article. ISSN: 2072-4292	Yes	3.180
	Author contributions: Responsible for research design; Processing of remote sensing data; Collection of ground reference data; Interpretation and discussion of results; Writing of the initial manuscript and handling of the review process.				
P4	BACHOFER, F., QUÉNÉHERVÉ, G. & MÄRKER, M., 2014 - *The Delineation of Paleo-Shorelines in the Lake Manyara Basin Using TerraSAR-X Data.* - Remote Sensing 6 (3): 2195-2212 (doi: 10.3390/rs6032195).	Published	Journal Article. ISSN: 2072-4292	Yes	3.180
	Author contributions: Responsible for research design; Processing of remote sensing data; Collection of ground reference data; Interpretation and discussion of results; Writing of the initial manuscript and handling of the review process.				
P5	BACHOFER, F., QUÉNÉHERVÉ, G., ZWIENER, T., MAERKER, M. & HOCHSCHILD, V., (Submitted 2015-04-27) - *Comparative Analysis of Edge Detection Techniques for SAR Images*. European Journal of Remote Sensing.	Submitted	Journal Article. ISSN: 2279-7254	Yes	1.360
	Author contributions: Responsible for research design; Processing of remote sensing data; Interpretation and discussion of results; Writing of the initial manuscript.				

P6	MAERKER, M., QUÉNÉHERVÉ, G., BACHOFER, F. & MORI, S., 2015 - *A simple DEM assessment procedure for gully system analysis in the Lake Manyara area, northern Tanzania*. Natural Hazards: 1-19 (doi: 10.1007/s11069-015-1855-y).	Published	Journal Article. ISSN: 0921-030X	Yes	1.719
	Author contributions: Preparation of DEMs and the WorldView-2 scene; Compiling of maps and contributing to writing of the manuscript; Contributing to the interpretation of the results.				
P7	MÄRKER, M., BACHOFER, F., QUÉNÉHERVÉ, G., HERTLER, C., SAANANE, C., GIEMSCH, L. & THIEMAYER, H., 2013 - *Modelling the Spatial Distribution of Archaeological Sites in the Makuyuni Region, Tanzania.* CAA'2010 Fusion of Cultures. Proceedings of the 38th Annual Conference on Computer Applications and Quantitative Methods in Archaeology, BAR International Series 2494: 523-529, Granada, Spain.	Published	Conference Proceedings. ISBN-10: 1407311085	Yes	-
	Author contributions: Preparation of the ASTER multispectral data; Contributing to the interpretation of the results.				

* Thomson Reuters Impact Factor 2014.

Tab. 2: Classification of publications: Remote sensing core papers (left column), publications with a remote sensing contribution (center column) and methodological papers (right column); the naming are short titles compiled from the original titles (Tab. 1).

Primarily remote sensing based publications (core - papers)	Method comparison remote sensing and image processing	Publications with remote sensing contribution
P2 Delineation of Lacustrine Sediments with SVM and Boosted Regression Trees		P1 Morphotectonic Interpretation
P3 Multisensoral Topsoil Mapping	P5 Edge Detection Methods	P6 Gully System Analysis
P4 Delineation of Paleo-Shorelines		P7 Modelling the Spatial Distribution of Sites

Chapter 2 – Study Area: Lake Manyara Basin

2.1 Geographical Setting

Lake Manyara (954 m a.s.l.) is located in the eastern arm of the East African Rift System (EARS) in northern Tanzania (Fig. 1). The shape of the Lake Manyara basin is typical for drainage basins associated with lithospheric divergence and especially for EARS lakes [Cohen 2003]. The primary structural unit of the basin is an asymmetrical shaped half-graben [Schwartz *et al.* 2012]. In the west of the lake the escarpment margin appears, which is elevated 250 – 900 m from the basin floor and ascends to the Mbulu plateau (Fig. 2). The Ngorongoro crater highlands appear on the northwestern boundary. To the north, the basin is adjacent to the Engaruka / Lake Natron basin. In the northeast, the volcanic peaks of Essimingor and Monduli dominate this landscape. A shoal, west dipping, monocline rises on the eastern side of the margin.

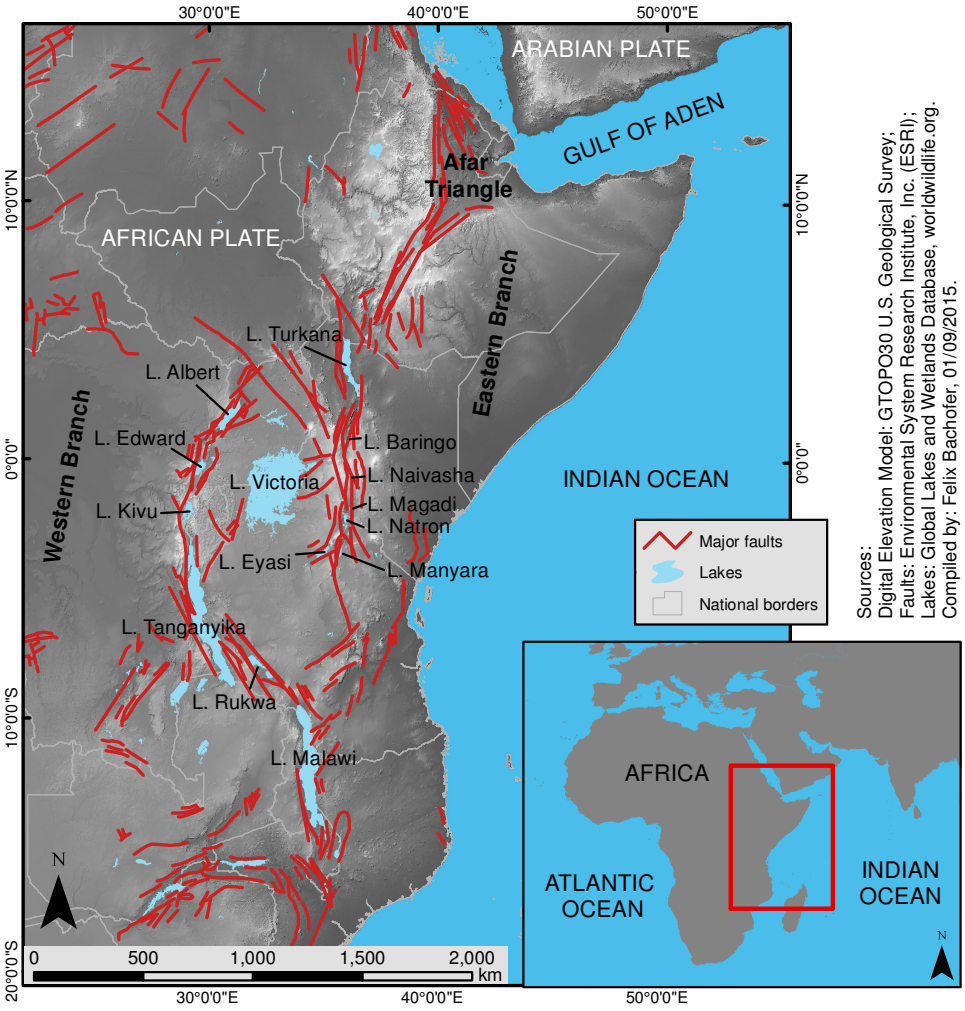

Fig. 1: The East African Rift System.

Lake Manyara is a shallow soda lake in an endorheic basin. The basin has an area of 18,480 km², based on a SRTM DEM [Slater *et al.* 2006]. With Lake Burungi exists a perched basin

within the greater Lake Manyara basin (Fig. 2). Lake Manyara showed a maximum water depth of 1.18 m and 0.81 m in average during a survey in May/June 2010 [Deus *et al.* 2013] after an average rain season (see Appendix VIII). With the exception of some pools, which are fed by springs from the rift escarpment, the lake periodically dries out completely [Deus & Gloaguen 2013]. The region is strongly influenced by the seasonal shift of the Inter-Tropical Convergence Zone (ITCZ).

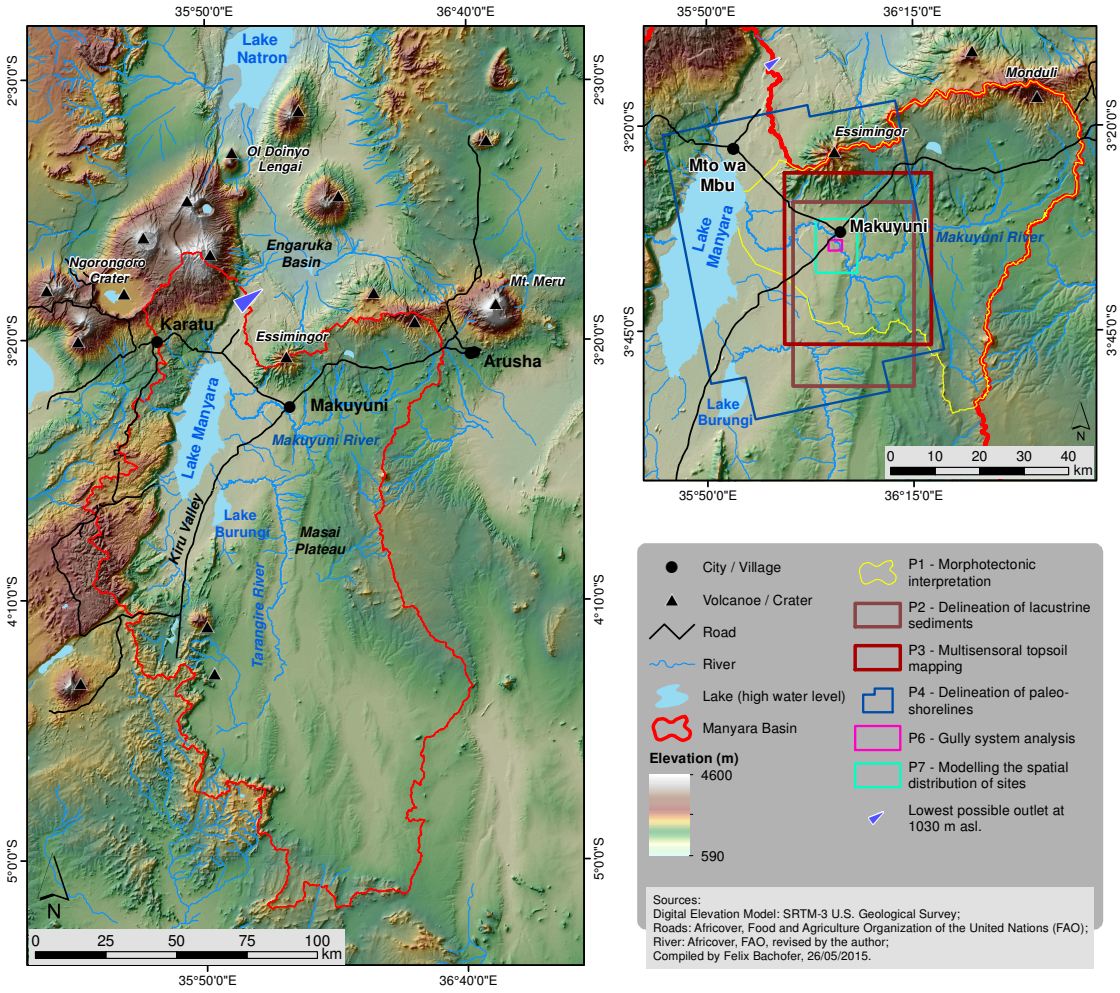

Fig. 2: The Lake Manyara basin in northern Tanzania.

The Tropical Rainfall Measurement Mission (TRMM) monthly Rainfall Estimate product 3B43 (V7) [Huffman *et al.* 2007] reveals a bimodal rainfall pattern for the basin with a short rainy season which peaks in November/December and a stronger rainy season with a peak in March/April (see Appendix VIII). For the years 2000 to 2014, the average annual precipitation ranges from 1200 mm at the escarpment to 650 mm at the plain lying east of the lake. The annual mean air temperature varies between 15 °C and 25 °C [Deus & Gloaguen 2013]. Deus & Gloaguen [2013] monitored the water balance pattern of the lake and identified high spatial and temporal variations. By modelling the water balance, they found the water level of the lake to be strongly influenced by precipitation, as also by climate fluctuations. Anthropogenic activities close to the rivers may also influence the water balance. This is due to the irrigation of intensified agriculture

of fertile areas [Ngana *et al.* 2003]. The dominating soil types in the basin are Chromic Luvisols on intermediate gneisses of the Masai Plateau (Masai Steppe), Mollic Andosols on volcanic ashes and volcanic slopes, Gleyic Solonetz on the eastern shore of the Lake and Nitisols on the rift plateau [De Pauw 1984]. The semi-arid Masai Plateau west of Lake Manyara is faced with overgrazing caused by the pastoralist Masai people, which leads to land-degradation and soil erosion [Kiunsi & Meadows 2006]. It is an undulating plain with bushed grassland vegetation dominated by umbrella thorn acacia (acacia tortilis). The slopes of the escarpment and the Essimingor volcano have dense montane forests, bushed woodland and degraded scrubland. Adjacent to the lake extends the Mto wa Mbo swamp area in the north and swamp areas in the Kiru Valley south of the lake and along the Tarangire River. Grassland and moderate forests are dominant here. Alkaline grasslands dominate the flats adjacent to the lake, which are frequently flooded.

2.2 Geology and Tectonic Development of North Tanzanian Divergence Zone (NTD)

The Manyara basin belongs to a set of EARS basins, which stretch from Ethiopia to Tanzania [Ebinger *et al.* 1997] (Fig. 1). The earliest signs for faulting in northern Tanzania are evident for the Miocene and Pliocene (5 – 8 Ma) and were initiated from older rift activities originating in Ethiopia at about 30 Ma [Dawson 2008, Ring 2014]. The Manyara basin is located mainly on Proterozoic basement rocks of the Mozambique orogenic fold belt (Fig. 4). The metasedimentary rocks (gneiss and quartz) result from different orogenic events and are dated to 2 Ga and 645 Ma [Dawson 2008]. The Victoria and the Masai Block were uplifted, which resulted in a tectonic depression and early divergence [Dawson 1992, Macdonald 2002]. As part of this process, shield volcanoes erupted. Nephelinite and phonolite from stratovolcano Essimingor was dated to 8.1 Ma – 6 Ma; 4.78 Ma, 3.22 Ma. The volcanic activity spread and Lemagrut and Sadiman erupted (5.5 – 4.5 Ma) [Evans *et al.* 1971, Bagdasaryan *et al.* 1973, Beloussov *et al.* 1974, Le Gall *et al.* 2008]. Instead of the K-Ar ages of 8.1 – 7.35 Ma for Essimingor by Bagdasaryan *et al.* [1973], Mana *et al.* [2012] received ages from 5.91 – 5.76 Ma with $^{40}Ar/^{39}Ar$ analysis. The volcanic activity between 8 Ma and 2 Ma is dominated by alkali basalt-trachyte / phonolite extrusions [Dawson 1997]. Lavas between Lake Manyara and the Engaruka Basin are dated between 5.4 Ma and 1.4 Ma [Bagdasaryan *et al.* 1973, Beloussov *et al.* 1974]. During that same time, the NTD formed. Lavas from the Ngorongoro massive have been dated with 2.8 Ma to 2.2 Ma (Fig. 5) [Evans *et al.* 1971], and massive explosive phases at 1.9 Ma [Le Gall *et al.* 2008]. The first evidence for subsidence for the Manyara basin are waterlain tuffs and ashes, which have an approximate age of 4.86 Ma [Foster *et al.* 1997, Dawson 2008].

EXCURSION: THE ELEVATION OF PRESENT-DAY LAKE MANYARA

For the lake level of current Lake Manyara different elevations can be found in the literature. Baumann [1894] assumed a lake level of 1,000 m a.s.l. for Lake Manyara. With a barometer, thermometer and three reference stations, Uhlig [1909] measured an average lake level height of 958 m with single measurements ranging from 943 to 971 m. Kohlschütter [1907] performed height measurements on his expedition and noted 963 m in average for "the border of the salt desert, old soil of the Manyara Lake". The height of the Lake Manyara water table was mentioned by Jaeger [1913] with 960 m; An elevation level which is repeatedly mentioned in literature and maps until today. It is not clear from where Jaeger adopted this height. Up to today, many authors rely on this height information. Casanova & Hillaire-Marcel [1992] and Deus & Gloaguen [2013] still used the lake level height of 960 m. Only Somi [1993] mentions that the level must be lower.

The Geoscience Laser Altimeter System (GLAS) onboard the IceSAT satellite data provides the possibility verify the true lake level. The sensor measures within a vertical accuracy of +/- 15 cm an averaged footprint of about 70 m in diameter and 172 m along track [Zwally *et al.* 2002, Carabajal & Harding 2005]. The ICESat elevations refer to the TOPEX/Poseidon ellipsoid. They have to be converted to orthometric heights with respect to the WGS84 reference system and the EGM96 geoid model.

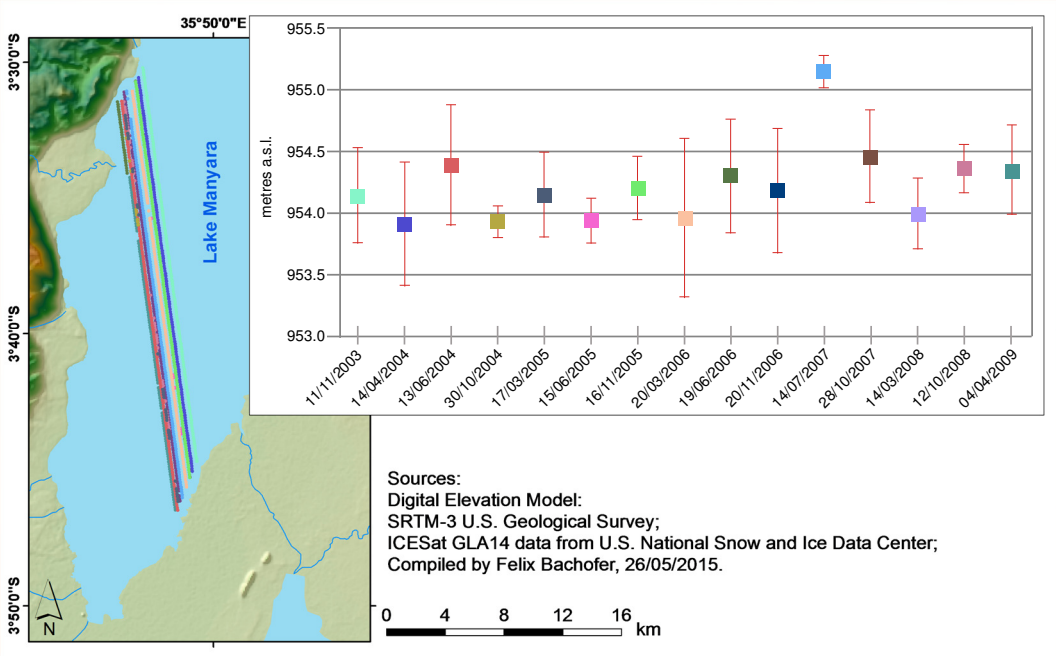

Fig. 3: Mean elevation of lake level for each ICESat track, with standard derivation.

15 ICESat overpasses were corrected for outliers and resulted in 1,424 valid points (GLA14 product) over Lake Manyara between 2003 and 2009 (Fig. 3). A mean lake level of 954.25 m was obtained (EGM96, stdv. 35 cm). Early global DEMs like SRTM-C band version 1 [Farr & Kobrick 2000], the SRTM-X band [DLR 2014] and the ASTER Global DEM version 1 + 2 [Holdship 1976, Tachikawa *et al.* 2011] show voids and irregular surfaces on water bodies and have a vertical shift of several metres compared to the ICESat elevations. The SRTM-C band data from version 2 provides correct height information with 954 m a.s.l. for Lake Manyara.

The shape of the current Tanzanian rift valley was initiated in a major phase of faulting between 1.2 Ma and 0.9 Ma. The tectonic events gave rise to the east facing escarpment and started the formation of the major inland drainage basins [Dawson 1992, 1997, Foster *et al.* 1997]. The EARS splayed further at the NTD in three arms, which are seismically active. The pre-existing structure of the lithosphere controls the volcanism and faulting of the NTD [Ebinger *et al.* 1997, Nyblade & Brazier 2002].

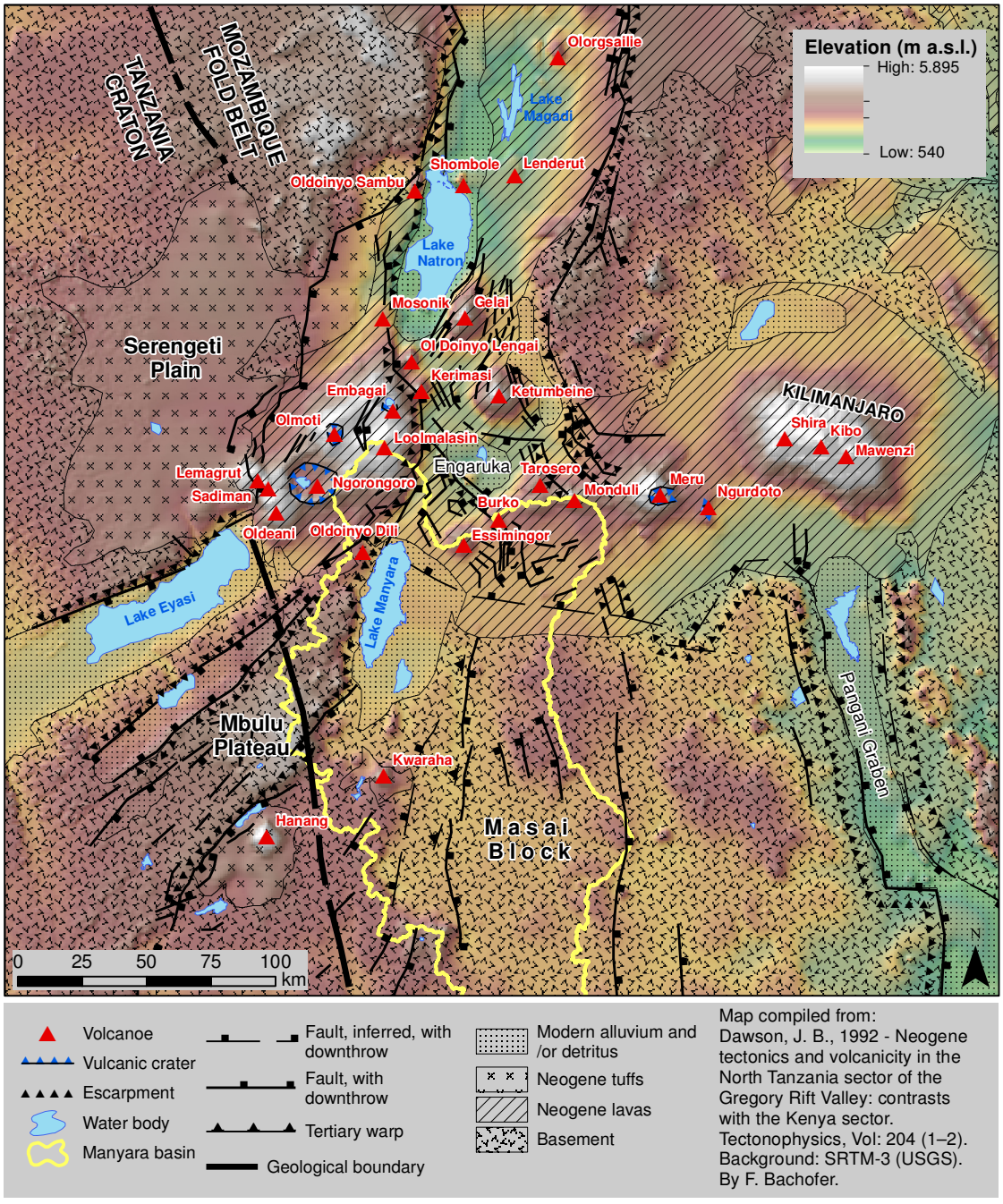

Fig. 4: Tectonic development, volcanism and geology after Dawson [1992] (Dawson compiled data from of the Quarter Degree Maps of the Tanzania and Kenya Geological Surveys and from the SK 57 Survey of Kenya [1967] and Series 1031 D.O.S. [1969]; modified by the author).

Bounded by the Pre-Cambrian intermediate gneisses of the Masai block, the tectonic disturbance bifurcates and results in the NE-trending Eyasi half-graben and the NNW-trending Pangani graben (Fig. 4) [Chorowicz 2005, Dawson 2008]. The rift depression close to the escarpment has a depth of approximately 3 km and is filled with Plio-Pleistocene sediments [Ebinger *et al.* 1997]. The Manyara Rift resulted in a W-dipping warp of basement rocks. Minor en échelon step faults dip to the NNE and E with offsets up to 100 m [Ring *et al.* 2005]. Phonolite, olivine free nephelinite and carbonatite lavas dominate the volcanic activity after 1.2 Ma. These Younger Extrusives belong to Kerimasi, Hanang and the still active Ol Doinyo Lengai volcanoes [Dawson 1992, 2012]. An investigation of the peak strength level of seismic events showed an N-S increase and deepening, which is consistent with a permanent southward movement of the rifting activity [Macheyeki *et al.* 2008, Albaric *et al.* 2009, Mulibo & Nyblade 2010]. Straight alignments of river sections allude to a structural control, caused by faulting or due to fractures [Vaidyanadhan *et al.* 1993]. Dawson [2008] provides a comprehensive overview about the research of the geology and the tectonic development of the region. He also provides an extensive collection on radiometric dates for northern Tanzania (Fig. 5). Radiometric dates, which could be located in adjacency to the study area by literature review, are illustrated in Fig. 6.

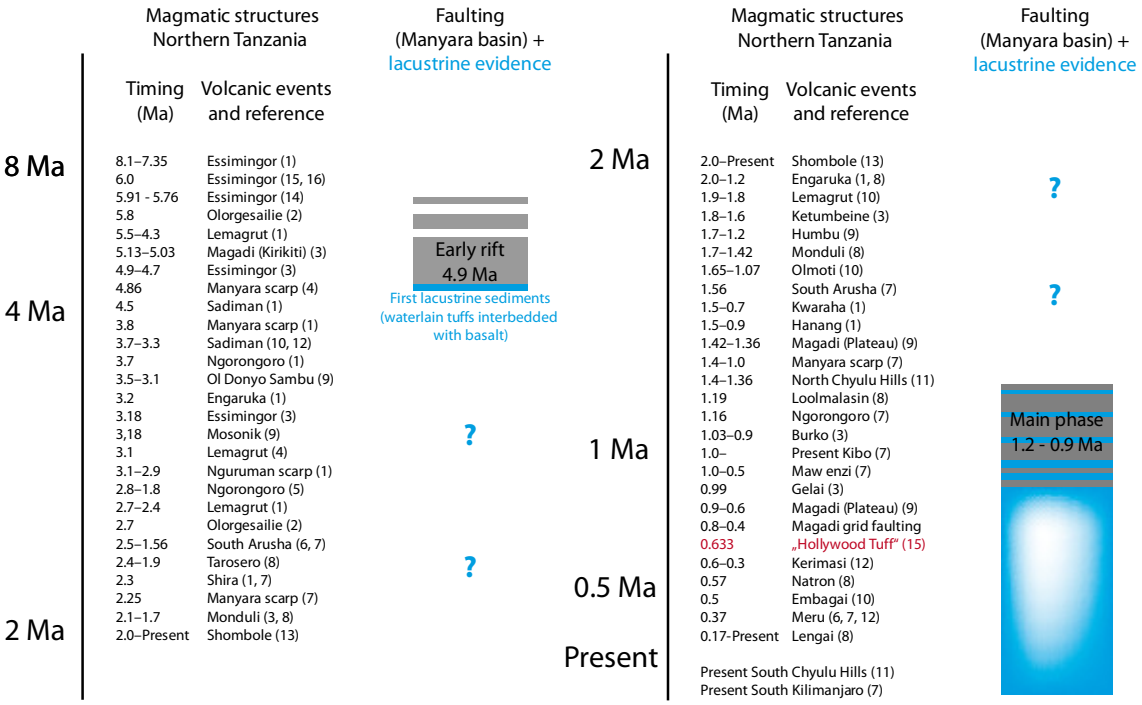

Fig. 5: NTD synrift volcanics after Le Gall *et al.* [2008], faulting after Dawson [2008], modified by the author. Grey bars indicate faulting events, blue bars lacustrine evidence. References: 1) Bagdasaryan *et al.* [1973]; 2) Evernden *et al.* [1965]; 3) Evans *et al.* [1971]; 4) Foster *et al.* [1997]; 5) Grommé *et al.* [1971]; 6) Wilkinson *et al.* [1986]; 7) Le Gall *et al.* [2008]; 8) Macintyre *et al.* [1974]; 9) Isaacs & Curtis [1974]; 10) Manega [1993]; 11) Haug & Strecker [1995]; 12) Hay [1976]; 13) Fairhead *et al.* [1972]; 14) Mana *et al.* [2012]; 15) Schwartz *et al.* [2012]; 16) Beloussov *et al.* [1974].

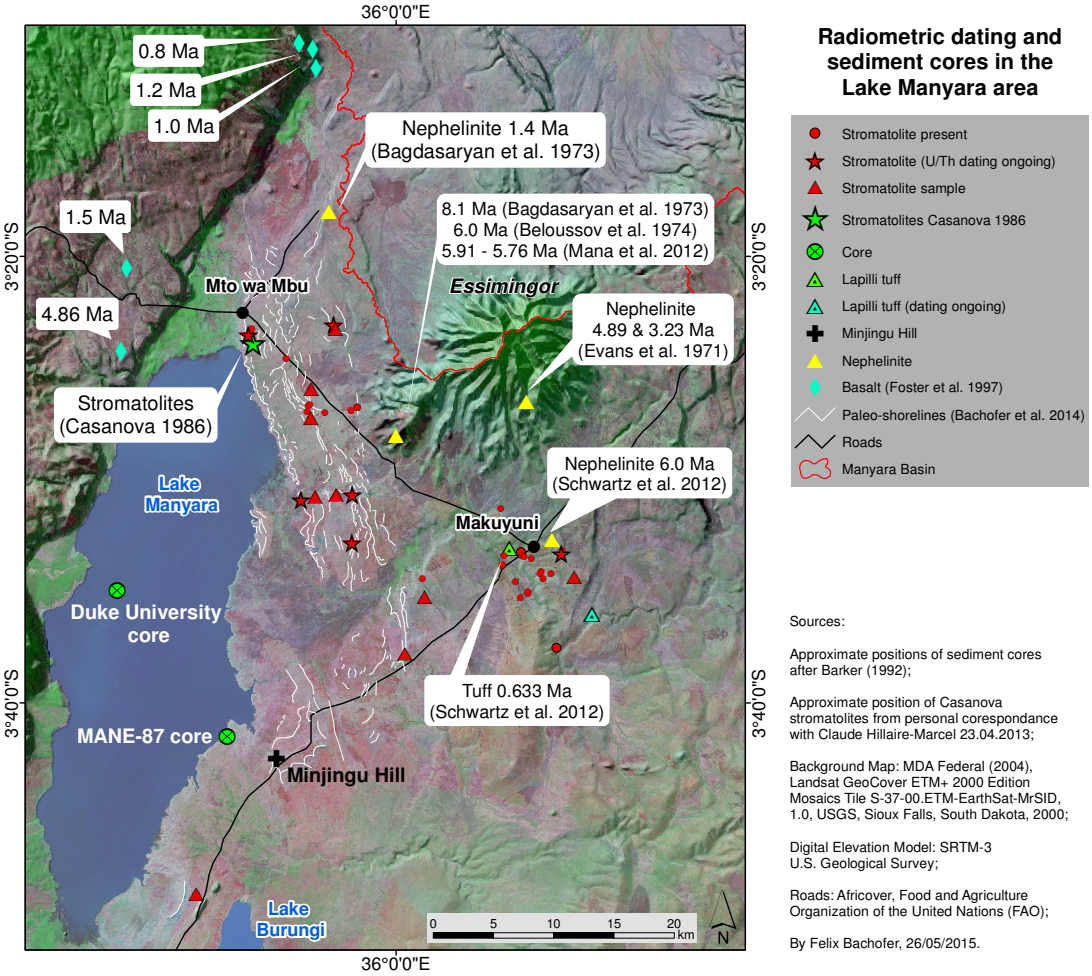

Fig. 6: Radiometric dating and sediment cores in the Lake Manyara area.

2.3 Paleo-Lake Manyara Evidence

Cohen [2003] states that normally two different kinds of paleo-limnological evidence are used to deduce lake level fluctuations. Both are abundant in the Lake Manyara basin. Adjacent to the eastern shore of the lake, shoreline terraces occur. The other piece of evidence is the development of stacked, prograding delta packages, which are abundant in lacustrine sediments close to Makuyuni village. Cohen [2003] also points out the fact that both kinds of evidence have to be interpreted carefully, as tectonic adjustments can influence their position.

Geographical travel reports from the end of the 19th century already mention the fact that Lake Manyara once had a higher water level. Werther [1898] assumed a connection between Lake Manyara and Lake Burungi. Baumann [1894] even suggested a connection to Lake Natron. Uhlig [1909] identified several paleo-shorelines between the present-day lake and the Essimingor on a survey in 1904. Jaeger [1913] mentioned paleo-lake sediments in his report and had followed the shorelines described by Uhlig up to 40 m above the current lake level. The shorelines were also obvious for Leakey [1931]. Other researchers propose an interconnection to the Natron-Magadi basin [Holdship 1976]. Older and more elevated evidence of lacustrine beds close to Makuyuni

was probably first described by Kent [1942], who was on an expedition together with Dr. L.S.B. Leakey in 1935. He investigated a section close to the Makuyuni River where he found different layers, which today are part of the Manyara Beds stratigraphy. They also identified vertebrate fossils and fish remains within those layers. He had no doubt that these lacustrine beds were once deposited by a larger Lake Manyara, which reached a lake level of 90 – 106 m above the present level. The following two sub-chapters give a more detailed overview of the Manyara Beds and the younger paleo-lake evidence.

a) The Manyara Beds

The lacustrine strata of the Manyara Beds define a maximum extent of the lake, more than 40 km east of the present shoreline and with an elevation of more than 140 m above the present lake level. Sections are best exposed close to the town of Makuyuni, where a thin layer of Holocene soils and caliche overlays the sediments partly and where the Makuyuni River and big gully systems incise into the savanna landscape. The sediments contain high amounts of vertebrate fossils, Acheulean lithics and possible Homo erectus remains [Kaiser *et al.* 2010]. The lacustrine sediments are underlain by a sequence of nephelinitic conglomerates, nephelinite lavas and rocks [Kent 1942]. The nephelenitic base was dated to a $^{40}Ar/^{39}Ar$ age of 6.0 +/- 0.03 Ma (Fig. 6) [Schwartz *et al.* 2012]. The sediments can be subdivided into a lacustrine grayish lower member (mudstones, siltstones, diatomites, marls and tuff) and a fluvial and terrestrial up to 13 m thick reddish brown upper member (siltstones, mudstones, conglomerates and breccias) (Fig. 7). The transition between both members is marked in most sections by distinct tephra layers. In the northern part of the Makuyuni area, a lightweight and poorly cemented tephra called "Hollywood Tuff" is abundant. In the southern part, in a stratigraphically equivalent position, a more cemented reddish tephra layer can be found which is called "Red Brick Tuff".

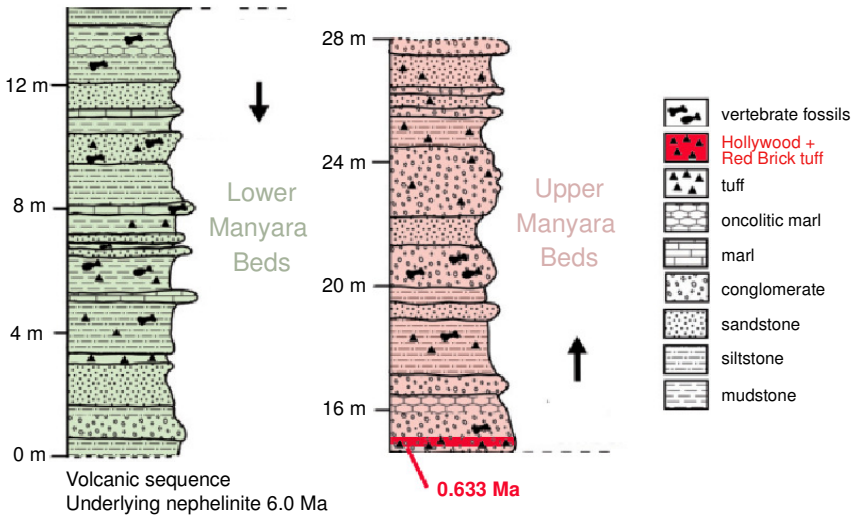

Fig. 7: Generalized stratigraphic column of the Manyara Beds [Ring *et al.* 2005], modified by the author.

Materials in both tephra layers indicate fluvial transport [Ring *et al.* 2005, Schwartz *et al.* 2012]. The $^{40}Ar/^{39}Ar$ age of "Hollywood Tuff" is 0.633 +/- 0.039 Ma. The source of the tephra is not clear. Essimingor was probably inactive (Fig. 8). Prevailing easterly winds suggest the volcanoes Burko, Monduli or Meru, but also a source from the Crater Highlands close to Ngorongoro is possible [Hay 1976, Schwartz *et al.* 2012]. Schwartz *et al.* [2012] conclude, from assumed sedimentation rates, the beginning of the deposition of the Lower Manyara Beds to be between 1.3 Ma and 0.98 Ma and that the top of the Upper Manyara Beds was deposited between 0.44 Ma and 0.27 Ma. Magnetostratigraphic analyses support these calculations. Geochronological analyses suggest that the Manyara Beds correlate with the famous Olduvai Gorge Beds II – IV and the Masek Beds (70 km, respectively 95 km northwest of Lake Manyara). Since there are still some ambiguities, further research is necessary [Schwartz *et al.* 2012].

The regression of the paleo-Lake Manyara after 0.633 Ma and consequently the transition from lacustrine deposition to fluvial/terrestrial deposition may have been caused by different drivers. The age of the Lower Manyara Beds overlaps with the so-called Mid-Pleistocene Revolution (MPR) (about 1.0 – 0.7 Ma), which was a period of intense glacial-interglacial climatic cycles. The MPR appears to be a humid and lake forming interval which appeared in East Africa between 1.1 Ma and 0.9 Ma [Trauth *et al.* 2005, Trauth *et al.* 2007, Schwartz *et al.* 2012]. Schwartz *et al.* [2012] argue that volcanic activity, and with it intense sedimentation rates, may have shifted the paleo-shoreline westwards. Ring *et al.* [2005] assume that the eastern shoreline of Lake Manyara did not only migrate westward but also to the south, due to the southward movement of faulting and volcanism in the Middle and Late Pleistocene. This may have changed the geometry of the basin at that time.

Deposits from Minjingu Hill (Fig. 6), which is a Proterozoic inselberg 5 km east of the present Lake Manyara shoreline, are likely correlative with the Manyara Beds [Schwartz *et al.* 2012], but may possibly be younger [Schlüter 1987, Schlüter 1993]. The hill was an island when the lake level was higher and mainly populated by cormorants, which produced large amounts of guano. The resulting phosphoric deposits are rich in fossil Tilly bones [Schlüter *et al.* 1992, Vaidyanadhan *et al.* 1993, Schlüter 1994, Schlüter & Kohring 2002].

b) Paleo-shorelines, stromatolites and sediment cores

Nearshore carbonate cementation in lakes forms beachrock. Those lithified pavements often develop around existing sand grains, algal bioherms and spring deposited tufas [Cohen 2003]. The type of carbonate sediment depends on the lake floor gradient and the local wave energy conditions [Platt & Wright 2009]. A lake with low gradients and low energy conditions can be expected on the eastern shore of paleo-Lake Manyara, where ramps of carbonate muds often occur. These carbonate muds are also characteristic for carbonate producing palustrine environments. Compared to sedimentary evidence, the shorelines mark a paleo-lake extent and allow an accurate reconstruction of the lake level [Hillaire-Marcel *et al.* 1986, Cohen 2003]. Cohen [2003] notes, that at shorelines of those types, stromatolites may occur. Stromatolites are laminated benthic deposits, which result from microbial mats [Kalkowsky 1908]. Cyanobacteria,

small algae and fungi formed the microbial mats and films, which often occur in hypersaline lake environments [Riding 2000, Dupraz & Visscher 2005].

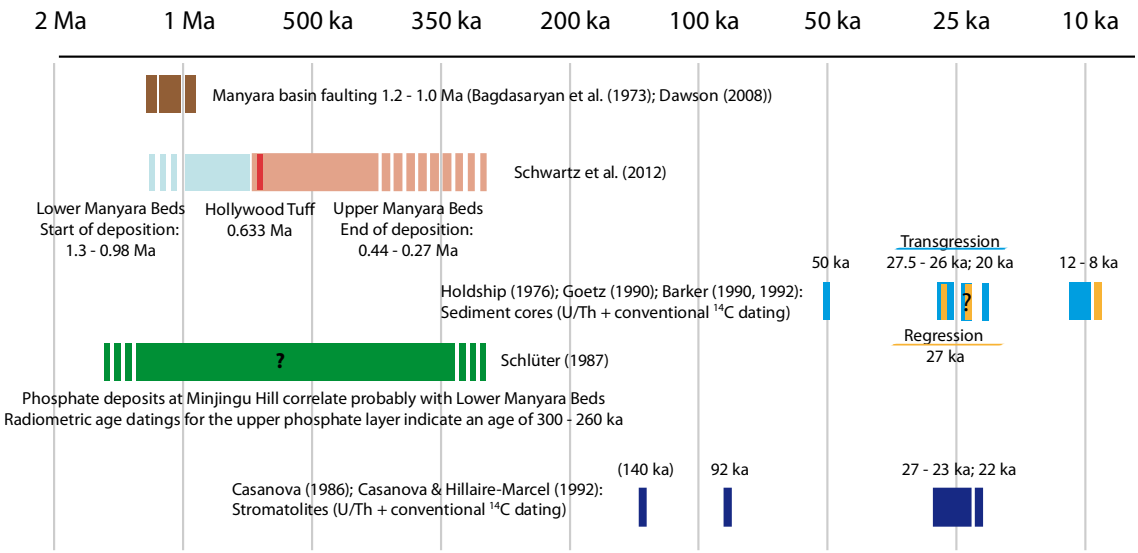

Fig. 8: Evidence for high paleo-lake levels in the Lake Manyara basin and basin faulting.

Between the current eastern shore of Lake Manyara and west of the Essimingor, Manyara Beds and the Masai Plateau, younger evidence (compared to the Manyara Beds) for paleo-lake extents are visible [Dixit 1984]. Carbonate ramps, paleo-lake terraces and ridges are abundant, and provide the basis for several scientific investigations and discussions. These landforms are composed of dolomitic or carbonate rocks, which are stromatolitic, oolitic or consist of coarse fragments and/or gravel. Keller *et al.* [1975] worked in the Lake Manyara basin and the Engaruka basin. They found eight main terraces and several beaches in the Lake Manyara Basin and mapped them along the road from Arusha to Dodoma. Somi [1993] found four stages and Dawson [2008] refers to at least five terraces. The researchers describe the terraces as well defined with clear back-slopes or old cliffs. The carbonate ramps resist erosion and weathering. They also identified two-step shorelines, which result from varying lake levels. Some ridges reach relative elevations of up to 7 m above adjacent ground [Vaidyanadhan *et al.* 1993]. They interpreted the presence of several paleo-shorelines and beaches as a result of a fluctuating lake level. Dixit [1984] investigated accompanied oncolites and stromatolites from the Lake Manyara Basin. He traced oncolites and other stromatolites on ridges for several kilometers in N–S direction. Without the possibility of drilling, he was not able to conclude what lies between these ridges, except that soil and caliche cover these areas. Oncolites and stromatolites are abundant on the ridges, while on the side of the ridges, rudaceous calcareous rocks dominate. He also provides a detailed description of the oncolites and stromatolites. Since Dixit [1984] found relatively large oncolites in the Lake Manyara area (> 10 cm) which are not attached to the ground, he concludes that they were formed in a rather high-energy littoral environment in which they were moved, at least occasionally, by strong waves. He deduces that the zone of the lake where the oncolites and stromatolites were formed was sublittoral to marginal with possible periods of subaerial exposure.

Casanova [1986] and Casanova & Hillaire-Marcel [1992] conducted ^{14}C and U/Th dating on 18 stromatolite samples, as well as ^{13}C, ^{18}O isotope analysis to assess paleo-hydrological conditions. Whereas Holdship [1976] and Schlüter [1987] suggest a paleo-lake level with a connection to the Engaruka and Natron-Magadi basins, Casanova & Hillaire-Marcel [1992] expect a lower maximum lake level at about 990 m, which precludes a connection to the other basins. Similar to another study at Lake Natron [Hillaire-Marcel *et al.* 1986], they also identified stromatolites from three generations, which can already be visibly classified due to their specific morphology. Often, though not always, second-generation stromatolites develop on first-generation stromatolites, and third-generation stromatolites encrust them both. They collected the samples on a distinct level of 20 m above the present lake level (Fig. 6). They conclude that at least those three lacustrine phases had the same lake extent [Casanova 1986, Casanova & Hillaire-Marcel 1992]. An uncertain U/Th age of 140 ka was calculated for a group of first-generation samples. Another, more confident, U/Th age was identified at 92 ka. Second- and third-generation stromatolites formed between 27 and 23 ka (U/Th + ^{14}C ka BP; Fig. 8). Third-generation samples, which isotope analyses indicate nutrient enrichment and a regression phase, yield ages about 21.8 ^{14}C ka BP. No stromatolite evidence occurs for a probable humid period between 12.5 and 8 ka [Holdship 1976], which is not unusual, since specific water chemistry and ecological conditions are necessary for their formation (Fig. 8). Somi [1993] also dated stromatolites from shorelines with different elevations. Due to technical problems, he considers his dates as less reliable as those from Casanova [1986], but the deviating dates can be assigned to those of Casanova [1986] and confirm the general trend.

The sediments of Lake Manyara provide a more continuous archive than the stromatolites. A 57 m long core was drilled close to the center of the lake by a team from Duke University in 1969 [Holdship 1976] and a second 14 m sediment core (MANE-87) was taken from the mudflats at the eastern shore of the lake in 1987 (Fig. 6) [Barker 1990, 1992]. Analyses of Barker [1992] and Holdship [1976] focused on the diatom assemblages in the cores. Diatoms, or Bacillariophyeae, are unicellular algae with siliceous frustules, which respond to changes in the water chemistry. They are strong environmental indicators which are often well preserved in sediment deposits [Barker 1990]. Holdship [1976] dated a maximum age of 35.55 ^{14}C ka BP, which was extrapolated to 55 ^{14}C ka BP for the base of the core. The results of both cores suggest transgressional phases between 27.5 and 26 ^{14}C ka BP, at 20 ^{14}C ka BP and between 12.5 and 8 ^{14}C ka BP [Holdship 1976, Barker 1990]. The ^{14}C results were confirmed by U/Th dating [Goetz 1990]. Because the analysis suggests a large amount of freshwater at the Pleistocene/Holocene transition, Holdship [1976] suggests a high water level up the outlet and an overspill in the Engaruka and Natron-Magadi basins for this period. Barker [1990] supports this hypothesis.

The development of the Lake Manyara lake level is still controversially debated. Vaidyanadhan *et al.* [1993] assume a gradual shrinking of Lake Manyara with just a few transgressions. Holdship [1976] and Barker [1990] on the contrary, assume stronger phases of transgression and regression and thereby different maximum lake levels.

c) Quaternary lake level fluctuations in East Africa

First analyses of lake level fluctuations of various lakes in Africa were presented by Washbourn [1967] and Butzer *et al.* [1972]. Street & Grove [1979] provided a global overview on paleo-lake fluctuations. A lake level arises from the balance of inputs and outputs. The inputs consist of precipitation, inflow of streams and inflow of groundwater. Outputs are outflow of streams, groundwater seepage and evapotranspiration. The importance of these parameters varies depending on climate and topographical characteristics of the lake basin [Street & Grove 1979, Barker 1990, Olaka *et al.* 2010, Trauth *et al.* 2010]. Currently the Lake Manyara is an endorheic basin with no outflow, making this parameter irrelevant. The same applies to several lakes following the Gregory rift valley from Kenya to Tanzania. The most prominent lakes are Turkana, Suguta, Baringo, Bogoria, Nakuru, Elmenteita, Naivasha, Magadi, Natron, Eyasi and Manyara. A review of paleo-limnological literature (Fig. 9) illustrates evidence for high lake levels in the according drainage basins. Two main phases of high lake levels are evident in the Middle and Late Pleistocene. One phase is apparent between 140 ka and 120 ka and another at the Pleistocene-Holocene transition between 12 ka and 8 ka.

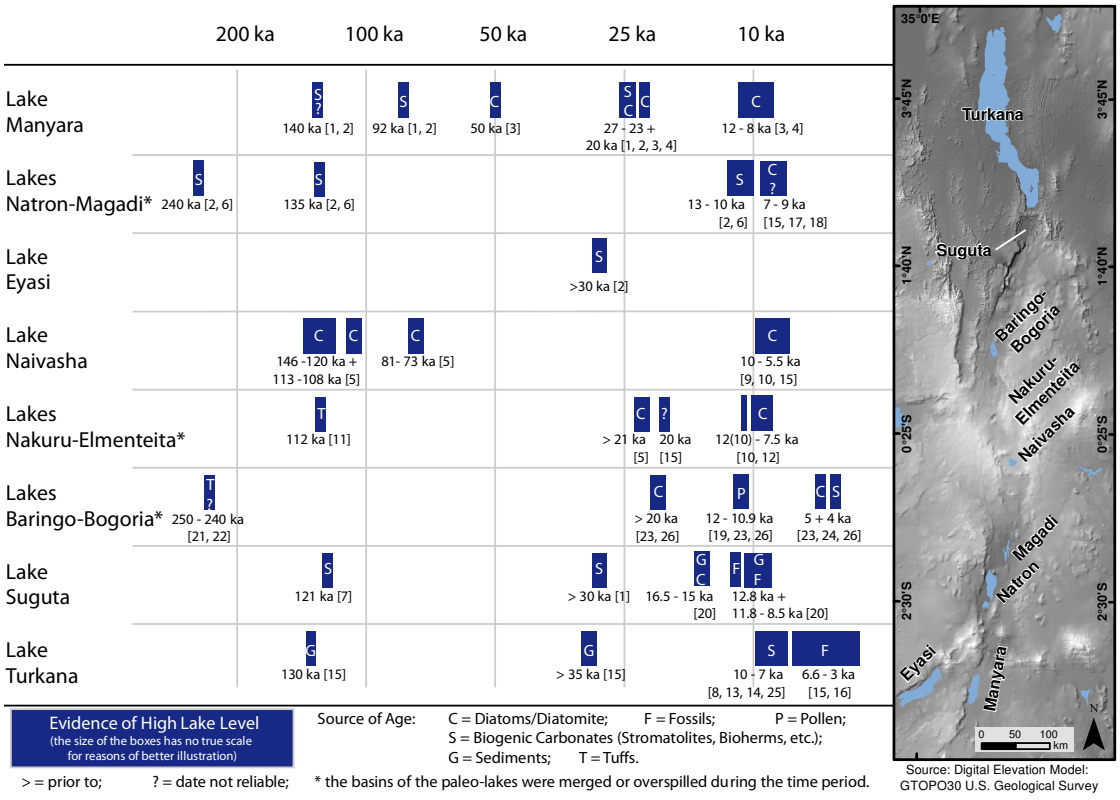

Fig. 9: Middle Pleistocene to Middle Holocene relative lake-level high stands in East Africa from literature review. Listed ages involve calibrated and conventional ^{14}C ages. References: 1) Casanova [1986]; 2) Casanova & Hillaire-Marcel [1992]; 3) Holdship [1976], Goetz [1990]; 4) Barker [1990]; 5) Bergner & Trauth [2004]; 6) Hillaire-Marcel *et al.* [1986]; 7) Casanova *et al.* [1988]; 8) Abell *et al.* [1982]; 9) Washbourn [1967]; 10) Richardson & Dussinger [1986]; 11) Bergner *et al.* [2009]; 12) Dühnforth *et al.* [2006]; 13) Vondra *et al.* [1971]; 14) Butzer [1980]; 15) Butzer *et al.* [1972]; 16) Thomson [1966]; 17) Hay [1968]; 18) Eugster [1967]; 19) Vincens [1986]; 20) Garcin *et al.* [2009]; 21) Hill *et al.* [1986]; 22) Cornelissen *et al.* [1990]; 23) Renaut & Tiercelin [1994]; 24) Vincens *et al.* [1986]; 25) Owen & Renaut [1986]; 26) Tiercelin *et al.* [1981].

The lowest possible present-day outlet (Fig. 2) for Lake Manyara drains to the Lake Natron-Magadi basin, traversing the small Engaruka basin. Therefore, the paleo-hydrology of the Natron-Magadi basin is especially important for Lake Manyara. Hillaire-Marcel *et al.* [1986] dated three generations of stromatolites from the Lake Natron-Magadi basin about 60 m above the present-day lake level. From ages of the ^{14}C and U/Th dated stromatolites samples they concluded to a maximum extension of the lake at 10,800 ^{14}C yr BP (third generation stromatolites; 646 – 656 m a.s.l. and 675 – 680 m a.s.l.; lake rise at 11,800 ^{14}C yr BP and lake recession ca. 9,100 ^{14}C yr BP). With U/Th methods, they dated the second generation of stromatolites (655 – 656 m asl.) to ca. 135,000 ka (+/- 10,000) and the first generation, with a high uncertainty to 240,000 ka (+34,000 / - 52,000). They conclude that the stromatolite dates of Lake Natron-Magadi have no equivalent in the Lake Manyara shoreline history and vice versa. Therefore, any correlation between dated stromatolites in East African Lakes may involve a methodological problem, as the encrusting benthic microbial communities react very sensitive to variations in water chemistry and hydrological conditions [Casanova & Hillaire-Marcel 1992]. This leads to the conclusion that stromatolites are not necessarily an indicator for all high paleo-lake levels, rather for some.

2.4 East African Paleo-Climate

The East African climate is characterized by a strong seasonality and spatial variability [Nicholson 1996]. Hession & Moore [2011] have shown that topographic variables have a strong influence on the local precipitation patterns in East Africa. Changes of vegetation cover result in an increase or decrease of albedo and can accentuate climatic effects [Vincens *et al.* 1993]. The present seasonal climatic situation, with a bimodal pattern of short rains in October/November and a stronger wet season in March/April (e.g. Manyara basin, see Appendix VIII), is strongly dependent on the southward and northward migration of the Inter-tropical Convergence Zone (ITCZ). The ITCZ follows the maximum insolation and receives most of the advective moisture from the Indian Ocean [Nicholson 1996, Levin *et al.* 2009]. Three major air streams dominate the climate of the region. The relatively dry NE monsoon and the SE monsoon originating from the Indian Ocean, which are separated by the ITCZ, as well as the humid Congo Air Stream, which reaches the region when the Congo Air Boundary (CAB) migrates east [Nicholson 1996, Barker & Gasse 2003, Levin *et al.* 2009]. The Congo Air Stream transports humid air from the Atlantic and the Congo basin [Levin *et al.* 2009]. The results of Junginger *et al.* [2014] suggest that a highstand of the paleo-Lake Suguta, during the African Humid Period (AHP), resulted from a north–eastwards shift of the CAB caused by a high pressure gradient between East Africa and India. The East African climate proves to be strongly influenced by remote drivers. The El Niño Southern Oscillation (ENSO) causes perturbations in the interdecadal and interannual precipitation pattern, which for example results in extremely wet conditions in equatorial East Africa during El Niño events, while southern Africa experiences dry conditions on the contrary [Camberlin *et al.* 2001, Schneider *et al.* 2014, Nicholson 2015]. Interdependent with the dominant impact of ENSO on the interannual rainfall variability, the variation of the SST gradient across

the Indian Ocean has a high impact on the East African hydroclimate when regarding multidecadal periods [Bergner & Trauth 2004, Tierney *et al.* 2013]. High SSTs off the East African coast are positively correlated with ENSO events in the region and with a strong east - west sea surface dipole on the Indian Ocean (Indian Ocean Dipole - IOD) [Nicholson & Kim 1997, Camberlin *et al.* 2001].

The research on the paleo-climate variability in East Africa led to the identification of several drivers in a complex system [Nicholson 1996]. The geological development of the EARS with its highly elevated plateau and rift shoulders influenced major airstreams and thus the paleo-climate [Sepulchre *et al.* 2006]. These long term paleo-climate changes in turn affected the morphology of the EARS drainage basins, the paleo-flora and paleo-fauna and played an important role in the evolution of hominins [deMenocal 1995, Trauth *et al.* 2005]. Cohen [2003] and Trauth *et al.* [2010] state that tropical and subtropical rift lakes react quite sensitive to climatic changes, particularly precipitation, because of the high evaporation rates compared to higher latitudes. Besides these morphotectonic influences, orbital caused variations of total solar irradiance is the main driver of long-term climate variability in the region [Nicholson 1996, Trauth *et al.* 2010].

For instance, Verschuren *et al.* [2000] found that the Naivasha lake records of humidity and aridity within the last millennium correlate with phases of direct high and low solar radiation due to sunspot variability. On longer time scales, the orbital parameter eccentricity (shape of the earth's orbit) [Milankovic 1941], the obliquity of the earth's axis and the precession of the earth influenced the insolation and thus greatly impacted the paleo-climate [Kutzbach & Street-Perrott 1985, Verschuren *et al.* 2000, Trauth *et al.* 2003, Trauth *et al.* 2007, Maslin & Trauth 2009, Trauth *et al.* 2009, Blaauw *et al.* 2011, Trauth *et al.* 2015]. Principally, the earth's orbital precession, with a frequency of 23 – 19 kyr, causes insolation and has a major impact on high and low lake levels in East Africa. The precession leads to a more intense gradient between low-pressure areas over the continents and high-pressure areas over the oceans and results in an increased moisture transport [Kutzbach & Street-Perrott 1985]. Based on these dynamics, equatorial East Africa is affected by half-precessional cycles (11 – 10 kyr). Once during and increasing gradient, and once during a decreasing gradient. This case, for example, was evident during the AHP between 14,500 and 5,500 ka [Kutzbach & Street-Perrott 1985, Barker *et al.* 2004, Garcin *et al.* 2009, Junginger *et al.* 2014, Schneider *et al.* 2014]. It also coincides well with lake level highstands at approximately >22 ka, >30 ka and between 60 and 50 ka (Fig. 9) [Rossignol-Strick 1983, Trauth *et al.* 2003]. Examples for influences of the earth's precession further back in time are the 2.7 – 2.55 year old sediments of the Lake Baringo basin [Kingston *et al.* 2007]. Prior to 2.7 Ma the 400 kyr component of the Earth's eccentricity cycle lead to periods of high climatic variability [Trauth *et al.* 2007]. Since 1 Ma, the 400 kyr cycles turned into 100 kyr-cycles also due to eccentricity as evident in many paleo-climate records of the area [Ruddiman *et al.* 1989, Trauth *et al.* 2005, Trauth *et al.* 2007, Trauth *et al.* 2009]. In addition to these clear correlations with changes in the earth's orbital parameter, East Africa's paleo-climate records also indicate correlations with substantial global climate transitions in the late Cenozoic, despite a general long term drying trend based on the

following [Trauth *et al.* 2005, Trauth *et al.* 2007]: i) a deep lake period at 1.1 – 0.9 Ma and the initiation of the Mid-Pleistocene Revolution [Berger & Jansen 2013]; ii) a deep lake period between 1.9 and 1.7 Ma and the development of the Walker circulation [Ravelo *et al.* 2004]; iii) as well as from an additional deep lake period at 2.7 – 2.5 Ma and the intensification of the Northern Hemisphere Glaciation after the Pliocene warmth period [Haug & Tiedemann 1998].

Between 2.7 Ma and 1 Ma, the 41 kyr earth's obliquity seem to have influenced the region [Tiedemann *et al.* 1994, Ravelo *et al.* 2004], however since the obliquity should not directly affect equatorial regions, remote controls may have triggered these events [Trauth *et al.* 2005, Trauth *et al.* 2007]. Remote tectonic activities, comparable to the uplift of Tibet, also influenced the global climate and in this case had a cooling effect on East Africa during the Late Cenozoic [Ruddiman & Kutzbach 1989].

2.5 Archaeological and Paleontological Evidence

The oldest uncovered hominid remains thus far (*Australopithecus bahrelghazali*; 7 – 6 Ma) were found in Chad [Brunet *et al.* 2002]. Nevertheless, the EARS is one of the most important regions with find localities of early hominids. Some of the most relevant hominid findings related to the EARS are: Ardi, a 4.4 Ma old *Ardipithecus ramidus* (from Ethiopia) [White *et al.* 1994]; Lucy a 3.2 Ma *Australopithecus afarensis* (from Ethiopia) [Johanson & Edey 1981]; A newly discovered oldest specimen of a *Homo* remain with 2.8 Ma so far (jawbone from Ethiopia) [Villmoare *et al.* 2015]; The *Homo rudolfensis* was found at Lake Malawi with an age of 2.5 Ma [Schrenk *et al.* 1993] and at Koobi (genus is under discussion, 1.9 Ma) in the east of Lake Turkana [Leakey 1973, Wood & Lonergan 2008] and the Nariokotome Boy (formerly known as Turkana Boy; *Homo erectus*, 1.6 – 1.5 Ma) close to Lake Turkana [Brown *et al.* 1985]. Different researchers assume a relationship between the three big paleo-climatic shifts mentioned in the previous chapter at 2.7 – 2.5 Ma, 1.9 – 1.7 Ma and 1.1 – 0.9 Ma and major events in early hominid evolution [deMenocal 1995, Trauth *et al.* 2005, Trauth *et al.* 2007, Bergner *et al.* 2009, Maslin & Trauth 2009, Trauth *et al.* 2010, Maslin *et al.* 2014].

In the northwest of the Lake Manyara basin lays one of the most important finding locations (Fig. 10). The Olduvai Gorge was first discovered by H. Reck in 1913 [Reck 1921, 1937]. L.S.B. and M. Leakey, who devoted the focus of their research to this location, brought the site to popular attention. In 1959, Mary Leakey found the remains of an *Australopithecus boisei [Leakey 1959]*. In the following years *Homo habilis* and *Homo erectus* remains were discovered [Leakey 1959, 1961, Leakey *et al.* 1964, Leakey *et al.* 1965]. Olduvai yields not only hominid remains, as the excavation of the Olduvai Beds and Masek Beds also brought out an enormous collection of vertebrate fossils and stone artefacts from the Acheulean, Middle Stone Age (MSA), and Later Stone Age (LSA) [Leakey & Roe 1995, Potts 2010]. Besides Olduvai is the Laetoli site (45 km SSE of Olduvai, Fig. 10) another important location [Kent 1941]. A fossil of *Australopithecus afarensis,* as well as bipedal footprints, were discovered by M. Leakey. Fossil from at least 23 individuals

were found and dated to 3.76 – 3.46 Ma [Leakey & Hay 1979]. In younger strata also a *Homo sapiens* was found, which was dated to 120 ka [Magori & Day 1983].

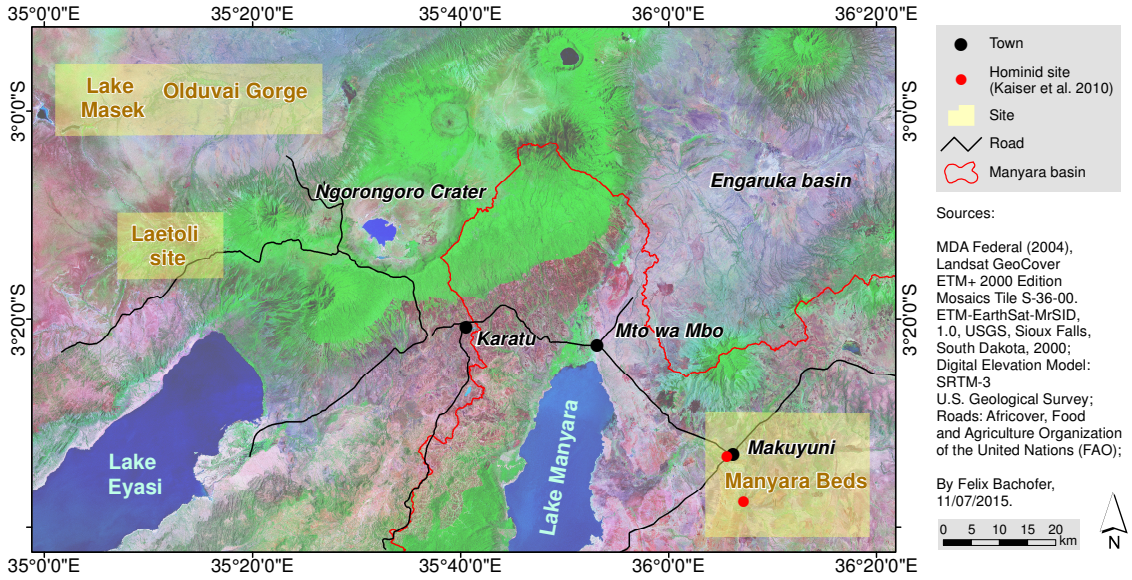

Fig. 10: Outlined sites of the Olduvai-, Masek-, Laetoli- and Manyara Beds, which comprise rich paleontological and archaeological findings.

The Manyara Beds were first described by Kent [1942] as a result of an excursion with L.S.B. Leakey in 1935. Between several vertebrate fossils, they found a mandible of a Hippopotamus, which indicated, that the Beds are Middle Pleistocene Age or younger. Keller *et al.* [1975] focused their survey on an area west of Makuyuni, reaching until the eastern shore of the lake and in the Engaruka basin. They found MSA and Later LSA assemblages of chert and quartz at different localities. The Manyara area came into focus of research activities again in 1994. This intense research period is ongoing up to today [Kaiser *et al.* 1995, Schwartz *et al.* 2012]. Researchers subdivided the area in the surroundings of Makuyuni, where the river system and gully system incise in the landscape and reveal the Manyara Beds best, into 'MK areas'.

Those areas and locations indicate places, which are rich in surficial vertebrate fossils and lithics (Fig. 11) [Kaiser *et al.* 2010, Schwartz *et al.* 2012]. At MK 2 and MK 4 fragments of hominid fossils were found and identified as a tooth and a parietal fragment of *Homo erectus* [Kaiser *et al.* 2010]. Frost *et al.* [2012] suggest that the fragments represent *Homo heidelbergensis*. Cut-marks on a bovid mandible proves the treatment of bones by hominins in the area [Frost *et al.* 2012]. Paleontological studies show relative differences in the abundance of faunal fossils in the Manyara Beds. Bovids are more frequent in the UMBs, while Equidae are more often found in the LMBs [Frost *et al.* 2012]. Based on the morphologic characters of the fossils, open grassland had dominated the landscape during the time of the deposition of the Manyara Beds and was later followed by bushed grassland [Kaiser *et al.* 2010, Wolf *et al.* 2010, Frost *et al.* 2012]. Giemsch [2015] analysed 1,337 Acheuléen lithic artefacts from different sites from the Manyara Beds near Makuyuni. They are comprised of 31.5 % handaxes, 30.7 % flakes and flake tools, 20.8 % cores and core tools, as well as others. The raw materials are made of locally available basalt and quartz (96.5 %). The finding locations comprise an age of 630 ka to 270 ka, considering other

archaeological sites. The density of the findings indicates that hominins were not only occasional in the Lake Manyara area. Since the hominin fragments and artifacts were found close to the contact zone between the LMBs and the UMBs, Frost *et al.* [2012] and Giemsch [2015] suggest that it was advantageous for hominins to tarry in a lakeshore environment.

Palaeontological and archaeological research is also conducted in other parts of the Manyara basin. Seitsonen [2006a] concentrates his work mainly to an area north of Lake Manyara and the Engaruka basin. He discovered 13 sites with MSA and LSA assemblages. Eleven of these sites have an elevation above 1032 m and are therewith above the lowest possible outlet (Fig. 2) and close to the escarpment. Charcoal from a rich preceramic LSA site was radiocarbon dated to 9,280 +/- 60 cal. yr BP. Prendergast *et al.* [2013] found LSA sites on the southern Mbulu plateau, and radiocarbon dated an ostrich eggshell to 9,280 +/- 25 cal. yr BP.

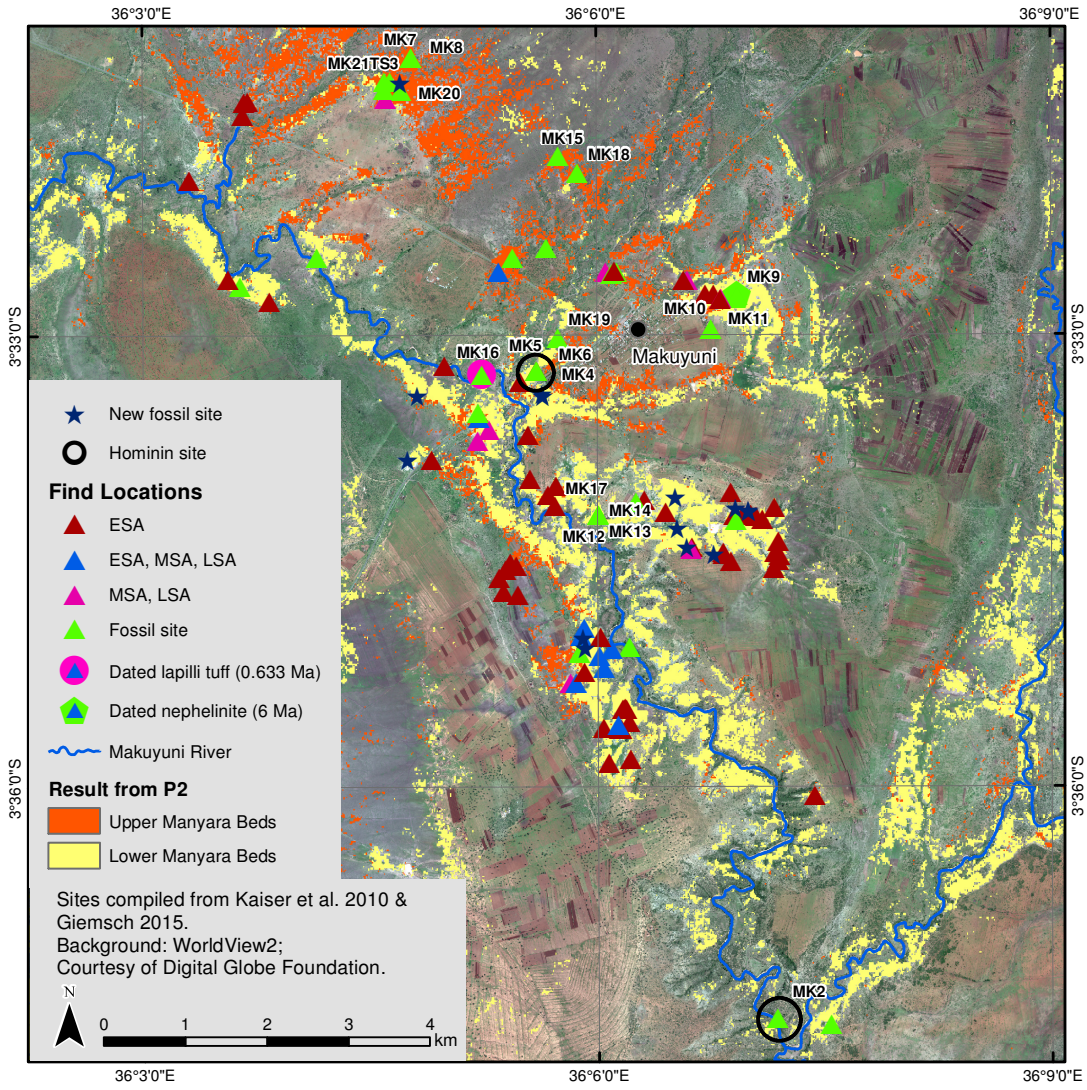

Fig. 11: Map showing important MK areas and the Manyara Beds.

CHAPTER 3 - PROPOSED RESEARCH METHODS

Remote sensing data and associated analysis technologies represent the central methodological approaches for this dissertation. Topographic analysis, as well as field work, strongly contributed to the analyses. This chapter provides a general introduction to satellite remote sensing, while the respective methods applied in this thesis are described in detail in the research papers (Appendices I – VII). The aim of this chapter is to introduce the fundamentals of remote sensing and topographic analyses. It enables interested readers to follow the methods applied to the gathered data in order to gain an understanding of the landscape, its forms and structures, as well its underlying processes. Detailed descriptions of physics and technologies are beyond the scope of this introduction.

3.1 REMOTE SENSING

Sabins [2000] describes remote sensing as a science, in which images are acquired, processed and interpreted that record the interaction of signals of the electromagnetic spectrum (Fig. 12) and physical matter. Other authors generalize this definition and speak of a science, which acquires information of objects and surfaces without direct physical contact [Albertz 2009, Lillesand *et al.* 2015]. Such definitions would include measurements that do not result in images and might include non-invasive, terrestrial geophysical measurements. The term remote sensing, as used in this thesis, is restricted to the acquisition, processing and interpretation of data from sensors, which are mounted on air- and spaceborne platforms. The fundamental principle of remote sensing analysis is the assumption, that different objects reflect, absorb transmit or emit electromagnetic radiation (EMR) with different intensities. These differences result from the chemical, physical and structural properties of an object. EMR transmits energy and consists of an electric field and a perpendicular magnetic field, which can be imagined as a stream of particles travelling in waves. Remote sensing sensors measure this radiation, which is also influenced by the atmosphere. The intensity in radiation of an object, which reaches a sensor, varies depending on the wavelength in the electromagnetic spectrum. With these measurements, remote sensing seeks to differentiate between different objects and materials [Mather & Koch 2011, Lillesand *et al.* 2015]. The electromagnetic spectrum (Fig. 12) illustrates sets of grouped waves. The atmosphere absorbs large parts of the wavelengths, which in conclusion cannot be used in terrestrial earth observation with spaceborne sensors. The regions, where the electromagnetic spectrum is transmissive of wavelengths, are called atmospheric windows [Jensen 2007]. Short-wave X and gamma rays are blocked by the atmosphere. Ultraviolet radiation enters the atmosphere, but is rarely measured by remote sensing sensors. The range of the electromagnetic spectrum between 0.4 and 0.7 µm is visible for the human eye, followed by the near-infrared up to a wavelength of 1 µm. The short-wave infrared has a bandwidth from 1 to 3 µm. The thermal infrared occupies wavelengths in the atmospheric windows between 3 to 5 µm and 8 – 14 µm.

Radio Detection and Ranging (Radar) and passive microwave signals operate between wavelengths of 1 mm and 1 m [Lillesand *et al.* 2015].

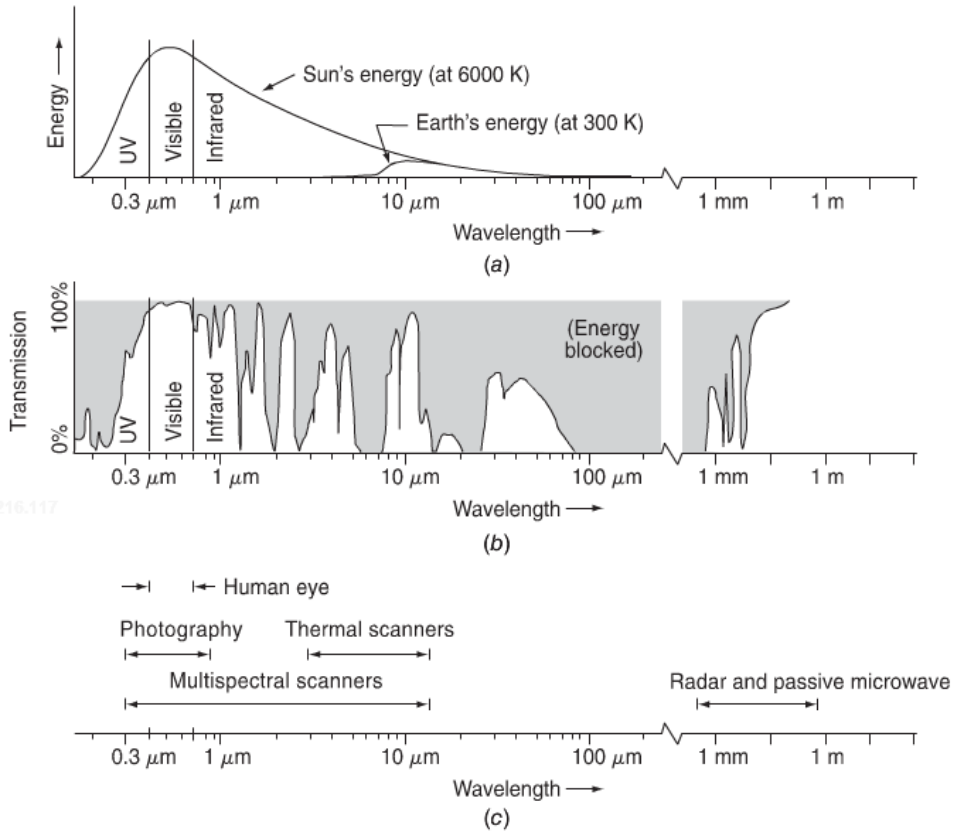

Fig. 12: The electromagnetic spectrum with spectral characteristics of: a) natural energy sources; b) atmospheric transmittance and spectral regions; c) remote sensing systems. The source of the figure is Lillesand *et al.* [2015].

Some characteristics, which help to assess the performance of sensors, are the following [Albertz 2009, Mather & Koch 2011]: i) Spatial resolution or ground sampling distance (GSD) is mostly provided by the length of an edge of a pixel (picture element). It thereby defines the degree of detail in which a sensor can distinguish objects and surfaces within the instantaneous field of view of a sensor; ii) Spectral resolution is an important characteristic for sensors, which measure EMR in the visible and in the infrared regions; While microwave sensors measure radiation of one wavelength, optical systems discriminate between different colours and acquire single images for distinct wavelengths; iii) The temporal resolution defines the time, which is necessary for a sensor, to revisit the same area and acquire a second image; iv) The radiometric resolution refers to the sensitivity of a sensor in measuring the upwelling energy and ability to store the signal with digital numbers various of quantization levels.

Remote sensing systems can be subdivided into active and passive systems. Optical multispectral sensors record reflected or emitted EMR. The source of the reflected EMR is the sun. Thermal infrared wavelengths transport emitted energy from the earth's surface (Fig. 12). Since the sensors measure the energy from external energy sources, they are considered passive systems. Most radar sensors are active remote sensing systems, which transmit the energy and

receive the same EMR after the interaction with an object [Richards 2009, Mather & Koch 2011, Lillesand *et al.* 2015].

a) Optical Remote Sensing

The spectral information of optical sensors is used in this thesis to identify fluvial features (P6), distinguish between vegetated and non-vegetated areas and to classify the surface substrates of the non-vegetated areas (P2, P3). The optical remote sensing systems utilized in this thesis are the visible- and near-infrared (VNIR) and shortwave infrared (SWIR) bands of the ASTER sensor and the spectral bands of the WorldView-2 satellite (Tab. 3). WorldView-2 has a very high spatial resolution. Its' eight multispectral bands have a GSD of 1.85 m and the panchromatic band of 0.46 m at nadir (surface point on earth, directly below the sensor). The WorldView-2 satellite carries a commercial multispectral sensor, launched in October 2009 [DigitalGlobe 2013]. Though the sensor has a high spectral resolution in relation to its' spatial resolution, the spectral range does barely exceed the near-infrared range. The ASTER VNIR and SWIR sensors were launched on-board NASA's TERRA spacecraft in December 1999 [Fujisada 1995, Yamaguchi *et al.* 1998]. The arrangement of the spectral bands was designed for vegetation, soil and mineral mapping. Even though sensors with a higher spatial resolution are available, the ASTER satellite offers a relatively high spectral resolution. The three on-board sensors provide three bands in the visible and near infrared regions (VNIR; 15 m GSD), six bands in the short wave infrared region (SWIR, 30 m GSD) and five bands in the thermal infrared region (TIR, 90 m GSD) [Fujisada 1995, Yamaguchi *et al.* 1998]. The only operational sensor with a similar spatial resolution, which is covering the soil and lithologically important short-wave infrared and thermal infrared regions, is currently the hyperspectral (220 bands) Hyperion sensor [Melesse *et al.* 2007, van der Meer *et al.* 2012]. The Hyperion sensor has a relatively narrow swath width of 7.75 km [Zhang & Pazner 2007], which results in a low global coverage and as a result, no data of the study area are available in the archive so far. Since the end of 2014, WorldView-3 images can be ordered. The satellite covers the spectral range of the VNIR and SWIR region, similar to the ASTER satellite but with a higher spatial resolution [Kruse & Perry 2013, SIC 2015].

Tab. 3: Multispectral images used in this thesis; RGB = red, green, blue spectral bands.

Sensor	Date	Time (UTC)	No. bands	Wavelength	GSD (nadir)	Applied in paper
WorldView-2 pansharpened	2010-10-15		8	0.40 – 1.04 µm	0.46 m	P6
WorldView-2 multispectral	2011-02-21	08:22	8	0.40 – 1.04 µm	1.85 m	P3
ASTER-VNIR	2006-08-23	08:07	3	0.52 – 0.86 µm	15 m	P2, P3, P7
ASTER-SWIR	2006-08-23	08:07	6	1.60 – 2.43 µm	30 m	P2, P3, P7
IKONOS (Google Earth)	2005-09-12	-	RGB	0.45 – 0.72 µm	0.82 m	P6
GeoEye1 (Google Earth)	2010-01-25	-	RGB	0.45 – 0.695 µm	0.46 m	P6

In the thesis, a strong emphasis is placed on the usage of spectral indices and ratios of ASTER images. The spectral rationing of band absorption features at distinct wavelengths highlights the relative presence or absence of distinct surface materials [Rowan *et al.* 2005]. P2 and P3 provide an extensive overview and literature review of spectral indices. Reports authored by Kalinowski & Oliver [2004] and Cudahy [2012], give a comprehensive overview of indices.

b) Radar Remote Sensing

SAR data offers some specific advantages compared to optical remote sensing images. SAR sensors can operate day and night, the SAR signals experience less influences by atmospheric effects and they provide supplementary information [Sabins 2000]. As mentioned previously, the chemical composition has a high impact on the EMR reflected in the visible and infrared region. The backscatter signal of active SAR sensors is sensitive on the surface roughness, the geometric shape of objects and the dielectric properties, which are dependent on the moisture content [Mather & Koch 2011]. A letter indicates the wavelength of a sensor: X stands for a wavelength of 3.75 – 2.5 cm (frequency: 8 – 12.5 GHz); C for a wavelength of 7.5 – 3.75 cm (frequency: 4 – 8 GHz) and L for a wavelength of 30 – 15 cm (frequency: 1 – 2 GHz). The higher the wavelength, the less influenced the signal is by the atmosphere and the better it can penetrate vegetation and surface sediments [Jensen 2007, Mather & Koch 2011, Lillesand *et al.* 2015]. The disposition of the electric field and the magnetic field is described by the polarization state of the EMR. It can be either horizontal (H) or vertical (V).

Tab. 4: SAR images used in this thesis; Asc. = ascending, Des. = descending, Pol. = polarization, AP = alternating polarization, Incident angle at scene center.

Sensor	Mode	Band	Date	Orbit	Incident angle	Pol.	GSD	Applied in paper
TSX1	StripMap	X	2011-08-28	Asc.	26.3°	HH	3 m	P3, P4
TSX1	StripMap	X	2011-09-02	Asc.	26.3°	HH	3 m	P4
TSX1	StripMap	X	2011-09-08	Asc.	44.4°	HH	3 m	P4
TSX1	StripMap	X	2011-09-13	Asc.	44.4°	HH	3 m	P3, P4, P5
TSX1	StripMap	X	2012-12-24	Asc.	25.8°	HH/HV	3 m	P4
TSX1	StripMap	X	2013-01-15	Asc.	24.49°	HH/HV	3 m	P1, P4
TSX1	StripMap	X	2013-01-26	Asc.	28.11°	HH	3 m	P1
ENVISAT ASAR	AP	C	2011-08-02	Des.	31.0 – 36.3° (scene range)	VV/VH	30 m	P1, P3
ENVISAT ASAR	AP	C	2011-10-01	Des.	31.0 – 36.3° (scene range)	VV/VH	30 m	P3
ALOS PALSAR	Fine Beam	L	2008-05-24	Asc.	38.78°	HH/HV	20 m	P4
ALOS PALSAR	Fine Beam	L	2010-07-15	Asc.	38.78°	HH/HV	20 m	P1, P4

When displayed with two letters, the first letters indicates the polarization of the emitted radiation while the second indicates polarization of the received radiation. SAR systems can have different modes of polarization. Single polarizations are HH, VV, HV or VH. Dual polarizations are HH and HV, VV and VH, or HH and VV. Full polarization or quadruple polarization systems allow all four combinations [Richards 2009, Mather & Koch 2011]. When EMR is reflected or scattered by an object it changes its polarization and thereby provides information about the characteristics of an object. The travel time of a signal indicates its backscatter position on the earths' surface. Imaging SAR systems are side-looking systems, since nadir looking systems would receive echoes from both sides of the nadir track. Those signals would be ambiguously for the receiver and could not be distinguished. Nevertheless, the side looking radar may cause specific distortions, which are called radar shadows, foreshortening and layover effects [Richards 2009]. The viewing geometry has a strong influence on these distortions, as well as on the strength of the backscatter signal. The local incidence angle of the sensor controls, together with the surface topography and surface properties, the backscatter signal [Mather & Koch 2011].

The applications for radar remote sensing in the study are the contribution to surface substrate classification and the detection of linear structures, which indicate paleo-shorelines or tectonic lineaments. The L-, C- and X-band SAR sensors interact differently with surface objects. High-frequency sensors are sensitive for minor variations of surface roughness, while sensors with lower frequencies are less sensitive to vegetation cover and are able to penetrate it [Dierking 1999, Gaber *et al.* 2009b, Mather & Koch 2011]. Hence, with TerraSAR-X (TSX1), ENVISAT ASAR and ALOS PALSAR were varying wavelengths utilized in the publications P1, P3, P4 and P5 of this thesis (Tab. 4).

3.2 Terrain Analysis and Spatial Modelling

DEMs are digital, mostly continuous, representations of the topographic landscape. DEMs of different sources and their derivatives were used for the assessment of the topographical, hydrological and sedimentological situation of the study area (Tab. 5). Since Light Detection and Ranging (LiDAR) products are not available for the study area, SAR interferometry and the stereo-correlation of optical images remain the sources of the DEMs in this study [Mulder *et al.* 2011].

Tab. 5: DEMs used in this thesis.

DEM	GSD	Applied in paper
SPOT DEM	20 m	P6
ASTER GDEM	30 m	P6
SRTM-X	30 m	P1, P2 ,P3, P4, P6, P7
SRTM-3	90 m	P4

Optical stereo-photogrammetry utilizes overlapping remote sensing acquisitions. The movement of the remote sensing platform causes the stereoscopic parallax, which describes the

displacement of an object caused by image acquisitions from different points of observation. The position and orientation of the sensor is known at the time of image acquisition. The stereoscopic method requires a co-registration of the input images in order to allow the identification of objects on the ground. The surface heights of these objects can be derived by the principle: the amount of parallax decreases with an increasing distance from the camera [Jacobsen 2003, Li *et al.* 2005, Albertz 2009, Lillesand *et al.* 2015]. A Satellite Pour l'observation De La Terre (SPOT) DEM was derived from stereo-pair images of forward- and backward-facing sensors of the SPOT-5 satellite by Incentive for the Scientific use of Images from the Spot system (ISIS), which is financed by the French Space Agency (CNES). The DEM was compiled with four pairs of satellite images (01/01/2006; 30/07/2004; 23/01/2005; and 27/06/2006) and has a GSD of 20 m. The ASTER VNIR sensor provides its band 3 in nadir looking and in backward looking orientation. This allows the stereoscopic generation of DEMs. The ASTER Global DEM (GDEM, version 2) is a global product (between 83° N and 83° S) provided by Ministry of Economy, Trade, and Industry (METI) of Japan and the United States National Aeronautics and Space Administration (NASA) [Hirano *et al.* 2003, San & Süzen 2005, Tachikawa *et al.* 2011].

SAR interferometry is a widely used method to derive height information [Jacobsen 2003, Büyüksalih & Jacobsen 2006, Passini & Jacobsen 2007, Jacobsen 2010]. The SAR echo has two components. One is the amplitude, the other component is the phase. SAR interferometry exploits the phase information, which precisely measures the path length between the SAR system and the illuminated surface. Two antennas, one antenna at each respective position, are necessary to calculate the phase difference between the two acquisitions. The baseline between both positions must be identified to conclude to the height information [Hanssen 2001, Richards 2009, Mather & Koch 2011]. The NASA SRTM DEM results from a series of SAR images, which were taken by a space shuttle mission with the objective of building a high-resolution topographic database of the entire world in February 2000 [Farr & Kobrick 2000, Farr *et al.* 2007]. SRTM employed two SAR systems. A C-band SAR with a wavelength of 5.6 cm (frequency 5.3 GHz) from NASA's Jet Propulsion Laboratory (JPL) and an X-band SAR with 3.1 cm wavelength (frequency 9.6 GHz) of the German Aerospace Centre (DLR). The SRTM-C band dataset provides a full global coverage between 60° north and 56° south latitude [Farr *et al.* 2007]. Until September 2014, the available C-band SRTM had only a spatial resolution of 3 arc-seconds, which are approximately 90 m GSD. Since September 2014 are also SRTM-C DEMs with 1 arc-second available, which is equal to a GSD of 30 m [LPDAAC 2014]. The SRTM-X band dataset has no full coverage worldwide, however still covers the study area and has a GSD of 30 m [DLR 2014].

From the DEMs, topographic parameters were processed which describe the topographic position of surfaces and objects. From these topographic parameters, it is also possible to derive hydrological and geomorphological surface processes. The parameters are described in the publications of this thesis. The following literature provides supplementary information on terrain analysis and spatial modelling: Zevenbergen & Thorne [1987], Dikau [1988], Moore *et al.* [1991, 1997], Li *et al.* [2005], Deng [2007], Zhou *et al.* [2008], Wilson [2012].

3.3 FIELD WORK

Field work is necessary for a proper understanding of the landforms, their processes, and ground reference point collection for the calibration and validation of the remote sensing analyses. The data for this study was collected during six field campaigns between 2010 and 2014. Extensive surveys were conducted in the focus areas (Fig. 2), though also in additional areas of the Manyara basin and in the Natron-Magadi basin.

Reference point collection

For the collection of ground reference data, 699 sites were visited to ensure an adequate number of reference points for the input datasets of supervised classifications and accuracy assessment following Congalton & Green [2009]. The collected parameters consist of: land use, texture, calcium carbonate ($CaCO_3$) content (with hydrochloride acid), soil color, visible mineral components of surface substrates, vegetation cover, topographic position, GPS and photo references. Since the remotely located parts in the south and east of the study area are partly inaccessible, it was decided to apply a random clustered sampling strategy [Congalton & Green 2009].

Soil sample collection

Surface substrate samples were collected in the study area, in addition to the reference points. For 36 reference locations, topsoil samples (0–2 cm) were collected, and physical and chemical analyses were conducted (see Appendix IX). Details of the analysis procedure are stated in P3.

Sample collection for radiometric dating

Stromatolites at 69 sites were visited during the field campaigns. East of Lake Manyara, 21 stromatolite samples were collected (Fig. 6). Most of them are related to shorelines and terraces (Appendix X). Some stromatolites were found in the Manyara Beds, yet it is not clear if they were transported and from which stratigraphic layer they originate. The stromatolites found in situ on paleo-shorelines have been sent to the Max Planck Institute for Evolutionary Anthropology for Uranium-series dating (U/Th) dating [Ku 2000]. A preliminary analysis of Uranium and Thorium contents appears auspicious, though the analysis are yet to be completed. Additionally, two samples of tuff were collected east of Makuyuni, at an outcrop in the Makuyuni River bed. The tuffs were under- and overlain by Nephelinite (X: 182868.76, Y: 9601576.85; UTM 37S, WGS84). They were sent to Department of Petrology of the Free University of Amsterdam for $^{40}Ar/^{39}Ar$ dating. Unfortunately, no final dating results are available thus far.

CHAPTER 4 - RESULTS AND DISCUSSION

4.1 ANSWERS TO THE RESEARCH QUESTIONS

Seven publications address the eight research questions and the main objective of this dissertation. The results of the scientific work, which is presented in detail in the research articles (Appendices I – VII), are elucidated in this section. Where necessary, short methodological explanations are given. The detailed methodologies can be found in the according publications (P1 – P7). The following figure (Fig. 13) displays the interrelations between the research questions and the publications, in which the research questions are addressed.

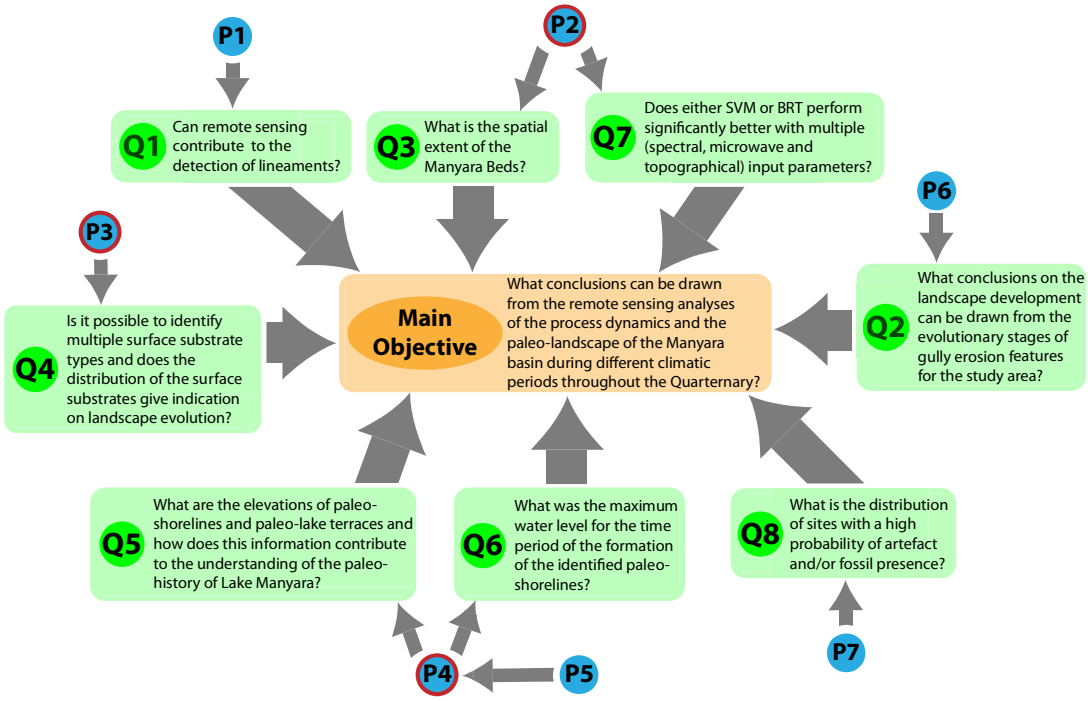

Fig. 13: Interrelation of publications and research questions. Core publications are displayed with a red corona.

Q1: Can remote sensing contribute to the detection of lineaments?

The relief and the landscape of the Lake Manyara basin reflect the evolution of a complex system in the EARS. The landscape simultaneously underwent tectonic processes inherent to its geology and Quaternary geomorphological processes. For the Makuyuni River catchment, lineaments were extracted from ENVISAT ASAR and TerraSAR-X images (P1). Manual and automatic edge extraction approaches were compared. With both methods, the same lineaments were identified, yet the automatic extraction produced many artefacts. The lineaments show an N-S orientation and reveal tectonic activity, which is characterized by the occurrence of erosional processes, as well as by deviations and knickpoints of streambeds. The lineaments were successfully detected from SAR scenes.

Q2: What conclusions on the landscape development can be drawn from the evolutionary stages of gully erosion features for the study area?

Features of gully erosion are abundant throughout the study area. Topographic analysis with various DEMs and the digitalization of drainage networks and gully features from high-resolution remote sensing data served as input data for a gully evolution model, which determines the gully development phases (P6). Gully channel formation is a very rapid, but short (approximately 5 % of a gullys' lifetime) process [Sidorchuk 1999]. The morphometric parameters, derived from the analysis, suggest that the gully systems are relatively stable and indicate that the bigger systems developed already at a more elevated base level. Hence, the age of the large gully systems is most likely beyond the last paleo-Lake Manyara highstand. Nevertheless, since this is an interpretation of a modelling outcome and no absolute dating result, the determination of the age has to be treated with caution.

Q3: What is the spatial extent of the Manyara Beds?

The lacustrine sediments LMBs are the paleo-lake evidence with the highest elevation in the Manyara basin [Frost *et al.* 2012, Schwartz *et al.* 2012]. Their elevation and their large extent on the plain east of present Lake Manyara makes them an important indicator for the paleo-Lake Manyara and the landscape development in the region. In addition, the Manyara Beds bear a multitude of artefacts and fossils, which allow conclusions of the paleo-environment [Kaiser *et al.* 2010, Giemsch 2015]. While lacustrine sediments and resulting initial soils adjacent to the present lake dominate the surface substrates, the Manyara Beds crop out where the fluvial network and gully systems incise into the landscape. For the mapping of the Manyara Beds, an ASTER multispectral satellite image (2006-08-23), spectral indices, and topographic information derived from an SRTM-X DEM, was used as input data sets in an SVM classification (P2). When classifying the UMBs and the LMBs into two separate classes, an overall classification accuracy (OA) of 80 % was reached. When merging the LMBs and UMBs, the OA increases to 92 %. The results exhibit the surface distribution of the LMB and UMB. The remote sensing approach proved to be highly suitable for the delineation of the Manyara Beds. The UMBs were identified mainly north and northeast of Makuyuni. The LMBs, or similar lacustrine / palustrine sediments, were found in the Tarangire valley up to 33 km south of Makuyuni and on the same elevation. Up to 18 km east of Makuyuni, more lacustrine / palustrine sediments were identified with an elevation 140 m above the LMB at Makuyuni.

Q4: Is it possible to delineate multiple surface substrate types and does the spatial distribution of the surface substrates give indication on landscape evolution?

The distribution of soils and rocks yields valuable information for the interpretation of landscape evolution. For the assessment of surface substrates (P3), nine soil and lithological target-classes were identified, through field work and laboratory analysis of surface soil samples (Appendix IX). Those classes are: 1) Carbonate rich substrates; 2) Calcaric topsoil; 3) Dark topsoil; 4) Tuff outcrop; 5) Reddish topsoil; 6) Silica-rich topsoil; 7) Topsoil with iron oxide properties; 8)

Mafic-dominated cover beds; 9) Mafic river beds. A non-linear SVM approach was used to classify the input datasets, which consists of a high-resolution WorldView-2 scene, the backscatter intensity information of TerraSAR-X and ENVISAT ASAR SAR images, ASTER spectral bands and corresponding spectral indices, as well as SRTM-X derived topographic indices. Based on these spectral, structural and topographical properties of the topsoil target-classes were identified with an OA of 71.9 %. This OA can be increased to 79 % by merging the similar target-classes "Carbonate rich substrates" and "Calcaric topsoil" together. "Carbonate rich substrates" can be associated with the LMBs, "Silica-rich topsoil", as well with "reddish topsoils" to a certain extent, and can be associated with the felsic Proterozoic basement of the Masai Plateau. "Dark topsoils" correlate with colluvial and fluvial deposits. "Topsoils with iron oxide properties" can be found on the slopes of the volcano Essimingor and on mafic ridges. These congruities allow conclusions to be drawn on the landscape development, which is discussed in the following chapter.

Q5: What are the elevations of paleo-shorelines and paleo-lake terraces and how does this information contribute to the understanding of the paleo-history of Lake Manyara?

Paleo-shorelines and paleo-lake terraces result from varying stages of Quaternary lake level highstands, and today are linear ridges that can be found east of Lake Manyara [Keller *et al.* 1975, Casanova & Hillaire-Marcel 1992]. An in-depth spatial consideration of the shorelines had thus far been missing. The paleo-shorelines could not be delineated with optical remote sensing images, because of the uniform surface cover compared to their surroundings. The attempt of a spectral analysis led to unsatisfying results. The application of SAR images seemed to be a promising alternative. The geometry and the surface roughness of the elongated landforms led to an intense backscatter signal in ALOS PALSAR and TerraSAR-X images (P4). The resulting features were extracted from the SAR scenes with edge detection techniques. A detailed methodological comparison was conducted to find a well performing algorithm (P5). The most promising edge detector techniques in this comparison were the Canny operator [Canny 1986] and the edge detection based on Discrete Wavelet Transformation [Mallat 1989]. The elevation for each identified segment was extracted from an SRTM-X DEM. A continuous distribution of shorelines between 960 and 1040 m a.s.l. indicates fluctuating paleo-lake levels. Several prominent paleo-lake levels were then identified at 970 m, 978 m, 1002 m to 1008 m, 1018 m and 1030 m and depict more steady paleo-environmental conditions. A validation with reference data from field surveys proved the analysis successful.

Q6: What was the maximum water level for the time period of the formation of the identified paleo-shorelines?

The maximum paleo-lake level, which was identified by the extraction of the SAR backscatter signals, is identified between 1030 m and 1040 m a.s.l.. This altitude resembles an identical elevation to the lowest possible outlet of the present-day endorheic Manyara basin at 1032 m a.s.l. (P4 & Fig. 2). The paleo-lake level was validated by stromatolites, which were found

on the slopes of the terrace. The location of the outlet indicates an overflow into the neighboring Engaruka and Natron-Magadi basins.

Q7: Does either SVM or BRT perform significantly better with multiple (spectral, microwave and topographical) input parameters?

The relationships of the surface substrates, the stratigraphy and the topographical position are complex in such a heterogeneous environment like the study area. Multiple input parameters were applied to identify them. For the delineation of the Manyara Beds (P2) SVM and BRT classification approaches were compared. Additionally, various combinations of input datasets were comprised of the ASTER spectral bands of the VNIR and SWIR spectral region and 35 spectral indices, as well as 25 additional topographic indices calculated from a SRTM-X DEM to serve as input datasets. The SVM classification was conducted with the Library of Support Vector Machines (LIBSVM) in a supervised classification approach [Chang & Lin 2011]. In an n-dimensional feature space, it maximizes the margin for input features classes according to the input samples. To achieve optimized margins between several input features, SVMs transfer the data into an n-dimensional feature space. Kernel functions are used to delineate the independent input features according to the designated target classes [Vapnik 1995, 1998]. Just as SVM's, regression trees are machine-learning algorithms. Their goal is to construct prediction models from the input datasets, by recursively partitioning the feature space and assigning simple predictions or classification rules to each part. The result can be represented as a structure similar to a tree [Elith *et al.* 2006]. Two BRT algorithms were applied in the comparison: The AdaBoost.M1 and the SAMME algorithm [Freund & Schapire 1996, Prasad *et al.* 2006, Zhu *et al.* 2009]. The comparison resulted in high OA for both methods, with minor advantages for the SVM approach. In general, no significant difference could be observed. In addition, the SVM algorithm performed well in the delineation of multiple surface substrate classes (P3).

Q8: What is the distribution of sites with a high probability of artefact and/or fossil presence?

A large number of sites with specimens of fossil vertebrates and artefacts were detected during different field campaigns [Kaiser *et al.* 2010, Giemsch 2015]. An integrative spatial modelling concept was developed, using GIS, satellite remote sensing data and the maximum entropy method (MaxEnt), a statistical methodology based on statistical mechanics [Jaynes 1957, Phillips *et al.* 2006] for a thorough analysis of the spatial distribution of these sites. The proposed analysis used 22 topographic indices, as well as ASTER VNIR and SWIR spectral bands and principle components as predictor variables (P7). Ninety-nine archaeological and paleontological sites served as training variables. The results indicate that the fossils and artefacts were transported towards the toeslopes, because of the high variable importance of the profile curvature [Zevenbergen & Thorne 1987]. The sites are also found at a certain height above the present river network and close to the boundary of the UMBs and LMBs, which points to a deposition close to the former lakeshore. This indicates the dependence of early hominids on

water resources and food resources such as game, which also concentrates in these ecological units. Geraldine Quénéhervé (University of Tuebingen) conducted a re-analysis of the dataset with 50 predictor variables, including various spectral indices derived from the ASTER data [Quénéhervé personal communication 15.05.2015]. The new analysis supports the results so far. More differentiated results are present, as the probabilities for Early Stone Age, MSA/LSA and fossil sites were modelled separately. The major difference is a higher elevation of paleontological sites in general, compared to Early Stone Age/MSA/LSA sites. In addition, fossils sites seem to be related to stable paleo-landscape features indicated by the Quartz Rich Rocks index [Rowan *et al.* 2005] and the Laterite index [Bierwirth 2002]. The spectral indices feature high variable importance.

4.2 Integration of the Results into the Landscape Evolution of the Study Area

The presented answers to Q1 – Q6 and Q8, centered on various remote sensing based methods, draw a comprehensive picture of the landscape development in the study area and in the Lake Manyara basin as a whole. The remote sensing analyses proposed in P1 reveal a dominant N–S orientation of lineaments. Most of the subbasins in the Makuyuni catchment show a strong asymmetry, especially in the northern section. The asymmetry suggests tectonic deformation, as well as subsidence of the central rift, which causes an increased westerly dipping of the monocline. Knickpoints, derived from longitudinal stream profiles, show spatial proximity to lineaments in the hydrological right part of the catchment. In the left part of the catchment, the knickpoints are related to the transition of Precambrian lithology of the Masai Plateau to the younger basalts. As a result, the northern section is considered hydrologically controlled with tectonic influence, while the southern section of the catchment is more stable. In conclusion, results of the morphological analysis on basin tilting, basin hypsometry and the morphology of the stream longitudinal profiles indicate that tectonic activity in the study area is an important factor for Quaternary geomorphological processes. The tectonic activity controls the landscape evolution of this region. P6 investigates gully erosion phases according to gully morphometric characteristics as proposed by Kosov *et al.* [1987] and by Sidorchuk [1999]. The relation of the contributing area at the gully head cut to the total contributing area at the gully mouth suggests that the gully systems in the area are stable. Their age can be considered as old, compared to the current base level. The sizes of some upstream gully systems indicate that they existed already when a base level of a higher lake level was predominant. Those gully systems were reactivated with the regression of the lake.

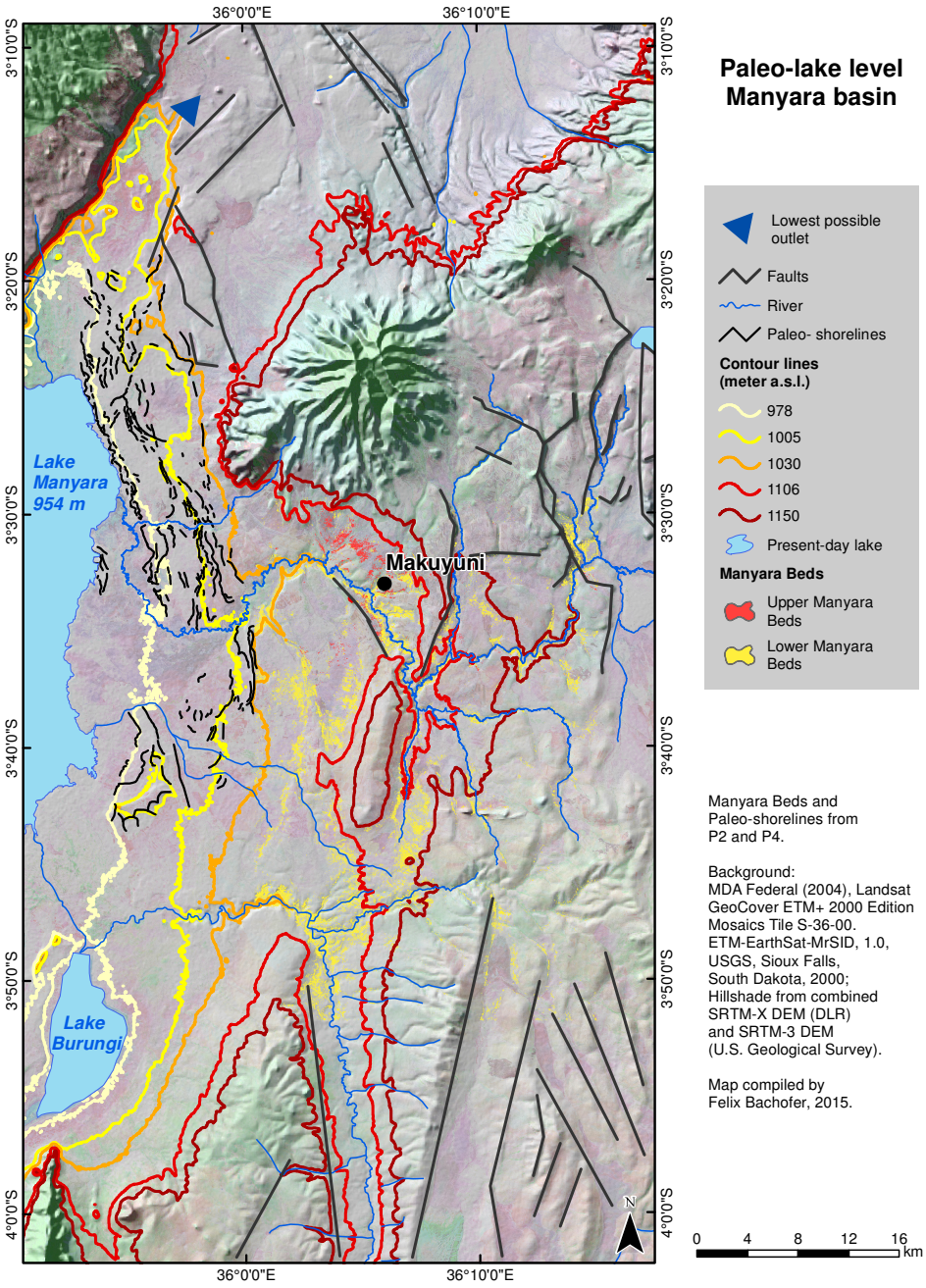

Fig. 14: Possible paleo-lake level of Lake Manyara based on current topography.

Lake systems with a large extent are quite sensitive to short-term and long-term climatic and tectonic variations because of their large evaporating surface relative to their depth. So far, the Manyara Beds have been identified up to 140 m above and 30 km east of the present-day lake level [Ring *et al.* 2005, Schwartz *et al.* 2012]. The results of P2 and P3 exhibit the surface distribution of the LMB and UMB in the study area. The LMBs, or similar lacustrine sediments were identified south of the Makuyuni River catchment in the Tarangire River system. The elevation of the lacustrine deposits in the Tarangire valley coincides with the LMBs. This indicates that no significant tectonic tilt occurred in NS direction since the deposition of the LMBs. The remote sensing analysis revealed that lacustrine deposits occur 10 to 18 km further east and up to 285 m above the current lake level (Fig. 14). A field visit confirmed the result and contemporary

vertebrate fossils were found at this location. Yet, no sediment profile was found during the field campaign for detailed stratigraphic analysis. The sediments may also result from carbonate muds, which deposited in a lacustrine/palustrine environment with a low gradient and low energy [Cohen 2003]. There are three plausible scenarios for the abundance of these high-elevated sediments, which have to be falsified in future research:

I) Cascading lake systems existed parallel to an extended paleo-Lake Manyara, following the main faults towards the east. The lake systems formed perched basins on inclined fault blocks and/or were separated by mafic ridges. They were subsequently cut and drained by the Makuyuni River.

II) The paleo-Lake Manyara was extended to the east, but was not as deep as the current topography suggests. The reason for the westerly migration of the water body to the present-day position of the lake may involve an onset of aridity in the Pleistocene, but is in any case related to an increased tilt of the downthrown block of the main rift fault by a series of minor movements or a big event. This scenario is also indicated by the analysis of the subbasins in P1. Ring *et al.* [2005] and Schwartz *et al.* [2012] propose a similar tectonic development. In this scenario, a less extensive lake level rise was necessary to flood the eastern area. Dawson [2008] contradicts this possibility. Tectonic movements must be involved in some way, if not the difference in elevation between the eastern lacustrine sediment and Manyara Beds to the lowest possible outlet could not be explained (Fig. 14).

III) The third scenario proposes a combination of scenario I and II. The perhaps climatic and tectonically based westerly regression of the paleo-Lake Manyara left several shallow perched basins behind, similar to the current Lake Burungi. The Makuyuni River subsequently cut and drained the small basins.

The results of P3 allow conclusions to be drawn on the landscape development. The results indicate a complex and heterogeneous evolution of the study area, and of the Manyara basin as a whole. “Topsoils with iron oxide properties” are predominant when associated with mafic outcrops on ridges or the slopes of the Essimingor volcano. The ridges are associated with tectonic faults. A subsequent radiometric dating of these ridges would allow a more accurate understanding of the timing of tectonic events and would help to learn more on the deposition environment of the Manyara Beds near Makuyuni. Andosols develop on stable positions, were tuffs are preserved from erosion. “Carbonate-rich sediments” most closely correspond to the LMBs, while “Calcaric topsoil” indicates initial soil development processes upon the LMBs or on soils influenced by translocated carbonates. At the stratigraphic border of the LMBs and UMBs, the thin outcrops of Hollywood and Red Brick tuffs were identified. “Silica-rich topsoil” results from quartz sand and grit enrichment on the soil surface by denudation processes. The respective soils developed on the Proterozoic intermediate basement of the Masai Plateau in the southern part of the study area. Quartzite hills of the basement crop out close to Makuyuni and within the Manyara Beds. In conclusion, the topsoils are controlled by the quartzite and intermediate gneisses of the Precambrian basement, by the Younger Extrusives, the lacustrine sediments and

in stable positions also by tuffs with a high $CaCO_3$ content. Those $CaCO_3$ rich tuffs, resulting from carbonatite volcanism, are probably one of the main sources of the $CaCO_3$ in the geosystem of the basin.

The Lake Manyara underwent various transgression and regression phases during the Quaternary. The paleo-shorelines, which can be found in the east of the present Lake Manyara, are younger than the Manyara Beds. Casanova & Hillaire-Marcel [1992] conducted radiometric dating of stromatolites on a distinct elevation 20 m above the present-day lake. They found an uncertain maximum age of 140 ky (Fig. 6). The fluctuation of the paleo-lake, as well as its' maximum elevation is controversially debated in various studies [Keller *et al.* 1975, Holdship 1976, Casanova 1986, Barker 1990, Casanova & Hillaire-Marcel 1992, Somi 1993]. The delineation of the paleo-shorelines with SAR intensity images and an edge detector is proposed in P4. Several stromatolite samples were collected from various distinct paleo-shoreline levels. The radiometric dating of these samples may resolve parts of the discussion. Unfortunately, while this thesis is compiled the dating of the samples is still ongoing. The paleo-shoreline or paleo-lake terrace with the highest elevation, which was identified in the analysis, holds approximately the same elevation than the lowest possible outlet of the Lake Manyara basin (Fig. 14). This specific paleo-terrace has the same shape than other terraces, but the dominating material consists of mafic blocks from the Essimingor volcano. Nevertheless, several stromatolites were found on two independent locations on the same level of the former shoreline. It is possible, that the carbonate material was weathered and the morphologic harder stromatolites had sustained. This would imply a high age for this paleo-lake level. The outlet leads to the shallow Engaruka basin, which is adjacent to the Natron-Magadi basin. All identified paleo-shoreline levels seem tectonically undisturbed, since the linear features continue consistently, except of disturbances by fluvial systems. The height levels on both sides of the fluvial incisions are the same. The same fact was observed by Somi [1993]. For the time and the area of the paleo-shoreline development, it can be assumed that no major tectonic events had disturbed the geomorphological features.

Information from remote sensing data can serve as input dataset for different specific geomorphological analyses. The capabilities of optical and microwave remote sensing supplement various analyses with wide-area data coverage, which is especially important in remote areas. This thesis confronted limitations as a consequence of remote sensing data and techniques, which should be made evident at this point. General challenges of this sort include limitations set by the spatial and spectral resolution of available sensors. Though the study area is located in a semiarid environment, vegetation cover complicates and partly prevents the spectral analyses of mineral composition and lithologies. That any spectral remote sensing analysis results predominantly in information of the earths' surfaces presents an additional limitation. Microwave data can deliver subsurface information, provided that particular conditions of the substrate, the viewing geometry of the sensor and the wavelength are fulfilled [Al-Bilbisi *et al.* 2004]. Furthermore, remote sensing is not capable of substituting field work [Church 2013]. For an understanding of landforms and processes, ground reference information is necessary for the calibration and validation of the remote sensing analyses

CHAPTER 5 - CONCLUSIONS

This thesis deciphers various aspects of the paleo-landscape in the Lake Manyara basin. It shows that remote sensing is a valuable technology, which can contribute to the assessment of landscape development. The application of SAR data and various optical sensors with high spatial and/or spectral resolution allowed for a detailed analysis of present-day and paleo-landscape features. Surface substrates, lithologies and lacustrine sediments were identified with spectral information, SAR backscatter and topographical information. Paleo-shorelines were competently mapped and it could be proven, that the paleo-Lake Manyara had overspilled into the Engaruka and almost certain into the Natron-Magadi basin as well. Remote sensing data and analyses contributed to the understanding of the tectonic development, the distribution and interpretation of geomorphologic forms and the assessment of gully and soil erosion. The proposed research was able to solve specific questions, which may contribute to the paleo-environmental reconstruction of hominin habitats. At the same time new questions have emerged, which shall be solved through future research. At present, the author desires to express clearly that remote sensing based techniques comprise merely one methodological approach among various others. Remote sensing provides area-wide information, which is not possible through field work, and provides extensive information going beyond the perception of the human eye. Thereby remote sensing enables detecting interrelations between objects on the earth's surface. Nevertheless, a holistic research design for paleo-landscape and/or paleo-environmental reconstruction will continually rely on the cooperation between different research disciplines, including geology, field based geomorphology, hydrology, climatology, archaeology, paleontology, and techniques like laboratory analyses of sediment samples, radiometric dating and the digital modelling of various spatial processes, to provide a non-conclusive list of selected disciplines.

Further research will focus on different methodological and thematically topics. Based on the obtained results further field campaigns have been planned. The radiometric dating of stromatolites has to be continued to reveal the timing of the paleo-lake level fluctuations. To assess the timing of tectonic events, mafic extrusions and tuff layer must be dated. The analysis shows the abundance of lacustrine sediments east of the Makuyuni area. Those sediments have to be validated in more detail. Coring could potentially reveal their depth and the time needed for deposition. A central question should be whether all paleo-lake sediments belonged to the paleo-Lake Manyara, or if parallel/cascading lake systems existed. Another important feature, which has not been sufficiently investigated yet, is the paleo-drainage system. The valley morphology indicates a stream capture of the Makuyuni River system of the Tarangire River system. Together with the assessment of the tectonic development, this may give more insight into the paleo-hydrological system and thereby allows better paleo-climate modelling. Furthermore, the interrelations with the neighbouring basins, especially the Engaruka and Natron-Magadi basins should be investigated in more detail.

We live in a stimulating time concerning capabilities of earth observation. The European Sentinel 1 & 2 missions provide, respectively will provide, SAR C-band and optical data with a high coverage and temporal resolution [Berger & Aschbacher 2012, Drusch *et al.* 2012, Torres *et al.* 2012, Agapiou *et al.* 2014]. Landsat 8 OLI contributes to the consistent Landsat mission [Knight & Kvaran 2014]. With WorldView-3 a commercial high-resolution satellite, with eight spectral bands in the VNIR and eight spectral bands in the SWIR regions, provides new possibilities for mineral mapping since 2015 [Kruse & Perry 2013]. Future satellite missions will provide great opportunities for these research questions as well as for others. The TerraSAR-L mission will penetrate the vegetation cover and will give more information on the surface of wooded and bushed areas [Eineder *et al.* 2014]. Hyperspectral missions will allow more precise mineral mapping and the possibilities to distinguish between more mineral compositions, and with a higher level of detail. The announced systems are EnMap [Guanter *et al.* 2015], PRISMA [Stefano *et al.* 2013] and HyspIRI [Abrams & Hook 2013].

REFERENCES

1 Abell, P. I., Awramik, S. M., Osborne, R. H. & Tomellini, S., 1982 - *Plio-pleistocene lacustrine stromatolites from lake Turkana, Kenya: Morphology, stratigraphy and stable isotopes*. Sedimentary Geology, Vol: 32 (1–2): 1-26.

2 Abrams, M. J. & Hook, S. J., 2013 - *NASA's Hyperspectral Infrared Imager (HyspIRI)*. - In: Thermal Infrared Remote Sensing, Kuenzer, C. & Dech, S. (Eds.); Springer Netherlands: Vol. 17: 117-130.

3 AbuBakr, M., Ghoneim, E., El-Baz, F., Zeneldin, M. & Zeid, S., 2013 - *Use of radar data to unveil the paleolakes and the ancestral course of Wadi El-Arish, Sinai Peninsula, Egypt*. Geomorphology, Vol: 194 (0): 34-45.

4 Agapiou, A., Alexakis, D., Sarris, A. & Hadjimitsis, D., 2014 - *Evaluating the Potentials of Sentinel-2 for Archaeological Perspective*. Remote Sensing, Vol: 6 (3): 2176-2194.

5 Al-Bilbisi, H., Tateishi, R. & Tetuko, J., 2004 - *A technique to estimate topsoil thickness in arid and semi-arid areas of north-eastern Jordan using synthetic aperture radar data*. International Journal of Remote Sensing, Vol: 25 (19): 3873-3882.

6 Albaric, J., Déverchère, J., Petit, C., Perrot, J. & Le Gall, B., 2009 - *Crustal rheology and depth distribution of earthquakes: Insights from the central and southern East African Rift System*. Tectonophysics, Vol: 468 (1–4): 28-41.

7 Albertz, J., 2009 - *Einführung in die Fernerkundung : Grundlagen der Interpretation von Luft- und Satellitenbildern*. 4, Wiss. Buchges., Darmstadt.

8 Alexakis, D., Sarris, A., Astaras, T. & Albanakis, K., 2011 - *Integrated GIS, remote sensing and geomorphologic approaches for the reconstruction of the landscape habitation of Thessaly during the neolithic period*. Journal of Archaeological Science, Vol: 38 (1): 89-100.

9 Altaweel, M., 2005 - *The use of ASTER satellite imagery in archaeological contexts*. Archaeological Prospection, Vol: 12 (3): 151-166.

10 Anderson, K. & Croft, H., 2009 - *Remote sensing of soil surface properties*. Progress in Physical Geography, Vol: 33 (4): 457-473.

11 Aubert, M., Baghdadi, N., Zribi, M., Douaoui, A., Loumagne, C., Baup, F., El Hajj, M. & Garrigues, S., 2011 - *Analysis of TerraSAR-X data sensitivity to bare soil moisture, roughness, composition and soil crust*. Remote Sensing of Environment, Vol: 115 (8): 1801-1810.

12 Bachofer, F., Quénéhervé, G., Hochschild, V. & Maerker, M., 2015a - *Multisensoral Topsoil Mapping in the Semiarid Lake Manyara Region, Northern Tanzania*. Remote Sensing, Vol: 7 (8): 9563-9586.

13 Bachofer, F., Quénéhervé, G. & Märker, M., 2014 - *The Delineation of Paleo-Shorelines in the Lake Manyara Basin Using TerraSAR-X Data*. Remote Sensing, Vol: 6 (3): 2195-2212.

14 Bachofer, F., Quénéhervé, G., Märker, M. & Hochschild, V., 2015b - *Comparison of SVM and Boosted Regression Trees for the Delineation of Lacustrine Sediments using Multispectral*

ASTER Data and Topographic Indices in the Lake Manyara Basin. Photogrammetrie, Fernerkundung, Geoinformation (PFG), Vol: 1 / 2015: 81-94.

15 Bagdasaryan, G., Gerasimovskiy, V., Polyakov, A., Gukasyan, R. & Vernadskiy, V., 1973 - *Age of volcanic rocks in the rift zones of East Africa*. Geochemistry International, Vol: 10: 66-71.

16 Bailey, G. N., Reynolds, S. C. & King, G. C., 2011 - *Landscapes of human evolution: models and methods of tectonic geomorphology and the reconstruction of hominin landscapes*. Journal of Human Evolution, Vol: 60 (3): 257-80.

17 Barker, P. A., 1990 - *Diatoms as palaeolimnological indicators: A reconstruction of Late Quaternary environments in two East African salt lakes.* Loughborough University of Technology, Dissertation, 267 pp.

18 Barker, P. A., 1992 - *Differential diatom dissolution in Late Quaternary sediments from Lake Manyara, Tanzania: an experimental approach*. Journal of Paleolimnology, Vol: 7 (3): 235-251.

19 Barker, P. A. & Gasse, F., 2003 - *New evidence for a reduced water balance in East Africa during the Last Glacial Maximum: implication for model-data comparison*. Quaternary Science Reviews, Vol: 22 (8–9): 823-837.

20 Barker, P. A., Talbot, M. R., Street-Perrott, F. A., Marret, F., Scourse, J. & Odada, E. O., 2004 - *Late Quaternary climatic variability in intertropical Africa.* - In: Past Climate Variability through Europe and Africa, Battarbee, R. W. et al. (Eds.); Kluwer Academic Publishers: 117-138.

21 Barr, W. A., in press - *Paleoenvironments of the Shungura Formation (Plio-Pleistocene: Ethiopia) based on ecomorphology of the bovid astragalus*. Journal of Human Evolution, Vol: xxx (2015): 1-11.

22 Baumann, O., 1894 - *Die kartographischen Ergebnisse der Massai-Expedition des Deutschen Antisklaverei-Comités*. Ergänzungsheft No. II zu "Petermanns Mitteilungen", Gotha : Perthes, 56 pp.

23 Beloussov, V. V., Geraimovsky, V. I., Polyakov, A. I. & SSSR, A. a. n., 1974 - *Vostochno-Afrikanskaya Riftovaya Sistema (The East African Rift System)*. Nauka (in Russian), Moscow, UDSSR.

24 Berger, M. & Aschbacher, J., 2012 - *Preface: The Sentinel missions—new opportunities for science*. Remote Sensing of Environment, Vol: 120: 1-2.

25 Berger, W. H. & Jansen, E., 2013 - *Mid-Pleistocene Climate Shift - The Nansen Connection.* - In: The Polar Oceans and Their Role in Shaping the Global Environment, Johannessen, O. M. et al. (Eds.); American Geophysical Union: Washington, D. C., USA, 295-311.

26 Bergner, A. G. N., Strecker, M. R., Trauth, M. H., Deino, A., Gasse, F., Blisniuk, P. & Dühnforth, M., 2009 - *Tectonic and climatic control on evolution of rift lakes in the Central Kenya Rift, East Africa*. Quaternary Science Reviews, Vol: 28 (25–26): 2804-2816.

27 Bergner, A. G. N. & Trauth, M. H., 2004 - *Comparison of the hydrological and hydrochemical evolution of Lake Naivasha (Kenya) during three highstands between 175 and 60 kyr BP*. Palaeogeography, Palaeoclimatology, Palaeoecology, Vol: 215 (1–2): 17-36.

28 Berking, J., 2011 - *Geoarchaeology in Drylands - Paleaoenvironmental Reconstructions in the Vicinity of Naga, Central Sudan. Physische Geographie, FB Geowissenschaften,* Freie Universität Berlin, Dissertation, 54 pp.

29 Berking, J., Beckers, B. & Schütt, B., 2010 - *Runoff in two semi-arid watersheds in a geoarcheological context: A case study of Naga, Sudan, and Resafa, Syria*. Geoarchaeology, Vol: 25 (6): 815-836.

30 Berking, J., Meister, J., Ullrich, B., Schott, M., Kaufmann, G. & Schütt, B., 2011 - *Geoarchaeological Methods for Landscape Reconstruction at the Excavation Site of Naga, Central Sudan*. Die Erde - Contributions to Geoarchaeology, Vol: 3: 289-313.

31 Berking, J. & Schütt, B., 2011a - *Geoarchaeology and Chronostratigraphy in the Vicinity of Meroitic Naga in Northern Sudan — A Review*. eTopoi - Journal for Ancient Studies, Vol: 1: 23-43.

32 Berking, J. & Schütt, B., 2011b - *Late Quaternary Morphodynamics in the Area of the Meroitic Settlement of Naga, Central Sudan*. Zeitschrift für Geomorphologie, Vol: 55 Suppl. 3: 1-24.

33 Bierwirth, P., 2002 - *Evaluation of ASTER Satellite Data for Geological Applications*. Consultancy Report to Geoscience Australia, 50 pp.

34 Bishop, W. W. & Pickford, M. H. L., 1975 - *Geology, fauna and palaeoenvironments of the Ngorora Formation, Kenya Rift Valley*. Nature, Vol: 254 (5497): 185-192.

35 Blaauw, M., van Geel, B., Kristen, I., Plessen, B., Lyaruu, A., Engstrom, D. R., van der Plicht, J. & Verschuren, D., 2011 - *High-resolution 14C dating of a 25,000-year lake-sediment record from equatorial East Africa*. Quaternary Science Reviews, Vol: 30 (21–22): 3043-3059.

36 Blumenschine, R. J., 1986 - *Early hominid scavenging opportunities : implications of carcass availability in the Serengeti and Ngorongoro ecosystems*. B.A.R., Oxford.

37 Branton, N., 2009 - *Landscape Approaches in Historical Archaeology: The Archaeology of Places.* - In: International Handbook of Historical Archaeology, Gaimster, D. & Majewski, T. (Eds.); Springer New York: 51-65.

38 Breeze, P. S., Drake, N. A., Groucutt, H. S., Parton, A., Jennings, R. P., White, T. S., Clark-Balzan, L., Shipton, C., Scerri, E. M. L., Stimpson, C. M., Crassard, R., Hilbert, Y., Alsharekh, A., Al-Omari, A. & Petraglia, M. D., in press - *Remote sensing and GIS techniques for reconstructing Arabian palaeohydrology and identifying archaeological sites*. Quaternary International, Vol: xxx (2015): 1-22.

39 Brown, F., Harris, J., Leakey, R. & Walker, A., 1985 - *Early Homo erectus skeleton from west Lake Turkana, Kenya*. Nature, Vol: 316 (6031): 788-792.

40 Brunet, M., Guy, F., Pilbeam, D., Mackaye, H. T., Likius, A., Ahounta, D., Beauvilain, A., Blondel, C., Bocherens, H., Boisserie, J.-R., De Bonis, L., Coppens, Y., Dejax, J., Denys, C., Duringer, P., Eisenmann, V., Fanone, G., Fronty, P., Geraads, D., Lehmann, T., Lihoreau, F., Louchart, A., Mahamat, A., Merceron, G., Mouchelin, G., Otero, O., Campomanes, P. P., De Leon, M. P., Rage, J.-C., Sapanet, M., Schuster, M., Sudre, J., Tassy, P., Valentin, X., Vignaud, P., Viriot, L., Zazzo, A. & Zollikofer, C., 2002 - *A new hominid from the Upper Miocene of Chad, Central Africa*. Nature, Vol: 418 (6894): 145-151.

41 Butzer, K. W., 1980 - *The Holocene Lake Plain of North Rudolph, East Africa*. Physical Geography, Vol: 1 (1): 42-58.

42 Butzer, K. W., Isaac, G. L., Richardson, J. L. & Washbourn-Kamau, C., 1972 - *Radiocarbon Dating of East African Lake Levels*. Science, Vol: 175 (4026): 1069-1076.

43 Büyüksalih, G. & Jacobsen, K., 2006 - *Generation and Validation of Digital Elevation Models based on Satellite Images*. IntArchPhRS. Band XXXVI WG I/5, 6, Paris, France.

44 Camberlin, P., Janicot, S. & Poccard, I., 2001 - *Seasonality and atmospheric dynamics of the teleconnection between African rainfall and tropical sea-surface temperature: Atlantic vs. ENSO*. International Journal of Climatology, Vol: 21 (8): 973-1005.

45 Campana, S., Dabas, M., Marasco, L., Piro, S. & Zamuner, D., 2009 - *Integration of remote sensing, geophysical surveys and archaeological excavation for the study of a medieval mound (Tuscany, Italy)*. Archaeological Prospection, Vol: 16 (3): 167-176.

46 Canny, J., 1986 - *A Computational Approach to Edge Detection*. Pattern Analysis and Machine Intelligence, IEEE Transactions on, Vol: PAMI-8 (6): 679-698.

47 Carabajal, C. C. & Harding, D. J., 2005 - *ICESat validation of SRTM C-band digital elevation models*. Geophysical Research Letters, Vol: 32 (10.1029/2005GL023957): 5.

48 Casanova, J., 1986 - *Les stromatolites continentaux : paléoécologie, paléohydrologie, paléoclimatologie. Application au Rift Gregory,. Faculte des sciences de Liminy,* Université Aix-Marseille - II, Dissertation, 256 pp.

49 Casanova, J. & Hillaire-Marcel, C., 1992 - *Chronology and paleohydrology of late Quaternary high lake levels in the Manyara basin (Tanzania) from isotopic data (18O, 13C, 14C, ThU) on fossil stromatolites*. Quaternary Research, Vol: 38 (2): 205-226.

50 Casanova, J., Hillaire-Marcel, C., Page, N., Taieb, M. & Vincens, A., 1988 - *Palaeohydrology and Late Quaternary stratigraphy of lacustrine deposits in the Suguta rift, Kenya*. Comptes Rendus - Academie des Sciencess, Serie II, Vol: 307 (10): 1251-1258.

51 Chang, C.-C. & Lin, C.-J., 2011 - *LIBSVM: A library for support vector machines*. ACM Transactions on Intelligent Systems and Technology, Vol: 2 (3): 1-27.

52 Chen, A., Darbon, J. & Morel, J.-M., 2014a - *Landscape evolution models: A review of their fundamental equations*. Geomorphology, Vol: 219: 68-86.

53 Chen, F., Masini, N., Yang, R., Milillo, P., Feng, D. & Lasaponara, R., 2014b - *A Space View of Radar Archaeological Marks: First Applications of COSMO-SkyMed X-Band Data*. Remote Sensing, Vol: 7 (1): 24-50.

54 Chorowicz, J., 2005 - *The East African rift system*. Journal of African Earth Sciences, Vol: 43 (1–3): 379-410.

55 Church, M., 2013 - *Refocusing geomorphology: Field work in four acts*. Geomorphology, Vol: 200: 184-192.

56 Cigna, F., Tapete, D., Lasaponara, R. & Masini, N., 2013 - *Amplitude Change Detection with ENVISAT ASAR to Image the Cultural Landscape of the Nasca Region, Peru*. Archaeological Prospection, Vol: 20 (2): 117-131.

57 Ciminale, M., Gallo, D., Lasaponara, R. & Masini, N., 2009 - *A multiscale approach for reconstructing archaeological landscapes: Applications in Northern Apulia (Italy)*. Archaeological Prospection, Vol: 16 (3): 143-153.

58 Cohen, A. S., 2003 - *Paleolimnology*. Oxford University Press, Oxford [i.a.].

59 Congalton, R. G. & Green, K., 2009 - *Assessing the accuracy of remotely sensed data : principles and practices*. 2. ed., CRC Press, Boca Raton, Fla. [i.a.].

60 Cornelissen, E., Boven, A., Dabi, A., Hus, J., Yong, K. J., Keppens, E., Langohr, R., Moeyersons, J., Pasteels, P., Pieters, M., Uytterschaut, H., Van Noten, F. & Workineh, H., 1990 - *The Kapthurin Formation revisited*. African Archaeological Review, Vol: 8 (1): 23-75.

61 Cudahy, T., 2012 - *Satellite ASTER Geoscience Product - Notes for Australia*. CSIRO, 26 pp.

62 Dabbagh, A. E., Al-Hinai, K. G. & Asif Khan, M., 1997 - *Detection of sand-covered geologic features in the Arabian Peninsula using SIR-C/X-SAR data*. Remote Sensing of Environment, Vol: 59 (2): 375-382.

63 Danese, M., Masini, N., Biscione, M. & Lasaponara, R., 2014 - *Predictive modeling for preventive Archaeology: overview and case study*. Open Geosciences, Vol: 6 (1): 42.

64 Dart, R. A., 1925 - *Australopithecus africanus The Man-Ape of South Africa*. Nature, Vol: 115: 195-199.

65 Dawson, J. B., 1992 - *Neogene tectonics and volcanicity in the North Tanzania sector of the Gregory Rift Valley: contrasts with the Kenya sector*. Tectonophysics, Vol: 204 (1–2): 81-92.

66 Dawson, J. B., 1997 - *Neogene; recent rifting and volcanism in northern Tanzania; relevance for comparisons between the Gardar Province and the East African Rift valley*. Mineralogical Magazine, Vol: 61 (4): 543-548.

67 Dawson, J. B., 2008 - *The Gregory rift valley and Neogene-recent volcanoes of northern Tanzania*. Geological Society, London.

68 Dawson, J. B., 2012 - *Nephelinite–melilitite–carbonatite relationships: Evidence from Pleistocene–recent volcanism in northern Tanzania*. Lithos, Vol: 152: 3-10.

69 De Laet, V., Paulissen, E. & Waelkens, M., 2007 - *Methods for the extraction of archaeological features from very high-resolution Ikonos-2 remote sensing imagery, Hisar (southwest Turkey)*. Journal of Archaeological Science, Vol: 34 (5): 830-841.

70 De Laet, V., van Loon, G., Van der Perre, A., Deliever, I. & Willems, H., 2015 - *Integrated remote sensing investigations of ancient quarries and road systems in the Greater Dayr al-Barshā Region, Middle Egypt: a study of logistics*. Journal of Archaeological Science, Vol: 55: 286-300.

71 De Pauw, E., 1984 - *Soils, Physiography and Agro-Ecological Zones of Tanzania*. Crop Monitoring and Early Warning Systems Project, FAO. GCPS/URT/047/NET., Ministry of Agriculture, Dar es Salaam.

72 deMenocal, P. B., 1995 - *Plio-Pleistocene African Climate*. Science, Vol: 270 (5233): 53-59.

73 Deng, Y. X., 2007 - *New trends in digital terrain analysis: landform definition, representation, and classification*. Progress in Physical Geography, Vol: 31 (4): 405-419.

74 Deus, D. & Gloaguen, R., 2013 - *Remote Sensing Analysis of Lake Dynamics in Semi-Arid Regions: Implication for Water Resource Management. Lake Manyara, East African Rift, Northern Tanzania*. Water, Vol: 5 (2): 698-727.

75 Deus, D., Gloaguen, R. & Krause, P., 2013 - *Water Balance Modeling in a Semi-Arid Environment with Limited in situ Data Using Remote Sensing in Lake Manyara, East African Rift, Tanzania*. Remote Sensing, Vol: 5 (4): 1651-1680.

76 Dewitte, O., Jones, A., Elbelrhiti, H., Horion, S. & Montanarella, L., 2012 - *Satellite remote sensing for soil mapping in Africa: An overview*. Progress in Physical Geography, Vol: 36 (4): 514-538.

77 Dierking, W., 1999 - *Quantitative roughness characterization of geological surfaces and implications for radar signature analysis*. Geoscience and Remote Sensing, IEEE Transactions on, Vol: 37 (5): 2397-2412.

78 DigitalGlobe, 2013 - *WorldView-2*. Accessed: 20.01.2015. Available from: https://www.digitalglobe.com/sites/default/files/DG_WorldView2_DS_PROD.pdf

79 Dikau, R., 1988 - *Entwurf einer geomorphographisch-analytischen Systematik von Reliefeinheiten*. Heidelberger Geographische Bausteine Heidelberger Geographische Bausteine Heidelberg, Germany, pp.

80 Dixit, P. C., 1984 - *Pleistocene lacustrine ridged oncolites from the Lake Manyara area, Tanzania, East Africa*. Sedimentary Geology, Vol: 39: 53-62.

81 DLR, 2014 - *DLR SRTM Digital Elevation Models / SRTM-X Specifications*. DLR. Accessed: 03.04.2015. Available from: https://centaurus.caf.dlr.de:8443/eoweb-ng/licenseAgreements/DLR_SRTM_Readme.pdf

82 Dore, N., Patruno, J., Pottier, E. & Crespi, M., 2013 - *New Research in Polarimetric SAR Technique for Archaeological Purposes using ALOS PALSAR Data*. Archaeological Prospection, Vol: 20 (2): 79-87.

83 Drusch, M., Del Bello, U., Carlier, S., Colin, O., Fernandez, V., Gascon, F., Hoersch, B., Isola, C., Laberinti, P., Martimort, P., Meygret, A., Spoto, F., Sy, O., Marchese, F. & Bargellini, P., 2012 - *Sentinel-2: ESA's Optical High-Resolution Mission for GMES Operational Services*. Remote Sensing of Environment, Vol: 120: 25-36.

84 Dühnforth, M., Bergner, A. N. & Trauth, M., 2006 - *Early Holocene water budget of the Nakuru-Elmenteita basin, Central Kenya Rift*. Journal of Paleolimnology, Vol: 36 (3): 281-294.

85 Dupraz, C. & Visscher, P. T., 2005 - *Microbial lithification in marine stromatolites and hypersaline mats*. Trends in Microbiology, Vol: 13 (9): 429-438.

86 Ebinger, C., Djomani, Y. P., Mbede, E., Foster, A. & Dawson, J. B., 1997 - *Rifting Archaean lithosphere: the Eyasi-Manyara-Natron rifts, East Africa*. Journal of the Geological Society, Vol: 154 (6): 947-960.

87 Eineder, M., Hajnsek, I., Krieger, G., Moreira, A. & Papathanassiou, K., 2014 - *Tandem-L - Satellite Mission Proposal for Monitoring Dynamic Processes on the Earth's Surface*. Satellite SAR Systems, German Aerospace Center, Oberpfaffenhofen, Germany, 28 pp.

88 Elith, J., Graham, C. H., Anderson, R. P., Dudík, M., Ferrier, S., Guisan, A., Hijmans, R. J., Huettmann, F., Leathwick, J. R., Lehmann, A., Li, J., Lohmann, L. G., Loiselle, B. A., Manion, G., Moritz, C., Nakamura, M., Nakazawa, Y., Overton, J. M. M., Townsend Peterson, A., Phillips, S. J., Richardson, K., Scachetti-Pereira, R., Schapire, R. E., Soberón, J., Williams, S., Wisz, M. S. & Zimmermann, N. E., 2006 - *Novel methods improve prediction of species' distributions from occurrence data*. Ecography, Vol: 29 (2): 129-151.

89 Elmahdy, S. I., 2012 - *Hydromorphological Mapping and Analysis for Characterizing Darfur Paleolake, NW Sudan Using Remote Sensing and GIS*. International Journal of Geosciences, Vol: 2012 (3): 25-36.

90 Esch, T., Himmler, V., Schorcht, G., Thiel, M., Wehrmann, T., Bachofer, F., Conrad, C., Schmidt, M. & Dech, S., 2009 - *Large-area assessment of impervious surface based on integrated analysis of single-date Landsat-7 images and geospatial vector data*. Remote Sensing of Environment, Vol: 113 (8): 1678-1690.

91 Espa, G., Benedetti, R., De Meo, A., Ricci, U. & Espa, S., 2006 - *GIS based models and estimation methods for the probability of archaeological site location*. Journal of Cultural Heritage, Vol: 7 (3): 147-155.

92 Eugster, H. P., 1967 - *Hydrous Sodium Silicates from Lake Magadi, Kenya: Precursors of Bedded Chert*. Science, Vol: 157 (3793): 1177-1180.

93 Evans, A. L., Fairhead, J. D. & Mitchell, J. G., 1971 - *Potassium—Argon Ages from the Volcanic Province of Northern Tanzania*. Nature, Vol: 229: 19-20.

94 Evernden, J. F., Curtis, G. H., Bishop, W., Brace, C. L., Clark, J. D., Damon, P. E., Hay, R. L., Hopkins, D. M., Howell, F. C., Knopf, A., Kretzoi, M., Leakey, L. S. B., Maude, H. E., Richards, J. R., Savage, D. E. & Wright, H. E., Jr., 1965 - *The Potassium-Argon Dating of Late Cenozoic Rocks in East Africa and Italy [and Comments and Reply]*. Current Anthropology, Vol: 6 (4): 342-385.

95 Fairhead, J. D., Mitchell, J. G. & Williams, L. A., 1972 - *New K/Ar Determinations on Rift Volcanics of S. Kenya and their Bearing on Age of Rift Faulting*. nature physical science, Vol: 238: 66-69.

96 Farr, T. G. & Kobrick, M., 2000 - *Shuttle radar topography mission produces a wealth of data*. Eos, Transactions American Geophysical Union, Vol: 81 (48): 583-585.

97 Farr, T. G., Rosen, P. A., Caro, E., Crippen, R., Duren, R., Hensley, S., Kobrick, M., Paller, M., Rodriguez, E., Roth, L., Seal, D., Shaffer, S., Shimada, J., Umland, J., Werner, M., Oskin, M., Burbank, D. & Alsdorf, D., 2007 - *The Shuttle Radar Topography Mission - Technique and Applications*. Reviews of Geophysics, Vol: 45 (2, RG2004): 1-33.

98 Flores-Prieto, E., Quénéhervé, G., Bachofer, F., Shahzad, F. & Maerker, M., in press - *Morphotectonic Interpretation of the Makuyuni Catchment in Northern Tanzania using DEM and SAR data*. Geomorphology, Vol: xxx (2015): 1-46.

99 Foerster, V., Junginger, A., Langkamp, O., Gebru, T., Asrat, A., Umer, M., Lamb, H. F., Wennrich, V., Rethemeyer, J., Nowaczyk, N., Trauth, M. H. & Schaebitz, F., 2012 - *Climatic change recorded in the sediments of the Chew Bahir basin, southern Ethiopia, during the last 45,000 years*. Quaternary International, Vol: 274: 25-37.

100 Foody, G. M. & Mathur, A., 2004 - *A relative evaluation of multiclass image classification by support vector machines*. Geoscience and Remote Sensing, IEEE Transactions on, Vol: 42 (6): 1335-1343.

101 Foster, A., Ebinger, C., Mbede, E. & Rex, D., 1997 - *Tectonic development of the northern Tanzanian sector of the East African Rift System*. Journal of the Geological Society, Vol: 154 (4): 689-700.

102 Freund, Y. & Schapire, R. E., 1996 - *Experiments with a New Boosting Algorithm*. Machine Learning: Proceedings of the Thirteenth International Conference, 148-156, Bari, Italy.

103 Frost, S. R., Schwartz, H. L., Giemsch, L., Morgan, L. E., Renne, P. R., Wildgoose, M., Saanane, C., Schrenk, F. & Harvati, K., 2012 - *Refined age estimates and Paleoanthropological investigation of the Manyara Beds, Tanzania*. Journal of Anthropological Sciences, Vol: 90: 151-161.

104 Fujisada, H., 1995 - *Design and performance of ASTER instrument*. Proceedings of SPIE: Advanced and Next-Generation Satellites, 2583: 16-25, Paris, France.

105 Gaber, A., Ghoneim, E., Khalaf, F. & El-Baz, F., 2009a - *Delineation of paleolakes in the Sinai Peninsula, Egypt, using remote sensing and GIS*. Journal of Arid Environments, Vol: 73 (1): 127-134.

106 Gaber, A., Koch, M. & El-Baz, F., 2009b - *Textural and Compositional Characterization of Wadi Feiran Deposits, Sinai Peninsula, Egypt, Using Radarsat-1, PALSAR, SRTM and ETM+ Data*. Remote Sensing, Vol: 2 (1): 52-75.

107 Gaber, A., Koch, M., Griesh, M. H., Sato, M. & El-Baz, F., 2013 - *Near-surface imaging of a buried foundation in the Western Desert, Egypt, using space-borne and ground penetrating radar*. Journal of Archaeological Science, Vol: 40 (4): 1946-1955.

108 Gaber, A., Soliman, F., Koch, M. & El-Baz, F., 2015 - *Using full-polarimetric SAR data to characterize the surface sediments in desert areas: A case study in El-Gallaba Plain, Egypt*. Remote Sensing of Environment, Vol: 162: 11-28.

109 Gallo, D., Ciminale, M., Becker, H. & Masini, N., 2009 - *Remote sensing techniques for reconstructing a vast Neolithic settlement in Southern Italy*. Journal of Archaeological Science, Vol: 36 (1): 43-50.

110 Garcin, Y., Junginger, A., Melnick, D., Olago, D. O., Strecker, M. R. & Trauth, M. H., 2009 - *Late Pleistocene–Holocene rise and collapse of Lake Suguta, northern Kenya Rift*. Quaternary Science Reviews, Vol: 28 (9–10): 911-925.

111 Gasse, F., 2000 - *Hydrological changes in the African tropics since the Last Glacial Maximum*. Quaternary Science Reviews, Vol: 19 (1–5): 189-211.

112 Gasse, F., Chalié, F., Vincens, A., Williams, M. A. J. & Williamson, D., 2008 - *Climatic patterns in equatorial and southern Africa from 30,000 to 10,000 years ago reconstructed from terrestrial and near-shore proxy data*. Quaternary Science Reviews, Vol: 27 (25–26): 2316-2340.

113 Gessner, U., Machwitz, M., Conrad, C. & Dech, S., 2013 - *Estimating the fractional cover of growth forms and bare surface in savannas. A multi-resolution approach based on regression tree ensembles*. Remote Sensing of Environment, Vol: 129 (0): 90-102.

114 Gharibreza, M., in press - *Evolutionary trend of paleoshorelines in the Coastal Makran zone (Southeast Iran) since the mid-Holocene*. Quaternary International, Vol: xxx (2015): 1-10.

115 Ghilardi, M. & Desruelles, S., 2008 - *Geoarchaeology: where human, social and earth sciences meet with technology*. S.A.P.I.EN.S, Vol: 1 (2): 1-9.

116 Ghoneim, E., Benedetti, M. & El-Baz, F., 2012 - *An integrated remote sensing and GIS analysis of the Kufrah Paleoriver, Eastern Sahara*. Geomorphology, Vol: 139–140 (0): 242-257.

117 Ghoneim, E. & El-Baz, F., 2007 - *The application of radar topographic data to mapping of a mega-paleodrainage in the Eastern Sahara*. Journal of Arid Environments, Vol: 69 (4): 658-675.

118 Giemsch, L., 2015 - *Makuyuni; Fundstellen des Acheuléen am Lake Manyara, Tansania. Ein Beitrag zur Erforschung der mittelpleistozänen Kultur in Ostafrika*. Verlag Marie Leidorf GmbH, Rahden, Germany.

119 Goetz, C., 1990 - *Traçage isotopique et chronologie des processus d'altération et de sédimentation par l'étude des déséquilibres U & Th: application aux systèmes lacustres de Magadi (Kenya) et Manyara (Tanzanie)*. Universite Aix-Marseille II, Dissertation, 217 pp.

120 Grommé, C. S., Reilly, T. A., Mussett, A. E. & Hay, R. L., 1971 - *Palaeomagnetism and Potassium-Argon Ages of Volcanic Rocks of Ngorongoro Caldera, Tanzania1*. Geophysical Journal of the Royal Astronomical Society, Vol: 22 (1): 101-115.

121 Guanter, L., Kaufmann, H., Segl, K., Foerster, S., Rogass, C., Chabrillat, S., Kuester, T., Hollstein, A., Rossner, G., Chlebek, C., Straif, C., Fischer, S., Schrader, S., Storch, T., Heiden, U., Mueller, A., Bachmann, M., Mühle, H., Müller, R., Habermeyer, M., Ohndorf, A., Hill, J., Buddenbaum, H., Hostert, P., van der Linden, S., Leitão, P., Rabe, A., Doerffer, R., Krasemann, H., Xi, H., Mauser, W., Hank, T., Locherer, M., Rast, M., Staenz, K. & Sang, B., 2015 - *The EnMAP Spaceborne Imaging Spectroscopy Mission for Earth Observation*. Remote Sensing, Vol: 7 (7): 8830-8857.

122 Hanssen, R., 2001 - *Radar interferometry*. Kluwer Academic Publishers, Dordrecht [i.a.].

123 Haug, G. H. & Strecker, M. R., 1995 - *Volcano-tectonic evolution of the Chyulu Hills and implications for the regional stress field in Kenya*. Geology, Vol: 23 (2): 165-168.

124 Haug, G. H. & Tiedemann, R., 1998 - *Effect of the formation of the Isthmus of Panama on Atlantic Ocean thermohaline circulation*. Nature, Vol: 393 (6686): 673-676.

125 Hay, R., 1968 - *Chert and its sodium-silicate precursors in sodium-carbonate lakes of East Africa*. Contributions to Mineralogy and Petrology, Vol: 17 (4): 255-274.

126 Hay, R. L., 1976 - *Geology of the Olduvai Gorge : a study of sedimentation in a semiarid basin*. University of California Press, Berkeley.

127 Hession, S. L. & Moore, N., 2011 - *A spatial regression analysis of the influence of topography on monthly rainfall in East Africa*. International Journal of Climatology, Vol: 31 (10): 1440-1456.

128 Hewson, R. D. & Cudahy, T. J., 2011 - *Issues Affecting Geological Mapping with ASTER Data: A Case Study of the Mt Fitton Area, South Australia.* - In: Land Remote Sensing and Global

Environmental Change, Ramachandran, B. et al. (Eds.); Springer New York: Vol. 11: 273-300.

129 Hewson, R. D., Cudahy, T. J. & Huntington, J. F., 2001 - *Geologic and alteration mapping at Mt Fitton, South Australia, using ASTER satellite-borne data.* Geoscience and Remote Sensing Symposium, 2001. IGARSS '01. IEEE 2001 International, 2, 724-726,

130 Hewson, R. D., Cudahy, T. J., Mizuhiko, S., Ueda, K. & Mauger, A. J., 2005 - *Seamless geological map generation using ASTER in the Broken Hill-Curnamona province of Australia*. Remote Sensing of Environment, Vol: 99 (1–2): 159-172.

131 Hill, A., Curtis, G. & Drake, R., 1986 - *Sedimentary stratigraphy of the Tugen Hills, Baringo, Kenya*. Geological Society, London, Special Publications, Vol: 25 (1): 285-295.

132 Hillaire-Marcel, C., Carro, O. & Casanova, J., 1986 - *14C and ThU dating of Pleistocene and Holocene stromatolites from East African paleolakes*. Quaternary Research, Vol: 25 (3): 312-329.

133 Hirano, A., Welch, R. & Lang, H., 2003 - *Mapping from ASTER stereo image data: DEM validation and accuracy assessment*. ISPRS Journal of Photogrammetry and Remote Sensing, Vol: 57 (5-6): 356-370.

134 Holcomb, D. W. & Shingiray, I. L., 2007 - *Imaging Radar in Archaeological Investigations - An Image Processing perspective*. Wiseman, J. R. & El-Baz, F. (Eds.) Remote Sensing in Archaeology. Springer New York.

135 Holdship, S. A., 1976 - *The paleolimnology of Lake Manyara, Tanzania : a diatom analysis of a 56 meter sediment core: a diatom analysis of a 56 meter sediment core.* Duke University, Dissertation, 133 pp.

136 Hritz, C., 2014 - *Contributions of GIS and Satellite-based Remote Sensing to Landscape Archaeology in the Middle East*. Journal of Archaeological Research, Vol: 22 (3): 229-276.

137 Huffman, G. J., Adler, R. F., Bolvin, D. T., Gu, G. J., Nelkin, E. J., Bowman, K. P., Hong, Y., Stocker, E. F. & Wolff, D. B., 2007 - *The TRMM multisatellite precipitation analysis (TMPA): Quasi-global, multiyear, combined-sensor precipitation estimates at fine scales*. Journal of Hydrometeorology, Vol: 8 (1): 38-55.

138 Irving, E., 2005 - *The role of latitude in mobilism debates*. Proc Natl Acad Sci U S A, Vol: 102 (6): 1821-8.

139 Isaacs, G. L. & Curtis, G. H., 1974 - *Age of early Acheulian industries from the Peninj Group, Tanzania*. Nature, Vol: 249 (5458): 624-627.

140 Jacobsen, K., 2003 - *DEM generation from satellite data*. Remote Sensing in Transition, Proceedings of the 23rd EARSeL Symposium 2003, 513–525, Ghent, Belgium.

141 Jacobsen, K., 2010 - *Vergleich von ASTER GDEM- mit SRTM-Höhenmodellen*. Konferenzband der Dreiländertagung von DGPF, OVG und SGPBF, 19: 581-588, Vienna, Austria.

142 Jaeger, F., 1913 - *Das Hochland der Riesenkrater und die umliegenden Hochländer Deutsch-Ostafrikas ; 2 Länderkundliche Beschreibung*. Mittler, Berlin.

143 Jaynes, E. T., 1957 - *Information Theory and Statistical Mechanics*. Physical Review, Vol: 106 (4): 620-630.

144 Jensen, J. R., 2007 - *Remote sensing of the environment : an earth resource perspective*. 2nd, Pearson Prentice Hall, Upper Saddle River, NJ.

145 Johanson, D. C. & Edey, M. A., 1981 - *Lucy, the beginnings of humankind*. Simon and Schuster, New York.

146 Johnson, J. K., 2006 - *Remote sensing in archaeology : an explicitly North American perspective*. University of Alabama Press, Tuscaloosa.

147 Junginger, A., Roller, S., Olaka, L. A. & Trauth, M. H., 2014 - *The effects of solar irradiation changes on the migration of the Congo Air Boundary and water levels of paleo-Lake Suguta, Northern Kenya Rift, during the African Humid Period (15–5ka BP)*. Palaeogeography, Palaeoclimatology, Palaeoecology, Vol: 396: 1-16.

148 Kaiser, T., Bromage, T. G. & Schrenk, F., 1995 - *Hominid Corridor Research Project update: New Pliocene fossil localities at Lake Manyara and putative oldest Early Stone Age occurrences at Laetoli (Upper Ndolanya Beds), northern Tanzania*. Journal of Human Evolution, Vol: 28 (1): 117-120.

149 Kaiser, T. M., Seiffert, C., Hertler, C., Fiedler, L., Schwartz, H. L., Frost, S. R., Giemsch, L., Bernor, R. L., Wolf, D., Semprebon, G., Nelson, S. V., Schrenk, F., Harvati, K., Bromage, T. G. & Saanane, C., 2010 - *Makuyuni, a new Lower Palaeolithic Hominid Site in Tanzania*. Mitteilungen Hamburgisches Zoologisches Museum und Institut, Vol: 106: 69-110.

150 Kalinowski, A. & Oliver, S., 2004 - *ASTER Mineral Index Processing Manual*. Remote Sensing Applications, Geoscience Australia 37 pp.

151 Kalkowsky, E., 1908 - *Oolith und Stromatolith im norddeutschen Buntsandstein*. Zeitschrift der Deutschen Geologischen Gesellschaft, Vol: 60: 68 - 125.

152 Keller, C. M., Hansen, C. & Alexander, C. S., 1975 - *Archaeology and Paleoenvironments in the Manyara and Engaruka Basins, Northern Tanzania*. Geographical Review, Vol: 65 (3): 364-376.

153 Kennedy, D., 2011 - *The "Works of the Old Men" in Arabia: remote sensing in interior Arabia*. Journal of Archaeological Science, Vol: 38 (12): 3185-3203.

154 Kent, P. E., 1941 - *The Recent History and Pleistocene Deposits of the Plateau North of Lake Eyasi, Tanganyika*. Geological Magazine, Vol: 78 (03): 173-184.

155 Kent, P. E., 1942 - *A Note on Pleistocene Deposits near Lake Manyara, Tanganyika*. Geological Magazine, Vol: 79 (01): 72-77.

156 Khan, S. D., Fathy, M. S. & Abdelazeem, M., 2014 - *Remote sensing and geophysical investigations of Moghra Lake in the Qattara Depression, Western Desert, Egypt*. Geomorphology, Vol: 207 (0): 10-22.

157 King, G. & Bailey, G., 2006 - *Tectonics and human evolution*. Antiquity, Vol: 80 (308): 265-286.

158 Kingston, J. D., Deino, A. L., Edgar, R. K. & Hill, A., 2007 - *Astronomically forced climate change in the Kenyan Rift Valley 2.7-2.55 Ma: implications for the evolution of early hominin ecosystems*. J Hum Evol, Vol: 53 (5): 487-503.

159 Kiunsi, R. B. & Meadows, M. E., 2006 - *Assessing land degradation in the Monduli District, northern Tanzania*. Land Degradation & Development, Vol: 17 (5): 509-525.

160 Knight, E. & Kvaran, G., 2014 - *Landsat-8 Operational Land Imager Design, Characterization and Performance*. Remote Sensing, Vol: 6 (11): 10286-10305.

161 Kohlschütter, E., 1907 - *Ergebnisse der Ostafrikanischen Pendel-Expedition der Königl. Gesellschaft der Wissenschaften zu Göttingen in den Jahren 1899 und 1900 : Verlauf und Ausrüstung der Expedition. Höhenmessungen*. Weidmann, Berlin.

162 Kosov, B. F., Nikol'skaya, I. I. & Zorina, Y., 1987 - *Eksperimental'nyye issledovaniya ovragoobrazovaniya.* - In: Eksperimental'naya geomorfologiya, Makkaveev, N. I. (Eds.); Moscow University: Moscow (in Russian), Vol. 3: 113–140.

163 Kruse, F. & Perry, S., 2013 - *Mineral Mapping Using Simulated Worldview-3 Short-Wave-Infrared Imagery*. Remote Sensing, Vol: 5 (6): 2688-2703.

164 Ku, T. L., 2000 - *Uranium-series methods.* - In: Quaternary Geochronology: Methods and Applications, (Eds.); AGU: Washington, DC, Vol. 4: 101-114.

165 Kutzbach, J. E. & Street-Perrott, F. A., 1985 - *Milankovitch forcing of fluctuations in the level of tropical lakes from 18 to 0 kyr BP*. Nature, Vol: 317 (6033): 130-134.

166 Lasaponara, R. & Masini, N., 2011 - *Satellite remote sensing in archaeology: past, present and future perspectives*. Journal of Archaeological Science, Vol: 38 (9): 1995-2002.

167 Lasaponara, R. & Masini, N., 2012 - *Satellite Remote Sensing: A New Tool for Archaeology*. Remote Sensing and Digital Image Processing, 16, Springer, Netherlands.

168 Lasaponara, R. & Masini, N., 2013 - *Satellite Synthetic Aperture Radar in Archaeology and Cultural Landscape: An Overview*. Archaeological Prospection, Vol: 20 (2): 71-78.

169 Layton, R. & Ucko, P. J., 1999 - *Introduction: gazing on the landscape and encountering the environment.* - In: The Archaeology and Anthropology of Landscape: Shaping Your Landscape, Layton, R. & Ucko, P. J. (Eds.); Routledge: London/New York, 1-20.

170 Le Gall, B., Nonnotte, P., Rolet, J., Benoit, M., Guillou, H., Mousseau-Nonnotte, M., Albaric, J. & Deverchère, J., 2008 - *Rift propagation at craton margin.: Distribution of faulting and volcanism in the North Tanzanian Divergence (East Africa) during Neogene times*. Tectonophysics, Vol: 448 (1–4): 1-19.

171 Leakey, L. S., Tobias, P. V. & Napier, J. R., 1964 - *A New Species of the Genus Homo from Olduvai Gorge*. Nature, Vol: 202: 7-9.

172 Leakey, L. S. B., 1931 - *East African Lakes*. The Geographical Journal, Vol: 77 (6): 497-508.

173 Leakey, L. S. B., 1959 - *A New Fossil Skull From Olduvai*. Nature, Vol: 491: 184: 491.

174 Leakey, L. S. B., 1961 - *New Finds at Olduvai Gorge*. Nature, Vol: 189: 649-650.

175 Leakey, L. S. B., Tobias, P. V. & Leakey, M. D., 1965 - *Olduvai Gorge, 1951-1961*. University Press, Cambridge Eng.

176 Leakey, M. D. & Hay, R. L., 1979 - *Pliocene footprints in the Laetolil Beds at Laetoli, northern Tanzania*. Nature, Vol: 278 (5702): 317-323.

177 Leakey, M. D. & Roe, D. A., 1995 - *Olduvai Gorge. Volume 5: Excavations in Beds III, IV and the Masek Beds 1968–1971*. Cambridge University Press,

178 Leakey, R. E. F., 1973 - *Evidence for an Advanced Plio-Pleistocene Hominid from East Rudolf, Kenya*. Nature, Vol: 242 (5398): 447-450.

179 Levin, N. E., Zipser, E. J. & Cerling, T. E., 2009 - *Isotopic composition of waters from Ethiopia and Kenya: Insights into moisture sources for eastern Africa*. Journal of Geophysical Research, Vol: 114 (D23306): 1-13.

180 Li, Z., Zhu, Q. & Gold, C., 2005 - *Digital terrain modeling : principles and methodology*. CRC, Boca Raton, FL [i.a.].

181 Lillesand, T. M., Kiefer, R. W. & Chipman, J. W., 2015 - *Remote sensing and image interpretation*. 7, Wiley, New York.

182 Linck, R., Busche, T., Buckreuss, S., Fassbinder, J. W. E. & Seren, S., 2013 - *Possibilities of Archaeological Prospection by High-resolution X-band Satellite Radar – a Case Study from Syria*. Archaeological Prospection, Vol: 20 (2): 97-108.

183 LPDAAC, 2014 - *NASA Shuttle Radar Topography Mission (SRTM) Global 1 arc second Data Released over Africa.* Land Processes Distributed Active Archive Center. Accessed: 12.08.2015. Available from: https://lpdaac.usgs.gov/nasa_shuttle_radar_topography_mission_srtm_global_1_arc_second_data_released_over_africa

184 Macdonald, R., 2002 - *Magmatism of the Kenya Rift Valley: a review*. Earth and Environmental Science Transactions of the Royal Society of Edinburgh, Vol: 93 (03): 239-253.

185 Macheyeki, A. S., Delvaux, D., Batist, M. D. & Mruma, A., 2008 - *Fault kinematics and tectonic stress in the seismically active Manyara–Dodoma Rift segment in Central Tanzania – Implications for the East African Rift*. Journal of African Earth Sciences, Vol: 51 (4): 163-188.

186 Macintyre, R. M., Mitchell, J. G. & Dawson, J. B., 1974 - *Age of Fault Movements in Tanzanian Sector of East African Rift System*. Nature, Vol: 247 (5440): 354-356.

187 Maerker, M., Quénéhervé, G., Bachofer, F. & Mori, S., 2015 - *A simple DEM assessment procedure for gully system analysis in the Lake Manyara area, northern Tanzania*. Natural Hazards, Vol: 1-19.

188 Magori, C. C. & Day, M. H., 1983 - *Laetoli Hominid 18: an early Homo sapiens skull*. Journal of Human Evolution, Vol: 12 (8): 747-753.

189 Mallat, S. G., 1989 - *A theory for multiresolution signal decomposition: the wavelet representation*. Pattern Analysis and Machine Intelligence, IEEE Transactions on, Vol: 11 (7): 674-693.

190 Mana, S., Furman, T., Carr, M. J., Mollel, G. F., Mortlock, R. A., Feigenson, M. D., Turrin, B. D. & Swisher, C. C., 2012 - *Geochronology and geochemistry of the Essimingor volcano:*

Melting of metasomatized lithospheric mantle beneath the North Tanzanian Divergence zone (East African Rift). Lithos, Vol: 155: 310-325.

191 Manega, P. C., 1993 - *Geochronology, geochemistry and isotopic study of the Plio-Pleistocene hominid sites and the Ngorongoro Volcanic Highland in northern Tanzania.* University of Colorado, Dissertation, pp.

192 Märker, M., Bachofer, F., Quénéhervé, G., Hertler, C., Saanane, C., Giemsch, L. & Thiemayer, H., 2013 - *Modelling the Spatial Distribution of Archaeological Sites in the Makuyuni Region, Tanzania.* CAA'2010 Fusion of Cultures. Proceedings of the 38th Annual Conference on Computer Applications and Quantitative Methods in Archaeology, BAR International Series 2494, 523-529, Granada, Spain.

193 Mars, J. C. & Rowan, L. C., 2010 - *Spectral assessment of new ASTER SWIR surface reflectance data products for spectroscopic mapping of rocks and minerals*. Remote Sensing of Environment, Vol: 114 (9): 2011-2025.

194 Maslin, M. A., Brierley, C. M., Milner, A. M., Shultz, S., Trauth, M. H. & Wilson, K. E., 2014 - *East African climate pulses and early human evolution*. Quaternary Science Reviews, Vol: 101: 1-17.

195 Maslin, M. A. & Trauth, M. H., 2009 - *Plio-Pleistocene East African Pulsed Climate Variability and Its Influence on Early Human Evolution.* - In: The First Humans – Origin and Early Evolution of the Genus Homo, Grine, F. E. et al. (Eds.); Springer Netherlands: 151-158.

196 Mather, P. M. & Koch, M., 2011 - *Computer processing of remotely-sensed images : an introduction*. 4th, Wiley-Blackwell, Chichester, West Sussex, UK ; Hoboken, NJ.

197 Mehrer, M. W. & Wescott, K. L., 2006 - *GIS and archaeological site location modeling.* Taylor & Francis, Boca Raton [i.a.].

198 Melesse, A., Weng, Q., Thenkabail, P. & Senay, G., 2007 - *Remote Sensing Sensors and Applications in Environmental Resources Mapping and Modelling*. Sensors, Vol: 7 (12): 3209-3241.

199 Menze, B. H. & Ur, J. A., 2014 - *Multitemporal Fusion for the Detection of Static Spatial Patterns in Multispectral Satellite Images - With Application to Archaeological Survey*. IEEE - Journal of Selected Topics in Applied Earth Observations and Remote Sensing, Vol: 7 (8): 3513-3524.

200 Milankovic, M., 1941 - *Kanon der Erdbestrahlung und seine Anwendung auf das Eiszeitenproblem*. Mihaila Curcica, Belgrade.

201 Montufo, A. M., 1997 - *The use of satellite imagery and digital image processing in landscape archaeology. A case study from the island of Mallorca, Spain*. Geoarchaeology, Vol: 12 (1): 71-85.

202 Moore, I. D., Grayson, R. B. & Ladson, A. R., 1991 - *Digital terrain modelling: A review of hydrological, geomorphological, and biological applications*. Hydrological Processes, Vol: 5 (1): 3-30.

203 Moore, I. D., Grayson, R. B. & Ladson, A. R., 1997 - *Digital terrain modelling: A review of hydrological, geomorphological, and biological applications*. Soil Science Society of America Journal, Vol: 57: 443-452.

204 Mulder, V. L., de Bruin, S., Schaepman, M. E. & Mayr, T. R., 2011 - *The use of remote sensing in soil and terrain mapping - A review*. Geoderma, Vol: 162 (1–2): 1-19.

205 Mulibo, G. D. & Nyblade, A. A., 2010 - *The 1994-1995 Manyara and Kwamtoro Earthquake Swarms: Variation in the Depth Extent of Seismicity in Northern Tanzania*. South African Journal of Geology, Vol: 112 (3-4): 387-404.

206 Ngana, J. O., Mwalyosi, R. B. B., Madulu, N. F. & Yanda, P. Z., 2003 - *Development of an integrated water resources management plan for the Lake Manyara sub-basin, Northern Tanzania*. Physics and Chemistry of the Earth, Parts A/B/C, Vol: 28 (20–27): 1033-1038.

207 Niang, I., Ruppel, O. C., Abdrabo, M. A., Essel, A., Lennard, C., Padgham, J. & Urquhart, P., 2014 - *Africa.* - In: Climate Change 2014: Impacts, Adaptation, and Vulnerability. Part B: Regional Aspects. Contribution of Working Group II to the Fifth Assessment Report of the Intergovernmental Panel on Climate Change, Barros, V. R. et al. (Eds.); Cambridge University Press: Cambridge, United Kingdom and New York, NY, USA, 1199-1265.

208 Nicholson, S. E., 1996 - *A review of climate dynamics and climate variability in eastern Africa.* - In: The Limnology, Climatology and Paleoclimatology of the East African Lakes, Johnson, T. C. & Odada, E. O. (Eds.); Gordon and Breach: Amsterdam, Netherlands, 25-56.

209 Nicholson, S. E., 2015 - *Long-term variability of the East African 'short rains' and its links to large-scale factors*. International Journal of Climatology, Vol: 1-12.

210 Nicholson, S. E. & Kim, J., 1997 - *The Relationship of the El-Niño Southern Oscillation to African Rainfall*. International Journal of Climatology, Vol: 17 (2): 117-135.

211 Ninomiya, Y., Fu, B. & Cudahy, T. J., 2005 - *Detecting lithology with Advanced Spaceborne Thermal Emission and Reflection Radiometer (ASTER) multispectral thermal infrared "radiance-at-sensor" data*. Remote Sensing of Environment, Vol: 99 (1-2): 127-139.

212 Nyblade, A. A. & Brazier, R. A., 2002 - *Precambrian lithospheric controls on the development of the East African rift system*. Geology, Vol: 30 (8): 755-758.

213 Olaka, L. A., Odada, E. O., Trauth, M. H. & Olago, D. O., 2010 - *The sensitivity of East African rift lakes to climate fluctuations*. Journal of Paleolimnology, Vol: 44 (2): 629-644.

214 Owen, R. B. & Renaut, R. W., 1986 - *Sedimentology, stratigraphy and palaeoenvironments of the Holocene Galana Boi Formation, NE Lake Turkana, Kenya*. Geological Society, London, Special Publications, Vol: 25 (1): 311-322.

215 Paillou, P., Grandjean, G., Baghdadi, N., Heggy, E., August-Bernex, T. & Achache, J., 2003 - *Subsurface imaging in south-central Egypt using low-frequency radar: Bir Safsaf revisited.* Geoscience and Remote Sensing, IEEE Transactions on, Vol: 41 (7): 1672-1684.

216 Paillou, P., Schuster, M., Tooth, S., Farr, T., Rosenqvist, A., Lopez, S. & Malezieux, J.-M., 2009 - *Mapping of a major paleodrainage system in eastern Libya using orbital imaging radar: The Kufrah River*. Earth and Planetary Science Letters, Vol: 277 (3-4): 327-333.

217 Pal, M. & Foody, G. M., 2010 - *Feature Selection for Classification of Hyperspectral Data by SVM*. Geoscience and Remote Sensing, IEEE Transactions on, Vol: 48 (5): 2297-2307.

218 Parcak, S. H., 2009 - *Satellite Remote Sensing for Archaeology*. Routledge, London [i.a.].

219 Passini, R. & Jacobsen, K., 2007 - *High Resolution SRTM Height Models* ISPRS Workshop 2007 - High-Resolution Earth Imaging for Geospatial Information, XXXVI-1/W51: 7, Hannover, Germany.

220 Patruno, J., Dore, N., Crespi, M. & Pottier, E., 2013 - *Polarimetric Multifrequency and Multi-incidence SAR Sensors Analysis for Archaeological Purposes*. Archaeological Prospection, Vol: 20 (2): 89-96.

221 Phillips, S. J., Anderson, R. P. & Schapire, R. E., 2006 - *Maximum entropy modeling of species geographic distributions*. Ecological Modelling, Vol: 190 (3-4): 231-259.

222 Platt, N. H. & Wright, V. P., 2009 - *Lacustrine Carbonates: Facies Models, Facies Distributions and Hydrocarbon Aspects.* - In: Lacustrine Facies Analysis, (Eds.); Blackwell Publishing Ltd.: 57-74.

223 Potts, R., 1998 - *Environmental Hypotheses of Hominin Evolution.* - In: Yearbook of Physical Anthropology, (Eds.); Vol. 41: 93-136.

224 Potts, R., 2010 - *Early hominid activities at Olduvai*. Transaction Publishers, New Brunswick, N.J.

225 Pour, A. B. & Hashim, M., 2011 - *Application of advanced spaceborne thermal emission and reflection radiometer (ASTER) data in geological mapping*. International Journal of the Physical Sciences, Vol: 6 (33): 7657-7668.

226 Pour, A. B. & Hashim, M., 2014 - *ASTER, ALI and Hyperion sensors data for lithological mapping and ore minerals exploration*. SpringerPlus, Vol: 3 (130): 1-19.

227 Prasad, A. M., Iverson, L. R. & Liaw, A., 2006 - *Newer classification and regression tree techniques: Bagging and random forests for ecological prediction*. Ecosystems, Vol: 9 (2): 181-199.

228 Prendergast, M. E., Mabulla, A. Z. P., Grillo, K. M., Broderick, L. G., Seitsonen, O., Gidna, A. O. & Gifford-Gonzalez, D., 2013 - *Pastoral Neolithic sites on the southern Mbulu Plateau, Tanzania*. Azania: Archaeological Research in Africa, Vol: 48 (4): 498-520.

229 Prinz, T., Lasar, B. & Krüger, K. P., 2010 - *High-resolution remote sensing and GIS techniques for geobase data supporting archaeological surveys: A case study of ancient Doliche, southeast Turkey*. Geoarchaeology, Vol: 25 (3): 352-374.

230 Pryce, T. O. & Abrams, M. J., 2010 - *Direct detection of Southeast Asian smelting sites by ASTER remote sensing imagery: technical issues and future perspectives*. Journal of Archaeological Science, Vol: 37 (12): 3091-3098.

231 Quénéhervé, G., personal communication 15.05.2015 - *Personal communication on predictive modelling in the Manyara basin*. Tuebingen, Germany.

232 Rapp, G. R. & Hill, C. L., 2006 - *Geoarchaeology : the earth-science approach to archaeological interpretation*. 2nd, Yale University Press, New Haven.

233 Ravelo, A. C., Andreasen, D. H., Lyle, M., Olivarez Lyle, A. & Wara, M. W., 2004 - *Regional climate shifts caused by gradual global cooling in the Pliocene epoch*. Nature, Vol: 429 (6989): 263-267.

234 Reck, H., 1921 - *Eine neue diluviale Säugetierfundstelle am Minjonjo in Deutsch-Ostafrika*. Sitzungsberichte der Gesellschaft Naturforschender Freunde zu Berlin, Vol: 1-3: 25-36.

235 Reck, H., 1937 - *Wissenschaftliche Ergebnisse der Oldoway-Expedition 1913*. Leipzig, Bornträger.

236 Renaut, R. W. & Tiercelin, J.-J., 1994 - *Lake Bogoria, Kenya Rift Valley—a Sedimentological Overview*. - In: Society for Sedimentary Geology - Special Publication, Renaut, R. W. (Eds.); Vol. 50: 101-123.

237 Richards, J. A., 2009 - *Remote sensing with imaging radar*. Springer, Heidelberg; New York.

238 Richardson, J. L. & Dussinger, R. A., 1986 - *Paleolimnology of mid-elevation lakes in the Kenya Rift Valley*. Hydrobiologia, Vol: 143 (1): 167-174.

239 Riding, R., 2000 - *Microbial carbonates: the geological record of calcified bacterial–algal mats and biofilms*. Sedimentology, Vol: 47: 179-214.

240 Ring, U., 2014 - *The East African Rift System*. Austrian Journal of Earth Sciences, Vol: 107 (1): 132-146.

241 Ring, U., Schwartz, H. L., Bromage, T. G. & Sanaane, C., 2005 - *Kinematic and sedimentological evolution of the Manyara Rift in northern Tanzania, East Africa*. Geological Magazine, Vol: 142 (4): 355-368.

242 Robertson, E. C., Jeffrey D. Seibert, Fernandez, D. C. & Zender, M. U., 2006 - *Space and Spatial Analysis in Archaeology*. University of Calgary Press, Calgary, Canada.

243 Robinson, C. A., El-Baz, F., Al-Saud, T. S. M. & Jeon, S. B., 2006 - *Use of radar data to delineate palaeodrainage leading to the Kufra Oasis in the eastern Sahara*. Journal of African Earth Sciences, Vol: 44 (2): 229-240.

244 Rossignol-Strick, M., 1983 - *African monsoons, an immediate climate response to orbital insolation*. Nature, Vol: 304 (5921): 46-49.

245 Rowan, L. C. & Mars, J. C., 2003 - *Lithologic mapping in the Mountain Pass, California area using Advanced Spaceborne Thermal Emission and Reflection Radiometer (ASTER) data*. Remote Sensing of Environment, Vol: 84 (3): 350-366.

246 Rowan, L. C., Mars, J. C. & Simpson, C. J., 2005 - *Lithologic mapping of the Mordor, NT, Australia ultramafic complex by using the Advanced Spaceborne Thermal Emission and Reflection Radiometer (ASTER)*. Remote Sensing of Environment, Vol: 99 (1-2): 105-126.

247 Ruddiman, W. F. & Kutzbach, J. E., 1989 - *Forcing of late Cenozoic northern hemisphere climate by plateau uplift in southern Asia and the American west*. Journal of Geophysical Research: Atmospheres, Vol: 94 (D15): 18409-18427.

248 Ruddiman, W. F., Raymo, M. E., Martinson, D. G., Clement, B. M. & Backman, J., 1989 - *Pleistocene evolution: Northern hemisphere ice sheets and North Atlantic Ocean*. Paleoceanography, Vol: 4 (4): 353-412.

249 Sabins, F. F., 2000 - *Remote sensing : principles and interpretation*. 3. ed., 3. print., Freeman, New York.

250 San, B. T. & Süzen, M. L., 2005 - *Digital elevation model (DEM) generation and accuracy assessment from ASTER stereo data*. International Journal of Remote Sensing, Vol: 26 (22): 5013-5027.

251 Schaber, G. G., McCauley, J. F. & Breed, C. S., 1997 - *The use of multifrequency and polarimetric SIR-C/X-SAR data in geologic studies of Bir Safsaf, Egypt*. Remote Sensing of Environment, Vol: 59 (2): 337-363.

252 Schlüter, T., 1987 - *Paleoenvironment of lacustrine phosphate deposits at Minjingu, northern Tanzania, as indicated by their fossil record.* - In: Current Research in African Earth Sciences, Matheis, G. & Schandelmeier, H. (Eds.); Berlin, 223-226.

253 Schlüter, T., 1993 - *Geological Development and Economic Significance of Lacustrine Phosphate Deposits in Northern Tanzania*. Documenta Naturae, Vol: 77: 73 - 79.

254 Schlüter, T., 1994 - *Lake Manyara basin, Tanzania*. Gierlowski-Kordesch, E. & Kelts, K. (Eds.) Global Geological Record of Lake Basins. Camebridge University Press.

255 Schlüter, T. & Kohring, R., 2002 - *Palaeopathological Fish Bones from Phosphorites of the Lake Manyara Area, Northern Tanzania – Fossil Evidence of a Physiological Response to Survival in an Extreme Biocenosis*. Environmental Geochemistry and Health, Vol: 24 (2): 131-140.

256 Schlüter, T., Kohring, R. & Mehl, J., 1992 - *Hyperostotic fish bones ("Tilly bones") from presumably Pliocene phosphorites of the Lake Manyara area, northern Tanzania*. Paläontologische Zeitschrift, Vol: 66 (1-2): 129-136.

257 Schmaltz, E., Märker, M., Rosner, H.-J. & Kandel, A. W., 2014 - *The integration of landscape processes in archaeological site prediction in the Mugello basin (Tuscany/Italy)*. 21st century Archaeology - Proceedings of the 42nd Annual Conference on Computer Applications and Quantitative Methods in Archaeology (CAA), 451-458, Paris, France.

258 Schmid, T., Koch, M., DiBlasi, M. & Hagos, M., 2008 - *Spatial and spectral analysis of soil surface properties for an archaeological area in Aksum, Ethiopia, applying high and medium resolution data*. Catena, Vol: 75 (1): 93-101.

259 Schneider, T., Bischoff, T. & Haug, G. H., 2014 - *Migrations and dynamics of the intertropical convergence zone*. Nature, Vol: 513 (7516): 45-53.

260 Schrenk, F., Bromage, T. G., Betzler, C. G., Ring, U. & Juwayeyi, Y. M., 1993 - *Oldest Homo and Pliocene biogeography of the Malawi Rift*. Nature, Vol: 365 (6449): 833-836.

261 Schwartz, H., Renne, P. R., Morgan, L. E., Wildgoose, M. M., Lippert, P. C., Frost, S. R., Harvati, K., Schrenk, F. & Saanane, C., 2012 - *Geochronology of the Manyara Beds, northern Tanzania: New tephrostratigraphy, magnetostratigraphy and 40Ar/39Ar ages*. Quaternary Geochronology, Vol: 7 (0): 48-66.

262 Seitsonen, O., 2006a - *Archaeological Research in the Northern Lake Manyara Basin, Tanzania, 2003-2004*. Azania: Journal of the British Institute in Eastern Africa, Vol: 41: 41-67.

263 Seitsonen, O., 2006b - *Archaeology and shoreline displacement in the Lake Manyara Basin*. Department of Archaeology, University of Helsinki, Finland, 4 pp.

264 Sepulchre, P., Ramstein, G., Fluteau, F., Schuster, M., Tiercelin, J.-J. & Brunet, M., 2006 - *Tectonic Uplift and Eastern Africa Aridification*. Science, Vol: 313 (5792): 1419-1423.

265 Sharp, R. P., 1982 - *Landscape evolution (A Review)*. Proceedings of the National Academy of Sciences of the United States of America, Vol: 79 (14): 4477-4486.

266 Siart, C., Eitel, B. & Panagiotopoulos, D., 2008 - *Investigation of past archaeological landscapes using remote sensing and GIS: a multi-method case study from Mount Ida, Crete*. Journal of Archaeological Science, Vol: 35 (11): 2918-2926.

267 SIC, 2015 - *WorldView-3 Satellite Sensor (0.31m)*. Satellite Imaging Corporation. Accessed: 06.09.2015. Available from: http://www.satimagingcorp.com/satellite-sensors/worldview-3/

268 Sidorchuk, A., 1999 - *Dynamic and static models of gully erosion*. Catena, Vol: 37 (3–4): 401-414.

269 Slater, J. A., Garvey, G., Johnston, C., Haase, J., Heady, B., Kroenung, G. & Little, J., 2006 - *The SRTM data 'finishing' process and products*. Photogrammetric Engineering & Remote Sensing, Vol: 72 (3): 237-247.

270 Smith, G. E., 1924 - *The evolution of man*. Oxford University Press, London, UK.

271 Somi, E. J., 1993 - *Paleoenvironmental Changes in Central and Coastal Tanzania During the Upper Cenozoic: Magnetostratigraphy, Sedimentary Records and Shorelevel Changes. Department of Geology and Geochemistry,* Paleogeophysics & Geodynamics, Department of Geology and Geochemistry , University of Stockholm, Dissertation, 100 pp.

272 Stefano, P., Angelo, P., Simone, P., Filomena, R., Federico, S., Tiziana, S., Umberto, A., Vincenzo, C., Acito, N., Marco, D., Stefania, M., Giovanni, C., Raffaele, C., Roberto, D. B., Giovanni, L. & Cristina, A., 2013 - *The PRISMA hyperspectral mission: Science activities and opportunities for agriculture and land monitoring*. Geoscience and Remote Sensing Symposium (IGARSS), 2013 IEEE International, 4558-4561, Melbourne, Australia.

273 Stern, R. J. & Abdelsalam, M. G., 1996 - *The origin of the great bend of the Nile from SIR-C/X-SAR imagery*. Science, Vol: 274 (5293): 1696-1698.

274 Stewart, C., Lasaponara, R. & Schiavon, G., 2013 - *ALOS PALSAR Analysis of the Archaeological Site of Pelusium*. Archaeological Prospection, Vol: 20 (2): 109-116.

275 Stewart, C., Lasaponara, R. & Schiavon, G., 2014 - *Multi-frequency, polarimetric SAR analysis for archaeological prospection*. International Journal of Applied Earth Observation and Geoinformation, Vol: 28: 211-219.

276 Street-Perrott, F. A. & Haarison, S. P., 1985 - *Lake level fluctuations.* - In: Paleoclimate analysis and modeling, Hecht, A. D. (Eds.); Wiley: New York, USA, 1-80.

277 Street, F. A., 1980 - *The relative importance of climate and local hydrogeological factors in influencing lake-level fluctuations.* - In: Palaeoecology of Africa, Coetzee, J. a. K. & Bakker, E. M. V. Z. (Eds.); CRC Press: Vol. 12: 137-158.

278 Street, F. A. & Grove, A. T., 1979 - *Global maps of lake-level fluctuations since 30,000 yr B.P.* Quaternary Research, Vol: 12 (1): 83-118.

279 Tachikawa, T., Hato, M., Kaku, M. & Iwasaki, A., 2011 - *Characteristics of ASTER GDEM version 2.* Geoscience and Remote Sensing Symposium (IGARSS), 2011 IEEE International, 3657-3660, Vancouver, Canada.

280 Tapete, D., Cigna, F., Masini, N. & Lasaponara, R., 2013 - *Prospection and Monitoring of the Archaeological Heritage of Nasca, Peru, with ENVISAT ASAR.* Archaeological Prospection, Vol: 20 (2): 133-147.

281 Thomson, K. S., 1966 - *Quaternary fish fossils from west of Lake Rudolf, Kenya*. Breviora, Vol: 243: 1-10.

282 Tiedemann, R., Sarnthein, M. & Shackleton, N. J., 1994 - *Astronomic timescale for the Pliocene Atlantic δ18O and dust flux records of Ocean Drilling Program Site 659.* Paleoceanography, Vol: 9 (4): 619-638.

283 Tiercelin, J. J., Renaut, R. W., Delibrias, G., Fournier, J. L. & Bieda, S., 1981 - *Late Pleistocene and Holocene lake level fluctuations in the Lake Bogoria basin, northern Kenya Rift Valley.* - In: Paleoecology of Africa, Coetzee, J. A. & Bakker, E. M. V. Z. (Eds.); Balkema: Rotterdam, Netherlands, Vol. 13: 105-120.

284 Tierney, J. E., Smerdon, J. E., Anchukaitis, K. J. & Seager, R., 2013 - *Multidecadal variability in East African hydroclimate controlled by the Indian Ocean.* Nature, Vol: 493 (7432): 389-392.

285 Torres, R., Snoeij, P., Geudtner, D., Bibby, D., Davidson, M., Attema, E., Potin, P., Rommen, B., Floury, N., Brown, M., Traver, I. N., Deghaye, P., Duesmann, B., Rosich, B., Miranda, N., Bruno, C., L'Abbate, M., Croci, R., Pietropaolo, A., Huchler, M. & Rostan, F., 2012 - *GMES Sentinel-1 mission*. Remote Sensing of Environment, Vol: 120: 9-24.

286 Trauth, M. H., Bergner, A. G., Foerster, V., Junginger, A., Maslin, M. A. & Schaebitz, F., 2015 - *Episodes of environmental stability versus instability in Late Cenozoic lake records of Eastern Africa*. J Hum Evol, Vol:

287 Trauth, M. H., Deino, A. L., Bergner, A. G. N. & Strecker, M. R., 2003 - *East African climate change and orbital forcing during the last 175 kyr BP*. Earth and Planetary Science Letters, Vol: 206 (3–4): 297-313.

288 Trauth, M. H., Larrasoaña, J. C. & Mudelsee, M., 2009 - *Trends, rhythms and events in Plio-Pleistocene African climate*. Quaternary Science Reviews, Vol: 28 (5-6): 399-411.

289 Trauth, M. H., Maslin, M. A., Deino, A. & Strecker, M. R., 2005 - *Late Cenozoic Moisture History of East Africa.* Science, Vol: 309 (5743): 2051-2053.

290 Trauth, M. H., Maslin, M. A., Deino, A. L., Junginger, A., Lesoloyia, M., Odada, E. O., Olago, D. O., Olaka, L. A., Strecker, M. R. & Tiedemann, R., 2010 - *Human evolution in a variable environment: the amplifier lakes of Eastern Africa*. Quaternary Science Reviews, Vol: 29 (23–24): 2981-2988.

291 Trauth, M. H., Maslin, M. A., Deino, A. L., Strecker, M. R., Bergner, A. G. N. & Dühnforth, M., 2007 - *High- and low-latitude forcing of Plio-Pleistocene East African climate and human evolution*. Journal of Human Evolution, Vol: 53 (5): 475-486.

292 Trier, Ø. D., Larsen, S. Ø. & Solberg, R., 2009 - *Automatic detection of circular structures in high-resolution satellite images of agricultural land*. Archaeological Prospection, Vol: 16 (1): 1-15.

293 Tucker, G. E. & Hancock, G. R., 2010 - *Modelling landscape evolution*. Earth Surface Processes and Landforms, Vol: 35 (1): 28-50.

294 Uhlig, C., 1909 - *Die Ostafrikanische Bruchstufe und die angrenzenden Gebiete zwischen den Seen Magad und Lawa ja Mweri sowie dem Westfuß des Meru*. Mittler, Leipzig.

295 Vaidyanadhan, R., Dixit, P. C. & Schlüter, T., 1993 - *Geomorphology and Sedimentology of Lake Manyara environs, Tanzania, East Africa*. Documenta Naturae, Vol: 77: 41-62.

296 van der Meer, F. D., van der Werff, H. M. A., van Ruitenbeek, F. J. A., Hecker, C. A., Bakker, W. H., Noomen, M. F., van der Meijde, M., Carranza, E. J. M., Smeth, J. B. d. & Woldai, T., 2012 - *Multi- and hyperspectral geologic remote sensing: A review*. International Journal of Applied Earth Observation and Geoinformation, Vol: 14 (1): 112-128.

297 Vapnik, V. N., 1995 - *The nature of statistical learning theory*. Springer, New York.

298 Vapnik, V. N., 1998 - *Statistical learning theory*. Wiley, New York.

299 Verschuren, D., Laird, K. R. & Cumming, B. F., 2000 - *Rainfall and drought in equatorial east Africa during the past 1,100 years*. Nature, Vol: 403 (6768): 410-414.

300 Verstraeten, G., 2013 - *The Relation between Archaeology and Geography in Studying Past Human-environment Interactions: Is Interdisciplinary Geoarchaeology the Answer?* - In: Exempli Gratia - Sagalassos, Marc Waelkens and Interdisciplinary Archaeology, Poblome, J. (Eds.); Leuven University Press: Leuven, Belgium, 71-80.

301 Vicente, L. E. & de Souza Filho, C. R., 2011 - *Identification of mineral components in tropical soils using reflectance spectroscopy and advanced spaceborne thermal emission and reflection radiometer (ASTER) data*. Remote Sensing of Environment, Vol: 115 (8): 1824-1836.

302 Villmoare, B., Kimbel, W. H., Seyoum, C., Campisano, C. J., DiMaggio, E. N., Rowan, J., Braun, D. R., Arrowsmith, J. R. & Reed, K. E., 2015 - *Early Homo at 2.8 Ma from Ledi-Geraru, Afar, Ethiopia*. Science, Vol: 347 (6228): 1352-1355.

303 Vincens, A., 1986 - *Diagramme pollinique d'un sondage Pleistocene superieur—Holocene du Lac Bogoria (Kenya)*. Review of Palaeobotany and Palynology, Vol: 47 (1–2): 169-192.

304 Vincens, A., Casanova, J. & Tiercelin, J. J., 1986 - *Palaeolimnology of Lake Bogoria (Kenya) during the 4500 BP high lacustrine phase*. Geological Society, London, Special Publications, Vol: 25 (1): 323-330.

305 Vincens, A., Chalié, F., Bonnefille, R., Guiot, J. & Tiercelin, J.-J., 1993 - *Pollen-Derived Rainfall and Temperature Estimates from Lake Tanganyika and Their Implication for Late Pleistocene Water Levels*. Quaternary Research, Vol: 40 (3): 343-350.

306 Vining, B. R. & Wiseman, J., 2006 - *Multispectral and synthetic aperture radar remote-sensing-based models for holocene coastline development in the Ambracian Gulf, Epirus, Greece*. Archaeological Prospection, Vol: 13 (4): 258-268.

307 Vogel, S. & Märker, M., 2010 - *Reconstructing the Roman topography and environmental features of the Sarno River Plain (Italy) before the AD 79 eruption of Somma–Vesuvius*. Geomorphology, Vol: 115 (1-2): 67-77.

308 Vogel, S., Märker, M., Rellini, I., Hoelzmann, P., Wulf, S., Robinson, M., Steinhübel, L., Di Maio, G., Imperatore, C., Kastenmeier, P., Liebmann, L., Esposito, D. & Seiler, F., in press - *From a stratigraphic sequence to a landscape evolution model: Late Pleistocene and Holocene volcanism, soil formation and land use in the shade of Mount Vesuvius (Italy)*. Quaternary International, Vol: xxx (2015): 1-25.

309 Vondra, C. F., Johnson, G. D., Bowen, B. E. & Behrensmeyer, A. K., 1971 - *Preliminary Stratigraphical Studies of the East Rudolf Basin, Kenya*. Nature, Vol: 231 (5300): 245-248.

310 Vrba, E. S., 1980 - *Evolution, species and fossils: How does life evolve?* South African Journal of Science, Vol: 76 (2): 61-84.

311 Washbourn, C. K., 1967 - *Lake Levels and Quaternary Climates in the Eastern Rift Valley of Kenya*. Nature, Vol: 216 (5116): 672-673.

312 Waters, M. R., 1992 - *Principles of geoarchaeology : a North American perspective*. University of Arizona Press, Tucson.

313 Werther, C. W., 1898 - *Die mittleren Hochländer des nördlichen Deutsch-Ost-Afrika : wissenschaftliche Ergebnisse der Irangi-Expedition 1896 - 1897 nebst kurzer Reisebeschreibung*. Paetel, Berlin.

314 White, T. D., Suwa, G. & Asfaw, B., 1994 - *Australopithecus ramidus, a new species of early hominid from Aramis, Ethiopia*. Nature, Vol: 371 (6495): 306-312.

315 Wilkinson, P., Mitchell, J. G., Cattermole, P. J. & Downie, C., 1986 - *Volcanic chronology of the Men–Kilimanjaro region, Northern Tanzania*. Journal of the Geological Society, Vol: 143 (4): 601-605.

316 Wilson, J. P., 2012 - *Digital terrain modeling*. Geomorphology, Vol: 137 (1): 107-121.

317 Wiseman, J. & El-Baz, F., 2007 - *Remote sensing in archaeology*. Springer, New York.

318 Wolf, D., Nelson, S. V., Schwartz, H. L., Semprebon, G. M., Kaiser, T. M. & Bernor, R. L., 2010 - *Taxonomy and paleoecology of the Pleistocene Equidae from Makuyuni, Northern Tanzania*. Palaeodiversity, Vol: 3: 249–269.

319 Wood, B. & Lonergan, N., 2008 - *The hominin fossil record: taxa, grades and clades*. Journal of Anatomy, Vol: 212 (4): 354-376.

320 Yamaguchi, Y., Kahle, A. B., Tsu, H., Kawakami, T. & Pniel, M., 1998 - *Overview of Advanced Spaceborne Thermal Emission and Reflection Radiometer (ASTER)*. Geoscience and Remote Sensing, IEEE Transactions on, Vol: 36 (4): 1062-1071.

321 Zevenbergen, L. W. & Thorne, C. R., 1987 - *Quantitative analysis of land surface topography*. Earth Surface Processes and Landforms, Vol: 12 (1): 47-56.

322 Zhang, X. & Pazner, M., 2007 - *Comparison of Lithologic Mapping with ASTER, Hyperion, and ETM Data in the Southeastern Chocolate Mountains, USA*. Photogrammetric Engineering and Remote Sensing, Vol: 73 (5): 555-561.

323 Zhou, Q., Lees, B. & Tang, G., 2008 - *Advances in digital terrain analysis*. Lecture notes in geoinformation and cartography, Springer, New York.

324 Zhu, J., Zou, H., Rosset, S. & Hastie, T., 2009 - *Multi-class AdaBoost*. Statistics and its Interface, Vol: 2: 349–360.

325 Zribi, M., Kotti, F., Lili-Chabaane, Z., Baghdadi, N., Ben Issa, N., Amri, R., Duchemin, B. & Chehbouni, A., 2012 - *Soil Texture Estimation Over a Semiarid Area Using TerraSAR-X Radar Data*. Geoscience and Remote Sensing Letters, IEEE, Vol: 9 (3): 353-357.

326 Zwally, H. J., Schutz, B., Abdalati, W., Abshire, J., Bentley, C., Brenner, A., Bufton, J., Dezio, J., Hancock, D., Harding, D., Herring, T., Minster, B., Quinn, K., Palm, S., Spinhirne, J. & Thomas, R., 2002 - *ICESat's laser measurements of polar ice, atmosphere, ocean, and land*. Journal of Geodynamics, Vol: 34 (3–4): 405-445.

APPENDIX I: PUBLICATION P1

Morphotectonic Interpretation of the Makuyuni Catchment in Northern Tanzania using DEM and SAR data.

Flores-Prieto, E., Quénéhervé, G., Bachofer, F., Shahzad, F. & Maerker, M., 2015 - *Morphotectonic Interpretation of the Makuyuni Catchment in Northern Tanzania using DEM and SAR data.* Geomorphology, Vol: 248: 427-439. (doi: 10.1016/j.geomorph.2015.07.049).

This research paper is available online at Elsevier (www.journals.elsevier.com/geomorphology):

http://www.sciencedirect.com/science/article/pii/S0169555X15301136

Paper History

The publication was developed on the basis of joint field work and the Master of Science Thesis of Elio Flores-Prieto "Morphotectonic interpretation of the Quaternary evolution of the Lake Manyara Basin using DEM and radar data analyses: a case study in the East African rift system, Tanzania" at the University of Tübingen in 2014. Michael Märker supervised this thesis. Data of the thesis was re-analysed and re-interpreted for the publication.

Journal: Geomorphology
ISSN: 0169-555X
Thomson Reuters Impact Factor 2014: 2.785
Type: Research Article.

Geomorphology 248 (2015) 427–439

Contents lists available at ScienceDirect

Geomorphology

journal homepage: www.elsevier.com/locate/geomorph

Morphotectonic interpretation of the Makuyuni catchment in Northern Tanzania using DEM and SAR data

Elio Flores-Prieto [a], Geraldine Quénéhervé [a], Felix Bachofer [a], Faisal Shahzad [b], Michael Maerker [c,d,*]

[a] Department of Geosciences, Institute of Geography, University of Tübingen, Rümelinstraße 19-23, 72070 Tübingen, Germany
[b] LiDAR Research and Development, Zoller and Froehlich GmbH, Simoniousstraße 22, 88299 Wangen im Allgaeu, Germany
[c] Heidelberg Academy of Sciences and Humanities, c/o Institute of Geography, University of Tübingen, Rümelinstraße 19-23, 72070 Tübingen, Germany
[d] Department of Earth Sciences, University of Florence, Italy

ARTICLE INFO

Article history:
Received 23 October 2014
Received in revised form 30 July 2015
Accepted 31 July 2015
Available online 4 August 2015

Keywords:
Morphotectonics
SAR data
TecDEM
Lineament extraction

ABSTRACT

Landscapes in the East African Rift System are formed by complex effects of the active continental extension zone. These effects are caused by the Somalian micro-plate's eastward drift away from the Nubian plate, as well as by volcanic, erosional and depositional processes. Tectonic processes in this region have significantly contributed to the formation of the current drainage systems and landforms. This study focuses on the morphotectonics of the Makuyuni catchment with an analysis of topography, drainage networks, stream longitudinal profiles and lineaments. This analysis reveals a morphostructural control with an N–S trend for the uplifted Masai Block, as well as tectonic deformation in the Makuyuni catchment area (NE of Lake Manyara). Whereas basin asymmetry analysis shows basin tilting associated with active faulting and uplifting near the Essimingor volcanic cone, in this catchment the steepness and concavity indices, coupled with lineaments obtained from interpretations of Synthetic Aperture Radar satellite scenes, show an uplifting along micro-faults. Hypsometry curves reveal that subcatchments on the right side of the Makuyuni River are in a mature equilibrium phase, whereas those at the left side are in a younger stage of maturity. An investigation of base level and statistical moments of the hypsometric curves provides evidences for the spatial distribution of gully erosion phenomena. Such erosion processes are due to tectonic deformation in the northern parts of the Makuyuni catchment. These results of regional tectonic instability suggest that tectonic processes are a significant factor for the current landscape evolution in the Lake Manyara basin.

1. Introduction

Quaternary evolution of landscapes in active rift areas is primarily formed by the effects of tectonic, volcanic and climatic factors. Tectonic factors are controlled by extensional processes of accommodating zones on major bounding faults (Ebinger and Scholz, 2011). Volcanic activity results from structural weaknesses in the crust and the high heat flow associated directly with rifting (Nichols, 2013). Climatic factors influence the weathering and water availability for transport, which determine the morphology and lithology of sedimentary bodies in rift regions (Tiercelin, 1990). Tectonic landscapes in rift areas are highly dynamic and are liable to undergo relatively rapid re-molding of its physical surface (Bailey et al., 2000). Traces of these dynamics are in part preserved in high escarpments, discontinuities in relief patterns, inland lake formation, and drainage network control, which are actively manifested by faulting and seismicity.

The study of relief structure and its morphology in tectonically active regions using geospatial data is usually called morphotectonics (Goudie, 2013). Morphotectonics is considered synonymous with tectonic geomorphology and defines the study of the interaction of tectonics and geomorphology (Scheidegger, 2004; Goudie, 2013). Morphotectonic studies are particularly addressed to locate anomalies in landform distribution, river courses, channel forms, terrace profiles, local relief or specific landforms such as slope breaks (Burbank and Anderson, 2011; Goudie, 2013). Digital Elevation Models (DEMs) and remote sensing data in general, are especially useful to analyze regional tectonic features from topography (Codilean et al., 2006; Wobus et al., 2006). The spatial data used as input in these analyses are commonly geomorphological and drainage pattern maps, DEMs and their various derivatives e.g., slope, aspect, and curvature (Burbank and Anderson, 2011). Morphotectonic analyses have been recently applied using global DEMs for active tectonic regions in the Himalayas, Andes, Alps and other mountain ranges showing their possibilities for applying geologic mapping and tectonic interpretations (Leverington et al., 2002; Jordan et al., 2005; Wulf et al., 2006; Gloaguen et al., 2007; Grohmann et al., 2007; Ramli et al., 2010; Shahzad and Gloaguen, 2011a, b; Anoop et al., 2012;

* Corresponding author at: Heidelberg Academy of Sciences and Humanities, c/o Institute of Geography, University of Tübingen, Rümelinstraße 19-23, 72070 Tübingen, Germany.
E-mail addresses: elio.flores_prieto@yahoo.de (E. Flores-Prieto), geraldine.queneherve@uni-tuebingen.de (G. Quénéhervé), felix.bachofer@uni-tuebingen.de (F. Bachofer), geoquaidian@gmail.com (F. Shahzad), michael.maerker@ggi.uni-tuebingen.de (M. Maerker).

http://dx.doi.org/10.1016/j.geomorph.2015.07.049
0169-555X/

Ferraris et al., 2012; Fisher et al., 2013; Gao et al., 2013; Soto-Pinto et al., 2013; Rahnama and Gloaguen, 2014; Scherler et al., 2014).

To investigate earth surface deformation due to tectonic processes, it is necessary to identify geomorphic markers that were displaced. The best markers are readily recognizable landforms, surfaces or linear trends (Burbank and Anderson, 2011). Linear trends can be identified in spatial data sets as lineaments. A lineament is a traceable, simple or composite linear feature shown on the surface whose parts are aligned in a rectilinear or slightly curvilinear relationship and which differs distinctly from the patterns of adjacent features, presumably reflects a subsurface phenomenon (O'Leary et al., 1976). Consequently, lineaments can be valley systems as well as rectilinear convex landforms. However, the automatic detection of valley features in the study area is difficult due to the ground resolution of the data in relation to the target structures as well as vegetation and shadowing effects. Therefore, we consider only convex rectilinear landforms as lineaments. Recent studies have demonstrated that remote sensing data are valuable sources for evaluating lineaments (Marghany and Hashim, 2010a; Soto-Pinto et al., 2013; Rahnama and Gloaguen, 2014). The appearance of lineaments is related to the occurrence of faults in the earth's crust and the depth of these faults. A fault which is close to the surface appears as a clear high-contrast lineament, and is better detectable in high resolution images. A deeper located fault is reflected in more subtle and often smeared lineaments, detectable in the lower-resolution and larger area images where the "noise", caused by fine details, is reduced (Arlegui and Soriano, 1998).

The aim of this study is to examine the morphotectonics of the Lake Manyara area focusing on the Makuyuni River basin, located in the East African Rift System (EARS). The tectonics of this region were previously studied in terms of i) kinematic and structural geology (Ring et al., 2005), ii) faulting, iii) Neogene tectonics and volcanism (Dawson, 1992, 2008; Le Gall et al., 2008; Albaric et al., 2009), iv) and structural geology (Albaric et al., 2010). Nevertheless, the link between landscape morphology and tectonics still has not been directly addressed.

This study identifies tectonic processes through a detailed analysis of topography, drainage networks, basins and river longitudinal profiles using DEMs derived from the Shuttle Radar Topography Mission (SRTM). This analysis is complemented by a lineament analysis performed using Synthetic Aperture Radar (SAR) data with different imaging geometry, wavelength and polarization. Different studies have proven the suitability of microwave remote sensing images for lineament detection and extraction (Tzong-Dar and Lee, 2007; Marghany and Hashim, 2010b). A specific focus of the study consists of assessing the suitability of different sensors for the detection of lineaments. The applied sensors are: ALOS Phased Array type L-band Synthetic Aperture Radar (PALSAR), Envisat Advanced Synthetic Aperture Radar (ASAR) and TerraSAR-X. We also investigate the role of tectonics as a triggering mechanism of gully erosion.

2. Regional setting

The EARS is one of the most remarkable geomorphic features in the African continent that results from the combination of the effects of the active continental extension zone caused by the eastward drift of the Somalia microplate away from the Nubian plate (Dawson, 2008) (Fig. 1). The EARS encompasses several Precambrian terrains that have experienced Cenozoic extension related to uplift and rifting. These terrains include the Archean Tanzanian craton, located in the center of the EARS that is mechanically strong and is surrounded by less resistant Proterozoic mobile belts, demonstrating strong control of lithospheric heterogeneities in strain localization during rift initiation (Ebinger et al., 1997; Ebinger and Scholz, 2011). The EARS splits into a western and an eastern branch around the Tanzania craton. The eastern branch runs over a distance of 2200 km through Ethiopia and Kenya up to northern Tanzania, largely following an N–S trend, composed of the Afar, Ethiopian, Kenya and Gregory rifts and the North Tanzania Divergence zone (NTD) from north to south (Tiercelin, 1990; Chorowicz, 2005; Dawson, 2008). As the EARS enters northern Tanzania, it splays into a 300 km wide zone of block faulting, in contrast to the well-defined, 80 km wide graben formed to the north of Kenya (Le Gall et al., 2008). The NTD is an elongated N–S depression flanked on its western side by a high, east-facing escarpment. The rift structures within the NTD are marked by a change in the rift morphology. Both sides of the depression are extensive areas of Neogene volcanic rocks (Dawson, 1992).

According to Dawson (1992) two intensive faulting processes took place in the NTD. The earlier was associated with the deformation of the mid Tertiary land surface and the uplifting of the Victoria and Masai Blocks causing a tectonic depression bounded by faults and warps. The second major phase of faulting took place at about 1.2 Ma during the Pleistocene phase of lower intensities, explosive nephelinite–phonolite–carbonatite volcanism (Dawson, 2012). Both episodes of faulting have created the present-day rift valley depression at the NTD.

The main manifestation of this faulting is seen in the major rift escarpment that runs from Lake Natron in the North to the South of Lake Manyara. This Eastern branch of the EARS has a relative elevation of ~500 m above the basin floor and is the surface expression of the major Manyara–Natron Fault (Macintyre et al., 1974).

The Lake Manyara basin is geographically located in the north-central part of Tanzania (3°00′–5°12′ S, 35°24′–36°48′ E), covers about 18,400 km^2 and lies between 954 and 3611 m a.s.l. It is an endorheic basin that straddles a complex occurrence of geological and geomorphological processes associated with volcanism, faulting, erosion and denudation (Dawson, 2008). The basin corresponds largely to the Manyara rift and has an asymmetrical geometry typical of a half-graben located in continental rift zones. In the west it is bordered by the Manyara escarpment, whose base is formed by several poorly sorted alluvial fan deposits. In the central part the shallow and saline Lake Manyara is located. The half-graben structure of the Lake Manyara basin is filled with continental sediments (Mutakyahwa, 2002). Today the seismic activity concentrates in the southern part of the basin (Macheyeki et al., 2008). East of Lake Manyara, paleolake terraces indicate former lake levels (Bachofer et al., 2014). A W-dipping warp in basement rocks is located in the east of the basin and minor *en echelon* step faults that dip to the NNE and to the E. (Macintyre et al., 1974; Ring et al., 2005).

The Makuyuni River catchment (3084 km^2) drains into Lake Manyara. The prevailing savannah climate is characterized by bi-modal rainy seasons with an annual rainfall of ca. 700 mm. The mean annual temperature is about 26 °C. In the north the border of the catchment is defined by steep valleys and volcanic sediments from the volcano Essimingor and the Monduli volcanoes and in general undulated structures (Fig. 2). The southern part is dominated by lowland areas followed by the undulating Masai plain stretching to the southeast. The Proterozoic metamorphic rocks are nearly completely covered by Holocene soils and lacustrine sediments adjacent to the lake. Close to the village of Makuyuni the so-called Manyara Beds are well exposed due to the incision of the Makuyuni River and gully erosion (Bachofer et al., 2015). They are divided in two sections: the Lower Members which are formed of lacustrine facies from the former paleolake Manyara (>0.633 Ma) and the Upper Members formed by floodplain, channel and debris flow facies (Ring et al., 2005; Frost et al., 2012).

3. Materials and methods

In this study we used multisensoral remote sensing data at various spatial scales. The data include: i) SRTM X-band data (SRTM-X) with 30 m ground resolution and those from three medium–high spatial resolution Synthetic Aperture Radar (SAR) sensors with different wavelengths and polarizations: ii) ALOS PALSAR (HH/HV polarization, L-band), iii) Envisat ASAR (HH/VV polarization, C-band) and iv) TerraSAR-X (HH polarization, X-band).

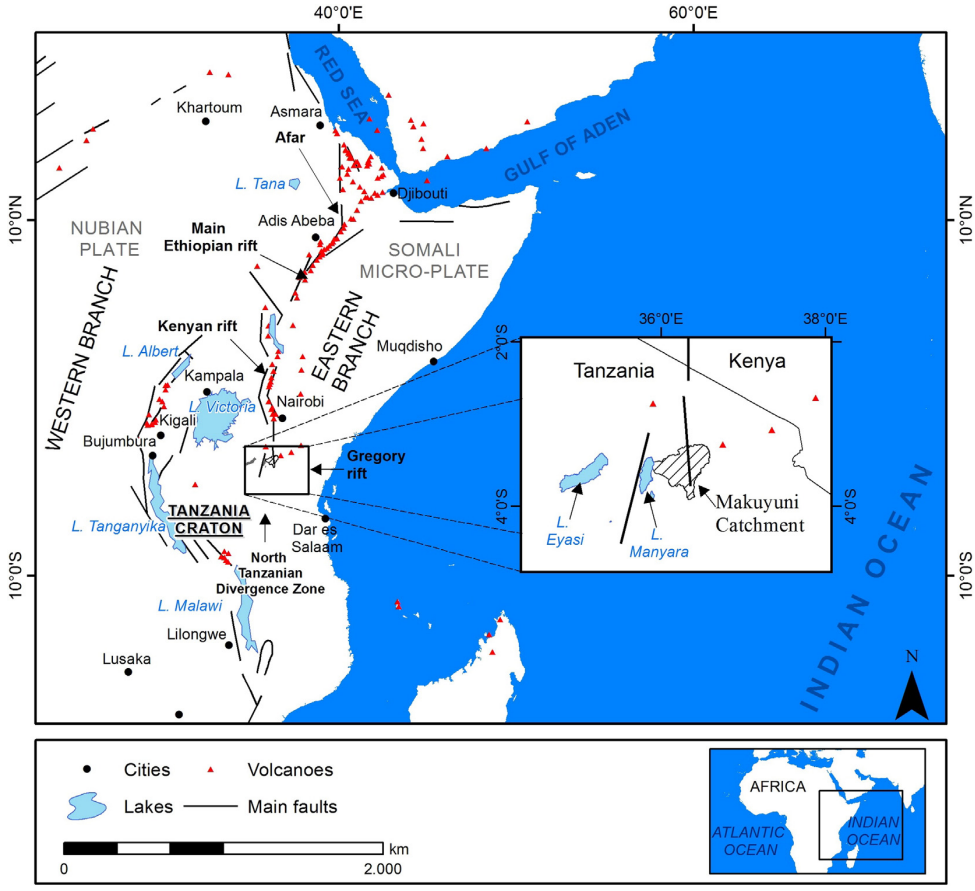

Fig. 1. Map of East Africa showing the EARS, its main structural units and associated volcanism, the location of the Lake Manyara and the Makuyuni River catchment in northern Tanzania. Source: Geology from the U.S. Geological Service (http://www.usgs.gov/), and Toponyms from Dawson (2008).

These data sets were examined to identify landscape elements reflecting recent tectonic activity such as drainage networks and lineaments. We combined morphotectonic parameters derived by terrain analysis to synthesize and visualize the results in a GIS (Geographic Information Systems) environment. This approach allows us to assess the influence of tectonics on current gully erosion processes.

3.1. Morphotectonic analyses

3.1.1. Stream profile analysis

For this analysis an SRTM-X DEM with a ground resolution of 30 m was used. Stream longitudinal profiles were extracted using TecDEM (http://www.tecdem.org). This toolbox is implemented into the MATLAB environment for understanding tectonics from DEMs and is able to generate stream profiles, determine flow directions, delineate watersheds, select knickpoints and generate morphometric maps for surface dynamics and basin analyses (Shahzad and Gloaguen, 2011a, b).

The first step is the extraction of the drainage network. This is based on the calculation of flow directions using the deterministic flow direction algorithm (D8) and contributing area. During the next step, on the basis of the extracted drainage system, longitudinal profiles of 22 channels were generated.

The stream profile analysis involved the calculation of the concavity (θ) and the steepness (k_s) indices.

θ and k_s values depend on basin morphology, underlying rock strengths and hydraulic geometry (Snyder et al., 2000; Shahzad and Gloaguen, 2011a; Anoop et al., 2012). They allow us to describe the stream longitudinal profiles through a relation between the channel gradient and the contributing drainage area (Schoenbohm et al., 2004). They are especially used for evaluating river system response to different landscape forming and modifying processes, including patterns of tectonic uplift and deformation (Wobus et al., 2006). This relation is expressed by the following predictable power law equation:

$$S = k_s A^{-\theta} \quad (1)$$

where S represents channel slope and A is the upstream drainage area. Because k_s is highly correlated to θ, we calculated a normalized steepness k_n using as reference $\theta = 0.45$ as suggested by Schoenbohm et al. (2004). θ and k_n values for concave segments along the longitudinal profiles were automatically calculated using a logarithmic regression analysis of area and slope values of selected trends. This calculation yields steepness distribution for the area with steady state landscape, as calculated by Shahzad and Gloaguen (2011a).

In the last step, knickpoints along the longitudinal profiles of the 22 tributaries were identified using a semi-automatic approach in TecDEM. This approach consists of the manual identification of the knickpoints in terms of slope breaks along the longitudinal profiles. The identification is based on expert knowledge and field work experience.

3.1.2. Drainage basin tilting

Drainage basin tilting was evaluated to examine the presence of tectonic tilting at the scale of the subcatchments. Therefore, we chose

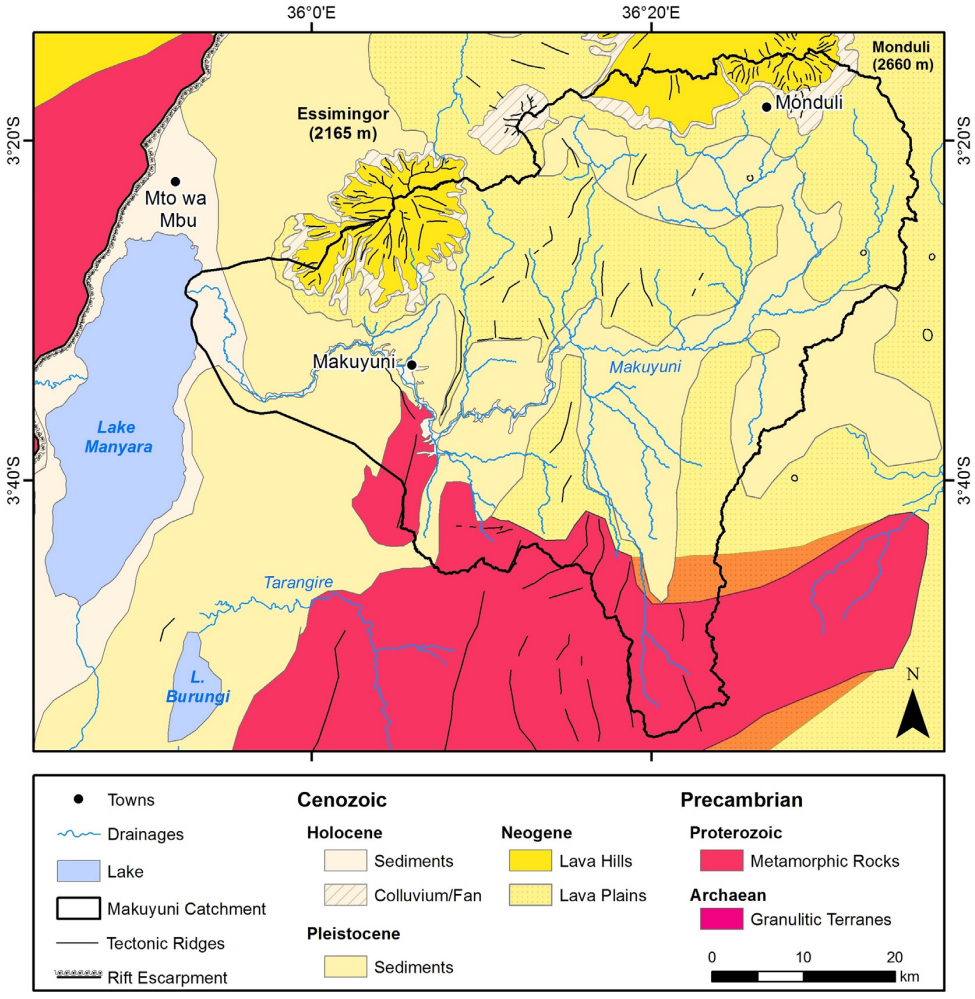

Fig. 2. Geological main units of the area. Based on field surveys and additional information from Vaidyanadhan et al. (1993) and Schlüter (2008).

Strahler order 4 which represents the mayor tributaries. Drainage basin tilting was estimated by means of the asymmetry factor *AF*, which is sensitive to tilting perpendicular to the direction of the stream (Hare and Gardner, 1985). *AF* values close to 50 show little or no tilting perpendicular to the direction of the trunk channel. *AF* values significantly above or below 50 results from drainage basin tilting, either due to tectonic activity or to lithological control. In order to determine the tilting direction of the subcatchments, following equation was used:

$$AF = 100 \cdot \frac{A_r}{A_t} \quad (2)$$

where A_r represents the basin area to the right side of the trunk stream, and A_t represents the total area of the drainage basin.

3.1.3. Basin hypsometry

Basin hypsometry is an appropriate parameter for identifying the stage of drainage evolution (Pérez-Peña et al., 2009). It represents the relative extent of the watershed area below or above a given height. The hypsometry integral (*HI*) and hypsometric curves can be used in classical conceptual geomorphic models of landscape and drainage evolution as follows: for *HI* values above 0.6, the area is at a youthful stage; for *HI* values in the range of 0.35–0.6 the area is in equilibrium (mature) phase; and *HI* values below 0.35 characterizes a monadnock phase in landscape evolution, a stage even more mature than the equilibrium stage (Strahler, 1957; Shahzad and Gloaguen, 2011b). Convex curves are typical for youthful stages of maturity whereas S-shaped curves and concave curves are typical for mature and old stages (Ohmori, 1993). Hypsometric curves and their statistical moments (skewness and kurtosis) were calculated using TecDEM software (see Shahzad and Gloaguen, 2011b). Skewness represents the asymmetry of the normal distribution in respect to the mean. Skewness is 0 when the variable distribution is symmetrical. Kurtosis is used to measure the "peakness" (>3) or "flatness" (<3) of the distribution in respect to the normal distribution (Pérez-Peña et al., 2009). These statistics can be interpreted in terms of erosion; skewness represents the amount of headward erosion in the upper reach of the basin, and kurtosis represents the erosion on both upper and lower reaches of a basin (Luo, 2000). Usually, these statistics are useful for hypsometric analysis when the basins present a similar hypsometry integral but different shapes (Pérez-Peña et al., 2009).

3.2. Lineament extraction

There are several algorithms that are available for automated lineament extraction, e.g. Hough Transform, Haar Transform and Segment Tracing (Jinfei and Howarth, 1990). In this study the automated lineament extraction was carried out by the LINE module of PCI

Geomatica software. This module is similar to the Segment Tracing algorithm and automatically detects a line of pixels as a vector element by evaluating local variance of the gray level in a digital image (Koike et al., 1998). All SAR scenes were radiometrically calibrated and topographically corrected. The automated lineament extraction method was performed for all available SAR scenes, and a complementary visual interpretation and manual extraction were conducted for the data of the Envisat ASAR (VH polarization) sensor. Complementary visual interpretation was performed only for this SAR sensor because its spatial scale resolution of 15 m provided the best basis for generalizing and identifying continuous linear features. The interpretation takes tonal and textural changes in the image as well as abrupt changes within the drainage network pattern into consideration — an example is shown in Fig. 3.

Manually and automatically extracted lineaments were compared using an overlay technique with a map of neotectonics created by

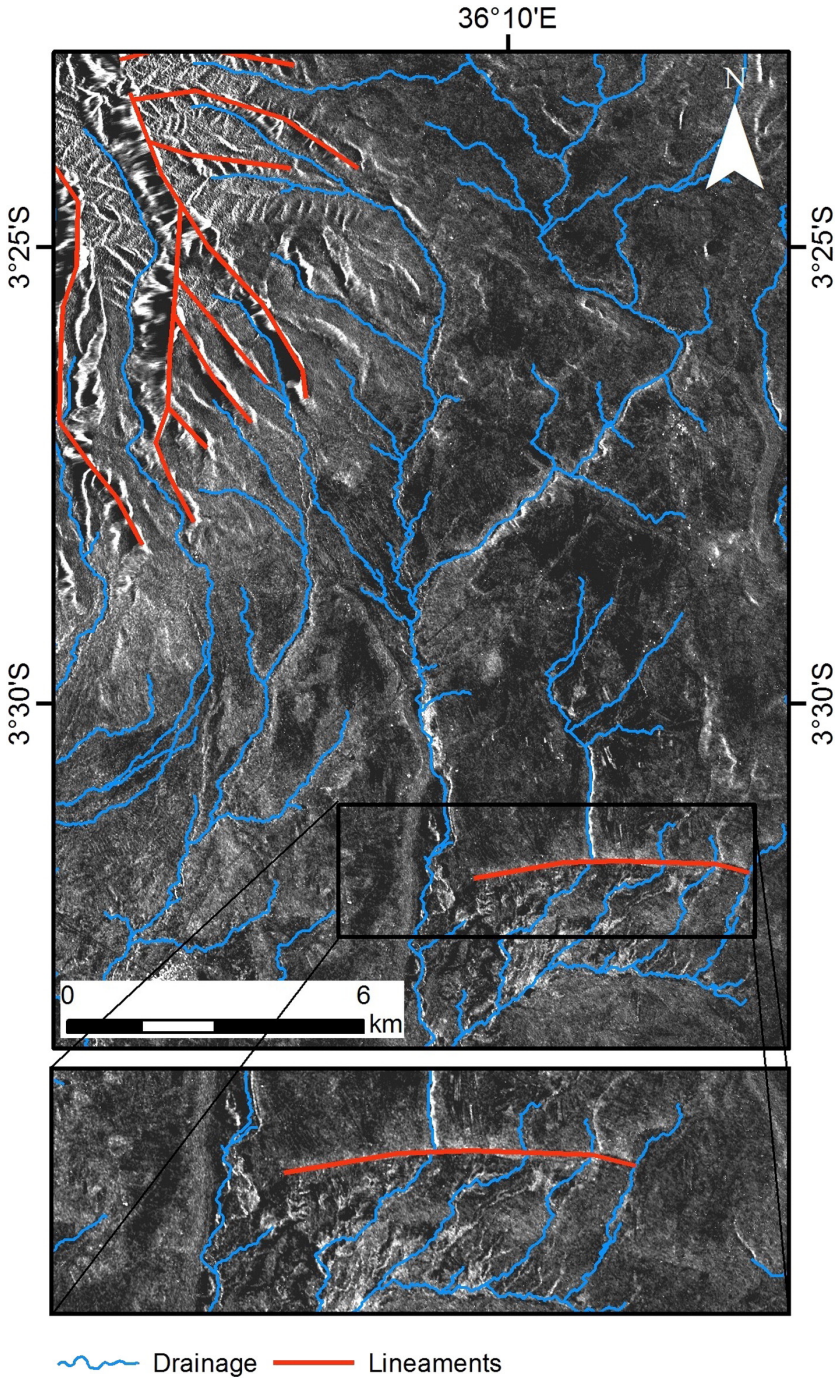

Fig. 3. Section of an Envisat ASAR scene (VH) of an area in the north of the Makuyuni catchment. Lineaments are indicated with segmented lines in white. The lineament in the enlarged section represents a local fault that deflects the four stream lines to the SW.

Dawson (2008). This allowed the classification of the lineaments into four types of linear tectonic structures: faults, inferred faults, escarpments and lithological contacts.

3.3. Base level maps and erosion areas

In a GIS environment we combined georeferenced tectonic structures (lineaments), morphotectonic data and a shapefile showing the current distribution of gully erosion phenomena digitalized from Google Earth™ images. We assessed the tectonic influence on the spatial distribution of gully erosion comparing the base level map with the current topography of the Makuyuni catchment shown by interpolated contours. The base level map was prepared in TecDEM by interpolating the elevation at the location of 2nd and 3rd Strahler order streams. Base levels can be used to study the dynamics of streams with different Strahler orders and topographic variations. Each base level surface is related to similar erosional stages, and can be considered a product of tectonic events (Golts and Rosenthal, 1993; Grohmann, 2004; Grohmann et al., 2007). To interpret the development and migration of knickpoints due to changes in the base level, they can be related to any geomorphological feature, e.g. the geomorphological evolution of a normal fault scarp. A response to the sudden base-level fall is knickpoint migration or propagation, which is an important aspect of channel incision and evolution in a wide range of geologic, tectonic, and climatic settings (Whipple and Tucker, 1999). Here we compared the knickpoint location with the location of gully systems in order to reveal a specific spatial correlation.

4. Results

All data and calculated results were validated during several field campaigns between 2010 and 2014. A total of 22 streams of the Makuyuni River were selected for a detailed analysis (Fig. 4). These streams correspond to the Strahler orders 3 and 4. Streams numbers 1 to 13 have their headwaters in the northern volcanic region, flowing southward to reach the Makuyuni River. The stream number 14 is part of the highest section of the Makuyuni River and follows an N–S trend for the first 10 km before undergoing a 45° deflection to an NE–SW direction. The streams numbers 15 to 22 flow northwards until they reach the Makuyuni main channel.

4.1. Stream longitudinal profiles

Longitudinal profiles of the 22 tributaries of the Makuyuni River consist of one to several channel segments. We identified these channel segments according to morphologic categories of the stream longitudinal profiles. These segments are frequently separated by knickpoints. The

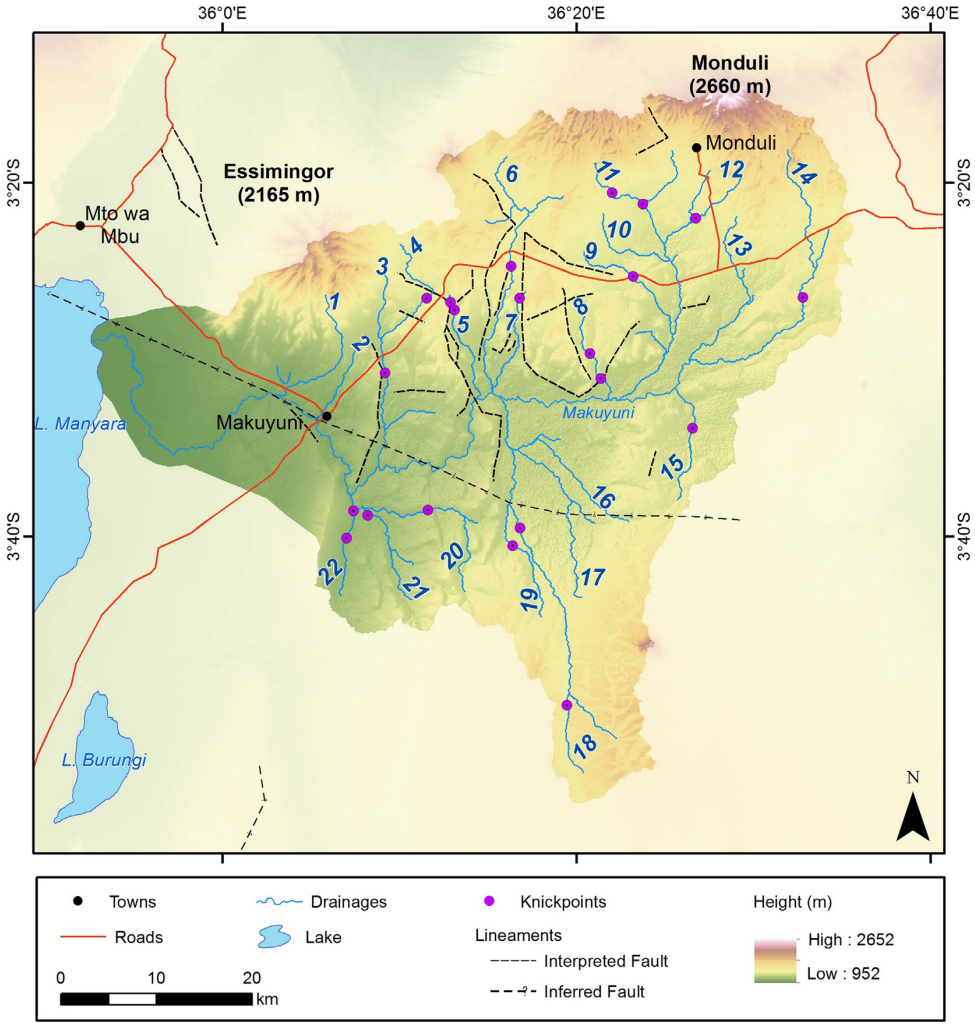

Fig. 4. Topographic map of the Makuyuni catchment showing the 22 selected tributaries, knickpoints and lineaments.

position of the channel segments allows the classification of the longitudinal profiles into four categories, corresponding to Fig. 5: A) fully equilibrated profiles without knickpoints (eight profiles), B) equilibrated profiles with knickpoints on their sections (nine profiles), C) profiles with two well-defined channel segments (two profiles), and D) profiles with three well-defined channel segments (three profiles).

θ and k_n values of the selected profiles are shown in the log area–log slope plots of Fig. 5. Values of θ and k_n of the 22 analyzed tributaries are grouped into three major segments that are defined by the morphology of the longitudinal profiles (Table 1), an upper segment that travels over the relict landscape, an intermediate segment corresponding to the middle section of the tributaries, and a lower segment dominated by fluvial incision. Table 1 shows increasing θ and k_n from the upper, middle to lower segments, as well as high variabilities of θ and k_n in the lower segments.

The distribution of knickpoints is related to the occurrence of faults (Fig. 4). The knickpoints located on the streams on the right side of the Makuyuni River (Nos. 3 to 8), coincide with minor lineaments detected through radar analysis, which were also classified by Dawson (2008) as micro or minor faults. Stream No. 14, situated in the eastern part of the catchment (Fig. 4), reveals one knickpoint located at the contact between Neogene rocks and recent alluvial deposits. No. 15, on the left side of the Makuyuni River, also shows a knickpoint located at this geological contact zone. The other knickpoints on the left side of the Makuyuni River are correspondingly related to a distinct lithological contact. There, the geological structure built by the Precambrian basement of the Masai Plateau is superimposed by the Quaternary alluvial and lacustrine deposits of the Manyara beds. Fig. 4 shows that the knickpoints of streams Nos. 20 to 22 are clearly alienated over this geological contact zone.

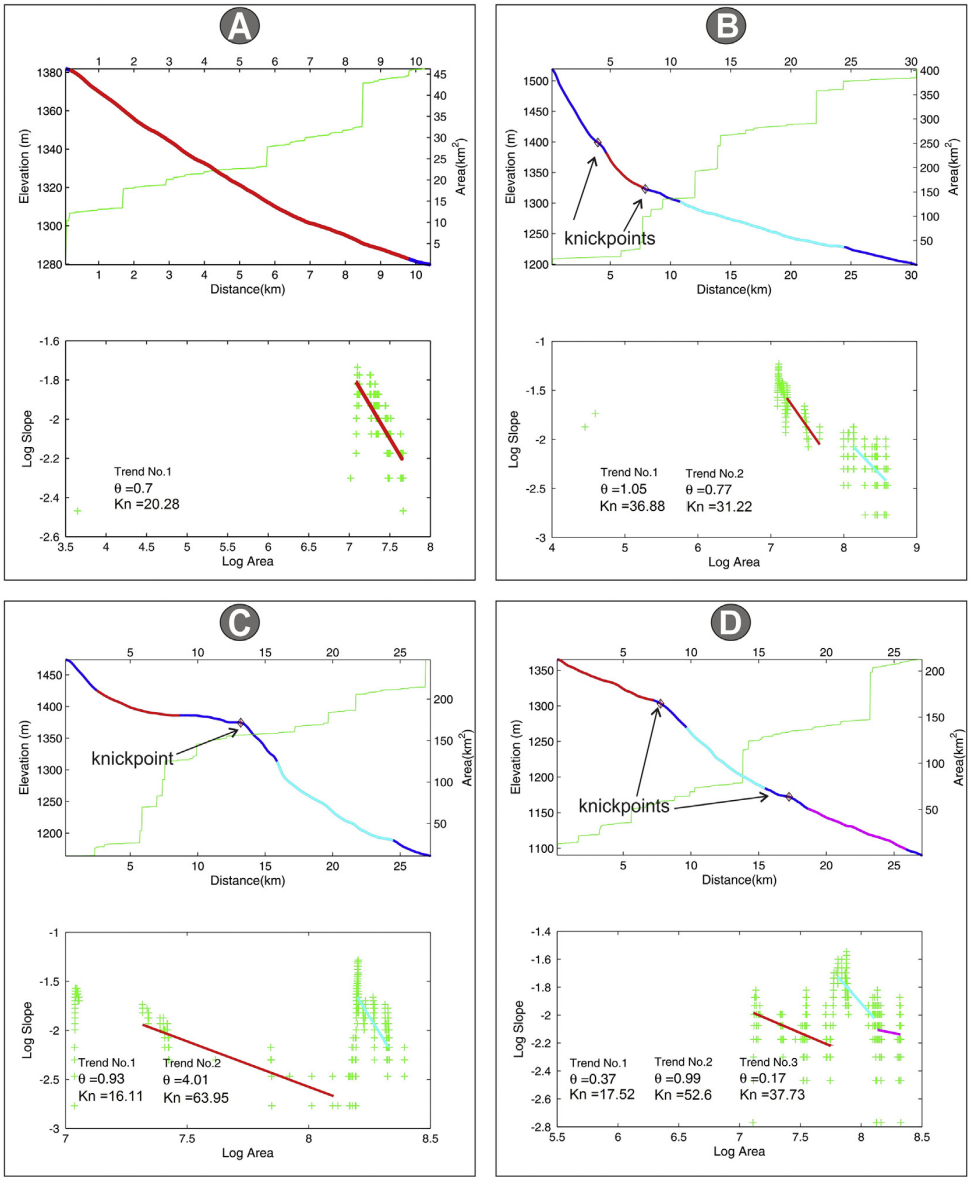

Fig. 5. Stream profile analysis (top of each set: longitudinal profile and cumulative catchment area, bottom: log area–log slope data) and knickpoints representing four categories of longitudinal profiles of the tributaries. (A) Fully equilibrated profile without knickpoints: stream No. 10. (B) Equilibrated profile with knickpoints on its section: No. 11. (C) Profile with two well-defined channel segments: No. 9. (D) Profile with three well-defined channel segments: No. 8.

Table 1
θ and k_n values.

Segment	Total segments	θ	k_n
Upper	22	1.394 ± 1.029	24.390 ± 11.890
Middle	9	3.731 ± 3.793	31.941 ± 16.835
Lower	2	9.070 ± 8.900	33.345 ± 43.850

4.2. Basin indices of tectonic activity

The calculated asymmetry index (*AF*) shows a strong asymmetry of the 12 subcatchments (Fig. 6A). The values of *AF* vary from 3.50 (almost symmetric; subcatchment 7) to 27.58 (highly asymmetric; subcatchment 8). The black arrows in Fig. 6A indicate the direction of tilt. All the subcatchments, with the exception of the Nos. 1 and 12, show an E–W direction of tilt.

Fig. 6B shows higher steepness values in the northern part of the Makuyuni catchment. This demonstrates higher tectonic deformation in this region of the catchment.

The hypsometric curves of the 12 subcatchments show two landscape maturity stages. A combined illustration of these subcatchments is shown in Fig. 7. Blue colored curves represent the subcatchments located on the right side of the Makuyuni River (northern subcatchments) and reveal a concave shape that suggests maturity, while the hypsometric curves of the subcatchments situated on the left side of the river (red curves) exhibit a more convex behavior (southern part). This shape type is attributed to more youthful drainage systems.

Statistical moments were used to quantify these hypsometric curves (Fig. 8A). In the case of the northern subcatchments, the values of hypsometric kurtosis are very irregular. They have a strong eastward increase up to subcatchment 3 and then a sudden decrease. Hypsometric skewness also increases slightly eastwards. In the southern subcatchments, there is an irregular behavior in hypsometric kurtosis and hypsometric skewness, with a general westward decrease (Fig. 8B). The hypsometric integral values are very similar for both northern and southern subcatchments.

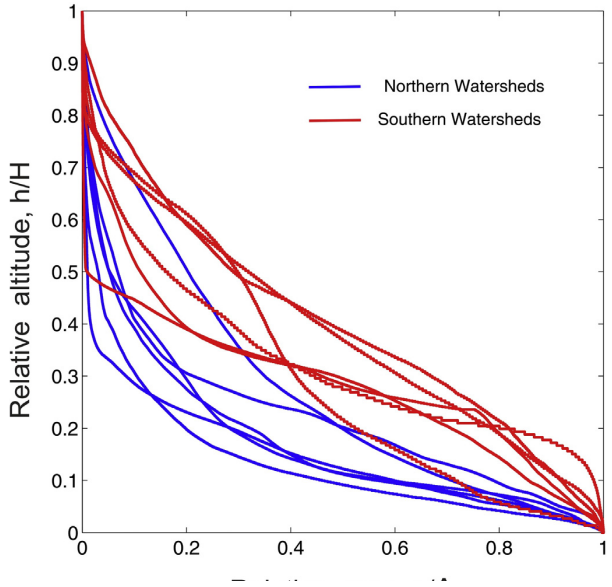

Fig. 7. Hypsometric curves for the northern and southern subcatchments of the Makuyuni River catchment. (H = maximum elevation difference of the basin; h = height of a given point in the basin; A = total area of the basin; a = surface area within basin above h).

4.3. Lineaments

The lineaments were automatically and manually extracted from the SAR images. The results of the automatic lineament extraction for each

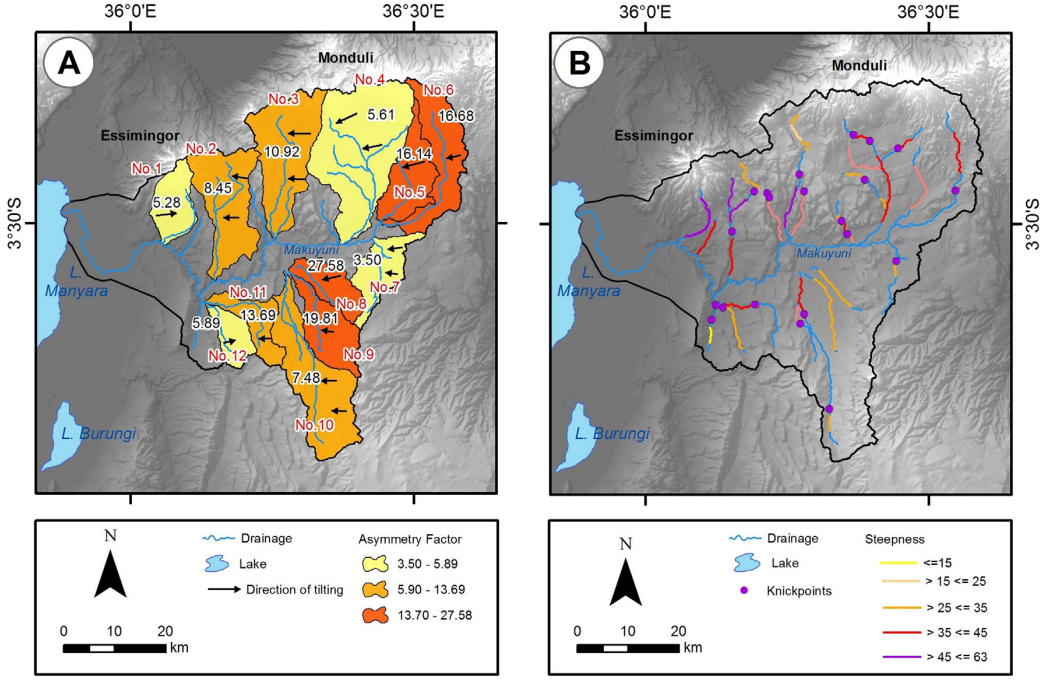

Fig. 6. Basin indices of tectonic activity. (A) Map showing subcatchments order 4 used to prepare hypsometric curves and their tilt directions according to the basin asymmetry. (B) Steepness and knickpoints of the Makuyuni River tributaries.

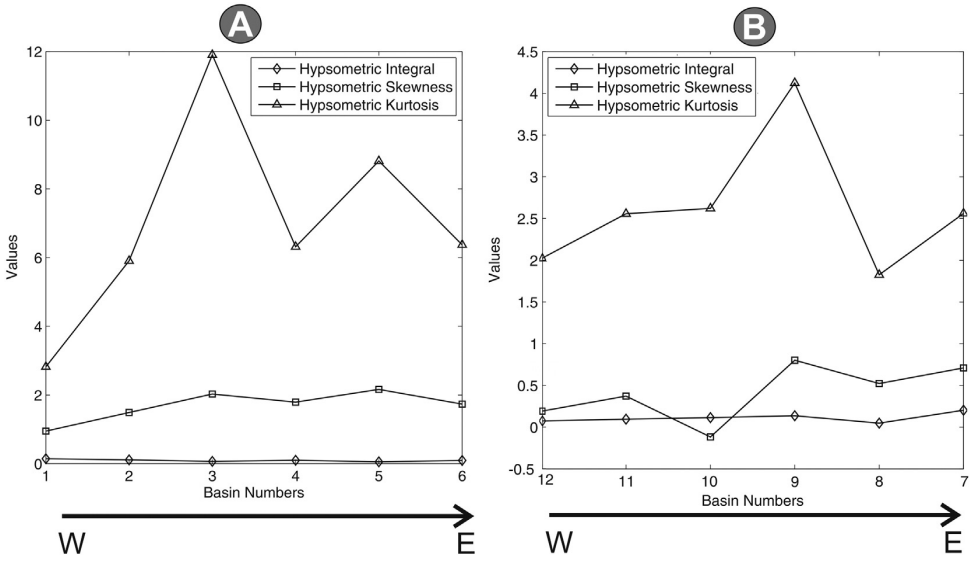

Fig. 8. Statistical moments of the hypsometric curves for the northern (A) and southern (B) subcatchments.

available SAR scene and all polarizations are summarized in Table 2 and Fig. 9. The length and number of detected lineaments were similar to the results computed with the ALOS PALSAR and Envisat ASAR data whereas the TerraSAR-X scenes provide a considerably higher number of lineaments. These differences are explained by the spatial resolution. Rose diagrams show a predominant N–S orientation of the extracted lineaments (Fig. 9A–C). Nonetheless, the Envisat ASAR Stripmap (VV; Fig. 9D) and the mosaicked TerraSAR-X Stripmap (HH; Fig. 9E) scenes indicate that a significant number of lineaments also have an NNE–SSW and an NNW–SSE orientation.

The visual interpretation was conducted for the Envisat scene, because the scene specific image acquisition geometry provided the best basis for the manual extraction of the lineaments. The automatically and the manually extracted lineaments are shown in Fig. 10. The number of automatically detected lineaments (503, Fig. 10A) is more than 24 times higher than the manually extracted ones (21, Fig. 10B). The most important reason for this is, that lineaments in automated analysis are shorter in length so that few of them could be combined to form one line as in the manually extracted map. The majority of the other detected lineaments are classified as artifacts, resulting from changes in vegetation cover, topography or geomorphologic structures and also roads and paths. The TerraSAR-X scenes in particular are highly affected by these artifacts, due to their high spatial resolution and a higher sensitivity to vegetation. Instead, the longer wavelengths of C- and L-band sensors show less sensitivity. The LINE algorithm cannot combine segmented lines. The total length of all the lineaments is higher in automated lineaments than the total length of the lineaments identified by manual extraction (342.3 vs 195.8 m). Nevertheless, the mean length of the lineaments from the manual interpretation is considerably higher than the automated ones.

Despite these differences, the spatial distribution of the lineaments in both maps is similar in that most of the lineaments are located in the north of the central Makuyuni catchment (Fig. 10).

4.4. Morphotectonics and current erosion processes

A base-level map of the 2nd and 3rd Strahler order streams and a colored shaded relief of the Makuyuni catchment are illustrated in Fig. 11. The base-level map gives a clear delimitation of the Makuyuni basin and the contour lines demarcate theoretical lines of equal uplift and hence, erosional surfaces (Fig. 11A). These lines show an E–W striking in the northern part of the Makuyuni catchment with a dip towards SSE, while the southern part is striking NE–SW and dipping towards NE. The proximity between these lines in the northern part suggests that this area is subject to tectonic activities. This might be in part correlated to uplift produced by the formation of the Monduli and Essimingor volcanoes. The major occurrence of knickpoints at considerably similar altitudes in this northern part indicates that they might have formed at similar stages of uplifting. In the northeastern and northern parts of the catchment, a high concentration of gully systems close to, or above the knickpoints can be observed. The knickpoints act as local erosion base level, and any changes in the knickpoint location leads to a response of erosional processes in the watershed above the knickpoints. Hence gully systems might indicate neotectonic activities as one of the triggering factors in gully formation.

Table 2
Automatically extracted lineaments from SAR data.

SAR sensor, mode & polarization	Acquisition date	Pass & incident angle (deg.)	Number of lineaments	Average length of lineaments (m)
ALOS PALSAR Fine Beam (HH)	2010-07-15	Ascending 38.78°	382	847
ALOS PALSAR Fine Beam (HV)	2010-07-15	Ascending 38.78°	310	824
Envisat ASAR Stripmap (VH)	2011-08-02	Descending 33.82°	503	680
Envisat ASAR Stripmap (VV)	2011-08-02	Descending 33.82°	391	633
TerraSAR-X Stripmap Mosaic (HH)	2013-01-25 & 2013-01-26	Ascending 24.49° & 28.11°	50,169	97

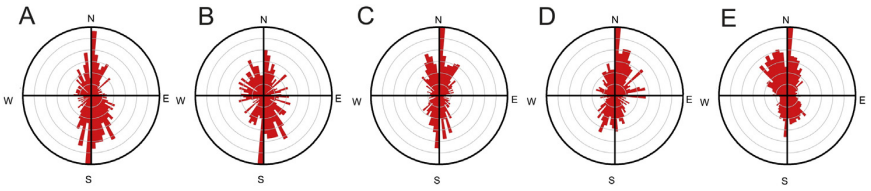

Fig. 9. Rose diagrams of the automatically delineated lineaments: (A) ALOS PALSAR Fine Beam (HH), (B) ALOS PALSAR Fine Beam (HV), (C) Envisat ASAR Stripmap (VH), (D) Envisat ASAR Stripmap (VV) and (E) Mosaicked TerraSAR-X Stripmap (HH).

5. Discussion

The assessment of morphotectonics based on DEM and SAR data analyses have yielded evidences of recent tectonics in the Makuyuni catchment.

5.1. Tilting of the subcatchments

Three categories of tectonic tilting for subcatchments of Strahler order 4 inferred from the *AF* value suggest that the drainage evolution in the Makuyuni catchment is sensitive to recent tectonics (Fig. 6A). These categories also reveal a non-uniform intensity of tilting. Highest values (>16) are located in the south-central and western parts of the Makuyuni catchment. There are several explanations for this result. Structural control caused by the boundary of the Pangani Rift at the western part of the Makuyuni catchment may have resulted in a strong shift of the basin midline of the subcatchments. Recent faulting and the contact of the tectonic depression of the Makuyuni River with the Masai Block (south) in the south-center of the Makuyuni River may also have affected the asymmetry of the subcatchments.

The *AF* factor also reveals a predominant E–W trend of tilting orientation for 10 out of 12 subcatchments. This trend can be explained by extensional E–W processes of the Manyara Rift and by the effects of local *en echelon* micro-faults. The other two subcatchments in the western part of the Makuyuni have a W–E tilt orientation. A possible explanation for this might be the local pushing forces of the ground movements (orogeny forces), associated with volcanism (Essimingor volcano).

5.2. Geomorphic stages of the subcatchments

The convexity of the hypsometric curves indicates erosional stages of the subcatchments. Older, more eroded drainage systems, show concave shapes. The difference in the curves of the northern and southern sides of the Makuyuni River reveals two stages of maturity (Fig. 7). Since the climatic conditions are similar for both sides of the river, these differences can be attributed to tectonic and lithological factors.

The northern part of the Makuyuni River catchment is affected by several *en echelon* micro-faults, while the southern part has no relevant fault lines (Fig. 4). The faults to the north of the Makuyuni River have been active during the late Pleistocene (Dawson, 2008) and were affected by uplifting. This uplifting is responsible for changes in the base level of the tributaries, which can also be interpreted as high incision rates. Thus, the subcatchments of the northern part of the Makuyuni River might have developed more concave hypsometric curves.

Lithological factors might also explain these differences in hypsometric curves. In the south of the catchment, where the Precambrian basement crops out, the relief is more resistant to the river incision, preserving convex stream profiles over time. In the north, the longitudinal profiles are more concave, revealing not only older states of maturity, but also major susceptibilities for the outcropping Quaternary deposits and Neogene rocks to river incision.

The statistical moments of the hypsometric curves provide additional information about the morphodynamics in the Makuyuni catchment. Since hypsometric integral values are very low and similar for both northern and southern curves (see Fig. 8), we had to use hypsometric skewness and kurtosis to interpret the spatial distribution and intensities of erosion processes.

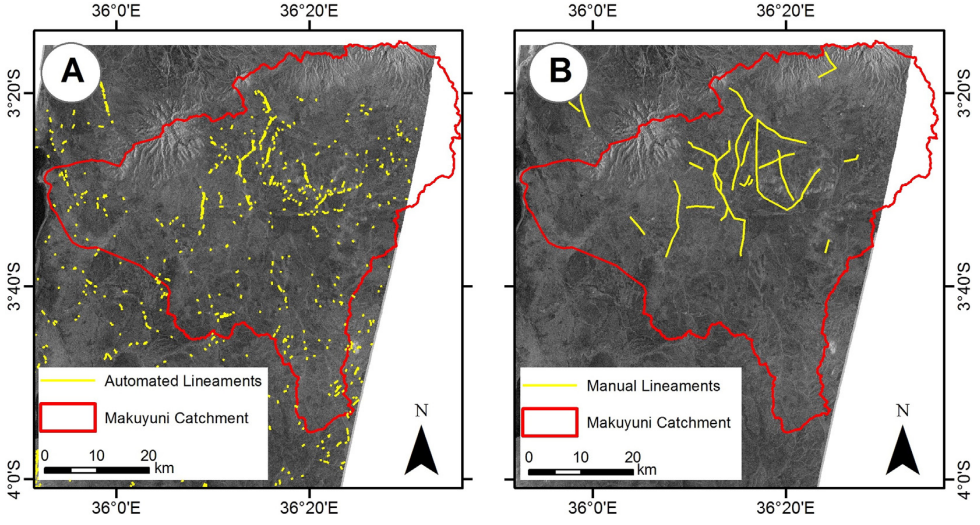

Fig. 10. Lineaments extracted (A) automatically and (B) manually.

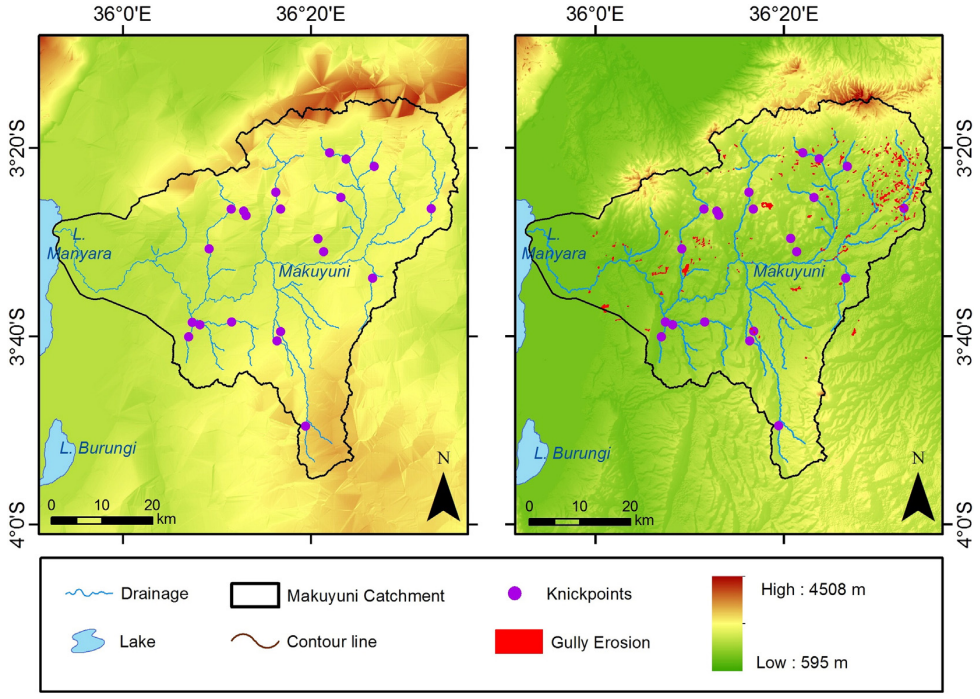

Fig. 11. Landforms reflecting: active tectonics and gully erosion. (A) Base-level map constructed for the 2nd and 3rd Strahler order streams and knickpoints. (B) Colored shaded relief, knickpoints of the Makuyuni catchment and gully erosion distribution. (For interpretation of the references to color in this figure legend, the reader is referred to the web version of this article.) Digitalized from Google Earth™ images and validated in the field.

Hypsometric skewness and kurtosis values increase eastwards in both the northern and southern hypsometric curves, revealing an increase in erosion in the upper and lower reaches of the subcatchments. These values also show a higher magnitude of incision on the northern side of the Makuyuni River around the Essimingor volcano, thus confirming the effect of the tectonic and lithological control on the erosion processes.

5.3. Evidence of tectonic activity in stream longitudinal profiles

Despite some irregularities that produced "noise" during the processing of some stream longitudinal profiles, the profile analysis seems to have yielded reliable results. Stream longitudinal profiles with different shapes suggest complex morphologies and morphodynamics that is primarily explained by changes in the lithology and tectonic activity.

A strong relationship between faults and the location of knickpoints was observed in the northern part of the Makuyuni catchment. The sequence of knickpoints on the tributaries Nos. 3 to 8 is directly related to tectonic control (micro-faults). The location of these knickpoints "over" the fault lines means that tectonic processes have taken place recently, and the location of knickpoints upstream of the fault lines is related to knickpoint migration (stream No. 8). Knickpoints on the streams Nos. 20, 21 and 22 (in the southern part) are spatially located over the lithological contact between Precambrian rocks and Quaternary deposits. One interpretation of the existence of these knickpoints might be that they are related to the low resistance of the Quaternary deposits. Once the streams reach the Quaternary deposits, the river incision increases, producing a distinct inflection in the river bed. Thus, these knickpoints are directly related to the predominant lithology. The latter was also confirmed by field observations in 2014. Stream longitudinal profiles classified as equilibrated profiles with knickpoints on their sections, and profiles with two and three well-defined channel segments are considered as a clear sign of tectonic activity and erosion.

The highest concavity index values were found in the lower channel segments. An explanation may be that the alluvial sediments which crop out close to the main channel of the Makuyuni River are less resistant to river incision. In the same way, the highest normalized steepness values in the lower channel segments are explained by the relative base level fall. The highest variability of these values in the middle segment is a consequence of the major uplift rates in the middle sections of the tributaries of the Makuyuni River.

Some authors (Whipple and Tucker, 1999; Snyder et al., 2000) argue that θ is relatively insensitive to tectonics (or climate), and that k_n is correlated with the rate of rock uplift. Streams that have different k_n values for different segments may be responding to tectonic perturbations to the fluvial system (e.g. tributaries Nos. 8 and 9 in Fig. 5), since uplift along a fault will send a wave of incision through the fluvial network which is directly reflected in steepened profiles and in knickpoint generation and migration (Wobus et al., 2006). Although tectonic forces are often responsible for these variations in the channel slopes and/or concavity, there are other factors such as lithological differences or variations in rock strength and debris flow or landslide frequency which can influence stream longitudinal profiles, including changes in incision rates, channel morphology, and bed condition (Whipple and Tucker, 1999). The estimation of steepness distribution from the concavity and steepness values was conducted by assuming steady state incision processes. The steepness map (Fig. 6B) confirms that in the northern side of the Makuyuni River, a more intense uplift has taken place in comparison to the southern side.

5.4. Landscape dynamics: active tectonics and gully erosion

Base-levels of the 2nd and 3rd Strahler order streams reveal that the northern part of the Makuyuni catchment was intensively affected by tectonic activity (Fig. 11A). This might have caused important differences in the effects of the geomorphic processes within the Makuyuni catchment. For example, the statistical moments of the hypsometric curves (Fig. 8) showed that the erosion in this northern part of the catchment is considerably higher. These findings are consistent with field validation

identifying a higher spatial occurrence of gully systems in the northern part, especially in the north-eastern part of the basin (Fig. 11B). This suggests that gully erosion processes in this area might be triggered by local active tectonics.

Similarly, stream longitudinal profiles with knickpoints and with two or three segments reveal changes at the base level of the tributaries of the Makuyuni River. Changes at the base level may lead to a subsequent incision of the streams, which result in a direct or indirect propagation of this incision in the upstream catchments (Harvey, 2002). This incision causes frequently a higher complexity of the drainage net, such as the development of tributaries of first order and gully formation. The distribution of gully erosion in Fig. 11B shows that several gully erosion systems are located upstream of the knickpoints in the northeastern part of the Makuyuni catchment. This points to a direct relation between the upstream migration of knickpoints and gully formation. Quantifying this relation is an important issue for future research for understanding the landscape dynamics in this part of the EARS.

6. Conclusions

The morphotectonics and the drainage evolution of the Lake Manyara area, with a focus on the Makuyuni River basin in the south of the EARS, were studied based on DEM analysis and lineament interpretations of SAR images. These analyses were performed using morphotectonic methods based on automated tools and software. Through these analyses the influence of tectonic activity on landscape evolution was investigated. The effect of the tectonics had already previously been consistently documented but without specific or local evidences. This study contributes to understanding the dynamics of Quaternary landscape evolution in this region as follows:

i. Relief and landscape patterns of the Lake Manyara basin reflect the evolution of a complex part of the rift systems that underwent the combined effects of tectonic factors inherent to its geological settings and Quaternary geomorphological processes. Generally, the morphostructures related to the EARS show a dominant N–S orientation. In the Makuyuni catchment, these structures reveal tectonic activity characterized by deviations and knickpoints of stream beds and the occurrence of erosion processes.
ii. The general increase of concavity and steepness values in the longitudinal profiles from the headwaters to lower sections indicate uplift associated with tectonic activity in the Makuyuni catchment.
iii. The spatial location of the knickpoints and its correlation with the lineament structures allowed the differentiation of the Makuyuni catchment into two distinctive areas: a) the hydrological controlled northern part of the catchment which is greatly influenced by tectonic activity, and b) a more stable southern part of the catchment, where the Precambrian lithology and less intense tectonics dominate.
iv. The data on the basin tilting, basin hypsometry and the morphology of the stream longitudinal profiles suggest that tectonic activity is an important factor governing Quaternary geomorphological processes, such as river incision and soil erosion, and hence, the landscape evolution of this region.

In summary, drainage network, stream longitudinal profiles, basin analysis and lineament extraction can be used as tools for identifying tectonic activity and related features in rift areas. The use of DEMs and SAR data in this kind of study permits the characterization and comparison of rift landscapes. Although there were initial limitations imposed by the low spatial resolution of the SRTM-X DEMs (30 m), their combination with high resolution radar data produced a better understanding of the superficial morphostructures. Moreover, in our case lineament interpretations for the regional analyses of morphotectonics, based on the use of C-band Envisat SAR images, yielded the best results with a medium spatial resolution. The above mentioned morphotectonic interpretations may be applicable to similar areas in the African rift, where landscapes are governed by extensional, tectonic, volcanic and erosional processes.

Acknowledgments

We are grateful for the support of the ROCEEH project: The Role of the Culture in Early Expansions of Humans, funded by the Heidelberg Academy of Sciences and Humanities. We would like to thank the DLR and the German Remote Sensing Data Center (DFS) for providing the TerraSAR-X and the SRTM/X-SAR data. Envisat ASAR and ALOS PALSAR data were provided by the European Space Agency. Furthermore, we would like to thank Jan Kalvoda and two more anonymous reviewers for their valuable comments.

References

Albaric, J., Déverchère, J., Petit, C., Perrot, J., Le Gall, B., 2009. Crustal rheology and depth distribution of earthquakes: insights from the central and southern East African Rift System. Tectonophysics 468 (1–4), 28–41.
Albaric, J., Perrot, J., Déverchère, J., Deschamps, A., Le Gall, B., Ferdinand, R.W., Petit, C., Tiberi, C., Sue, C., Songo, M., 2010. Contrasted seismogenic and rheological behaviours from shallow and deep earthquake sequences in the North Tanzanian Divergence, East Africa. J. Afr. Earth Sci. 58 (5), 799–811.
Anoop, A., Prasad, S., Basavaiah, N., Brauer, A., Shahzad, F., Deenadayalan, K., 2012. Tectonic versus climate influence on landscape evolution: a case study from the upper Spiti valley, NW Himalaya. Geomorphology 145–146, 32–44.
Arlegui, L.E., Soriano, M.A., 1998. Characterizing lineaments from satellite images and field studies in the central Ebro basin (NE Spain). Int. J. Remote Sens. 19 (16), 3169–3185.
Bachofer, F., Quénéhervé, G., Märker, M., 2014. The delineation of Paleo-Shorelines in the Lake Manyara Basin using TerraSAR-X data. Remote Sens. 6 (3), 2195–2212.
Bachofer, F., Quénéhervé, G., Märker, M., Hochschild, V., 2015. Comparison of SVM and Boosted regression trees for the delineation of lacustrine sediments using multispectral ASTER data and topographic indices in the Lake Manyara Basin. Photogrammetrie - Fernerkundung - Geoinformation (PFG) 1, 81–94.
Bailey, G., Manighetti, I., King, G., Bailey, G., Manighetti, I., King, G., 2000. Tectonics, volcanism, landscape structure and human evolution in the African Rift. In: Bailey, G., Charles, R., Winder, N., Bailey, G., Charles, R., Winder, N. (Eds.), Human Ecodynamics. Symposia of the Association for Environmental Archaeology en_GB. Oxbow Books, pp. 31–46.
Burbank, D., Anderson, R., 2011. Tectonic geomorphology. John Wiley & Sons 480 pp.
Chorowicz, J., 2005. The East African rift system. J. Afr. Earth Sci. 43 (1–3), 379–410.
Codilean, A.T., Bishop, P., Hoey, T.B., 2006. Surface process models and the links between tectonics and topography. Prog. Phys. Geogr. 30 (3), 307–333.
Dawson, J.B., 1992. Neogene tectonics and volcanicity in the North Tanzania sector of the Gregory Rift Valley: contrasts with the Kenya sector. Tectonophysics 204 (1–2), 81–92.
Dawson, J., 2008. The Gregory Rift Valley and Neogene-recent Volcanoes of Northern Tanzania. Geological Society (102 pp.).
Dawson, J.B., 2012. Nephelinite–melilitite–carbonatite relationships: evidence from Pleistocene—recent volcanism in northern Tanzania. Lithos 152, 3–10.
Ebinger, C., Scholz, C.A., 2011. Continental rift basins: the East African perspective, tectonics of sedimentary basins. John Wiley & Sons, Ltd, pp. 183–208.
Ebinger, C., Djomani, Y.P., Mbede, E., Foster, A., Dawson, J.B., 1997. Rifting Archaean lithosphere: the Eyasi–Manyara–Natron rifts, East Africa. J. Geol. Soc. 154 (6), 947–960.
Ferraris, F., Firpo, M., Pazzaglia, F.J., 2012. DEM analyses and morphotectonic interpretation: the Plio-Quaternary evolution of the eastern Ligurian Alps, Italy. Geomorphology 149–150, 27–40.
Fisher, G.B., Bookhagen, B., Amos, C.B., 2013. Channel planform geometry and slopes from freely available high-spatial resolution imagery and DEM fusion: Implications for channel width scalings, erosion proxies, and fluvial signatures in tectonically active landscapes. Geomorphology 194, 46–56.
Frost, S., Schwartz, H., Giemsch, L., Morgan, L., Renne, P., Wildgoose, M., Saanane, C., Schrenk, F., Harvati, K., 2012. Refined age estimates and Paleoanthropological investigation of the Manyara Beds, Tanzania. J. Anthropol. Sci. 90, 151–161.
Gao, M., Zeilinger, G., Xu, X., Wang, Q., Hao, M., 2013. DEM and GIS analysis of geomorphic indices for evaluating recent uplift of the northeastern margin of the Tibetan Plateau, China. Geomorphology 190, 61–72.
Gloaguen, R., Marpu, P.R., Niemeyer, I., 2007. Automatic extraction of faults and fractal analysis from remote sensing data. Nonlinear Process. Geophys. 14 (2), 131–138.
Golts, S., Rosenthal, E., 1993. A morphotectonic map of the northern Arava in Israel, derived from isobase lines. Geomorphology 7 (4), 305–315.
Goudie, A., 2013. Encyclopedia of geomorphology. Taylor & Francis (1200 pp.).
Grohmann, C.H., 2004. Morphometric analysis in geographic information systems: applications of free software GRASS and R. Comput. Geosci. 30 (9–10), 1055–1067.
Grohmann, C.H., Riccomini, C., Alves, F.M., 2007. SRTM-based morphotectonic analysis of the Poços de Caldas Alkaline Massif, southeastern Brazil. Comput. Geosci. 33 (1), 10–19.
Hare, P.W., Gardner, T., 1985. Geomorphic indicators of vertical neotectonism along converging plate margins, Nicoya Peninsula, Costa Rica. In: Morisawa, M., Hack, J. (Eds.), Tectonic Geomorphology. Allen and Unwin, pp. 75–104.
Harvey, A.M., 2002. Effective timescales of coupling within fluvial systems. Geomorphology 44 (3–4), 175–201.

Jinfei, W., Howarth, P.J., 1990. Use of the Hough transform in automated lineament. IEEE Trans. Geosci. Remote Sens. 28 (4), 561–567.
Jordan, G., Meijninger, B.M.L., Hinsbergen, D.J.J.v., Meulenkamp, J.E., Dijk, P.M.v., 2005. Extraction of morphotectonic features from DEMs: development and applications for study areas in Hungary and NW Greece. Int. J. Appl. Earth Obs. Geoinf. 7 (3), 163–182.
Koike, K., Nagano, S., Kawaba, K., 1998. Construction and analysis of interpreted fracture planes through combination of satellite-image derived lineaments and digital elevation model data. Comput. Geosci. 24 (6), 573–583.
Le Gall, B., Nonnotte, P., Rolet, J., Benoit, M., Guillou, H., Mousseau-Nonnotte, M., Albaric, J., Deverchère, J., 2008. Rift propagation at craton margin. Tectonophysics 448 (1–4), 1–19.
Leverington, D.W., Teller, J.T., Mann, J.D., 2002. A GIS method for reconstruction of late Quaternary landscapes from isobase data and modern topography. Comput. Geosci. 28 (5), 631–639.
Luo, W., 2000. Quantifying groundwater-sapping landforms with a hypsometric technique. J. Geophys. Res. 105 (E1), 1685–1694.
Macheyeki, A.S., Delvaux, D., Batist, M.D., Mruma, A., 2008. Fault kinematics and tectonic stress in the seismically active Manyara–Dodoma Rift segment in Central Tanzania — implications for the East African Rift. J. Afr. Earth Sci. 51 (4), 163–188.
Macintyre, R.M., Mitchell, J.G., Dawson, J.B., 1974. Age of fault movements in Tanzanian Sector of East African rift system. Nature 247 (5440), 354–356.
Marghany, M., Hashim, M., 2010a. Lineament mapping using multispectral remote sensing satellite data. Res. J. Appl.Sci. 5 (2), 126–130.
Marghany, M., Hashim, M., 2010b. Developing adaptive algorithm for automatic detection of geological linear features using RADARSAT-1 SAR data. Int. J. Phys. Sci 5, 2223–2229.
Mutakyahwa, M.K.D., 2002. Mineralogy and chemistry of bentonite (?) deposits at Minjingu, Lake Manyara, North Tanzania. J. Afr. Earth Sci. 34 (3–4), 213–221.
Nichols, G., 2013. Sedimentology and stratigraphy. Wiley (423 pp.).
Ohmori, H., 1993. Changes in the hypsometric curve through mountain building resulting from concurrent tectonics and denudation. Geomorphology 8 (4), 263–277.
O'Leary, D.W., Friedman, J.D., Pohn, H.A., 1976. Lineament, linear, lineation: some proposed new standards for old terms. Geol. Soc. Am. Bull. 87 (10), 1463.
Pérez-Peña, J.V., Azañón, J.M., Azor, A., 2009. CalHypso: an ArcGIS extension to calculate hypsometric curves and their statistical moments. Applications to drainage basin analysis in SE Spain. Comput. Geosci. 35 (6), 1214–1223.
Rahnama, M., Gloaguen, R., 2014. TecLines: a MATLAB-based toolbox for tectonic lineament analysis from satellite images and DEMs, part 1: line segment detection and extraction. Remote Sens. 6 (7), 5938–5958.
Ramli, M.F., Yusof, N., Yusoff, M.K., Juahir, H., Shafri, H.Z.M., 2010. Lineament mapping and its application in landslide hazard assessment: a review. Bull. Eng. Geol. Environ. 69 (2), 215–233.
Ring, U.W.E., Schwartz, H.L., Bromage, T.G., Sanaane, C., 2005. Kinematic and sedimentological evolution of the Manyara Rift in northern Tanzania, East Africa. Geol. Mag. 142 (04), 355.
Scheidegger, A.E., 2004. Morphotectonics. Springer (197 pp.).
Scherler, D., Bookhagen, B., Strecker, M.R., 2014. Tectonic control on ^{10}Be-derived erosion rates in the Garhwal Himalaya, India. J. Geophys. Res. Earth Surf. 119 (2), 83–105.
Schlüter, T., 2008. Geological Atlas of Africa. With notes on stratigraphy, tectonics, economic geology, geohazards, geosites and geoscientific education of each country. Springer (307 pp.).
Schoenbohm, L.M., Whipple, K.X., Burchfiel, B.C., Chen, L., 2004. Geomorphic constraints on surface uplift, exhumation, and plateau growth in the Red River region, Yunnan Province, China. Geol. Soc. Am. Bull. 116 (7), 895.
Shahzad, F., Gloaguen, R., 2011a. TecDEM: a MATLAB based toolbox for tectonic geomorphology, Part 1: drainage network preprocessing and stream profile analysis. Comput. Geosci. 37 (2), 250–260.
Shahzad, F., Gloaguen, R., 2011b. TecDEM: a MATLAB based toolbox for tectonic geomorphology, part 2: surface dynamics and basin analysis. Comput. Geosci. 37 (2), 261–271.
Snyder, N.P., Whipple, K.X., Tucker, G.E., Merritts, D.J., 2000. Landscape response to tectonic forcing: digital elevation model analysis of stream profiles in the Mendocino triple junction region, northern California. Geol. Soc. Am. Bull. 112 (8), 1250–1263.
Soto-Pinto, C., Arellano-Baeza, A., Sánchez, G., 2013. A new code for automatic detection and analysis of the lineament patterns for geophysical and geological purposes (ADALGEO). Comput. Geosci. 57, 93–103.
Strahler, A., 1957. Quantitative analysis of watershed geomorphology. Defense Technical Information Center, pp. 913–920.
Tiercelin, J.J., 1990. Rift-basin sedimentation: responses to climate, tectonism and volcanism. Examples of the East African Rift. J. Afr. Earth Sci. 10 (1–2), 283–305.
Tzong-Dar, W., Lee, M.T., 2007. Geological lineament and shoreline detection in SAR images, Geoscience and Remote Sensing Symposium, 2007. IGARSS 2007. IEEE International, pp. 520–523.
Vaidyanadhan, R., Dixit, P.C., Schlüter, T., 1993. Geomorphology and sedimentology of Lake Manyara Environs, Tanzania, East Africa. Doc. Naturae 77, 41–62.
Whipple, K.X., Tucker, G.E., 1999. Dynamics of the stream-power river incision model: implications for height limits of mountain ranges, landscape response timescales, and research needs. J. Geophys. Res. 104 (B8), 17661–17674.
Wobus, C., Whipple, K.X., Kirby, E., Snyder, N., Johnson, J., Spyropolou, K., Crosby, B., Sheehan, D., 2006. Tectonics from topography: procedures, promise, and pitfalls. Geol. Soc. Am. Spec. Pap. 398, 55–74.
Wulf, H., Schoenbohm, L., Strecker, M., 2006. Analysis of large-scale Quaternary landslide deposits: El Cajon basin, south-eastern Puna margin, NW Argentina, geophysical research abstracts. European Geosciences Union General Assembly.

APPENDIX II: PUBLICATION P2

Comparison of SVM and Boosted Regression Trees for the Delineation of Lacustrine Sediments using Multispectral ASTER Data and Topographic Indices in the Lake Manyara Basin.

BACHOFER, F., QUÉNÉHERVÉ, G., MÄRKER, M. & HOCHSCHILD, V., 2015 - *Comparison of SVM and Boosted Regression Trees for the Delineation of Lacustrine Sediments using Multispectral ASTER Data and Topographic Indices in the Lake Manyara Basin*. Photogrammetrie, Fernerkundung, Geoinformation (PFG) 1 / 2015 81-94 (doi: 10.1127/pfg/2015/0251).

This research paper is available online at *Schweizerbart and Borntraeger Science Publishers* (www.schweizerbart.de):

https://www.schweizerbart.de/papers/pfg/detail/2015/84627

Journal: Photogrammetrie, Fernerkundung, Geoinformation (PFG)
ISSN: 1432-8364
Thomson Reuters Impact Factor 2014: 0.733
Type: Research Article.

PFG 2015 / 1, 0081 – 0094
Stuttgart, February 2015

Article

Comparison of SVM and Boosted Regression Trees for the Delineation of Lacustrine Sediments using Multispectral ASTER Data and Topographic Indices in the Lake Manyara Basin

Felix Bachofer, Geraldine Quénéhervé, Michael Märker & Volker Hochschild, Tübingen

Keywords: SVM, boosted regression trees, ASTER, multispectral, topographic indices

Summary: The lower member of the so called Manyara Beds is a distinct lacustrine sedimentary layer which indicates, with an elevation of more than 140 m above today's lake level, a high stand of the paleolake Manyara in the Monduli District in northern Tanzania. The Manyara Beds are rich in Pleistocene vertebrate fossils. In this study we focus on the delineation of this specific stratigraphic layer in order to yield new insights into paleontological settings, landscape evolution and to plan paleontological fieldwork. We compare the performance of a support vector classifier with a linear as well as a Gaussian kernel, with boosted regression tree approaches to identify the lithostratigraphic layers of the Manyara Beds. For the identification of the lacustrine sediments, multispectral information of ASTER satellite imagery and topographic indices derived from a digital elevation model were utilized as input feature sets. Acceptable classification accuracies were obtained with all methods. Thus, the Manyara Beds can be delineated and new sites with paleolake sediments were detected. The highest overall accuracy with 92% was provided by the support vector machine approach with a linear kernel for a binary classification problem. For a multi-class classification problem with three target classes the support vector classifier achieved 80% accuracy with a linear, as well as a Gaussian kernel.

Zusammenfassung: *Vergleich von SVM und Boosted Regression Trees zur Abgrenzung von lakustrinen Sedimenten anhand von multispektralen ASTER Daten und topographischen Parametern im Einzugsgebiet des Manyara Sees*. Die aus vornehmlich lakustrinen Sedimenten bestehende ältere Gruppe der stratigraphischen Einheit der Manyara Beds beschreibt mit einer Höhe von mehr als 140 m über dem heutigen Seespiegel einen Hochstand des Paläosees Manyara im Monduli Distrikt im nördlichen Tansania. Die Manyara Beds sind reich an pleistozänen Wirbeltierfossilien. Die vorliegende Arbeit beschäftigt sich mit der räumlichen Abgrenzung dieser stratigraphischen Einheit um mehr über die paläontologischen Ablagerungsbedingungen und die Landschaftsgeschichte zu erfahren, sowie die Planung von paläontologischen Geländearbeiten zu unterstützen. Wir vergleichen anhand der lithostratigraphischen Einheit der Manyara Beds die Leistungsfähigkeit eines Support Vector (Stützvektoren) Klassifizierungsansatzes, mit einem linearen und einem Gaußschen Kernel, und mit Klassifizierungsbäumen (Boosted Regression Trees). Um die lakustrinen Sedimente zu unterscheiden, wurden multispektrale Informationen einer ASTER Satellitenaufnahme und topographische Parameter von einem digitalen Höhenmodell als Eingangsvariablen genutzt. Mit allen Klassifizierungsmethoden wurden zufriedenstellende Genauigkeiten erzielt. Somit konnte das Auftreten der Manyara Beds räumlich abgegrenzt und bisher nicht dokumentierte Flächen mit lakustrinen Sedimenten erfasst werden. Die höchste Klassifizierungsgenauigkeit von 92% wurde von der Support Vector Machine Klassifizierung mit einem linearen Kernel für eine binäre Klassifizierung erreicht. Für eine Aufgabenstellung mit Support Vector Machines für drei Zielklassen wurde eine Genauigkeit von 80% sowohl mit einem linearen, als auch mit einem Gaußschen Kernel erreicht.

www.schweizerbart.de
DOI: 10.1127/pfg/2015/0251 1432-8364/15/0251 $ 3.50

1 Introduction

Lacustrine sediments and paleo-shorelines of different Quaternary lake-level high stands can be observed in the north, south and east of the Lake Manyara basin of northern Tanzania. The study area is located in the Gregory Rift in Central North Tanzania. The basin is of paleontological and archeological interest documented by several investigations in recent years (e.g. Schlüter et al. 1992, Kaiser et al. 2010, Prendergast et al. 2013). One of the richest stratigraphic units in vertebrate fossils and artifacts in the region are the Manyara Beds, which indicate a high level of the paleolake Manyara at more than 140 m above today's lake level. The identification of the Manyara Beds contributes to the understanding of landscape evolution and the spatial distribution of potential paleontological sites. Thus, the study also serves for the planning of future fieldwork in the study area.

Remote sensing images are used in different studies to derive information on the extent of paleolakes and other paleo-landscape forms. ElSheikh et al. (2011) and Elmahdy (2012) used remote sensing, GIS and geophysical methods to delineate a paleolake in northern Darfur. Ghoneim et al. (2012) used an integrated approach with optical and microwave data to map a paleo-drainage system. The use of remote sensing in combination with topographic analysis for the delineation of paleolakes has been successfully applied by Gaber et al. (2009) on the Sinai Peninsula.

Mountrakis et al. (2011) review the application of support vector machines (SVM) in the classification of remotely sensed images. SVM and boosted regression tree analysis (BRT) were more and more used in the last decade and yield high accuracies (Foody & Ajay 2004, Esch et al. 2009, Wang et al. 2011, Gómez et al. 2012, Gessner et al. 2013). SVM and BRT analyses are capable of handling multiple input features, outliers, non linear tasks and redundant data (Foody & Ajay 2004, Elith et al. 2008). Hahn & Gloaguen (2008) used SVM to classify soil types and soil texture from ASTER multispectral data and topographic parameters in the Erzgebirge in Germany. BRT methods have been assessed with remote sensing data for land use issues (Pal & Mather 2003, Chan & Paelinckx 2008). The mapping of lithological units and the distribution of soil with multispectral data and terrain attributes as well as classification methods were reviewed by Mulder et al. (2011). In this study we compare the accuracy of SVM and BRT classifier in identifying the Manyara Beds in a small scaled, heterogeneous environment. Pal & Foody (2010) showed that an increase of input features may lead to a decline of classification accuracy. Therefore, we apply a feature selection to choose a subset of different ASTER spectral bands, multispectral indices and topographical indices. From this selected set of features, we expect also improved model interpretability, as well as an enhanced generalisation of the resulting models.

2 Regional setting and data preparation

2.1 *Study Area*

The Lake Manyara catchment in northern Tanzania is an endorheic basin and part of the eastern branch of the East African Rift System (Fig. 1). Today Lake Manyara is a shallow soda lake (954 m a.s.l.) with a maximum depth of 1.18 m (Deus et al. 2013). The basin is an asymmetrically shaped half graben, with a 200 m to 600 m high escarpment along the western shoulder. The eastern shoulder of the Rift is lower in elevation and consists of tectonic blocks that are dipping towards the west. The North-eastern parts of the catchment area are dominated by the volcano Essimingor. Paleo-shorelines can be found especially on the Eastern part of the rift tracing different paleolake levels up to 80 m above today's lake level. The latter forms also the lowest possible outlet into the Engaruka and Lake Natron basin (Keller et al. 1975, Bachofer et al. 2014). The maximum age of the paleo-shorelines was established with radiocarbon dating (Th/U series) to 140,000 a BP (Casanova & Hillaire-Marcel 1992). Besides the springs at the base of the escarpment, Lake Manyara is mainly fed with seasonal drainages of the Tarangire and Makuyuni rivers. Today a bimodal precipitation pattern with an average annual rainfall of about 700 mm can be observed for

the study area. The resulting semiarid vegetation cover is sparse and dominated by bushed grassland (Bachofer et al. 2014).

2.2 *The Manyara Beds*

The lacustrine and fluvial stratigraphic units, known as the Manyara Beds in the east of Lake Manyara, reach up to approximately 140 m above today's lake surface. They describe the maximum extent of the lake (Schwartz et al. 2012). The Manyara Beds are rich in Pleistocene vertebrate fossils. In the Lake Manyara area, especially close to the village of Makuyuni, two hominin-bearing sites (0.63 and 0.78 Ma), vertebrate fossils and handaxes from different periods were found (Kaiser et al. 2010, Frost et al. 2012). The Manyara Beds consist of a lacustrine grayish lower member (mudstones, siltstones, diatomites, marls and tuff) which was deposited between 1.03 and 0.633 Ma, and a fluvial and terrestrial upper member which is composed of up to 13 m thick reddish brown upper member (siltstones, mudstones, conglomerates and breccias) deposited between 0.633 and 0.44 (0.27) Ma. The transition between both members is in most sections marked by a distinct tephra layer (Frost et al. 2012). Sections of the Manyara Beds are best exposed in the surroundings of the town Makuyuni, where Holocene soils and caliche overlay the sediments and where various gully systems erode into the savanna landscape. Laboratory analysis of representative samples of alluvial material of the Low-

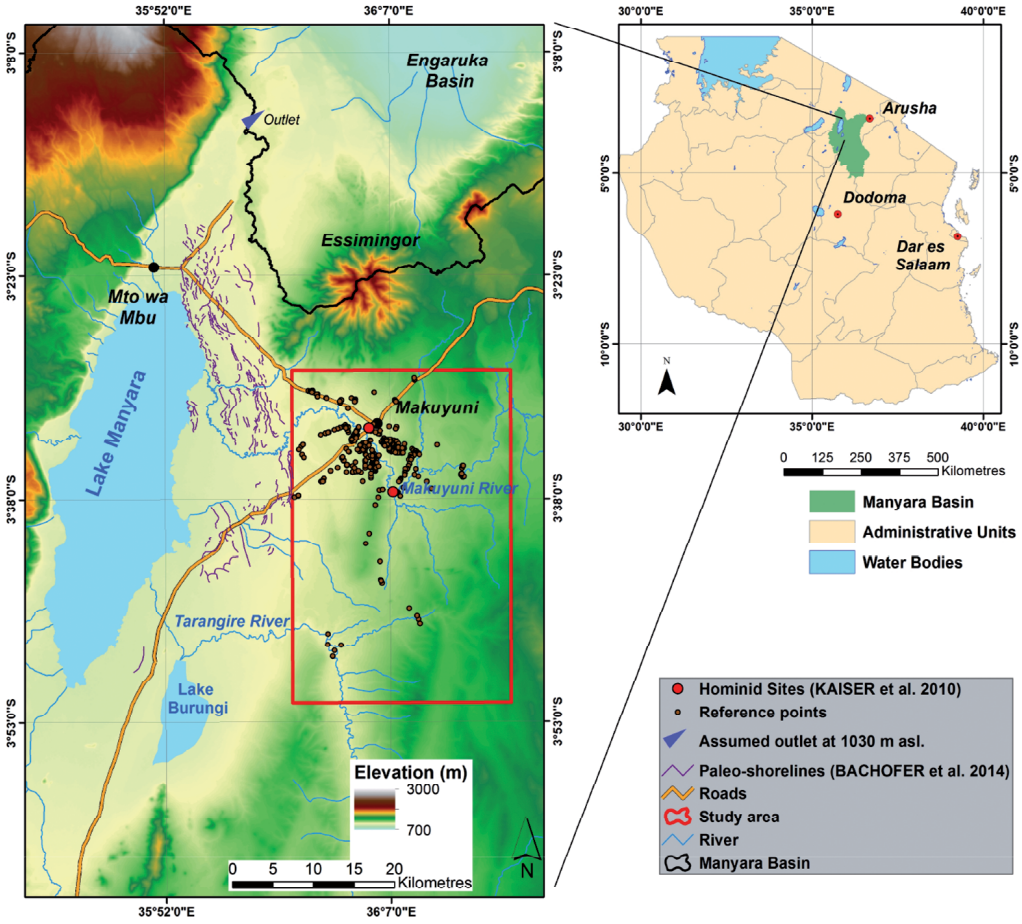

Fig. 1: The study area and the regional setting of Lake Manyara.

er Manyara Beds (LMB) and Upper Manyara Beds (UMB) were taken from the slopes of the Makuyuni river valley. They show heterogeneous texture, but distinct higher carbonate content in LMB and Fe^{2+} content in UMB. Organic carbon is dependent on the topographic position and adjacent soils and vegetation cover. Hence, the Manyara Beds show specific spectral and positional properties. Consequently, a successful delineation of the Manyara Beds with spectral bands, multispectral indices and topographical indices seem possible.

2.3 *ASTER Multispectral Data*

The Advanced Spaceborne Thermal Emission and Reflection Radiometer (ASTER) was launched with NASA's TERRA spacecraft in December 1999 (Yamaguchi et al. 1998). Its subsystems cover three bands in the visible-near infrared (VNIR), six bands in the shortwave infrared (SWIR) and five bands in the thermal infrared (TIR) wavelength regions (Tab. 1). The ground resolution is 15 m, 30 m and 90 m respectively (Fujisada 1995). Yamaguchi et al. (1998) stated that the VNIR spectral information was designed for use in mapping vegetation and iron oxides in soil and rocks, while the SWIR wavelengths were designed for soil and mineral mapping.

A cloud free ASTER L1B scene was obtained at August 23, 2006, 8:07 UTC during dry season. Because the SWIR bands of the L1B data is not corrected for a cross-detector leakage, crosstalk correction was applied following Iwasaki et al. (2002) using the correction software product from Earth Remote Sensing Data Applications Centre (ERSDAC).

The average geometric accuracy of the ASTER scene was validated by own ground control points (GCP) measurements and high resolution WorldView-2 imagery. A mean locational residual error of 61.4 m could be estimated which is close to the residual error calculated by Hewson et al. (2005). The GCPs and a Landsat ETM+ (L1T) panchromatic scene with 15 m ground resolution were used to improve the geometric accuracy using an automatic point matching algorithm. For our GCPs the Landsat scene showed a total RMSE of 16.5 m. The ASTER scene could be aligned with an RMSE of 0.9. However, the TIR bands were excluded from the analysis because of their low spatial resolution and some artifacts which were visible in the L1B and also in the surface emissivity product (AST05). To preserve the spectral information of the VNIR bands, the SWIR bands were resampled to the respective ground resolution of 15 m.

2.4 *Spectral Indices*

Multispectral indices derived from ASTER spectral bands are used in a broad range of studies with a main emphasis on vegetation, soil and lithology (Mulder et al. 2011, Pour & Hashim 2011). The spectral rationing of selective band absorption features of different materials at distinct wavelengths is utilized to emphasize the presence or absence of distinct mineral compositions or vegetation. From an extensive literature review a broad range of indices were collected and processed for this analysis (Tab. 2). Not all minerals, for which the indices were developed, are abundant in the study area. In addition, many of the indices carry redundant information because of the use of similar input bands and band combinations.

Tab. 1: ASTER spectral bands with the minimum lower and maximum upper band edges.

VNIR Green	0.52–0.60 µm	SWIR 3	2.185–2.225 µm
VNIR Red	0.63–0.69 µm	SWIR 4	2.235–2.285 µm
VNIR Near Infrared	0.76–0.86 µm	SWIR 5	2.295–2.365 µm
SWIR 1	1.600–1.700 µm	SWIR 6	2.360–2.430 µm
SWIR 2	2.145–2.185 µm	TIR 1 - 5	8.125–11.65 µm

Tab. 2: Spectral indices of ASTER VNIR and SWIR bands.

Index and literature reference	Formula	Index and literature reference	Formula
AlOH Group (Cudahy 2012)	(5/7)	AKP (Rowan & Mars 2003)	(4+6)/5
Alteration/Laterite (Bierwirth 2002)	(4/5)	Amphibole (Bierwirth 2002)	(6/8)
Alunite (Pour & Hashim 2011)	(7/5)*(7/8)	Calcite (Pour & Hashim 2011)	(6/8)*(9/8)
CCE (Rowan & Mars 2003)	(7+9)/8	Dolomite (Rowan & Mars 2003)	(6+8)/7
Clay 1 (Rowan & Mars 2003)	(5+7)/6	MgOH Group (Cudahy 2012)	(6+9)/(7+8)
Clay 2 (Bierwith 2002)	(5*7)/(6*6)	MgOH 1 (Hewson et al. 2005)	(6+9)/8
Kaolinitic (Hewson et al. 2005)	(7/5)	MgOH 2 (Cudahy 2012)	(7/8)
Kaolin Group (Cudahy 2012)	(6/5)	Ferric Iron³ (Rowan & Mars 2003)	(2/1)
Kaolinite (Pour & Hashim 2011)	(4/5)*(8/6)	Ferrous Iron 1 (Rowan et al. 2005)	(1/2)
Muscovite (Hewson et al. 2005)	(7/6)	Ferrous Iron 2 (Rowan & Mars 2003)	(5/3)+(1/2)
OH 1 (Pour & Hashim 2011)	(7/6)*(4/6)	Ferric Oxide (Cudahy 2012)	(4/3)
OH 2 (Ninomiya et al. 2005)	(4*7/6)/6	Gossan (Volesky et al. 2003)	(4/2)
OH 3 (Ninomiya et al. 2005)	(4*7/5)/5	Opaque Index (Cudahy 2012)	(1/4)
PHI (Hewson et al. 2005)	(5/6)	Ferrous Iron/Silicates (Cudahy 2012)	(5/4)
RBD6 (Rowan et al. 2005)	(4+7)/(6*2)	Burn Index (Hudak et al. 2004)	(3-5)/(3+6)
RBD8 (Rowan et al. 2005)	(7+9)/(8*2)	VI (Tucker 1979)	(3/2)
NDVI (Rouse et al. 1974)	(3-2)/3+2)	Salinity (Al-Khaier 2003)	(4-5)/(4+5)
STVI (Pour & Hashim 2011)	(3/2)*(1/2)		

Tab. 3: Topographic indices.

Slope (Travis et al. 1975)	Aspect (Travis et al. 1975)
Slope height (Boehner & Conrad 2008)	Valley Depth (Boehner & Conrad 2008)
Standardized Height (Boehner & Conrad 2008)	Normalized Height (Boehner & Conrad 2008)
Mid Slope Position (Boehner & Conrad 2008)	Downslope Distance Gradient (Hjerdt et al. 2004)
Plan Curvature (Zevenbergen & Thorne 1987, Dikau 1988)	Profile Curvature (Zevenbergen & Thorne 1987, Dikau 1988)
Negative Openness (Yokoyama et al. 2002)	Positive Openness (Yokoyama et al. 2002)
Morphometric Protection I. (Yokoyama et al. 2002)	Terrain Ruggedness Index (Riley et al. 1999)
Multiresolution Index of Valley Bottom Flatness (Gallant & Dowling 2003)	Multiresolution Index of Ridge Top Flatness (Gallant & Dowling 2003)
Relative Slope Position (Conrad 2005)	Geomorphones (Jasiewicz & Stepinski 2013)
Stream Power Index (Moore et al. 1991)	LS Factor (Moore et al. 1991)
Terrain Classification Index for Lowlands (Bock et al. 2007)	Topographic Position Index (Guisan et al. 1999, Jenness 2006)
Topographic Wetness Index (Beven & Kirkby 1979)	Vertical Distance to Channel Network (Conrad 2005)
Elevation (height above sea level; a.s.l) (DLR 2012)	

2.5 *Topographic Indices*

A track of the shuttle radar topography mission X-band (SRTM-X) digital elevation model (DEM) with 25 m ground resolution covers the study area. To eliminate the noise in the SRTM-X DEM, a multidirectional Lee filter was applied to preserve topographic features (Lee 1980). Different topographic indices (Tab. 3) were derived from the DEM to serve as independent features in the classification. The indices are used to characterize the topographic conditions of the Manyara Bed's location. The selected indices are listed in Tab. 3.

2.6 *Training and Reference Data*

As reference for this study, 498 ground reference points were collected during field campaigns between 2010 and 2014. Because of the time gap between the acquisition of the ASTER scene and the reference point selection, all points were taken with care even though the landscape is considered as relatively stable in relation to the ground resolution of the ASTER and SRTM-X data. Moreover, we assume that the mineral components of the Manyara Beds are conservative, means that in the study area environment they will change insignificantly over such a time period.

Some parts in the south and southeast of the study area are remote and partly inaccessible. Therefore, we applied a random clustered sampling strategy. The reference points are imbalanced with 40 points describing the UMBs, 139 points describing the LMBs, and 320 points with dissimilar landcover. To the latter class we refer to as "other landcover", which involves a rather complete reference selection of soils, minerals and vegetation within the study area, which were merged to take into account a potential landcover change. UMBs are not as abundant in the field as LMBs, which are the more important sediments for the reconstruction of the paleolake history. 20% of points from each class were randomly selected to serve exclusively as test datasets. Soils which are adjacent to or developed from the Manyara Beds were not classified as Manyara Beds. Reference points were collected describing the relative spatial distribution of the Manyara Beds with a minimum size of at least the VNIR resolution (15 m^2) for the UMBs and at least 30 m^2 for LMBs and "other landcover". The relatively small area for the UMBs was defined because they generally appeared as small sections or outcrops of red tuffs on the valley slopes.

3 Methodology

3.1 *Support Vector Machines*

The concept of support vector machines (SVM) based supervised classification originates from machine learning methodology and was introduced by Vapnik (1995, 1999). Due to different characteristics, the SVM algorithm has become very popular for pattern recognition and classification (Foody & Mathur 2004). While most remote sensing classification methods are mainly based on statistical properties of pixel and objects, SVMs maximizes the boundaries between intended classes. The problem of linear separating classes in an n-dimensional feature space, resulting from multiple independent input features is solved by applying kernel functions. By maximizing the margin between classes, an optimal separating hyperplane is strived for (Burges 1998, Hearst 1998). Only a small selection of feature values in the training data, which are close to the margin, are needed to define the hyperplane. These features are referred to as support vectors. Too many outliers within the training dataset would result in an over-fitting of the hyperplane. The cost parameter *C* determines a penalty for the support vectors which excludes outliers and results in a so called "soft margin". *C* controls thereby the balance between over-fitting (high values) and generalization (low values) of the maximum margin and must be selected carefully (Vapnik 1995 & 1999, Schölkopf & Smola 2002, Foody & Mathur 2004).

For this analysis, support vector classifier (C-SVC) from the *Library for Support Vector Machines* (LIBSVM) developed by Chang & Lin (2011) was utilized. It implements a "one-against-one" approach, which builds a classifier for each target value pair. The classification was conducted with a linear kernel and

the radial basis kernel function (RBF) which is widely used when a nonlinear relation is expected (Foody & Mathur 2004). The width of the RBF or Gaussian kernel is controlled by the constant γ, with high values describing a far reaching influence of the training sample and a low value for influencing the adjacent feature space. A grid search was applied by iteratively cross-validating the accuracy of test data classification, while optimizing the constants *C* and γ. All input feature sets were scaled to the range [-1, +1]. For the selection of features we applied the recursive feature elimination (RFE) technique which is widely used with SVM approaches following Guyon & Elisseeff (2003). In an iterative process the features are weighted according to their ability of discriminating the target classes. At each step the most insignificant features are eliminated recursively.

3.2 *Boosted Regression Trees*

Boosted regression trees (BRT), also known as stochastic gradient boosting (Elith et al. 2006), combine classification and regression trees with the gradient boosting algorithm (Friedman 2001). This method employs a learning algorithm to identify a model that fits best the relationship between a feature set and the class label of the target classes. We ran the model using the free statistical programming language R (R Development Core Team 2008) with the package *adabag* (Alfaro et al. 2013). The boosting algorithm used in *adabag* is the AdaBoost (adaptive boosting) algorithm based on Freund & Schapire (1996). The goal of the algorithm is to improve the accuracy of a tree by combining single predictor variables into classifiers. The points along the tree where the features are split are called nodes. Bagging reduces the variance and hence increases the prediction accuracy by taking repeated samples from the training dataset to build a prediction model and then averages the resulting predictions. Boosting constructs each tree on the original dataset but each tree is grown using information from previously grown trees. When a binary classification problem is extended to a multi-class classification problem, most boosting algorithms have to reduce the multi-class classification problem to multiple binary-class problems. However, the AdaBoost.M1 and the SAMME algorithms extend the AdaBoost algorithm to the multi-class case (Zhu et al. 2009). The difference between the algorithms is the calculation of the α constant, which estimates the error of the classifier for each tree iteration. For binary classifications SAMME is equivalent to AdaBoost.M1. The measure of the relative importance of the input features uses the gain of the Gini index (Alfaro et al. 2013), which measures the divergences between the probability distribution of the values of a feature. Best results for both approaches were achieved with the building of 500 trees and 5 nodes for each tree.

4 Results

The classification of the Manyara Beds for two classes (LMB, "other landcover") and three classes (LMB, UMB, "other landcover") with SVM and BRT was conducted with different sets of input feature combinations. As shown in Tabs. 4 and 5, the nine "Spectral Bands" of ASTER, the derived "Spectral Indices" and "Topographic Indices" derived from the DEM were considered for classification separately. Additionally, we show also the model performance considering "All Features" as well as a "Selection of Features" which were identified for SVM and BRT as the features with the highest importance for solving the classification problem (Fig. 2). The number of relevant features varies between the different methods and parameterizations. The smallest number of features (20) was identified for the SVM with an RBF kernel and the binary classification problem, the highest number (66) for the BRT approaches (Tabs. 4 and 5). The BRT methods stabilized with about 80 trees for the binary classification and for the multi-class problem between 130 and 500, depending on the feature set (Fig. 3).

The highest accuracy with 92% was achieved with SVM (linear kernel) and all "Spectral Bands" as well as "Spectral Indices" and "Topographic Indices" for the binary classification of LMB against "other landcover" (Tab. 4). Both linear and RBF kernels perform for the two classes with similar ac-

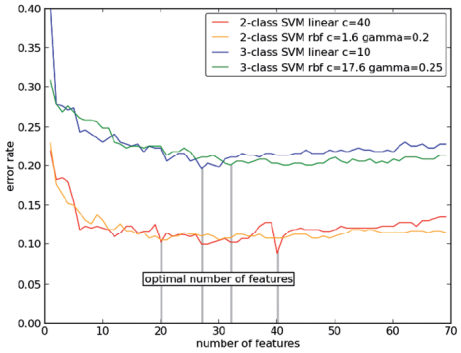

Fig. 2: Relationship between error rate and number of features selected by SVM-RFE.

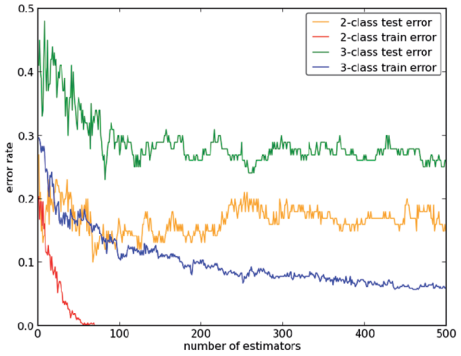

Fig. 3: AdaBoost SAMME error rate in relation to the number of trees for selected features.

Tab. 4: Overall accuracy and applied parameters for SVM and BRT. Binary classification scheme: LMB & "other landcover". Highest overall accuracy displayed in boldface (no = number of features).

	Spectral Bands (no: 9)	Spectral Indices (no: 35)	Topographic Indices (no: 25)	All Features (no: 69)	Selected Features
SVM linear	85% *C*: 75	86% *C*: 8	86% *C*: 8	**92%** *C*: 50	91% (no: 40) *C*: 40
SVM RBF	84% *C*: 29 γ: 1.5	87% *C*: 39.5 γ: 0.135	88% *C*: 50 γ: 1	89% *C*: 1.5 γ: 0.16	89% (no: 20) *C*: 1.6 γ: 0.2
BRT AdaBoost.M1	82%	85%	86%	89%	90% (no: 66)

Tab. 5: Overall accuracy and applied parameters for SVM and BRT. Three-class classification scheme: LMB, UMB & "other landcover". Highest overall accuracy displayed in boldface (no = number of features).

	Spectral Bands (no: 9)	Spectral Indices (no: 35)	Topographic Indices (no: 25)	All Features (no: 69)	Selected Features
SVM linear	74% *C*: 2	73% *C*: 4	72% *C*: 8	79% *C*: 1.5	**80%** (no: 27) *C*: 10
SVM RBF	75% *C*: 20 γ: 1.6	78% *C*: 12.5 γ: 0.105	73% *C*: 3 γ: 0.15	**80%** *C*: 3 γ: 0.235	**80%** (no: 32) *C*: 17.6 γ: 0.25
BRT AdaBoost.M1	75%	76%	72%	78%	78% (no: 66)
BRT SAMME	72%	75%	73%	79%	79% (no: 66)

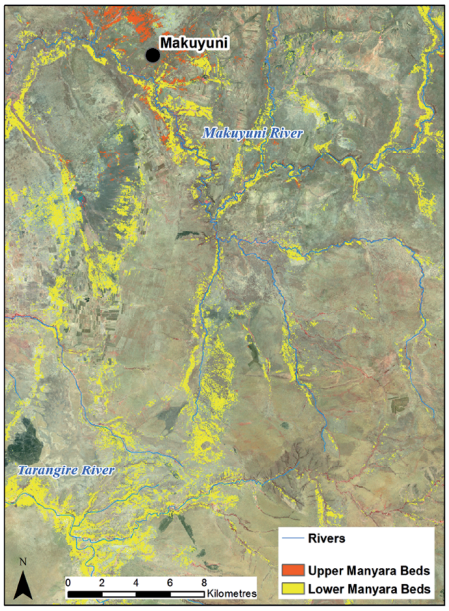

Fig. 4: Three-class SVM RBF result with "All Features", ASTER false colour infrared image (near-infrared, red, green) as background.

curacies. Only for the classification with "All Features" and the "Selected Features" the linear kernel can achieve a higher accuracy. The accuracies show a slightly lower performance for BRT than for both SVM methods.

When expanding the classification problem with the LMBs as the third class the overall accuracy drops with all possible combinations. The RBF kernel and the linear kernel perform similarly well and achieve 80% accuracy with "All Features" (Tab. 5). Fig. 4 shows the associated spatial distribution of the LMBs and UMBs. Stratigraphic units with similar topographic and spectral properties compared to the LMBs were identified in the south of the study area in the Tarangire River valley and further east in the Makuyuni River valley.

5 Discussion

In comparing the SVM classifier with linear and RBF kernels, as well as with the BRT AdaBoost.M1, results show that the binary classification problem can be solved with high accuracies of up to 92%. Regarding the binary

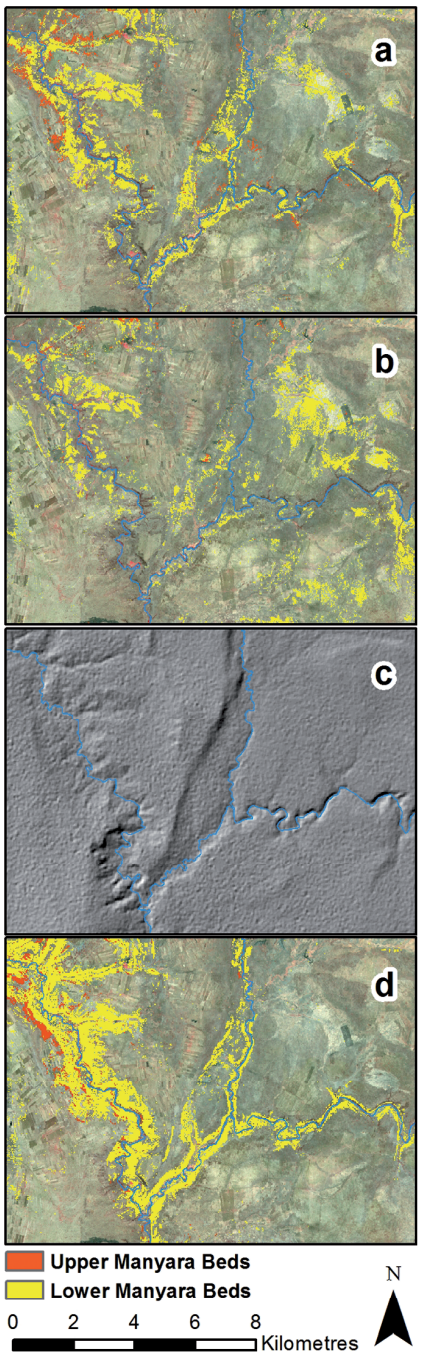

Fig. 5: Three-class SVM RBF comparison of different input features. ASTER false colour infrared image as background; a) SVM RBF with "All Features"; b) SVM RBF with 9 "Spectral Bands" of ASTER; c) hillshade of DEM; d) SVM RBF with "Topographic Indices".

classification problem, the linear and the RBF kernels yielded a very good performance. The BRT model performs marginally lower, but also at a high level. By enlarging the classification problem to three classes the overall accuracy drops by nearly 12% on average (Tabs. 4 and 5). The small number of UMB training features and their irregular spatial distribution result in an imbalanced training set and cause a lower overall accuracy. As for the three-class classification, the SVM with the RBF kernel as well as the SVM paired with the linear kernel perform slightly better than the BRT methods. The SVM three-class problem requires a higher generalization, leading to a wider hyperplane margin. The SVM binary problem however displays no such requirement (lower C values).

"Spectral Bands", "Spectral Indices" and "Topographic Indices" may be used as input features to explain the location of LMBs and UMBs. Both SVM methods perform similarly when using "All Features" and the RFE-"Selected Features". The same is true for the BRT methods. When using only "Topographic Indices" the binary classification approach detects the distribution of the Lower Manyara Beds better than with spectral information. Though for the three-class approach, the Lower and the Upper Manyara Beds seem to be separated better by spectral input features. "Spectral Bands" and "Spectral Indices" identify areas where the spectral information of the target classes is not (or only marginally) disturbed by heterogeneous land cover (Fig. 5b). The use of solely "Topographic Indices" results in a separation of the different topographic positions of the Manyara Beds within the study area (Fig. 5c, d). Consequently, the "Topographic Indices" with the multiclass scheme achieved the lowest accuracies because the topographic characteristics of the LMBs and the UMBs partly overlap. Accordingly, the combination of both spectral and topographic features best explains the distribution of the Manyara Beds (Fig. 5a).

Several optimized feature sets were identified which explain the distribution of the target classes with the training data (Fig. 2). Eight input features are common in all optimized feature sets (Tab. 6). The spectral feature VNIR Green (ASTER band 1) correlates with the

Tab. 6: Features which are common in all feature selection results.

VNIR Green	SWIR 6
Opaque Index	Stream Power Index
Multiresolution Index of Valley Bottom Flatness	Positive Openness
Plan Curvature	Elevation (height a.s.l.)

Manyara Beds. The spectral "Opaque Index" (Cudahy 2012) is sensitive to magnetite-bearing rocks, maghemite gravels, and manganese oxides. Whether the value distribution of the "Opaque Index" for this ASTER scene results from those specific absorption features can only be determined through further laboratory analysis or field spectroscopy. The spectral reflection characteristics may also result from other materials. The topographic information "Elevation (height a.s.l.)" describes the deposition on a distinct paleolake level. The topographic index "Positive Openness" expresses the degree of geometric dominance of one or several convex relief features. It therefore accurately highlights elevated areas (Yokoyama et al. 2002). "Plan Curvature" differentiates between ridges and valleys and may describe the incision of streams and gully systems into the lacustrine sediments. The "Multiresolution Index of Valley Bottom Flatness" (Gallant & Dowling 2003) may describe the depositional areas of the Manyara Beds.

Lacustrine sediments similar to the LMB are identified in the eastern part of the study area. After the first classification results we conducted a field check proving the predicted lacustrine sediments in the eastern part of the study area. In addition, vertebrate fossils are abundant at this location. Since the elevation of these sediments is higher than the LMBs, their elevation can be explained by a tectonic downshift of the block with the LMB as is proposed by Schwartz et al. (2012). This must have happened after or during the sedimentation of the Manyara Beds. The second explanation would propose a lake or swamp situation parallel to the paleolake Manyara. A gneissic ridge that is incised today by the Makuyuni River would have functioned as a barrier. The drainage of this lake was directed into the Tarangire River

in the south. Knick points of tributary river valleys indicate a change of the drainage direction. The third possibility would be a combination of both scenarios. For a further deciphering of the lake history a better dating of volcanic ridges and tuffs is needed.

6 Conclusions

This paper focused on a comparison between SVM and BRT methods, as well as the use of different sets of input features. All methods had performed with similar overall accuracies for the multi-class and the binary problem respectively. The best results were obtained using all spectral and topographic features to explain the distribution of the Manyara Beds. The highest accuracy for the binary classification of LMBs and "other landcover" were achieved with the SVM method and a linear kernel. For the classification of three classes (LMBs, UMBs, "other landcover") the SVM method with a RBF, as well as with a linear kernel performed best. In the case of the Lake Manyara area, small scale lithostratigraphic units could be delineated in a challenging environment, which entails a heterogeneous landcover with spectral similarity between different soils and a patchy vegetation cover. Besides the already known finding localities, new sites with paleolake sediments east of Makuyuni could be identified and may contribute to assessing the paleolake history of Lake Manyara. Lacustrine sediments in the south of the study area have to be validated in the field and their paleontological importance must be evaluated.

Acknowledgements

We would like to thank the editor and the reviewers for their time and valuable remarks. This study was financed by the Heidelberg Academy of Sciences and Humanities research center: "The Role of Culture in Early Expansions of Humans" (ROCEEH). The ASTER L1B data were obtained through the online Data Pool at the NASA Land Processes Distributed Active Archive Center (LP DAAC), USGS/Earth Resources Observation and Science (EROS) Center, Sioux Falls, South Dakota, USA. We would like to thank the DLR and the German Remote Sensing Data Center (DFS) for providing the SRTM/X-SAR data.

References

Alfaro, E., Gamez, M. & García, N., 2013: adabag: An R Package for Classification with Boosting and Bagging. – Journal of Statistical Software **54** (2): 1–35.

Al-Khaier, F., 2003: Soil Salinity Detection Using Satellite Remote Sensing. – Thesis, ITC Enschede, Netherlands.

Bachofer, F., Quénéhervé, G. & Märker, M., 2014: The Delineation of Paleo-Shorelines in the Lake Manyara Basin Using TerraSAR-X Data. – Remote Sensing **6** (3): 2195–2212.

Beven, K. & Kirkby, M.J., 1979: A physically based, variable contributing area model of basin hydrology. – Hydrological Sciences Journal **24** (1): 43–69.

Bierwirth, P., 2002: Evaluation of ASTER Satellite Data for Geological Applications. – Consultancy Report to Geoscience Australia.

Bock, M., Böhner, J., Conrad, O., Köthe, R. & Ringeler, A., 2007: XV. Methods for creating Functional Soil Databases and applying Digital Soil Mapping with SAGA GIS. – JRC Scientific and technical Reports, Office for Official Publications of the European Communities, Luxemburg.

Boehner, J. & Conrad, O., 2008: Terrain Parameters described in the SAGA-GIS Software, v.2.1.0. http://sourceforge.net/projects/saga-gis/files/latest/download?source=files (16.6.2014).

Burges, C., 1998: A Tutorial on Support Vector Machines for Pattern Recognition. – Data Mining and Knowledge Discovery **2** (2): 121–167.

Casanova, J. & Hillaire-Marcel, C., 1992: Chronology and paleohydrology of late Quaternary high lake levels in the Manyara basin (Tanzania) from isotopic data (18O, 13C, 14C, ThU) on fossil stromatolites. – Quaternary Research **38** (2): 205–226.

Chan, J.C.-W. & Paelinckx, D., 2008: Evaluation of Random Forest and Adaboost tree-based ensemble classification and spectral band selection for ecotope mapping using airborne hyperspectral imagery. – Remote Sensing of Environment **112** (6): 2999–3011.

Chang, C.C. & Lin, C.J., 2011: LIBSVM: A library for support vector machines. – ACM Transac-

tions on Intelligent Systems and Technology **2** (3): 1–27.

Conrad, O., 2005: Terrain Parameters described in the SAGA-GIS Software, v.2.1.0. http://sourceforge.net/projects/saga-gis/files/latest/download?source=files (16.6.2014).

Cudahy, T., 2012: Satellite ASTER Geoscience Product. – Notes for Australia; CSIRO: http://c3dmm.csiro.au/WA_ASTER/WA%20ASTER%20Geoscience%20Product%20Notes%2015112011.pdf (16.6.2014).

Deus, D., Gloaguen, R. & Krause, P., 2013: Water Balance Modeling in a Semi-Arid Environment with Limited in situ Data Using Remote Sensing in Lake Manyara, East African Rift, Tanzania. – Remote Sensing **5** (4): 1651–1680.

Dikau, R., 1988: Entwurf einer geomorphographisch-analytischen Systematik von Reliefeinheiten. – Heidelberger Geographische Bausteine, Heidelberg.

DLR, 2012: SRTM X-SAR Digital Elevation Models. Status: 2012-09-28. http://eoweb.dlr.de:8080/eoweb-ng/licenseAgreements/DLR_SRTM_Readme.pdf (23.12.2013).

Elith, J., Graham, C.H., Anderson, R.P., Dudík, M., Ferrier, S., Guisan, A., Hijmans, R.J., Huettmann, F., Leathwick, J.R., Lehmann, A., Li, J., Lohmann, L.G., Loiselle, B.A., Manion, G., Moritz, C., Nakamura, M., Nakazawa, Y., Overton, J.M.M., Townsend Peterson, A., Phillips, S.J., Richardson, K., Scachetti-Pereira, R., Schapire, R.E., Soberón, J., Williams, S., Wisz, M.S. & Zimmermann, N.E., 2006: Novel methods improve prediction of species' distributions from occurrence data. – Ecography **29** (2): 129–151.

Elith, J., Leathwick, J.R. & Hastie, T., 2008: A working guide to boosted regression trees. – Journal of Animal Ecology **77** (4): 802–813.

Elmahdy, S.I., 2012: Hydromorphological Mapping and Analysis for Characterizing Darfur Paleolake, NW Sudan Using Remote Sensing and GIS. – International Journal of Geosciences **2012** (3): 25–36.

ElSheikh, A., Abdelsalam, M.G. & Mickus, K., 2011: Geology and geophysics of the West Nubian Paleolake and the Northern Darfur Megalake (WNPL-NDML): Implication for groundwater resources in Darfur, northwestern Sudan. – Journal of African Earth Sciences **61** (1): 82–93.

Esch, T., Himmler, V., Schorcht, G., Thiel, M., Wehrmann, T., Bachofer, F., Conrad, C., Schmidt, M. & Dech, S., 2009: Large-area assessment of impervious surface based on integrated analysis of single-date Landsat-7 images and geospatial vector data. – Remote Sensing of Environment **113** (8): 1678–1690.

Foody, G.M. & Ajay, M., 2004: A relative evaluation of multiclass image classification by support vector machines. – IEEE Transactions on Geoscience and Remote Sensing **42** (6): 1335–1343.

Foody, G.M. & Mathur, A., 2004: Toward intelligent training of supervised image classifications: directing training data acquisition for SVM classification. – Remote Sensing of Environment **93** (1–2): 107–117.

Freund, Y. & Schapire, R.E., 1996: Experiments with a New Boosting Algorithm. – Thirteenth International Conference on Machine Learning, 148–156, Bari, Italy.

Friedman, J.H., 2001: Greedy function approximation: a gradient boosting machine. – Annals of Statistics, 1189–1232.

Frost, S.R., Schwartz, H.L., Giemsch, L., Morgan, L.E., Renne, P.R., Wildgoose, M., Saanane, C., Schrenk, F. & Harvati, K., 2012: Refined age estimates and Paleoanthropological investigation of the Manyara Beds, Tanzania. – Journal of Anthropological Sciences **90:** 1–12.

Fujisada, H., 1995: Design and performance of ASTER instrument. – SPIE, the Advanced and Next generation Satellites **2583:** 16–25, Paris, France.

Gaber, A., Ghoneim, E., Khalaf, F. & El-Baz, F., 2009: Delineation of paleolakes in the Sinai Peninsula, Egypt, using remote sensing and GIS. – Journal of Arid Environments **73** (1): 127–134.

Gallant, J.C. & Dowling, T.I., 2003: A multiresolution index of valley bottom flatness for mapping depositional areas. – Water Resources Research **39** (12): 1347.

Gessner, U., Machwitz, M., Conrad, C. & Dech, S., 2013: Estimating the fractional cover of growth forms and bare surface in savannas. A multi-resolution approach based on regression tree ensembles. – Remote Sensing of Environment **129:** 90–102.

Ghoneim, E., Benedetti, M. & El-Baz, F., 2012: An integrated remote sensing and GIS analysis of the Kufrah Paleoriver, Eastern Sahara. – Geomorphology **139–140:** 242–257.

Gómez, C., Wulder, M.A., Montes, F. & Delgado, J.A., 2012: Modeling Forest Structural Parameters in the Mediterranean Pines of Central Spain using QuickBird-2 Imagery and Classification and Regression Tree Analysis (CART). – Remote Sensing **4** (1): 135–159.

Guisan, A., Weiss, S. & Weiss, A., 1999: GLM versus CCA spatial modeling of plant species distribution. – Plant Ecology **143** (1): 107–122.

Guyon, I. & Elisseeff, A., 2003: An Introduction to Variable and Feature Selection. – Journal of Machine Learning Research **3:** 1157–1182.

Hahn, C. & Gloaguen, R., 2008: Estimation of soil types by non linear analysis of remote sensing

data. – Nonlinear Processes in Geophysics **15** (1): 115–126.

Hearst, M.A., 1998: Support Vector Machines. – IEEE Intelligent Systems **13** (4): 18–28.

Hewson, R.D., Cudahy, T.J., Mizuhiko, S., Ueda, K. & Mauger, A.J., 2005: Seamless geological map generation using ASTER in the Broken Hill-Curnamona province of Australia. – Remote Sensing of Environment **99** (1–2): 159–172.

Hjerdt, K.N., Mcdonnell, J.J., Seibert, J. & Rodhe, A., 2004: A new topographic index to quantify downslope controls on local drainage. – Water Resources Research **40** (5): W05602.

Hudak, A.T., Robichaud, P., Evans, J.S., Clark, J., Lannom, K., Morgan, P. & Stone, C., 2004: Field validation of Burned Area Reflectance Classification (BARC) products for post fire assessment. – University of Nebraska, Lincoln, NE, USA.

Iwasaki, A., Fujisada, H., Akao, H., Shindou, O. & Akagi, S., 2002: Enhancement of spectral separation performance for ASTER/SWIR. – SPIE, Infrared Spaceborne Remote Sensing **IX 4486:** 42–50, San Diego, CA, USA.

Jasiewicz, J. & Stepinski, T.F., 2013: Geomorphons – a pattern recognition approach to classification and mapping of landforms. – Geomorphology **182:** 147–156.

Jenness, J., 2006: Topographic Position Index (TPI) v.1.3a. – TPI_Documentation.pdf. http://www.jennessent.com/arcview/tpi.htm (17.6.2013).

Kaiser, T.M., Seiffert, C., Hertler, C., Fiedler, L., Schwartz, H.L., Frost, S.R., Giemsch, L., Bernor, R.L., Wolf, D., Semprebon, G., Nelson, S.V., Schrenk, F., Harvati, K., Bromage, T.G. & Saanane, C., 2010: Makuyuni, a new Lower Palaeolithic Hominid Site in Tanzania. – Mitteilungen Hamburgisches Zoologisches Museum und Institut **106:** 69–110.

Keller, C.M., Hansen, C. & Alexander, C.S., 1975: Archaeology and Paleoenvironments in the Manyara and Engaruka Basins, Northern Tanzania. – Geographical Review **65** (3): 364–376.

Lee, J.S., 1980: Digital image enhancement and noise filtering by use of local statistics. – IEEE Transactions on Pattern Analysis and Machine Intelligence **2** (2): 165–168.

Moore, I.D., Grayson, R.B. & Ladson, A.R., 1991: Digital terrain modelling: A review of hydrological, geomorphological, and biological applications. – Hydrological Processes **5** (1): 3–30.

Mountrakis, G., Im, J. & Ogole, C., 2011: Support vector machines in remote sensing: A review. – ISPRS Journal of Photogrammetry and Remote Sensing **66** (3): 247–259.

Mulder, V.L., De Bruin, S., Schaepman, M.E. & Mayr, T.R., 2011: The use of remote sensing in soil and terrain mapping – A review. – Geoderma **162** (1–2): 1–19.

Ninomiya, Y., Fu, B. & Cudahy, T.J., 2005: Detecting lithology with Advanced Spaceborne Thermal Emission and Reflection Radiometer (ASTER) multispectral thermal infrared "radiance-at-sensor" data. – Remote Sensing of Environment **99** (1–2): 127–139.

Pal, M. & Mather, P.M., 2003: An assessment of the effectiveness of decision tree methods for land cover classification. – Remote Sensing of Environment **86** (4): 554–565.

Pal, M. & Foody, G.M., 2010: Feature Selection for Classification of Hyperspectral Data by SVM. – IEEE Transactions on Geoscience and Remote Sensing **48** (5): 2297–2307.

Pour, A.B. & Hashim, M., 2011: Application of advanced spaceborne thermal emission and reflection radiometer (ASTER) data in geological mapping. – International Journal of the Physical Sciences **6** (33): 7657–7668.

Prendergast, M.E., Mabulla, A.Z.P., Grillo, K.M., Broderick, L.G., Seitsonen, O., Gidna, A.O. & Gifford-Gonzalez, D., 2013: Pastoral Neolithic sites on the southern Mbulu Plateau, Tanzania. – Azania: Archaeological Research in Africa **48** (4): 498–520.

R Development Core Team, 2008: R: A Language and Environment for Statistical Computing. – R Foundation for Statistical Computing, Vienna, Austria.

Riley, S.J., Degloria, S.D. & Elliot, R., 1999: A Terrain Ruggedness Index that quantifies topographic heterogeneity. – Intermountain Journal of Sciences **5** (1–4): 23–27.

Rouse, J.W., Haas, R.H., Shell, J.A., Deering, D.W. & Harlan, J.C., 1974: Monitoring the vernal advancement of retrogradation of natural vegetation. – Final Report, Type III, NASA/GSFC, Greenbelt, MD, USA.

Rowan, L.C. & Mars, J.C., 2003: Lithologic mapping in the Mountain Pass, California area using Advanced Spaceborne Thermal Emission and Reflection Radiometer (ASTER) data. – Remote Sensing of Environment **84** (3): 350–366.

Rowan, L.C., Mars, J.C. & Simpson, C.J., 2005: Lithologic mapping of the Mordor, NT, Australia ultramafic complex by using the Advanced Spaceborne Thermal Emission and Reflection Radiometer (ASTER). – Remote Sensing of Environment **99** (1–2): 105–126.

Schlüter, T., Kohring, R. & Mehl, J., 1992: Hyperostotic fish bones ("Tilly bones") from presumably Pliocene phosphorites of the Lake Man-

yara area, northern Tanzania. – Paläontologische Zeitschrift **66** (1–2): 129–136.

Schölkopf, B. & Smola, A.J., 2002: Learning with kernels: support vector machines, regularization, optimization, and beyond. – MIT Press, Cambridge, MA, USA.

Schwartz, H., Renne, P.R., Morgan, L.E., Wildgoose, M., Lippert, P.C., Frost, S.R., Harvati, K., Schrenk, F. & Saanane, C., 2012: Geochronology of the Manyara Beds, northern Tanzania: New tephrostratigraphy, magnetostratigraphy and 40Ar/39Ar ages. – Quaternary Geochronology **7:** 48–66.

Travis, M.R., Elsner, G.H., Iverson, W.D. & Johnson, C.G., 1975: VIEWIT: computation of seen areas, slope, and aspect for land-use planning. – Report PSW-11, Berkeley, CA, USA.

Tucker, C.J., 1979: Red and photographic infrared linear combinations for monitoring vegetation. – Remote Sensing of Environment **8** (2): 127–150.

Vapnik, V.N., 1995: The nature of statistical learning theory. – Springer, New York, NY, USA.

Vapnik, V.N., 1999: An overview of statistical learning theory. – Neural Networks, IEEE Transactions **10** (5): 988–999.

Volesky, J.C., Stern, R.J. & Johnson, P.R., 2003: Geological control of massive sulfide mineralization in the Neoproterozoic Wadi Bidah shear zone, southwestern Saudi Arabia, inferences from orbital remote sensing and field studies. – Precambrian Research **123** (2-4): 235–247.

Wang, X., Niu, R. & Wu, K., 2011: Lithology intelligent identification using support vector machine and adaptive cellular automata in multispectral remote sensing image. – Optical Engineering **50** (7): 076201, 1–12.

Yamaguchi, Y., Kahle, A.B., Tsu, H., Kawakami, T. & Pniel, M., 1998: Overview of Advanced Spaceborne Thermal Emission and Reflection Radiometer (ASTER). – IEEE Transactions on Geoscience and Remote Sensing **36** (4): 1062–1071.

Yokoyama, R., Shirasawa, M. & Pike, R.J., 2002: Visualizing topography by openness: a new application of image processing to digital elevation models. – Photogrammetric engineering and remote sensing **68** (3): 257–266.

Zevenbergen, L.W. & Thorne, C.R., 1987: Quantitative analysis of land surface topography. – Earth Surface Processes and Landforms **12** (1): 47–56.

Zhu, J., Zou, H., Rosset, S. & Hastie, T., 2009: Multi-class AdaBoost. – Statistics and its Interface **2:** 349–360.

Address of the Authors:

Dipl.-Geogr. Felix Bachofer, Dipl.-Geogr. Geraldine Quénéhervé, Prof. Dr. Volker Hochschild, Eberhard Karls Universität Tübingen, Geographisches Institut, D-72070 Tübingen, Tel.: +49-7071-29-77528, Fax: +49-7071-29-5378, e-mail: felix.bachofer@uni-tuebingen.de

Dr. Michael Märker, Heidelberger Akademie der Wissenschaften, ROCEEH, D-72070 Tübingen, Tel.: +49-7071-29-72135, e-mail: michael.maerker@geographie.uni-tuebingen.de

Manuskript eingereicht: Juni 2014
Angenommen: September 2014

APPENDIX III: PUBLICATION P3

Multisensoral Topsoil Mapping in the Semiarid Lake Manyara Region, Northern Tanzania.

BACHOFER, F., QUÉNÉHERVÉ, G., HOCHSCHILD, V. & MAERKER, M., 2015 - *Multisensoral Topsoil Mapping in the Semiarid Lake Manyara Region, Northern Tanzania*. Remote Sensing, Vol: 7 (8): 9563-9586 (doi:10.3390/rs70809563).

This research paper is available online at *Multidisciplinary Digital Publishing Institute* (MDPI; www.mdpi.com):

http://www.mdpi.com/2072-4292/7/8/9563

Journal: Remote Sensing
ISSN: 2072-4292
Thomson Reuters Impact Factor 2014: 3.180
Type: Research Article.

Remote Sens. **2015**, *7*, 9563-9586; doi:10.3390/rs70809563

OPEN ACCESS

remote sensing

ISSN 2072-4292

www.mdpi.com/journal/remotesensing

Article

Multisensoral Topsoil Mapping in the Semiarid Lake Manyara Region, Northern Tanzania

Felix Bachofer [1,*], Geraldine Quénéhervé [1], Volker Hochschild [1] and Michael Maerker [2,3]

[1] Institute of Geography, University of Tuebingen, Ruemelinstr. 19-23, 72070 Tuebingen, Germany; E-Mails: geraldine.queneherve@uni-tuebingen.de (G.Q.); volker.hochschild@uni-tuebingen.de (V.H.)

[2] Heidelberg Academy of Sciences and Humanities, Ruemelinstr. 19-23, 72070 Tuebingen, Germany; E-Mail: michael.maerker@geographie.uni-tuebingen.de

[3] Earth Science Department, University of Florence, Via G. La Pira, 50121 Florence, Italy

* Author to whom correspondence should be addressed; E-Mail: felix.bachofer@uni-tuebingen.de; Tel.: +49-7071-29-77528; Fax: +49-7071-29-5378.

Academic Editors: Nicolas Baghdadi and Prasad S. Thenkabail

Received: 21 May 2015 / Accepted: 20 July 2015 / Published: 28 July 2015

Abstract: This study pursues the mapping of the distribution of topsoils and surface substrates of the Lake Manyara area of northern Tanzania. The nine soil and lithological target classes were selected through fieldwork and laboratory analysis of soil samples. High-resolution WorldView-2 data, TerraSAR-X intensity data, medium-resolution ASTER spectral bands and indices, as well as ENVISAT ASAR intensity and SRTM-X-derived topographic parameters served as input features. Objects were derived from image segmentation. The classification of the image objects was conducted applying a nonlinear support vector machine approach. With the recursive feature elimination approach, the most input-relevant features for separating the target classes were selected. Despite multiple target classes, an overall accuracy of 71.9% was achieved. Inaccuracies occurred between classes with high $CaCO_3$ content and between classes of silica-rich substrates. The incorporation of different input feature datasets improved the classification accuracy. An in-depth interpretation of the classification result was conducted with three soil profile transects.

Keywords: topsoil mapping; ASTER; SAR; WorldView-2; topographical indices; multisensoral; SVM; multiscale

1. Introduction

The spatial distribution of soils and lithology provides essential input information for different scientific and economic applications, including landscape reconstruction [1], digital soil mapping (DSM) and mineral exploration for agricultural [2] or mining applications [3]. Though the soil must be considered as a three dimensional medium, a wide range of remote sensing sensors provide useful information in assessing various details of the mineral composition and other physical and/or chemical properties of the uppermost parts of the soils, as well as for spatially contiguous areas [4–6]. The topsoil is generally the most relevant part of the soil, considering food production, degradation and soil management [7]. Although the definition of topsoil varies in different soil taxonomies [7–10], the uppermost part of the soil belongs to the topsoil. The topsoil thickness is related to local conditions of pedogenesis, erosion and deposition processes. Normally, topsoil is characterized by a thickness of 10–30 cm [7,8]. In this study, we regard the soil surface properties as topsoil/lithology proxy. We hypothesize that the analysis of physical-chemical properties, the collection of field reference data and the remote sensing analysis of the upper surface strata yield valuable information about the topsoil and/or lithologic characteristics. Moreover, the topographic position and geomorphological processes also influence the topsoil characteristics and, hence, should be included in a comprehensive analysis of the spatial distribution of topsoils.

The surface reflectance of the mineral composition of a surface, which is received by a multi- or hyper-spectral sensor, is influenced by soil organic matter, moisture content, as well as texture and surface roughness [11]. Backscatter signals from Synthetic Aperture Radar (SAR) sensors of different wavelengths are dependent on the surface roughness and are sensitive to the dielectric properties of soils [12–14]. Soil mapping using remote sensing data show limitations due to the complex physical and chemical nature of soils. Remotely derived datasets can characterize the surface (optical remote sensing systems) or the uppermost part of soils (SAR systems) [5,15]. Since soils are complex three-dimensional structures, the surface characteristics may not represent the underlying layers of soil. The remote sensing signal may also be a product of different soil surface properties. This effect will increase with a lower spatial resolution of the datasets. Very high-resolution sensors, like WorldView-2 and GeoEye-1, provide a high spatial differentiation. On the other hand, lower spatial resolution sensors, like the Landsat series or ASTER, provide a better spectral coverage, especially in the mid-infrared region, which is important for mineral mapping purposes [5,16]. Vegetation cover is another important factor to consider. Already sparse vegetation cover may influence the identification of soil attributes using remote sensing methods [17,18]. Spectral indices from multi- or hyper-spectral remote sensing images are effective tools for the classification and evaluation of photosynthetic vegetation activity. Vegetation indices (VI), like the Normalized Difference Vegetation Index (NDVI), utilize the difference of absorption and reflection in the spectral wavelengths of the red (0.625–0.74 μm) and near-infrared (IR; 0.74–1 μm) [19]. Dead materials in grasslands blur VI, making it hard to distinguish between dead materials and some other land cover [20]. This is especially a problem in arid and semiarid regions, due to relatively long dry periods. A strategy to resolve these problems consists of long-term monitoring via remote sensing and collection of ground information [21,22].

A wide range of studies proved the applicability of techniques using remote sensing data for topsoil mapping. In the following, some of them are described. Landsat 5 TM imagery was used to detect basalt

outcrops for supporting soil mapping, applying reflectance values, band ratios and indices [23]. Landsat 7 ETM+ data were used to determine surface soil properties with the help of laboratory-analyzed surface soil samples [24]. The ASTER multispectral bands and derived indices and ratios were often utilized for lithological mapping [25–28]. ASTER data were also used to identify mineral components in tropical soils using reflectance spectroscopy signatures from soil samples [29].

Various studies include additional variables, especially in geostatistical approaches of the spatial soil distribution [5]. Topographical features, in particular, provide information on the terrain and, hence, on soil formation processes [30]. Mulder *et al.* [31] used ASTER data and derivatives, as well as elevation as topographical proxy for DSM. Hahn and Gloaguen [32] compared different input variable combinations of ASTER-derived land use, geology, topographical parameters and others to estimate soil distribution by support vector machines (SVM). Rossel and Chen [33] used Landsat data and derivatives, topographical derivatives, climate parameters, as well as soil, geological and radiometric maps and spectrometry results from soil samples to determine the surface soil properties for Australia. Selige *et al.* [34] found out that soil organic matter and soil texture of topsoil correlate with the spectral properties of a hyperspectral sensor. They were also able to model the distribution of sand, clay, organic carbon (C_{org}) and nitrogen. SAR backscatter intensity information from X-, C- and L-band sensors proved to be sensitive for soil moisture differences, surface roughness and, to some extent, also to soil texture [13,14,35–41]. Hengl *et al*. [42] applied an automated random forest approach to map soil properties of Africa with DEM-based landforms parameters and MODIS data at a spatial resolution of 250 m for the Africa Soil Information Service (AfSIS) project. A comprehensive overview about remote sensing in soil mapping is provided by Mulder *et al.* [5] and with a special focus on Africa by Dewitte *et al*. [6].

The lithologies and the soils of the Lake Manyara basin have complex genetic origins. The Proterozoic gneissic basement, tectonic and volcanic processes, as well as the (paleo-)hydrological processes and the sedimentation of the paleolake Manyara influence soil formation. This results in a small-scale distribution and fuzzy transitions of today's soils, topsoils and outcropping lithology, which cannot be depicted by the available soil map for the region with a scale of 1:2,000,000 [43]. Consequently, the categorization of soils is a complex process due to their three-dimensional nature. Hence, remotely-sensed surface features yield auxiliary information of topsoil characteristics and their distribution. Combined with topographic information, the analysis results in valuable information that allows also a rough identification of soil types.

The aim of this study is to map the distribution of the topsoil and surface substrate characteristics using multispectral, topographical and SAR input data. The laboratory analysis of surface samples provides soil properties used to categorize and characterize the topsoils and surface substrates. In order to improve the topsoil classification, we followed a multiscale approach using: (i) image object segments from a high-resolution WorldView-2 scene; (ii) low-resolution ASTER multispectral data and indices; (iii) X- and C-band SAR backscatter; as well as (iv) topographical derivatives. We compare and discuss the final mapping results with soil catenae covering characteristic transects of the study area.

2. Study Area

The study area is located within the East African Rift System of northern Tanzania; in the surroundings of the Makuyuni village. The area is drained towards the west by the Makuyuni River

disemboguing into the endorheic Lake Manyara Basin (Figure 1). The precipitation calculations from the daily Rainfall Estimate Product 3B42 (V7) of the Tropical Rainfall Measurement Mission (TRMM) show a bimodal rainfall pattern for the years 2000–2013 [44]. For this period, the average annual precipitation of 651 mm is mainly caused by two wet seasons. One occurs between November and January and a second between March and May [45]. This results in a sparsely-vegetated semiarid environment dominated by bushy grassland. The study area is also characterized by a variety of degradation processes due to long dry periods and short, but intensive rainfall events, as well as contributing anthropological factors, like overgrazing [46].

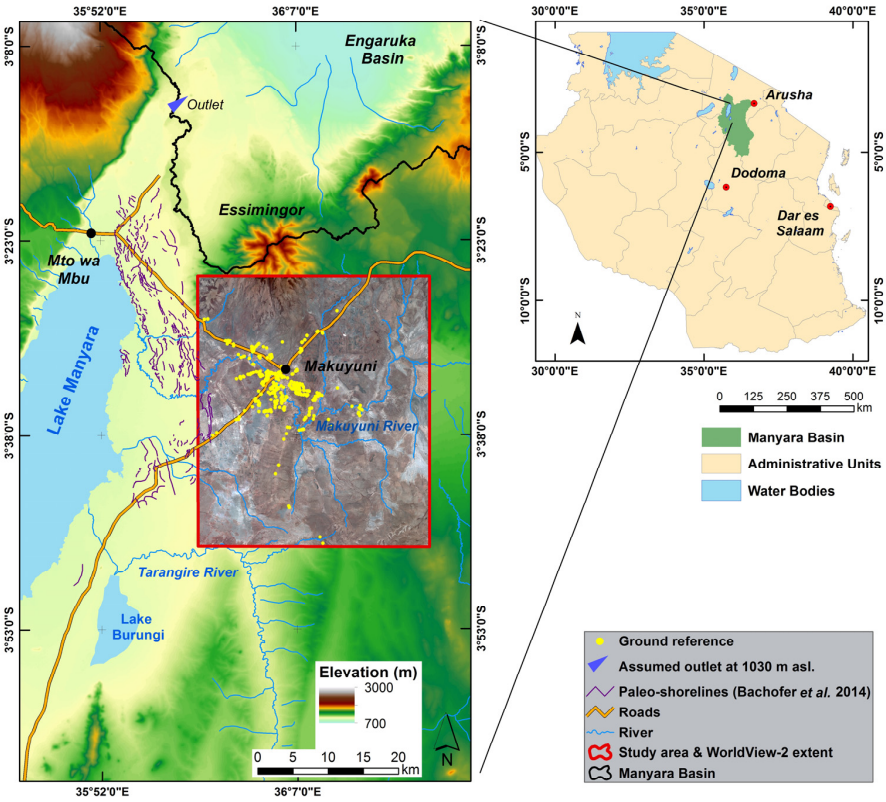

Figure 1. Study area.

The lithology of the study area is very complex, because different lithological units interleave here. The underlying basement of the Masai Plateau is formed of Proterozoic intermediate quartzite and gneisses and is exposed by tectonic faults [47]. Explosive volcanism, especially from the volcano Essimingor, and faulting associated with the rifting of the basin produced alkaline lavas, like alkali basalt, phonolite, nephelinite and tuffs. The volcano Ol Doinyo Lengai (90 km north of the study area) has a carbonate volcanism, and its carbonate tephra deposits are widespread [47–49]. Lacustrine and fluvially deposited sediments can be found 140 m above today's level of Lake Manyara. The so-called Manyara Beds crop out where the Makuyuni River and gully system incise into the lacustrine and terrestrial deposits. The lower member of the Manyara Beds is of lacustrine origin and is composed mainly of mudstones, siltstones, diatomites, marls and tuff that have been deposited in a reducing

environment. These sediments have an age of approximately 1.03–0.633 Ma. A tephra layer, which was dated to 0.633 Ma, marks the transition of the younger upper member of the Manyara Beds [50–52].

3. Input Data and Pre-Processing

Multiscale remote sensing data and their derivatives, as well as topographic indices delineated from a Shuttle Radar Topography Mission (SRTM) DEM served as input information for the analysis. All image datasets were co-registered to ensure complementary datasets.

3.1. WorldView-2

WorldView-2 is a commercial multispectral sensor, which was launched in October 2009. It has a very high geometrical resolution for its' eight multispectral bands (MS) at 1.85 m ground resolution and for the panchromatic band of 0.46 m at nadir [53]. The scene was acquired on 21 February 2011 (Table 1); following the winter wet season and a strong precipitation event mid-February (Figure 2).

Table 1. Optical remote sensing sensors. MS: multispectral.

Sensor	Date	Time (UTC)	No. of Bands	Wavelength	Spatial Resolution
WorldView-2	21 February 2011	08:22	8	0.40–1.04 µm	1.85 m (MS)
ASTER-VNIR	23 August 2006	08:07	3	0.52–0.86 µm	15 m
ASTER-SWIR	23 August 2006	08:07	6	1.60–2.43 µm	30 m

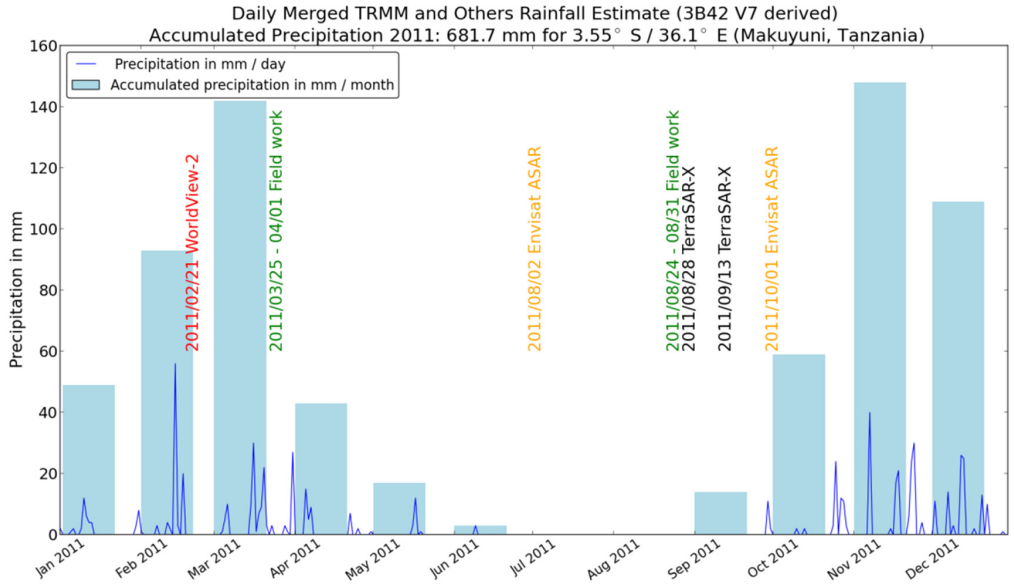

Figure 2. Precipitation, fieldwork and remote sensing data of the year 2011.

3.2. ASTER Bands and Indices

The Advanced Spaceborne Thermal Emission and Reflection Radiometer (ASTER) consists of three subsystems with a spectral coverage in the visible-near infrared (VNIR), the shortwave infrared (SWIR) and the thermal infrared (TIR) wavelength regions (Table 1). ASTER was launched onboard NASA's

TERRA spacecraft in December 1999. The spectral resolution was mainly designed for vegetation, soil and mineral mapping [54]. An ASTER L1B scene was obtained on 23 August 2006 after a long dry season. Because of the cross-detector leakage between the SWIR bands, crosstalk correction was applied using a correction tool from the Earth Remote Sensing Data Applications Centre (ERSDAC) [55].

The six spectral bands of the SWIR system were selected as input features for the analysis. Spectral indices derived from the ASTER VNIR and SWIR bands were also included as input parameters (Table 2). The purpose of these indices is a relative amplification of selective absorption and reflection features, which are caused by different surface materials at distinct wavelengths. They help to detect different mineral compositions, but also to emphasize the spectral differences of target objects. The indices listed in Table 2 are based on a comprehensive literature review.

Table 2. Spectral indices of ASTER VNIR and SWIR bands.

Index with Literature Reference	Formula	Index with Literature Reference	Formula
Alunite/Kaolinite/Pyrophyllite Index [25]	(4 + 6)/5	AlOH Group Index [56]	(5/7)
Alteration/Laterite Index [57]	(4/5)	Alunite Index [28]	(7/5) × (7/8)
Calcite Index [28]	(6/8) × (9/8)	Carbonate/Chlorite/Epidot Index [25]	(7 + 9)/8
Clay—1 Index [25]	(5 + 7)/6	Clay—2 Index [57]	(5 × 7)/(6 × 6)
Dolomite Index [25]	(6 + 8)/7	Ferric Iron (Fe^{3+}) Index [25]	(2/1)
Ferric Oxide Index [56]	(4/3)	Ferrous Iron (Fe^{2+})—1 Index [26]	(1/2)
Ferrous Iron (Fe^{2+})—2 Index [26]	(5/3) + (1/2)	Ferrous Iron/Silicates Index [56]	(5/4)
Kaolinite Index [28]	(4/5) × (8/6)	Kaolin Group Index [56]	(6/5)
Kaolinitic Index [58]	(7/5)	MgOH—1 Index [58]	(6 + 9)/8
MgOH—2 Index [56]	(7/8)	Muscovite Index [58]	(7/6)
OH Bearing Altered Minerals—1 Index [28]	(7/6) × (4/6)	OH Bearing Altered Minerals—2 Index [59]	(4 × 7/6/6)
OH Bearing Altered Minerals—3 Index [59]	(4 × 7/5/5)	Opaque Index [56]	(1/4)
Phengitic Index [58]	(5/6)	Relative Band Depth 6 (RBD6) [26]	(4 + 7)/(6 ×2)
Relative Band Depth 8 (RBD8) [26]	(7 + 9)/(8 × 2)		

3.3. Topographic Indices

During the Shuttle Radar Topography Mission (SRTM) in the year 2000, X-band data were acquired, which provided a DEM with 25 m ground resolution. The SRTM-X dataset has no full coverage worldwide; however, one track covers the study area. The DEM was projected to the Earth Gravitational Model (EGM96) vertical datum. The short wave X-band-derived DEM resulted in good elevation accuracy [60], but also yielded small-scale noise at the surface. To reduce this effect while preserving the topography, we applied a multidirectional Lee filter [61]. The DEM was used to calculate different topographic indices, which characterize the topographic position of the topsoils in the study area (Table 3).

Table 3. Topographic indices.

Index with Literature Reference	Index with Literature Reference
Elevation (height above sea level; a.s.l) [62]	Geomorphons [63]
Slope Length Factor [64]	Morphometric Protection Index [51]
Multiresolution Index of Ridge Top Flatness (MRRTF) [65]	Multiresolution Index of Valley Bottom Flatness [65]
Negative Openness [66]	Positive Openness [51]
Plan Curvature [67,68]	Slope [69]
Stream Power Index [64]	Terrain Classification Index for Lowlands [70]
Terrain Ruggedness Index [71]	Topographic Position Index [72]
Topographic Wetness Index [73]	Vertical Distance to Channel Network [74]

3.4. SAR Data

We acquired two TerraSAR-X (TSX1) (~9.65 GHz; X-band) StripMap and two Envisat ASAR (~5.331 GHz; C-band) scenes for different dates (Table 4). Precise orbits were applied to the ASAR scenes. All SAR scenes were calibrated and radiometrically corrected for topographic effects to gamma naught (γ) using the local incident angle derived from the SRTM-X DEM. The scenes were terrain corrected, and speckle effects were reduced by applying a Lee filter [61]. The two TSX1 scenes were mosaicked to a single dataset in order to cover the whole study area. The images were acquired in the dry season (Table 4; Figure 2), to minimize the influence of soil moisture on the backscatter intensity signal [36–38,75].

Table 4. SAR images. TSX1, TerraSAR-X.

Sensor	Mode	Date	Time (UTC)	Orbit	Incident Angle Range (Degrees)	Polarization	Spatial Resolution
Envisat ASAR	AP	2 August 2011	07:22	Descending	31.0–36.3°	VV/VH	30 m
Envisat ASAR	AP	1 October 2011	07:22	Descending	31.0–36.3°	VV/VH	30 m
TSX1	StripMap	28 August 2011	15:46	Ascending	26.3° (scene center)	HH	3 m
TSX1	StripMap	13 September 2011	15:54	Ascending	44.4° (scene center)	HH	3 m

3.5. Field Reference Data, Laboratory Analysis and Target Classes

During six field campaigns from 2010 to 2014, 602 reference sites were visited within the study area, including fieldwork conducted one month after the acquisition of the WV-2 scene. Because the southern and eastern parts of the study area are remote and partly inaccessible, we decided on a random clustered sampling strategy (Figure 1). The landscape is considered as stable and the mineral components as conservative in relation to the resolution of the input data. The collected parameters consist of: texture, calcium carbonate ($CaCO_3$) content (with hydrochloride acid), soil color, visible mineral components of surface substrates, vegetation cover, topographic position, GPS and photo references. The reference points serve as training and test data for the SVM analysis.

The categorization of soils and topsoils is a complex process. In addition to the description of field reference points, we also conducted laboratory analyses for a better understanding and for the target class selection. From 27 reference locations, surface substrate samples (0–2 cm) were collected and physical and chemical analyses conducted (Table 5). Soil samples were air-dried and sieved (<2 mm).

Texture was analyzed with the Bouyoucos hydrometer method after dispersing the samples with 1N sodium hexametaphosphate and represented according to the United States Department of Agriculture (USDA) classification [8]. $CaCO_3$ was measured using the methods proposed in Buurman *et al.* [76]. C_{org} was determined using the Springer and Klee method [77]. Available fractions of heavy metals (Fe and Mn) were extracted according to the Lindsay–Norwell procedure [78]. Exchangeable bases (K, Ca, Mg and Na) are analyzed based on the Mehlich 3 method [79]. The field reference collection and the laboratory samples resulted in seven topsoil classes (Table 5), two additional lithological classes (Figure 3) and a class for surface water (Class 1), which includes the Makuyuni River and water reservoirs for cattle farming and irrigation.

Table 5. Laboratory analysis of topsoil samples (meq = milliequivalents; mmol = millimoles).

		Laboratory Analysis														
Class	Number of topsoil Samples	Coarse Sand (0.5–2 mm) in g/kg	Fine/Medium Sand (0.05–0.5 mm) in g/kg	Silt (0.002– 0.05 mm) in g/kg	Clay (<0.002 mm) in g/kg	Calcium Carbonate $CaCO_3$ in g/kg	Organic Carbon (C_{org}) in ^{o}/k^{o}	Iron (Fe) in mg/kg	Manganese (Mn) in mg/kg	Aluminium (Al) in mg/kg	Calcium Cation (Ca^{2+}) in meq/100 g	Magnesium Cation (Mg^{2+}) in meq/100 g	Sodium Cation (Na^{+}) in meq/100 g	Potassium Cation (K^{+}) in meq/100 g	Chlorides (Cl) in mg/kg	Water soluble Sulfate (SO_4) in mmol/kg
2	4	117.25	503.75	166.00	279.50	128.00	2.75	4.01	7.60	0.28	7.53	4.40	4.87	0.97	91.37	8.87
3	5	74.80	344.80	143.80	367.60	115.60	20.62	6.54	20.72	0.17	18.88	5.09	6.77	1.80	59.90	45.78
4	4	92.60	216.00	416.60	274.80	26.79	14.61	9.64	36.80	0.21	24.13	6.07	6.31	1.88	13.86	8.54
5	1	83.00	280.00	134.00	475.00	2.00	9.80	9.17	20.14	0.22	22.46	3.70	6.10	1.08	7.20	7.80
6	7	134.86	327.57	317.14	220.43	12.29	15.47	9.09	49.80	0.25	14.98	4.66	5.81	2.24	10.01	6.94
7	4	384.00	374.50	156.75	120.75	0.75	10.05	5.70	40.48	0.25	4.79	1.54	0.26	1.46	18.68	10.20
8	2	41.00	235.50	101.00	278.50	25.00	15.85	26.40	76.04	0.47	18.25	7.77	0.21	2.44	14.25	8.90

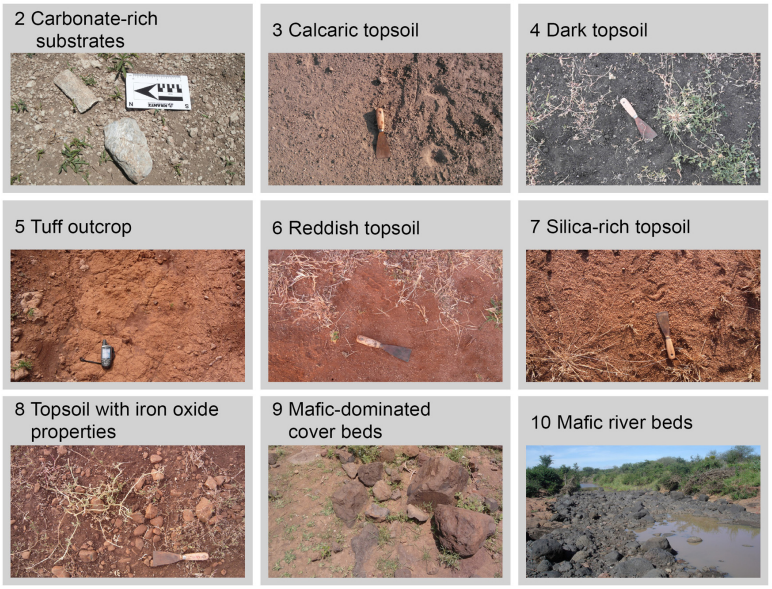

Figure 3. Target classes identified by field surveys and laboratory analysis (Class 1 = water).

"Carbonate-rich substrate" (Class 2) mostly consists of erosive areas with lacustrine sediments and more than 20% carbonate gravel or concretions. Class 2 appears with the Lower Manyara Beds, associated calcaric Regosols and secondary hardened carbonates. The $CaCO_3$ content is rather high (128 g/kg) and the C_{org} content relatively low (2.75 g/kg). "Calcaric topsoil" (Class 3) features a high $CaCO_3$ content and a comparatively high clay content. "Dark topsoil" (Class 4) shows the highest silt content, is dark in color (Munsell® color: hue of 7.5 or 10 YR (yellow red); values of ≤3 or lower; chroma of ≤2), has a low $CaCO_3$ content compared to "Class 3" and a low Fe content compared to "Class 8". It is associated with colluvial and fluvial deposits. "Tuff outcrop" (Class 5) defines distinct outcropping layers of hardened tuff. "Reddish topsoil" (Class 6) has a distinct hue of 5 YR or redder (Munsell® color) and can be distinguished from "Class 3" by a low $CaCO_3$ content, from "Class 4" by color and texture, from "Class 7" by texture, cations and Fe content and from "Class 8" by Fe and Mn content. "Silica-rich topsoil" (Class 7) is associated with the felsic basement and the high quartz sand and grit content, which is a surface residual due to selective erosion. The hue of the soil is 5–7.5 YR; the color value is 4; and the chroma 6–4 (Munsell® color). The "Topsoil with iron oxides properties" (Class 8) class describes a soil associated with mafic lithology (Class 9) and with a high Fe and Mn content, which makes it clearly distinguishable from "Class 3" and "Class 4". "Mafic-dominated cover beds" (Class 9) describe outcroppings and weathered mafic (nephelinite, phonolite, basalt) ridges and the Essimingor volcano. "Mafic river beds" (Class 10) are the same material as "Class 9", but the boulders are hardly weathered, which results in different spectral properties and concentrates within the river beds.

In order to validate and interpret the results of the topsoil and surface substrates' classification procedure, we conducted three soil catenae consisting of 24 soil profiles with detailed profile descriptions according to the World Reference Base for Soil Resources (WRB) 2014 [80].

4. Methods

The workflow consists of several steps (Figure 4): (I) image segmentation based on the high-resolution WorldView-2 images; (II) vegetation and areas affected by clouds and shadowing effects were excluded from further processing; (III) for each remaining segment, mean values of the input feature sets listed in the previous section (Tables 3 and 4) were extracted; (IV) an SVM model was built; (V) SVM-recursive feature elimination (RFE) reduced the number of variables before classifying the segments with the SVM approach; (VI) we compared the results of various input feature set combinations; (VII) accuracy assessment; and (VIII) external validation using soil catenae.

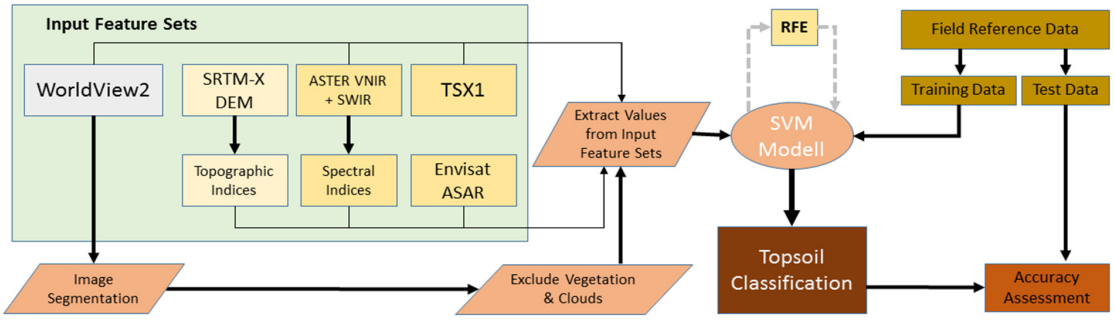

Figure 4. Proposed workflow. RFE, recursive feature elimination.

4.1. Image Object Segmentation

Image objects, which represent contiguous areas in the image, were delineated by multi-resolution segmentation [81]. The segmentation is purely based on the WorldView-2 bands. The reasons for applying an object-oriented approach are reduced processing costs, the possibility to extract values from multiple scales and the option to generate additional object-based input features. The multi-resolution segmentation is a bottom-up approach, which applies region merging beginning with the pixel level [82]. The heterogeneity measurement f (Equation 1), which defines if objects are merged, is controlled by a threshold. If the heterogeneity measure exceeds the threshold, which is determined by the scale parameter, the merging of image objects is terminated. Δh_{color} defines the difference in spectral heterogeneity and Δh_{shape} the consideration of the smoothness and compactness of the image objects. w_{color} and w_{shape} are the according weight measures [82].

$$f = w_{\text{color}} \times \Delta h_{\text{color}} + w_{\text{shape}} \times \Delta h_{\text{shape}}, w_{\text{color}} \in [0, 1,], w_{\text{shape}} \in [0, 1,] \, w_{\text{color}} + w_{\text{shape}} = 1 \quad (1)$$

Roads and buildings were easily identified from the resulting segments by spectral values, shape and spatial relations. Since the image acquisition took place shortly after the winter rainy season, we could verify in the field that, with the exception of some rare occasions, all vegetation cover was photosynthetic active. Therefore, vegetation cover was determined by NDVI thresholding, utilizing a histogram. These three land cover types were excluded from further processing, since they are not the focus of the research objective. This is especially important for the vegetation, because the influence on the spectral response (dead organic materials, as well as photosynthetic vegetation) is considered high [20].

After this pre-selection, 47% of the study area of 1200 km^2 was considered as open soil or vegetation-free lithology. Some of the reference points had to be excluded from further analysis, leading to 432 vegetation-free reference points. The 1,005,058 image segments result in an average mapping unit of 550 km^2. For these image objects, mean values from the SAR images, ASTER bands and indices, as well as from topographic parameters were extracted. The following additional input features were computed from WV2: (i) standard deviation for all spectral bands; (ii) NDVI [19]; (iii) spectral brightness; and (iv) texture homogeneity measure following Haralick *et al.* [83].

4.2. Support Vector Machines

The machine learning concept of SVM was developed to solve binary problems in pattern recognition applications. The development and theoretical background is published by Vapnik [84,85], Hearst [86], Burges [87] and Schölkopf and Smola [88]. Remote sensing studies make use of SVM properties, like high computation performance and high classification accuracies with small numbers of training samples [89]. Recent studies used SVM approaches to identify lithological units with remote sensing data [90,91].

The fundamental principle of SVM is the maximization of margins between training samples of two target classes. Not all features of the training dataset are used for this approach; only those samples that are close to the margin. They serve as support vectors, which are used to define the boundaries of the margin. A maximized margin is referred to as the optimal separating hyperplane [87]. To prevent an over-fitting of the hyperplane caused by outliers in the training dataset, a "soft margin" approach was introduced [92]. This approach uses a cost parameter (C), which determines a penalty for the support

vectors. Low *C* values indicate a stronger generalization of the model; high values provide more influence for single input features [93].

For this study, we utilized a support vector classifier (C-SVC) provided by the Library for Support Vector Machines (LIBSVM) [94]. C-SVC works as a "one-against-one" classifier that discriminates between two target classes. A multi-class approach is solved by constructing multiple target value pairs. In some cases, including soil-related issues, it is hardly possible to separate the target classes in a single input space with a linear function [32]. SVMs therefore project the input features in an n-dimensional feature space. To avoid the computational effort of projecting all input features into a multi-dimensional feature space, kernels can be used to calculate their dot product in the feature space. Various kernels can be applied with SVMs. In this study, a radial basis kernel function (RBF) was utilized, which is widely used when a nonlinear distribution of feature values is expected [32,95]. A linear kernel serving as reference was also applied. The width of the RBF, and hence, the influence of a training sample on the adjacent feature space, is controlled by the constant γ. High values indicate a strong influence, whereas low values indicate a weak influence. Thirty percent of the reference samples (130) were randomly selected to serve exclusively as test datasets, and the remaining 70% was used for the training of the SVM model. All input feature sets were scaled to a range of [−1, +1]. For the derivation of the constants *C* and γ, a grid search was conducted by an iterative cross-validation of the performance of fitting the model to the training data [94].

4.3. Recursive Feature Selection

In order to identify a minimum subset of features that contribute to the discrimination of the target classes, a RFE technique was applied [96]. Many of the spectral and topographical input features carry redundant information. A subset of features provides, in addition to a higher computation performance, the possibility for a better interpretation of the interrelation between the topsoil reference and the spectral and topographic parameters of the datasets explaining the topsoil distribution. RFE is a backward elimination method, which starts with a full set of features and iteratively reduces their number according to their contribution to the classification accuracy [97]. For this, the SVM classifier is trained at each iteration, and a ranking criterion is computed for all features. The feature with the smallest criterion is then removed before the next iteration [98]. SVM-RFE was performed with the e1071 package [99].

5. Results and Discussion

The comparison of different input feature groups shows that all additional input features increase the overall accuracy of the classification (Table 6). The classification of only the spectral bands of WorldView-2 with an RBF-kernel reaches an accuracy of 62.9%. By incorporating more features from the ASTER data, SAR scenes and topographic indices, an overall accuracy of 70.4% was achieved. By conducting the classification with the parameters selected by RFE (Table 7), the highest accuracy of 71.9% was reached. The application of a linear kernel instead of an RBF-kernel led to lower accuracies.

Table 6. Overall accuracies for different input feature groups. RBF, radial basis function.

Input Feature Groups	No. of Input Features	*C*	g	Overall Accuracy
WorldView-2	8	1896.0	0.0625	62.9%
WorldView-2 + WV2 derivatives	8 + 11	185,363	0.00006	63.7%
WorldView-2 and SAR scenes	8 + 5	16	0.0625	65.2%
WorldView-2 and ASTER bands / indices	8 + 33	181.02	0.0055	64.4%
WorldView-2 and topographic parameters	8 + 16	65,536.0	0.00005	67.4%
All available parameters	73	2.82	0.0883	70.4%
Selection from RFE (linear kernel)	24	1.41	-	66.6%
Selection from RFE (RBF-kernel)	38	4.00	0.1250	71.9%

Table 7. Relevance ranking of RFE selected input features. SD, standard deviation.

RFE Rank	Input Feature	RFE Rank	Input Feature	RFE Rank	Input Feature
1	Geomorphons	2	MRRTF	3	WV2—Band 3
4	Ferric Iron (Fe^{3+}) Index	5	WV2—Band 1	6	Calcite Index
7	AlOH Group Index	8	WV2—SD Band 3	9	Ferrous Iron 1 Index
10	Ferric Oxide Index	11	RBD8	12	WV2—Band 8
13	WV2—Band 4	14	WV2—SD Band 1	15	Alteration/ Laterite Index
16	ASTER SWIR Band 6	17	Opaque Index	18	Clay 2 Index
19	MgOH 2 Index	20	WV2—SD Band 4	21	WV2—Band 2
22	Kaolinite Index	23	Terrain Ruggedness Index	24	TSX1 HH intensity
25	Envisat ASAR (1 October 2011 VV)	26	WV2 NDVI	27	ASTER SWIR Band 4
28	Morphometric Protection Index	29	WV2—Band 7	30	ASTER SWIR Band 3
31	WV2—SD Band 8	32	WV2—Brightness	33	Envisat ASAR (2 August 2011 VV)
34	Elevation (height a.s.l.)	35	Topographic Wetness Index	36	Texture (homogeneity)

An RFE was performed for the dataset with all 73 input features. The RFE shows that with seven input features, an accuracy exceeding 60% can be attained (Figure 5). The classification accuracy for the SVM, with an RBF-kernel, peaks with a selection of 36 input features, then performs relatively stable until the maximum number of input features is reached. The so-called Hughes phenomenon, which describes the decrease in classification accuracy when additional input features are added to an already large dataset, cannot be observed with the RBF-kernel [100]. Yet, a small decrease can be noted for the linear kernel (Figure 5). The 36 input features from the RFE selection represent all input feature groups (Table 7). Out of the first seven input features, two are topographic indices. The MRRTF results in high values for flat elevated areas [65], and the geomorphons (geomorphologic phonotypes) classify the topography into landscape elements [63]. Both features describe the position of the target classes in the study area. WV2 contributes, along with the spectral Bands 3 and 1, two further

input datasets. The ASTER Calcite Index and the Ferric Iron (Fe^{3+}) Index may explain the distribution of the two target classes with high $CaCO_3$ content (Classes 2 and 3) and the topsoil class with iron oxide properties (Class 8). The AlOH Group Index may support the discrimination of clay minerals [56].

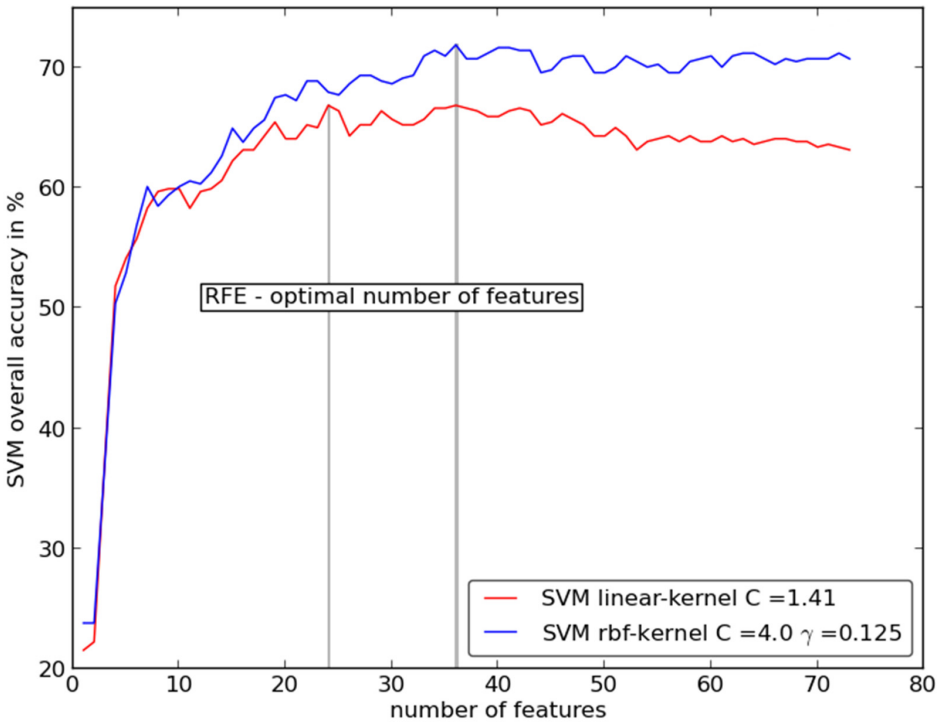

Figure 5. Accuracy curves from RFE for a linear and an RBF-kernel.

The confusion matrix of the RFE-selected input feature dataset reveals that the most competitive classes, concerning the user's and the producer's accuracy, are Class 2 "carbonate-rich substrates" and Class 3 "calcaric topsoil" (Table 8). Both classes have high carbonate content, and the topographic position is overlapping. The difference between both classes is related to the amount of $CaCO_3$ concretions, which are much higher in the lacustrine deposits. If we were to merge both classes, the overall accuracy would reach 79%. However, the visual validation shows a reasonable distribution for both classes. Class 3 also overlaps with Class 4 "dark topsoil". Class 4 is associated mainly with colluvial and fluvial deposits and shows low $CaCO_3$ content. The transition to Class 3 is gradual. The low producer's accuracy of Class 5 "tuff outcrop" can be explained by the relatively small area of these outcrops. The producer's accuracy of this particular class is higher (75%) when only applying the WV2-related input parameters, but the medium-resolution information of the ASTER- and DEM-derived features seems to corrupt the correct identification.

Table 8. Confusion matrix for RFE classification with RBF-kernel (C = 4, g = 0.125).

		Classified Data										Producers Accuracy
		1	**2**	**3**	**4**	**5**	**6**	**7**	**8**	**9**	**10**	
Reference Class	**1**	6	0	0	0	0	0	0	0	0	0	100%
	2	0	8	5	0	0	0	0	0	0	0	62%
	3	0	5	12	3	0	0	0	0	0	0	60%
	4	0	0	2	19	0	0	0	0	0	1	86%
	5	0	1	0	0	5	1	2	1	0	0	50%
	6	0	0	0	0	0	9	3	0	0	0	75%
	7	0	1	1	0	0	0	12	0	0	0	86%
	8	0	0	1	2	0	0	1	10	2	0	63%
	9	0	0	2	2	0	0	0	0	6	0	60%
	10	0	0	2	0	0	0	0	0	0	10	83%
Users Accuracy		100%	53%	48%	73%	100%	90%	67%	91%	75%	91%	Overall Accuracy 97/135 = 71.9%

"Carbonate-rich substrates" mainly represent the lacustrine lower member of the Manyara Beds, which are exposed prevalently at the foot of slope and mid-slope positions of the Makuyuni River system, as well as in associated gully systems (Figure 6). The class "calcaric topsoil" indicates soils that show an enrichment of $CaCO_3$ due to inputs from carbonatic volcanic ash deposits or development processes upon the "carbonate-rich substrates". In some cases, $CaCO_3$-rich soils developed on secondary translocated carbonates or consist of eroded soils exposing $CaCO_3$ concretions. The latter ones were identified during fieldwork in areas with higher slope degrees or large specific catchment areas. "Tuff outcrops" (Class 5) were recognized at a stratigraphic position above the lower member of the Manyara Beds, which coincides with the results of fieldwork and reviewed scientific literature [47]. The outcrops are too minuscule to be displayed in the map (Figure 6). The class "reddish topsoil" is identified with satisfying accuracy. This class is located mainly on stable flat ridge tops and is used agriculturally. Consequently, topsoils are disturbed and reworked by ploughing activity, bringing leached $CaCO_3$ back to the surface (Table 5). This makes the difference in Class 7 "silica-rich topsoil". These soils are not disturbed, and consequently, silica enriches at the surface due to selective erosion processes. "Silica-rich topsoils" and "reddish topsoils" developed on the Proterozoic intermediate quartzite and gneisses of the Masai Plateau, occur especially in the south of the study area. However, also, these areas were subject to carbonatic volcanic ash deposits. The topsoils with iron oxide properties (Class 8) occur in association with mafic ridges (phonolite, nephelinite) or along the slopes of the Essimingor volcano (Figure 6). Class 9 "Mafic-dominated cover beds" was identified well. Like Class 8, Class 9 can be found at the volcano slopes and on the mafic ridges. Since the cover beds are densely vegetated by shrubs, only small, vegetation-sparse areas were used for the classification. The "mafic river beds" are often covered by vegetation and water. Nevertheless, the mafic material at point bars in the Makuyuni River was traced with high accuracies.

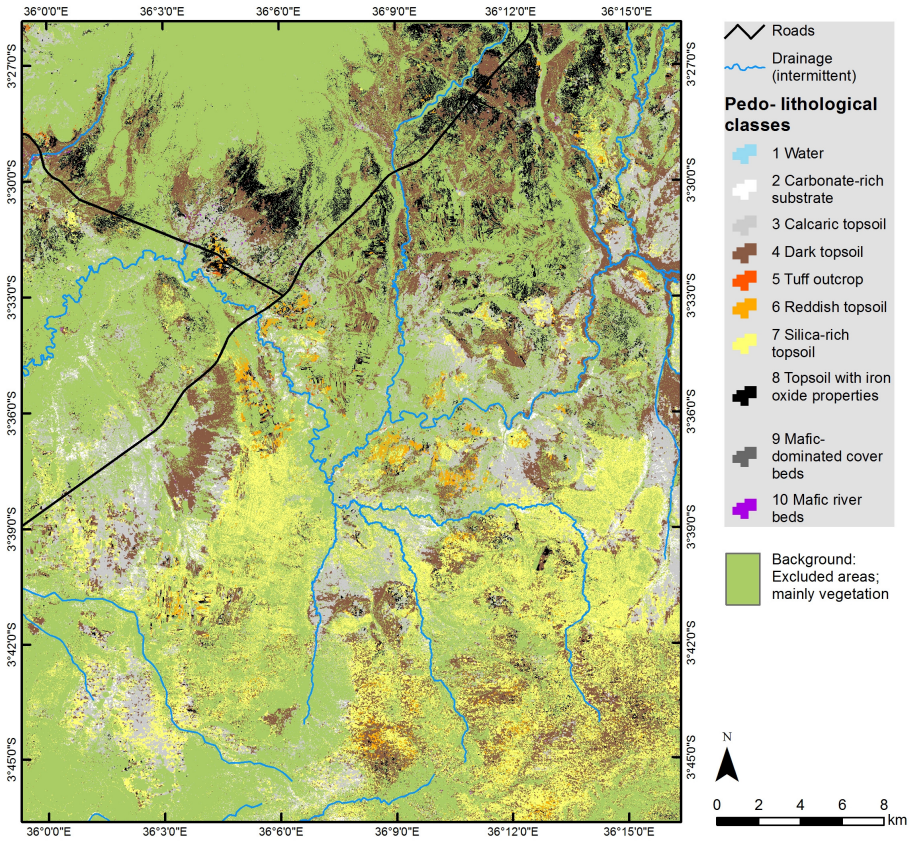

Figure 6. Final classification of topsoil distribution in the study area.

Out of 24 soil profile analyses conducted in the study area, we identified seven main soil types (see Figure 7). In the following, we show that these topsoils can be related to or associated with specific WRB soil types according to the applied catena approach. Vertisols are found in flat areas and in depressions characterized by high clay contents and representing formerly wet positions, related to a high biomass production. They are associated with "dark topsoil" (Class 4). Vertisols occur in association with Vertic Cambisols (Clayic) (Soil Profile 1; Figure 7b) that also relates to the pedo-lithological Class 4 "dark topsoil". In the study area, Calcisols occur with lacustrine "carbonate-rich substrates" (Class 2) and "calcaric topsoils" (Class 3), which are characterized by eroded Luvisols exposing $CaCO_3$ concretions.

Andosols are located on flat and stable ridge positions with low erosion potential. These soils developed from parent material of volcanic origin, such as volcanic ash, tuff and pumice. They show high mineral proportions indicating fertile soils suitable for crop production. In our analysis, Andosols co-exist with "reddish topsoils" (Class 6). Cambisols are widely distributed in the study area and occur mainly on relatively flat mid-slope positions. Along the Makuyuni River terraces, they are distinguished as Cambisols (Colluvic) (Soil Profiles 15–17; Figure 7). On flat ridge positions, they develop as Andic Cambisol (Soil Profiles 6, 8 and 9, Figure 7). Rhodic Cambisols (Soil Profile 20; Figure 7c) are particularly located on intensively-used agricultural fields and correlate with "reddish topsoils" (Class 6), showing a dark reddish brown 5 YR 3/4 Munsell® color for the first 15 cm of soil depth. Cambisols and Luvisols are associated with each other and correlate with "silica-rich topsoils" (Class 7) and

"reddish topsoils" (Class 6). The Haplic Ferralsol (Soil Profile 14; Figure 7d) correlates with "silica-rich topsoil" (Class 7). These soils developed on a weathered felsic basement.

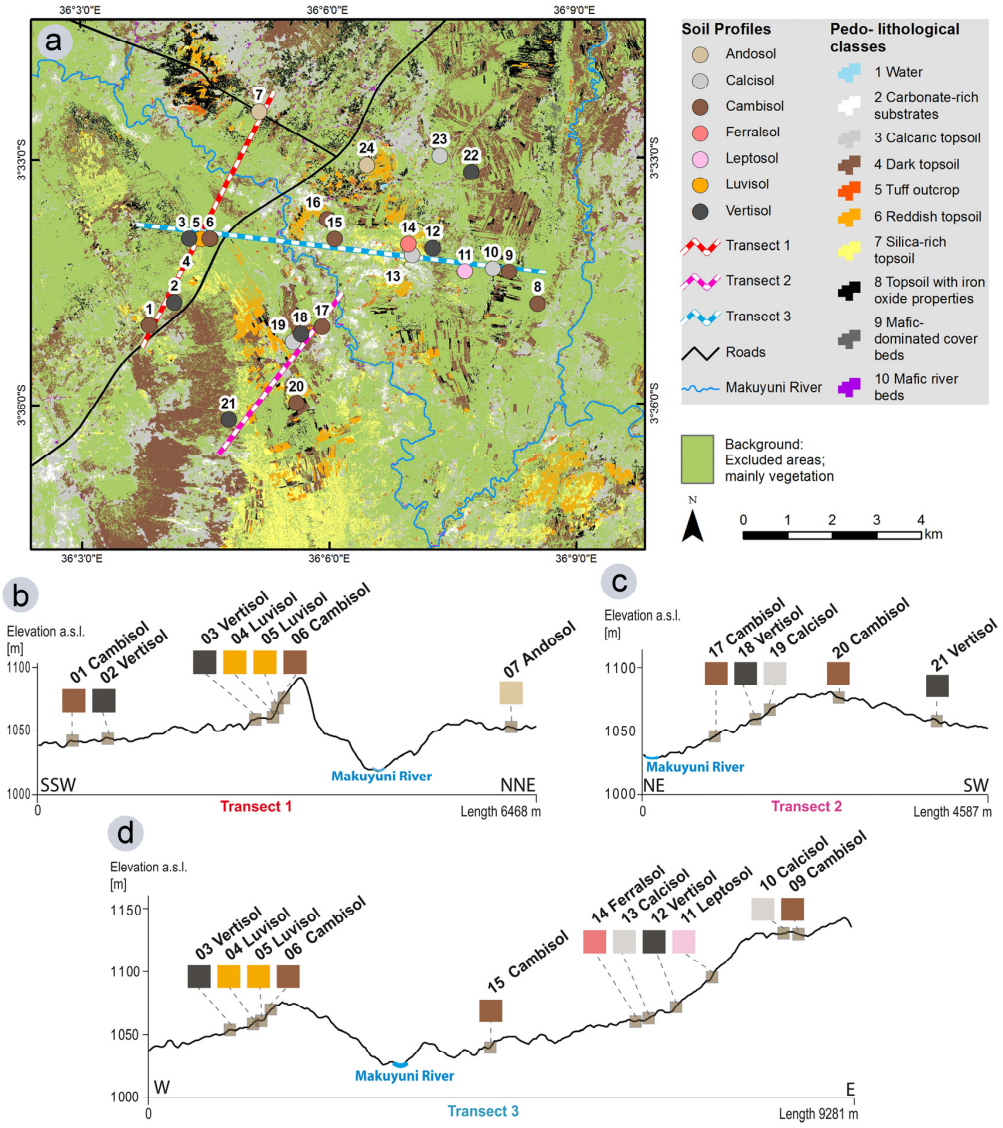

Figure 7. Section of the classification with soil profile transects. (**a**) Map with soil profile transects; (**b**) Soil profile transect 1 (SSW – NNE orientation); (**c**) Soil profile transect 2 (NE–SW orientation); (**d**) Soil profile transect 3 (W–E orientation).

The resulting map provides a very detailed distribution of topsoils and surface substrates for the study area, which outcompetes other spatial soil information available for this region, like the official soil map by De Pauw [43], the 250 m Africa Soil Information Service (AfSIS) product [42] or the products from the Soil and Terrain Database (SOTER) program [101]. Furthermore, the comparison with the soil profile catenae shows that the detailed topsoil information can be related to specific WRB-based soil types with little additional fieldwork and/or expert knowledge. Nevertheless, providing detailed

information on topsoils and surface substrates in comparison to other DSM studies [31,32,42] remains the main intention of the paper.

6. Conclusions

The introduced study has mapped the distribution of topsoils and lithology in a study area in the semiarid Lake Manyara Basin. Applying an integrated approach, combining surface characteristics and terrain features, the spatial distribution of topsoils and related soil types was derived. The topsoils have complex genetic origins related to different substrates, resulting in a high spatial heterogeneity. The non-vegetated areas were classified with a multisensoral approach, which included WV2 and ASTER multispectral data, the TSX1 and Envisat ASAR SAR scenes, and topographical indices were derived from SRTM-X data. With a C-SVC and an RBF-kernel, an overall accuracy of 71.9% was achieved for a challenging classification depth of 10 target classes. The final map is coherent with field observations and laboratory analysis of 27 soil samples. The applied methodological approach seems suitable for multiscale and multisensoral datasets of large areas. We show that the topsoil classification can be associated with soil profiles obtained by fieldwork and certain terrain positions derived from DEM, thus allowing a distinct spatial attribution of soil types.

The results of the topsoil classification and the related soil type association give valuable information, which can help to find locations for agricultural projects in the region and may thereby support the transition to the sustainable self-subsistence of the local population. This may contribute to a reduction of cattle-induced overgrazing and subsequent land degradation. For many applications, like archaeological field studies and paleontological surveys, high-resolution topsoil and surface substrate information yields greater insight than low-resolution soil type maps. The results of this work also help to explain the geological situation of the study area and the landscape evolution. Despite the potential influence of different fluvial and mass movement processes on the topsoil distribution, this study draws a valuable picture of the general situation.

Acknowledgments

This study was financed by the Heidelberg Academy of Sciences and Humanities research center: “The Role of Culture in Early Expansions of Humans” (ROCEEH). The WorldView-2 scene is courtesy of the DigitalGlobe Foundation. We would like to thank the DLR and the German Remote Sensing Data Center (DFD) for providing the TerraSAR-X and the SRTM/X-SAR data. The European Space Agency (ESA) provided the Envisat ASAR data. We acknowledge the support of Deutsche Forschungsgemeinschaft and Open Access Publishing Fund of Tuebingen University. We also want to acknowledge the EU International Research Staff Exchange Scheme (IRSES) Fluvial processes and sediment dynamics of slope channel systems (FLUMEN) (PIRSES-GA-2012-318969) project financing the exchange of researchers.

Author Contributions

Felix Bachofer designed and implemented the research of this study. He processed the remote sensing data, conducted the analysis and drafted the manuscript. Geraldine Quénéhervé analyzed the soil profiles. Felix Bachofer, Geraldine Quénéhervé and Michael Maerker contributed to the collection of

ground reference data during three field campaigns from 2010–2014. Furthermore, Felix Bachofer, Geraldine Quénéhervé, Volker Hochschild and Michael Maerker contributed to the data interpretation and supervised the manuscript construction.

Conflicts of Interest

The authors declare no conflict of interest.

References

1. Solomon, A.M.; Webb, T., III. Computer-aided reconstruction of late-quaternary landscape dynamics. *Annu. Rev. Ecol. Syst.* **1985**, *16*, 63–84.
2. Moore, I.D.; Gessler, P.E.; Nielsen, G.A.; Peterson, G.A. Soil attribute prediction using terrain analysis. *Soil Sci. Soc. Am. J.* **1993**, *57*, 443–452.
3. Sabins, F.F. Remote sensing for mineral exploration. *Ore Geol. Rev.* **1999**, *14*, 157–183.
4. Anderson, K.; Croft, H. Remote sensing of soil surface properties. *Prog. Phys. Geogr.* **2009**, *33*, 457–473.
5. Mulder, V.L.; de Bruin, S.; Schaepman, M.E.; Mayr, T.R. The use of remote sensing in soil and terrain mapping—A review. *Geoderma* **2011**, *162*, 1–19.
6. Dewitte, O.; Jones, A.; Elbelrhiti, H.; Horion, S.; Montanarella, L. Satellite remote sensing for soil mapping in Africa: An overview. *Prog. Phys. Geogr.* **2012**, *36*, 514–538.
7. FAO. *Topsoil Characterization for Sustainable Land Management, Draft*; Food and Agriculture Organization of the United Nations, Land and Water Development Division, Soil Resources, Management and Conservation Service: Rome, Italy, 1998; p. 74. Available online: ftp://ftp.fao.org/agl/agll/docs/topsoil.pdf (accessed on 23 July 2015).
8. USDA (United States Department of Agriculture). *Soil Survey Manual*; Soil Survey Division: Washington, DC, USA, 1993; p. 437.
9. Broll, G.; Brauckmann, H.J.; Overesch, M.; Junge, B.; Erber, C.; Milbert, G.; Baize, D.; Nachtergaele, F. Topsoil characterization-recommendations for revision and expansion of the FAO-Draft (1998) with emphasis on humus forms and biological features. *J. Plant Nutr. Soil Sci.* **2006**, *169*, 453–461.
10. Graefe, U.; Baritz, R.; Broll, G.; Kolb, E.; Milbert, G.; Wachendorf, C. Adapting humus form classification to WRB principles. In Proceedings of the 4th International Congress of the European Soil Science Societies—Eurosoil, At Bari, Italy, 2–6 July 2012; p. 954.
11. Ben-Dor, E.; Goldlshleger, N.; Benyamini, Y.; Agassi, M.; Blumberg, D.G. The spectral reflectance properties of soil structural crusts in the 1.2- to 2.5-μm spectral region. *Soil Sci. Soc. Am. J.* **2003**, *67*, 289–299.
12. Baghdadi, N.; Cerdan, O.; Zribi, M.; Auzet, V.; Darboux, F.; El Hajj, M.; Kheir, R.B. Operational performance of current synthetic aperture radar sensors in mapping soil surface characteristics in agricultural environments: Application to hydrological and erosion modelling. *Hydrol. Process.* **2008**, *22*, 9–20.

13. Aubert, M.; Baghdadi, N.; Zribi, M.; Douaoui, A.; Loumagne, C.; Baup, F.; El Hajj, M.; Garrigues, S. Analysis of TerraSAR-X data sensitivity to bare soil moisture, roughness, composition and soil crust. *Remote Sens. Environ.* **2011**, *115*, 1801–1810.
14. Aubert, M.; Baghdadi, N.N.; Zribi, M.; Ose, K.; El Hajj, M.; Vaudour, E.; Gonzalez-Sosa, E. Toward an operational bare soil moisture mapping using TerraSAR-X data acquired over agricultural areas. *IEEE J. Sel. Top. Appl. Earth Obs. Remote Sens.* **2013**, *6*, 900–916.
15. Schmugge, T.J.; Kustas, W.P.; Ritchie, J.C.; Jackson, T.J.; Rango, A. Remote sensing in hydrology. *Adv. Water Resour.* **2002**, *25*, 1367–1385.
16. Ben-Dor, E.; Chabrillat, S.; Demattê, J.A.M.; Taylor, G.R.; Hill, J.; Whiting, M.L.; Sommer, S. Using imaging spectroscopy to study soil properties. *Remote Sens. Environ.* **2009**, *113* (Suppl. 1), S38–S55.
17. Bartholomeus, H.; Epema, G.; Schaepman, M. Determining iron content in Mediterranean soils in partly vegetated areas, using spectral reflectance and imaging spectroscopy. *Int. J. Appl. Earth Obs. Geoinf.* **2007**, *9*, 194–203.
18. Grebby, S.; Cunningham, D.; Tansey, K.; Naden, J. The impact of vegetation on lithological mapping using airborne multispectral data: A case study for the north Troodos region, Cyprus. *Remote Sens.* **2014**, *6*, 10860–10887.
19. Rouse, J.W.; Haas, R.H.; Shell, J.A.; Deering, D.W.; Harlan, J.C. *Monitoring the Vernal Advancement of Retrogradation of Natural Vegetation*; NASA/GSFC: Greenbelt, MD, USA, 1974; p. 371.
20. Yang, X.; Guo, X. Quantifying responses of spectral vegetation indices to dead materials in mixed grasslands. *Remote Sens.* **2014**, *6*, 4289–4304.
21. Pickup, G.; Chewings, V.H.; Nelson, D.J. Estimating changes in vegetation cover over time in arid rangelands using landsat MSS data. *Remote Sens. Environ.* **1993**, *43*, 243–263.
22. Trodd, N.M.; Dougill, A.J. Monitoring vegetation dynamics in semi-arid African rangelands: Use and limitations of earth observation data to characterize vegetation structure. *Appl. Geogr.* **1998**, *18*, 315–330.
23. Mitchell, J.; Shrestha, R.; Moore-Ellison, C.; Glenn, N. Single and multi-date Landsat classifications of basalt to support soil survey efforts. *Remote Sens.* **2013**, *5*, 4857–4876.
24. Dogan, H.M.; Kılıç, O.M. Modelling and mapping some soil surface properties of Central Kelkit Basin in Turkey by using Landsat-7 ETM+ images. *Int. J. Remote Sens.* **2013**, *34*, 5623–5640.
25. Rowan, L.C.; Mars, J.C. Lithologic mapping in the Mountain Pass, California area using Advanced Spaceborne Thermal Emission and Reflection Radiometer (ASTER) data. *Remote Sens. Environ.* **2003**, *84*, 350–366.
26. Rowan, L.C.; Mars, J.C.; Simpson, C.J. Lithologic mapping of the Mordor, NT, Australia ultramafic complex by using the Advanced Spaceborne Thermal Emission and Reflection Radiometer (ASTER). *Remote Sens. Environ.* **2005**, *99*, 105–126.
27. Mars, J.C.; Rowan, L.C. Spectral assessment of new ASTER SWIR surface reflectance data products for spectroscopic mapping of rocks and minerals. *Remote Sens. Environ.* **2010**, *114*, 2011–2025.
28. Pour, A.B.; Hashim, M. Application of advanced spaceborne thermal emission and reflection radiometer (ASTER) data in geological mapping. *Int. J. Phys. Sci.* **2011**, *6*, 7657–7668.

29. Vicente, L.E.; de Souza Filho, C.R. Identification of mineral components in tropical soils using reflectance spectroscopy and advanced spaceborne thermal emission and reflection radiometer (ASTER) data. *Remote Sens. Environ.* **2011**, *115*, 1824–1836.
30. Conacher, A.J.; Dalrymple, J.B. The nine unit land surface model and pedogeomorphic research. *Geoderma* **1977**, *18*, 127–144.
31. Mulder, V.L.; de Bruin, S.; Weyermann, J.; Kokaly, R.F.; Schaepman, M.E. Characterizing regional soil mineral composition using spectroscopy and geostatistics. *Remote Sens. Environ.* **2013**, *139*, 415–429.
32. Hahn, C.; Gloaguen, R. Estimation of soil types by non linear analysis of remote sensing data. *Nonlinear Process. Geophys.***2008**, *15*, 115–126.
33. Rossel, R.A.V.; Chen, C. Digitally mapping the information content of visible–near infrared spectra of surficial Australian soils. *Remote Sens. Environ.* **2011**, *115*, 1443–1455.
34. Selige, T.; Böhner, J.; Schmidhalter, U. High resolution topsoil mapping using hyperspectral image and field data in multivariate regression modeling procedures. *Geoderma* **2006**, *136*, 235–244.
35. Gaber, A.; Koch, M.; El-Baz, F. Textural and compositional characterization of Wadi Feiran deposits, Sinai Peninsula, Egypt, using Radarsat-1, PALSAR, SRTM and ETM+ Data. *Remote Sens.* **2010**, *2*, 52–75.
36. Zribi, M.; Chahbi, A.; Shabou, M.; Lili-Chabaane, Z.; Duchemin, B.; Baghdadi, N.; Amri, R.; Chehbouni, A. Soil surface moisture estimation over a semi-arid region using ENVISAT ASAR radar data for soil evaporation evaluation. *Hydrol. Earth Syst.Sci.* **2011**, *15*, 345–358.
37. Zribi, M.; Kotti, F.; Lili-Chabaane, Z.; Baghdadi, N.; Ben Issa, N.; Amri, R.; Duchemin, B.; Chehbouni, A. Soil texture estimation over a semiarid area using TerraSAR-X radar data. *IEEE Geosci. Remote Sens. Lett.* **2012**, *9*, 353–357.
38. Baghdadi, N.; Aubert, M.; Zribi, M. Use of TerraSAR-X data to retrieve soil moisture over bare soil agricultural fields. *IEEE Geosci. Remote Sens. Lett.* **2012**, *9*, 512–516.
39. Vaudour, E.; Baghdadi, N.; Gilliot, J.M. Mapping tillage operations over a peri-urban region using combined SPOT4 and ASAR/ENVISAT images. *Int. J. Appl. Earth Obs. Geoinf.* **2014**, *28*, 43–59.
40. Gorrab, A.; Zribi, M.; Baghdadi, N.; Mougenot, B.; Chabaane, Z. Potential of X-band TerraSAR-X and COSMO-SkyMed SAR data for the assessment of physical soil parameters. *Remote Sens.* **2015**, *7*, 747–766.
41. Baghdadi, N.; Cresson, R.; El Hajj, M.; Ludwig, R.; la Jeunesse, I. Estimation of soil parameters over bare agriculture areas from C-band polarimetric SAR data using neural networks. *Hydrol. Earth Syst. Sci.* **2012**, *16*, 1607–1621.
42. Hengl, T.; Heuvelink, G.B.M.; Kempen, B.; Leenaars, J.G.B.; Walsh, M.G.; Shepherd, K.D.; Sila, A.; MacMillan, R.A.; Mendes de Jesus, J.; Tamene, L.; *et al*. Mapping soil properties of Africa at 250 m resolution: Random forests significantly improve current predictions. *PLoS One* **2015**, *10*, e0125814.
43. De Pauw, E. Soils, physiography and agro-ecological zones of tanzania. In *Crop Monitoring and Early Warning Systems Project, Food and Agriculture Organization of the United Nations. GCPS/URT/047/NET*; Ministry of Agriculture: Dar es Salaam, Tanzania, 1983.

44. Huffman, G.J.; Adler, R.F.; Bolvin, D.T.; Gu, G.J.; Nelkin, E.J.; Bowman, K.P.; Hong, Y.; Stocker, E.F.; Wolff, D.B. The TRMM multisatellite precipitation analysis (TMPA): Quasi-global, multiyear, combined-sensor precipitation estimates at fine scales. *J. Hydrometeorol.* **2007**, *8*, 38–55.
45. Bachofer, F.; Quénéhervé, G.; Märker, M. The delineation of paleo-shorelines in the Lake Manyara basin using TerraSAR-X data. *Remote Sens.* **2014**, *6*, 2195–2212.
46. Kiunsi, R.B.; Meadows, M.E. Assessing land degradation in the Monduli District, northern Tanzania. *Land Degrad. Dev.* **2006**, *17*, 509–525.
47. Schwartz, H.; Renne, P.R.; Morgan, L.E.; Wildgoose, M.M.; Lippert, P.C.; Frost, S.R.; Harvati, K.; Schrenk, F.; Saanane, C. Geochronology of the Manyara Beds, northern Tanzania: New tephrostratigraphy, magnetostratigraphy and 40Ar/39Ar ages. *Quat. Geochronol.* **2012**, *7*, 48–66.
48. Dawson, J.B. *The Gregory Rift Valley and Neogene-Recent Volcanoes of Northern Tanzania*; Geological Society: London, UK, 2008; p. 102.
49. Dawson, J.B. Neogene tectonics and volcanicity in the North Tanzania sector of the Gregory Rift Valley: Contrasts with the Kenya sector. *Tectonophysics* **1992**, *204*, 81–92.
50. Ring, U.; Schwartz, H.L.; Bromage, T.G.; Sanaane, C. Kinematic and sedimentological evolution of the Manyara Rift in northern Tanzania, East Africa. *Geol. Mag.* **2005**, *142*, 355–368.
51. Frost, S.R.; Schwartz, H.L.; Giemsch, L.; Morgan, L.E.; Renne, P.R.; Wildgoose, M.; Saanane, C.; Schrenk, F.; Harvati, K. Refined age estimates and Paleoanthropological investigation of the Manyara Beds, Tanzania. *J. Anthropol. Sci.* **2012**, *90*, 151–161.
52. Bachofer, F.; Quénéhervé, G.; Märker, M.; Hochschild, V. Comparison of SVM and boosted regression trees for the delineation of lacustrine sediments using multispectral ASTER data and topographic indices in the Lake Manyara basin. *Photogramm. Fernerkund. Geoinf.* **2015**, *1*, 81–94.
53. DigitalGlobe WorldView-2. Available online: https://www.digitalglobe.com/sites/default/files/DG_WorldView2_DS_PROD.pdf (accessed on 20 January 2015).
54. Yamaguchi, Y.; Kahle, A.B.; Tsu, H.; Kawakami, T.; Pniel, M. Overview of advanced spaceborne thermal emission and reflection radiometer (ASTER). *IEEE Trans. Geosci. Remote Sens.* **1998**, *36*, 1062–1071.
55. Iwasaki, A.; Fujisada, H.; Akao, H.; Shindou, O.; Akagi, S. Enhancement of spectral separation performance for ASTER/SWIR. *Proc. SPIE* **2002**, *4486*, 42–50.
56. Cudahy, T. *Satellite ASTER Geoscience Product—Notes for Australia*; Commonwealth Scientific and Industrial Research Organisation (CSIRO): Dickson, Australia, 2012; p. 26.
57. Bierwirth, P. *Evaluation of ASTER Satellite Data for Geological Applications*; Consultancy Report to Geoscience Australia: Canberra, Australia, 2002; p. 50.
58. Hewson, R.D.; Cudahy, T.J.; Mizuhiko, S.; Ueda, K.; Mauger, A.J. Seamless geological map generation using ASTER in the Broken Hill-Curnamona province of Australia. *Remote Sens. Environ.* **2005**, *99*, 159–172.
59. Ninomiya, Y.; Fu, B.; Cudahy, T.J. Detecting lithology with Advanced Spaceborne Thermal Emission and Reflection Radiometer (ASTER) multispectral thermal infrared "radiance-at-sensor" data. *Remote Sens. Environ.* **2005**, *99*, 127–139.
60. Hoffmann, J.; Walter, D. How complementary are SRTM-X and -C band digital elevation models? *Photogramm. Eng. Remote Sens.* **2006**, *72/3*, 261–268.

61. Lee, J.S. Digital image enhancement and noise filtering by use of local statistics. *IEEE Trans. Pattern Anal. Mach. Intell.* **1980**, *2*, 165–168.
62. DLR SRTM Digital Elevation Models/SRTM-X Specifications. Available online: https://centaurus.caf.dlr.de:8443/eoweb-ng/licenseAgreements/DLR_SRTM_Readme.pdf (accessed on 3 April 2015).
63. Jasiewicz, J.; Stepinski, T.F. Geomorphons—A pattern recognition approach to classification and mapping of landforms. *Geomorphology* **2013**, *182*, 147–156.
64. Moore, I.D.; Grayson, R.B.; Ladson, A.R. Digital terrain modelling: A review of hydrological, geomorphological, and biological applications. *Hydrol. Process.* **1991**, *5*, 3–30.
65. Gallant, J.C.; Dowling, T.I. A multiresolution index of valley bottom flatness for mapping depositional areas. *Water Resour. Res.* **2003**, *39*, 1347.
66. Yokoyama, R.; Shirasawa, M.; Pike, R.J. Visualizing topography by openness: A new application of image processing to digital elevation models. *Photogramm. Eng. Remote Sens.* **2002**, *68*, 257–266.
67. Zevenbergen, L.W.; Thorne, C.R. Quantitative analysis of land surface topography. *Earth Surf. Proc. Landf.* **1987**, *12*, 47–56.
68. Dikau, R. *Entwurf Einer Geomorphographisch-Analytischen Systematik von Reliefeinheiten*; Heidelberger Geographische Bausteine: Heidelberg, Germany, 1988.
69. Travis, M.R.; Elsner, G.H.; Iverson, W.D.; Johnson, C.G. *VIEWIT: Computation of Seen Areas, Slope, and Aspect for Land-Use Planning*; Pacific Southwest Research Station, Forest Service, U.S. Department of Agriculture: Berkeley, CA, USA, 1975.
70. Bock, M.; Böhner, J.; Conrad, O.; Köthe, R.; Ringeler, A. Methods for Creating Functional Soil Databases and Applying Digital Soil Mapping with SAGA GIS. In *Status and Prospect of Soil Information in South-Eastern Europe*; Office for Official Publications of the European Communities: Luxembourg, 2007; pp. 149–162.
71. Riley, S.J.; DeGloria, S.D.; Elliot, R. A terrain ruggedness index that Quantifies topographic heterogeneity. *Intermt. J. Sci.* **1999**, *5*, 23–27.
72. Guisan, A.; Weiss, S.; Weiss, A. GLM *versus* CCA spatial modeling of plant species distribution. *Plant Ecol.* **1999**, *143*, 107–122.
73. Beven, K.; Kirkby, M.J. A physically based, variable contributing area model of basin hydrology. *Hydrol. Sci. J.* **1979**, *24*, 43–69.
74. Conrad, O. Terrain Parameters described in the SAGA-GIS Software v.2.1.0. Available online: http://sourceforge.net/projects/saga-gis/files/latest/download?source=files (accessed on 10 February 2015).
75. Baghdadi, N.; Camus, P.; Beaugendre, N.; Issa, O.M.; Zribi, M.; Desprats, J.F.; Rajot, J.L.; Abdallah, C.; Sannier, C. Estimating surface soil moisture from TerraSAR-X data over two small catchments in the Sahelian part of western Niger. *Remote Sens.* **2011**, *3*, 1266–1283.
76. Buurman, P.; Lagen, B.V.; Velthorst, E.J.; Lagen, B.; Velthorst, E. *Manual for Soil and Water Analysis*; Backhuys: Leiden, The Netherlands, 1996.
77. Springer, U.; Klee, J. Prüfung der Leistungsfähigkeit von einigen wichtigeren Verfahren zur Bestimmung des Kohlenstoffs mittels Chromschwefelsäure sowie Vorschlag einer neuen Schnellmethode. *J. Soil Sci. Plant Nutr.* **1954**, *64*, 1–26.

78. Lindsay, W.L.; Norvell, W.A. Development of a dtpa soil test for zinc, iron, manganese, and copper. *Soil Sci. Soc. Am. J.* **1978**, *42*, 421–428.
79. Mehlich, A. Mehlich-3 soil test extractant—A modification of mehlich-2 extractant. *Commun. Soil Sci. Plant Anal.* **1984**, *15*, 1409–1416.
80. FAO. *World Reference Base for Soil Resources 2014—International Soil Classification System for Naming Soils and Creating Legends for Soil Maps*; Food and Agriculture Organization of the United Nations: Rome, Italy, 2014.
81. Baatz, M.; Schäpe, A. Multiresolution Segmentation: An optimization approach for high quality multi-scale image segmentation. In *Angewandte Geographische Informationsverarbeitung XII. Beiträge zum AGIT-Symposium Salzburg*; Strobl, J., Blaschke, T., Griesebner, G., Eds.; Wichmann: Heidelberg, Germany, 2000; Volume 12, pp. 12–23.
82. Benz, U.C.; Hofmann, P.; Willhauck, G.; Lingenfelder, I.; Heynen, M. Multi-resolution, object-oriented fuzzy analysis of remote sensing data for GIS-ready information. *ISPRS J. Photogramm. Remote Sens.* **2004**, *58*, 239–258.
83. Haralick, R.M.; Shanmugam, K.; Dinstein, I.H. Textural features for image classification. *IEEE Trans. Syst. Man Cybern.* **1973**, *SMC-3*, 610–621.
84. Vapnik, V.N. *The Nature of Statistical Learning Theory*; Springer: New York, NY, USA, 1995; p. 188.
85. Vapnik, V.N. An overview of statistical learning theory. *IEEE Trans. Neural Netw.* **1999**, *10*, 988–999.
86. Hearst, M.A. Support vector machines. *IEEE Intell. Syst.* **1998**, *13*, 18–28.
87. Burges, C. A tutorial on support vector machines for pattern recognition. *Data Min. Knowl. Discov.* **1998**, *2*, 121–167.
88. Schölkopf, B.; Smola, A.J. A short introduction to learning with kernels. In *Advanced Lectures on Machine Learning*; Mendelson, S., Smola, A.J., Eds.; Springer-Verlag: Berlin/Heidelberg, Germany, 2003; pp. 41–64.
89. Mountrakis, G.; Im, J.; Ogole, C. Support vector machines in remote sensing: A review. *ISPRS J. Photogramm. Remote Sens.* **2011**, *66*, 247–259.
90. Wang, X.; Niu, R.; Wu, K. Lithology intelligent identification using support vector machine and adaptive cellular automata in multispectral remote sensing image. *Opt. Eng.* **2011**, *50*, 076201.
91. Othman, A.; Gloaguen, R. Improving lithological mapping by SVM classification of spectral and morphological features: The discovery of a new chromite body in the Mawat ophiolite complex (Kurdistan, NE Iraq). *Remote Sens.* **2014**, *6*, 6867–6896.
92. Cortes, C.; Vapnik, V. Support-vector networks. *Mach. Learn.* **1995**, *20*, 273–297.
93. Schölkopf, B.; Smola, A.J. *Learning with Kernels: Support Vector Machines, Regularization, Optimization, and Beyond*; MIT Press: Cambridge, MA, USA, 2002; p. 626.
94. Chang, C.C.; Lin, C.J. LIBSVM: A library for support vector machines. *ACM Trans. Intell. Syst. Technol.* **2011**, *2*, 1–27.
95. Foody, G.M.; Mathur, A. Toward intelligent training of supervised image classifications: Directing training data acquisition for SVM classification. *Remote Sens. Environ.* **2004**, *93*, 107–117.
96. Guyon, I.; Elisseeff, A. An introduction to variable and feature selection. *J. Mach. Learn. Res.* **2003**, *3*, 1157–1182.

97. Kohavi, R.; John, G.H. Wrappers for feature subset selection. *Artif. Intell.***1997**, *97*, 273–324.
98. Guyon, I.; Weston, J.; Barnhill, S.; Vapnik, V. Gene selection for cancer classification using support vector machines. *Mach. Learn.* **2002**, *46*, 389–422.
99. Karatzoglou, A.; Meyer, D.; Hornik, K. Support vector machines in R. *J. Stat. Softw.* **2006**, *15*, 1–28.
100. Pal, M.; Foody, G.M. Feature selection for classification of hyperspectral data by SVM. *IEEE Trans. Geosci. Remote Sens.* **2010**, *48*, 2297–2307.
101. ISRIC; Global and National Soils and Terrain Databases (SOTER). *Procedures Manual, Version 2.0*; ISRIC—World Soil Information: Wageningen, The Netherlands, 2013; p. 198.

APPENDIX IV: PUBLICATION P4

The Delineation of Paleo-Shorelines in the Lake Manyara Basin Using TerraSAR-X Data.

BACHOFER, F., QUÉNÉHERVÉ, G. & MÄRKER, M., 2014 - *The Delineation of Paleo-Shorelines in the Lake Manyara Basin Using TerraSAR-X Data.* - Remote Sensing 6 (3): 2195-2212 (doi: 10.3390/rs6032195).

This research paper is available online at *Multidisciplinary Digital Publishing Institute* (MDPI; www.mdpi.com):

http://www.mdpi.com/2072-4292/6/3/2195

Journal: Remote Sensing
ISSN: 2072-4292
Thomson Reuters Impact Factor 2014: 3.180
Type: Research Article.

Remote Sens. **2014**, *6*, 2195-2212; doi:10.3390/rs6032195

OPEN ACCESS

remote sensing

ISSN 2072-4292

www.mdpi.com/journal/remotesensing

Article

The Delineation of Paleo-Shorelines in the Lake Manyara Basin Using TerraSAR-X Data

Felix Bachofer [1,*], Geraldine Quéneherv é [1] and Michael Märker [2,3]

[1] Institute of Geography, University of Tuebingen, Ruemelinstr, 19-23, D-72070 Tuebingen, Germany; E-Mail: geraldine.queneherve@uni-tuebingen.de

[2] Heidelberg Academy of Sciences and Humanities, Ruemelinstr, 19-23, D-72070 Tuebingen, Germany; E-Mail: michael.maerker@geographie.uni-tuebingen.de

[3] Earth Science Department, University of Florence, Via G. La Pira 4, I-50121 Florence, Italy

***** Author to whom correspondence should be addressed; E-Mail: felix.bachofer@uni-tuebingen.de; Tel.: +49-7071-29-77528; Fax: +49-7071-29-5378.

Received: 31 December 2013; in revised form: 18 February 2014 / Accepted: 27 February 2014 / Published: 10 March 2014

Abstract: The purpose of this paper is to describe the delineation of paleo-shorelines using high resolution microwave images and digital image processing tools, and with that to contribute to the understanding of the complex landscape evolution of the Lake Manyara Basin. The surroundings of Lake Manyara are the focus of several paleo-archeological investigations, since the location is close to Olduvai Gorge, where paleo-anthropological findings can be traced back to homo habilis. In the catchment of Lake Manyara two hominin-bearing sites (0.78 to 0.63 Ma), lots of vertebrate fossils and hand axes from different periods were found. Understanding the development and extent of the lake is crucial for understanding the regional paleo-environment of the Quaternary. Morphological structures of shorelines and terraces east of Lake Manyara were identified from TerraSAR-X StripMap images. By applying a Canny edge detector, linear features were extracted and revised for different image acquisitions using a contextual approach. Those features match literature and field references. A digital elevation model of the region was used to map the most distinct paleo-shorelines according to their elevation.

Keywords: Synthetic Aperture Radar (SAR); paleo-lake; TerraSAR-X; canny filter; edge detection

1. Introduction

Many authors have used lakes as indicators for climate and landscape changes in the Quaternary [1-6]. Lakes associated with the East African Rift System (EARS) respond in a quite sensitive way to tectonic and climatic changes [1]. Different studies therefore deal with the paleo-climate and the paleo-environment of this focus region [1,7–9]. Moreover, the direct and indirect influences of some of the EARS lakes on human evolution are intensively discussed. These lakes functioned as migration corridors or mixing barriers, and therefore contributed considerably to the development of biodiversity in the region [10].

The Lake Manyara Basin has been frequented by early hominins since the Early Middle Pleistocene. Hominin fragments of *Homo heidelbergensis* (see Figure 1), Acheulian material and a rich vertebrate fauna indicate the paleoanthropological importance of the region [11–13]. In addition, the vicinity to the hominin sites at Olduvai Gorge highlights the relevance of the Lake Manyara area in terms of paleo-landscape ecology and paleo-landscape development. Findings between Lake Manyara and the Engaruka Basin and in the vicinity of Makuyuni (see Figure 1) show that archaeological evidence is closely related to different paleolake stages [12,14]. One example is evidence from the Late Stone Age [14] (with radiocarbon dated findings from 9280 ± 60 y BP), which is related to a high lake level between 12,700 to 10,000 y BP [15,16].

Figure 1. The Lake Manyara Basin in Northern Tanzania.

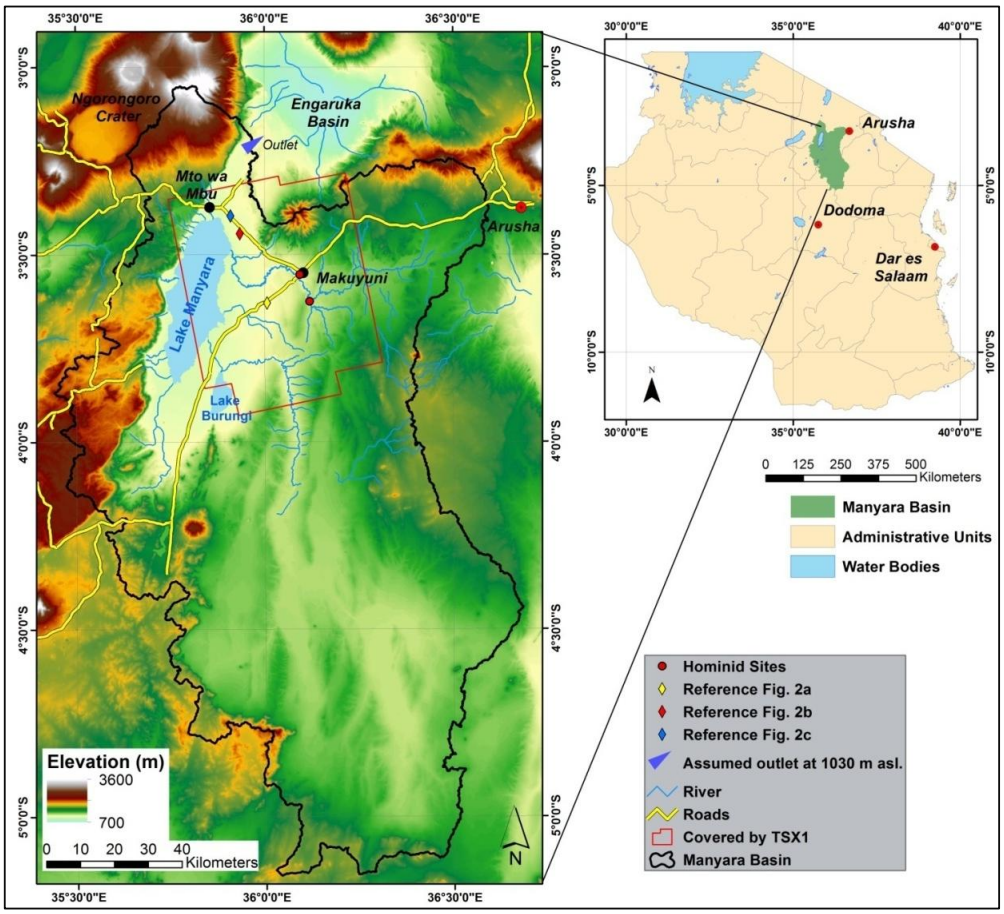

The Lake Manyara area is characterized by different lake levels that are related to specific paleo-shorelines, which appear mainly as terraces and beaches. These features and forms have been investigated only partly by detailed mapping and radiometric dating methods [17–19]. To the knowledge of the authors, a synoptic investigation of the spatial distribution of the paleolake shorelines, paleolake terraces and related features is not available. Thus, the objective of this study is to contribute to the understanding of the complex landscape evolution in the Lake Manyara area by delineating paleo-shorelines. The elevation of the shorelines in relation to the lowest outlet of the closed basin is also a focus point of the study. Because a delineation of the mentioned paleolake features was not feasible with optical remote sensing methods, backscatter intensity information from TerraSAR-X StripMap and ALOS PALSAR images were used. The morphological structures of shorelines and terraces east of Lake Manyara are characterized by high backscatter values, due to their geometric structure and texture. Linear features representing the paleo-shorelines were extracted from the intensity information of Synthetic Aperture Radar (SAR) images with a Canny edge detector and mapped in the study area. The results were linked to other studies of the Paleolake Manyara. A methodological approach in a similar context is not documented in the literature, to the knowledge of the authors.

In the last decades airborne and satellite remote sensing methodologies have been utilized increasingly for related tasks to detect paleo-landscape pattern, features and forms: Paleolakes on the Sinai Peninsula [20] were detected with IKONOS high resolution satellite imagery in combination with topographic analysis. Remote Sensing and topographical analysis were also used to delineate a paleolake in northern Darfur [21]. With Radarsat-1, Landsat ETM+ and a Shuttle Radar Topography Mission (SRTM), digital elevation model (DEM) paleo-shorelines and the paleolake highstand were identified in a megalake in Sudan [22]. SAR data was successfully applied in different studies for the mapping of subsurface geology and paleo-landscape [23,24]. Abdelsalam *et al.* [25] provide a thorough overview about the use of this methodology in arid regions. The integrated application of optical and microwave remote sensing and geospatial analysis also led to the successful delineation of buried paleo-drainages in Egypt, Sudan and Libya [26–28]. Single optical multispectral (e.g., ASTER) or high resolution (e.g., QuickBird) remote sensing data only allow the detection of the most prominent landscape features because of the spectral similarity of the covering material with its surroundings. Thus, in this study we utilize the TerraSAR-X sensor with its high resolution X-band images. This sensor offers the possibility to delineate distinct morphological structures due to the relation of backscatter intensity and geometry, texture and surface roughness [29,30].

Extracting line features is necessary for the delineation of paleo-shorelines. A general overview about line extraction methods is provided by Quackenbush [31]. Hellwich *et al.* [32] used a Markov Random Model and Bayesian classification for the extraction of linear objects from interferometric SAR data. Chanussot *et al.* [33] utilized a fuzzy fusion technique and a morphological line detector to extract a road network from multitemporal SAR images. Different Lee filters have been applied to derive linear features like coastlines from RADARSAT-1 and ERS-1 SAR data [34,35]. Using a Canny algorithm, Marghany [36] successfully delineated shoreline erosion from multitemporal SAR images.

2. Study Area and Paleolake Evidence

Lake Manyara (954 m a.s.l.) is located in an endorheic basin in the eastern branch of the EARS in northern Tanzania (Figure 1). The Manyara Basin is an asymmetrically shaped half graben, with a 200 to 600 m high escarpment in the west and a west dipping monocline in the east. The morphology of the landscape is strongly related to Quaternary volcanism and tectonic activity, which is still ongoing [36]. The basin is affected by minor *en echelon* step faults (NNE and E), whereas the lake sediments and the shorelines between Makuyuni and the lake are not disturbed by faulting [37–39]. The water supply originates from perennial springs and streams of the rift escarpment and from several seasonal drainages, of which the Makuyuni River and the Tarangire River are the largest. Today Lake Manyara is a shallow alkaline lake covering a varying area of up to approximately 550 km^2, with a maximum depth of 1.18 m, and can episodically dry out nearly completely [40]. The lowest possible outlet of the basin is located in the north of the lake along the main rift system, 78 to 80 m above today's lake level, and drains into the Engaruka Basin (Figure 1). The Tropical Rainfall Measurement Mission (TRMM) monthly Rainfall Estimate product 3B43 (V7) shows a bimodal rainfall pattern for the study area for the years 2000 to 2012, with a wet season from November to January and a second more intense wet season between March and May. The average annual precipitation ranges from 1200 mm at the escarpment to 700 mm at the plain east of the lake [41]. This results in a tropical semihumid vegetation cover with highland forests on the elevated areas west of the lake, and in a semiarid environment with bushed grassland east of the lake.

The oldest lacustrine strata within the Manyara Basin are known as the Manyara Beds and were first mentioned in 1942 [42]. They appear in the east of Lake Manyara and, based on sediments, define a maximum paleolake extent, approximately 140 m above today's lake surface. The Manyara Beds can be subdivided into a lacustrine grayish lower member (mudstones, siltstones, diatomite, marls and tuff) that was deposited between 1.3 to 0.98 Ma and 0.633 Ma, and a fluvial and terrestrial, up to 13 m thick, reddish-brown upper member (siltstones, mudstones, conglomerates and breccias) deposited between 0.633 Ma and 0.44 to 0.27 Ma. In most sections, the transition between both members is marked by a distinct tephra layer which was used for Ar^{40}/Ar^{39} dating [11,37,43]. The sections are best exposed close to the town of Makuyuni, where the sediments are partly overlain by a thin layer of Holocene soils and caliche and where big gully systems eroded into the savanna landscape.

The predominantly N-S aligned shorelines west of Lake Manyara vary from small beaches with a local relief of about 1 m to terraces that are several meters high. These terraces consist of up to three steps, indicating fluctuations of the distinct paleolake levels (Figure 2a). The terraces consist of conglomerates with different grain sizes up to 30 cm in diameter. The scarps are covered by coarse carbonates. The treads are sometimes vegetated by densely growing shrubs and small trees. Stromatolites and oncolites can be found along most of the ridges (Figure 2c). The areas between the shorelines are mostly covered by young carbonate rich soils, few are covered by carbonate gravel.

Figure 2. (**a**) Distinct paleo-shoreline (Lon. 36.006 °, Lat. −3.629 °); (**b**) Shoreline section (Lon. 35.909 °, Lat. −3.396 °); (**c**) Stromatolites and oncolites (Lon. 35.934 °, Lat. −3.444 °); Compare with Figure 1.

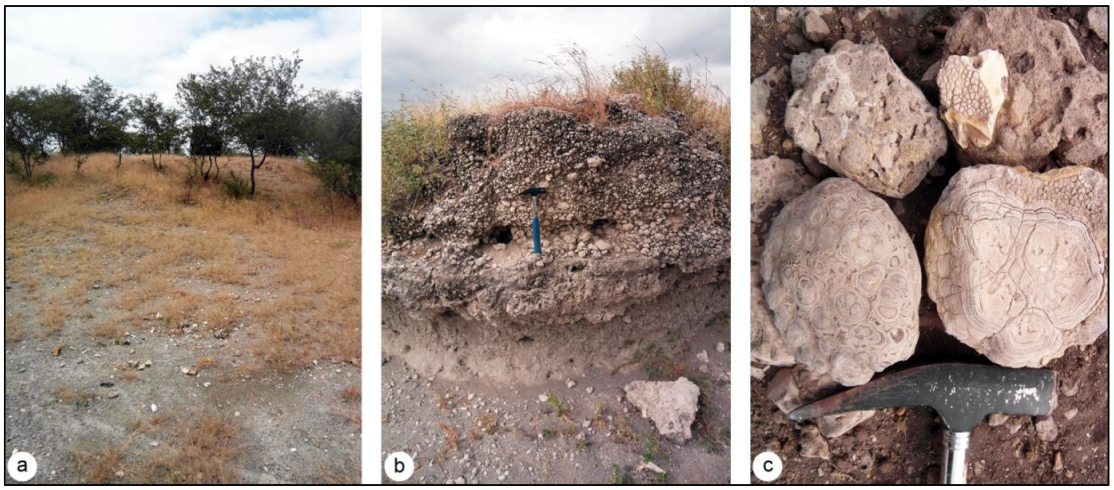

Several authors mention younger evidence of different paleolake phases than the lower member of the Manyara Beds. At the beginning of the 20th century, former shorelines and beaches up to 40 m above today's lake level were detected [44,45]. A complete series of beach terraces was found and identified as different shorelines of pluvial periods [46]. A first systematic documentation of shorelines was published in 1975 for the Lake Manyara and the Engaruka Basin [17]. The authors found eight main terraces and several beaches in the Lake Manyara Basin and mapped them without taking elevation information in the vicinity of the road leading from Makuyuni to the southern part of the lake. Another study identified four different lake levels about 6 m, 21 m, 43 to 52 m and 82 m above the current level, respectively, during field visits. The highest level also marks the threshold of a lowest possible outlet to the Engaruka and Natron-Magadi Basin [19]. These terraces have not been mapped for the whole basin yet, and the description of their location remains vague.

Other research has focused on oncolites and stromatolites, which are closely connected to flat tidal environments and therefore, have been documented as evidence for paleo-shorelines [18,47]. In an analysis of stromatolites from the northwestern area of today's lake extent close to the town of Mto Wa Mbu (Figure 1) [18], late Pleistocene and Holocene stromatolites collected on a distinct level of 20 m above today's lake level were dated by ^{14}C and Th/U series. Results showed humid periods with high lake levels for 22,000 y BP (increased water residence time, nutrient enrichment), 27,000 to 23,000 y BP (stable hydrological conditions with diluted fresh water), 35,000 to 32,000 y BP, 90,000 y BP, and an uncertain age of about 140,000 y BP [18,48]. Other research groups dated the humid period between 27,500 and 26,000 y BP, and an even younger high stand between 12,700 to 10,000 y BP by diatom analysis of two drilling cores from Lake Manyara [15,16]. All radiocarbon ages corroborate other studies of lake level fluctuations along the EARS. For the Nakuru-Elmenteita and the Naivasha Basin high lake level stands were postulated for the periods 146,000 to 73,300 y BP and 15,200 to 9600 y BP [1,49]. Trauth *et al.* [7] studied the nearby Ol Njorowa Gorge where they detected high level stands at 146,000 to 141,000 y BP and ca. 93,000 to 89,000 y BP (amongst other time intervals for the Upper Pleistocene). Garcin *et al.* [50] suggested high paleolake levels for Lake Suguta

for the periods 16,500 to 15,000 y BP, a high stand at 12,800 y BP and a high lake level from 11,800 y BP to 8500 y BP. For the Lake Natron-Magadi Basin north of Lake Manyara ages for stromatolites and related shorelines (ca. 240,000 y BP, 135,000 ± 10,000 y BP and from 12,000 to 10,000 y BP) have been found to differ from the ages of stromatolites of the Lake Manyara Basin, but agree with the ages of the other lake systems mentioned before, and the ages of the drilling cores of Lake Manyara [3,48]. The comparison of stromatolite ages in East African lake systems may involve a methodological problem, because the encrusting benthic microbial communities react very sensitively to changes in water chemistry and hydrological conditions. Therefore, stromatolites do not necessarily indicate all paleolake levels and radiometric dating and interpretation should not focus solely on these materials [18]. Trauth *et al.* [7] provide a synoptic view on East African climate change and lake systems for the last 175,000 y.

3. Methodology

3.1. SAR Processing

Six TerraSAR-X (TSX1) (~9.65 GHz; X-band) StripMap and two ALOS PALSAR (~1.27 GHz; L-band) scenes for different dates were acquired for the delineation of the paleo-shorelines (Table 1). All scenes were ordered in SLC format. The precipitation induced soil moisture increases the backscattering intensity for the soil covered areas and reduces the ability to discriminate the relevant structures of the paleo-shorelines [29,30]. Because soil moisture information with a sufficient resolution was not available, TRMM daily Rainfall Estimate product 3B42 (V7) was used to examine the days preceding the acquisition dates for relevant precipitation [41]. Relevant precipitation was measured only for the days prior to the 2013-01-15 TSX1 scene. Visual inspection confirmed a reduced contrast between the probable paleo-shorelines and their surroundings for the 2013-01-15 scene, but the most distinctive structures were still recognizable and therefore, the scene was not excluded from further processing.

Table 1. List of SAR images of the study area. Inc. Ang., incident angle at scene center; Pol., polarization; deg., degrees; Asc., Ascending.

Nr.	Sensor	Mode	Date	Time (UTC)	Orbit	Inc. Ang. (deg.)	Pol.
1	TSX1	StripMap	2011-09-08	15:46:08	Asc.	26.3 °	HH
2	TSX1	StripMap	2011-08-28	15:46:08	Asc.	26.3 °	HH
3	TSX1	StripMap	2011-09-13	15:54:39	Asc.	44.4 °	HH
4	TSX1	StripMap	2011-09-02	15:54:39	Asc.	44.4 °	HH
5	TSX1	StripMap	2012-12-24	15:46:10	Asc.	25.8 °	HH/HV
6	TSX1	StripMap	2013-01-15	15:46:08	Asc.	24.5 °	HH/HV
7	ALOS PALSAR	Fine Beam	2008-05-24	20:22:03	Asc.	38.8 °	HH/HV
8	ALOS PALSAR	Fine Beam	2010-07-15	20:25:27	Asc.	38.8 °	HH/HV

The TSX1 and ALOS PALSAR scenes were radiometrically calibrated to sigma naught (σ°) by applying a correction factor to the radar brightness product (β°). Further, radiometric normalization was applied to correct for topography using a SRTM-X DEM and the local incident angle resulting in gamma naught (γ°) [51,52]. Multilooking was applied to all scenes and they were terrain corrected. To

reduce speckle effects in the images and to pronounce morphological features they were filtered using a Lee filter [53]. Whereas the paleo-shorelines are hardly noticeable in optical remote sensing images, they are highlighted by their intense backscatter in TSX1 (Figure 3a,b). The resulting images were resampled to 3 m pixel resolution for TSX1 and to 20 m resolution for PALSAR images. The inter-scene spatial conformity is important for the following image processing steps. The high accuracy of orbital parameters of TSX1 data makes a further co-registration unnecessary [54]. The co-registration from ALOS PALSAR to the TSX1 scenes appeared insufficient for the purposes of this study, due to the different spatial resolution. Since the PALSAR images also did not show additional information of the relevant structures they were excluded from further processing.

Figure 3. Example of the workflow for a small area; (**a**) Optical reference image; (**b**) TSX1 image (13 September 2011); (**c**) Result of the Canny edge detector (background: transparent TSX1 image); (**d**) Results of shoreline extraction after post-processing.

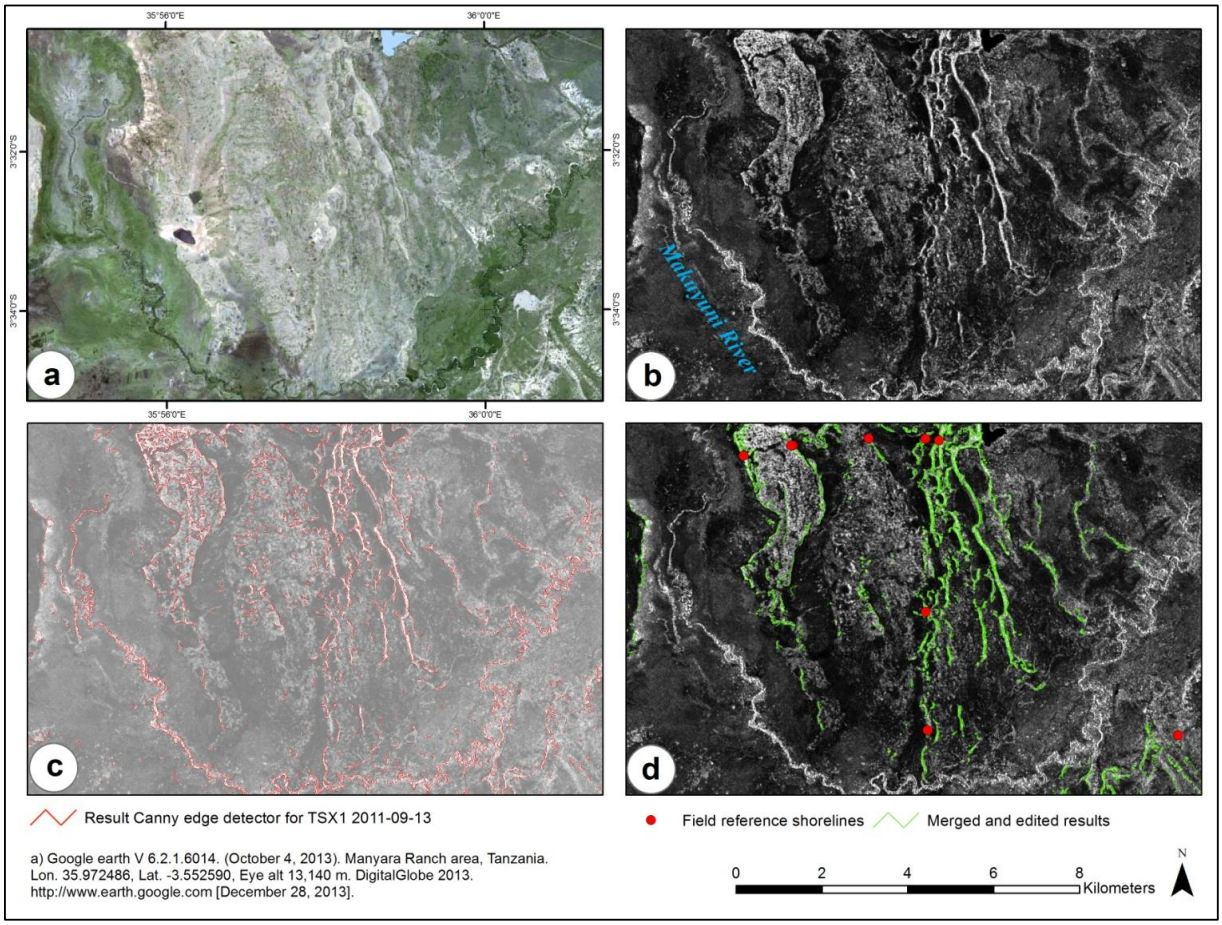

3.2. Filtering and Further Image Processing

The speckle effect makes the detection of linear features in SAR images more difficult than in optical images [34]. With the Lee filter (5 × 5) the speckle noise could be reduced while the contrast of the linear features could be preserved. The linear structures of the images were extracted from the derived image products using a Canny edge detector from the Python scikit-image module for the

SciPy library [55]. Edge detectors in general reduce the information content of an image to the structural information about objects [56]. To enhance the results of the edge detector and to be able to use similar weighting parameters for the Canny filter, all images were contrast stretched and normalized to a range from 0 to 1. The Canny procedure first applies a Gaussian filter to reduce noise in the original image. Subsequently, the strength of value gradients between the image pixels is computed by applying a directional Sobel operator. In addition, the direction of edges is approximated to vertical, horizontal and $\pm 45°$ directions. This is followed by a nonmaximum suppression, which suppresses all values along the magnitude of gradients that are not considered to be an edge to zero. Finally hysteresis thresholding is applied resulting in a lower and an upper threshold to reduce streaking effects. To achieve a good trade-off between the detection of a maximum of linear features including small beaches and the suppression of unnecessary features, the weighting parameters for the standard deviation of the Gaussian filter had to be adjusted for each scene. For hysteresis thresholding good results could be achieved with a ratio of high to low threshold of 3.5:1 (Figure 3c). The results are binary raster files with the value one representing linear features.

Morphological image processing was applied using a closing operator (dilation & erosion) to close gaps between detected lines (adjacent pixel elements) [31]. The resulting raster maps were added up to a single raster layer where structures detected in multiple scenes hold values greater than one. Only those structures were considered for further processing. An opening procedure (erosion & dilation) was applied to minimize the number of artifacts [31]. The remaining structures were reduced to their skeletons and converted into vector format. Contextual information was used to exclude features like roads and river beds (Figure 3c,d), as well as forests of the Lake Manyara National Park to the north and west of the lake, and a forested flood plain north of Lake Burungi. Many linear structures were identified on the slopes of the volcanic cone of the Essimingor northeast of the lake. The radial valleys of the volcano result in linear structures similar to shorelines (Figure 4). The western and northwestern slopes of Essimingor may have been reached by the lake during a high stand but other lines on the volcanic cone were deleted. Some of the areas between the shorelines west of Essimingor are covered by rough gravel and resulted in some artifacts that were verified in the field and removed by manual editing (Figure 3c,d; compare northwestern parts of the displayed areas).

3.3. Lake Level

SRTM-X DEM (30 m) data covers nearly the whole Manyara Basin and was seamlessly combined with a SRTM-3 DEM (90 m) to achieve coverage of the whole basin. A morphology preserving multidirectional Lee Filter for noise and artifact reduction was applied [53]. High accuracy ICESat altimetry data from 15 overpasses over Lake Manyara between 2003 and 2009 were processed to calculate a mean lake level of 954.25 m (EGM96, standard deviation of 35 cm) [57]. The SRTM-X lake level was adjusted to this height. SRTM data as well as most studies used a height of 960 m for the lake surface and as base height for relative measurements for the elevation of shorelines [18,19]. The identified paleo-shoreline features were converted to points and the corresponding heights where extracted from the DEM. The different levels of the shorelines can be traced and distinguished on the eastern side of Lake Manyara (Figure 4). The derived elevation values from SRTM-X are within a relative vertical accuracy of ± 6 m [58,59].

Figure 4. Identified shorelines (generalized for mapping issues) and field reference data from June 2013.

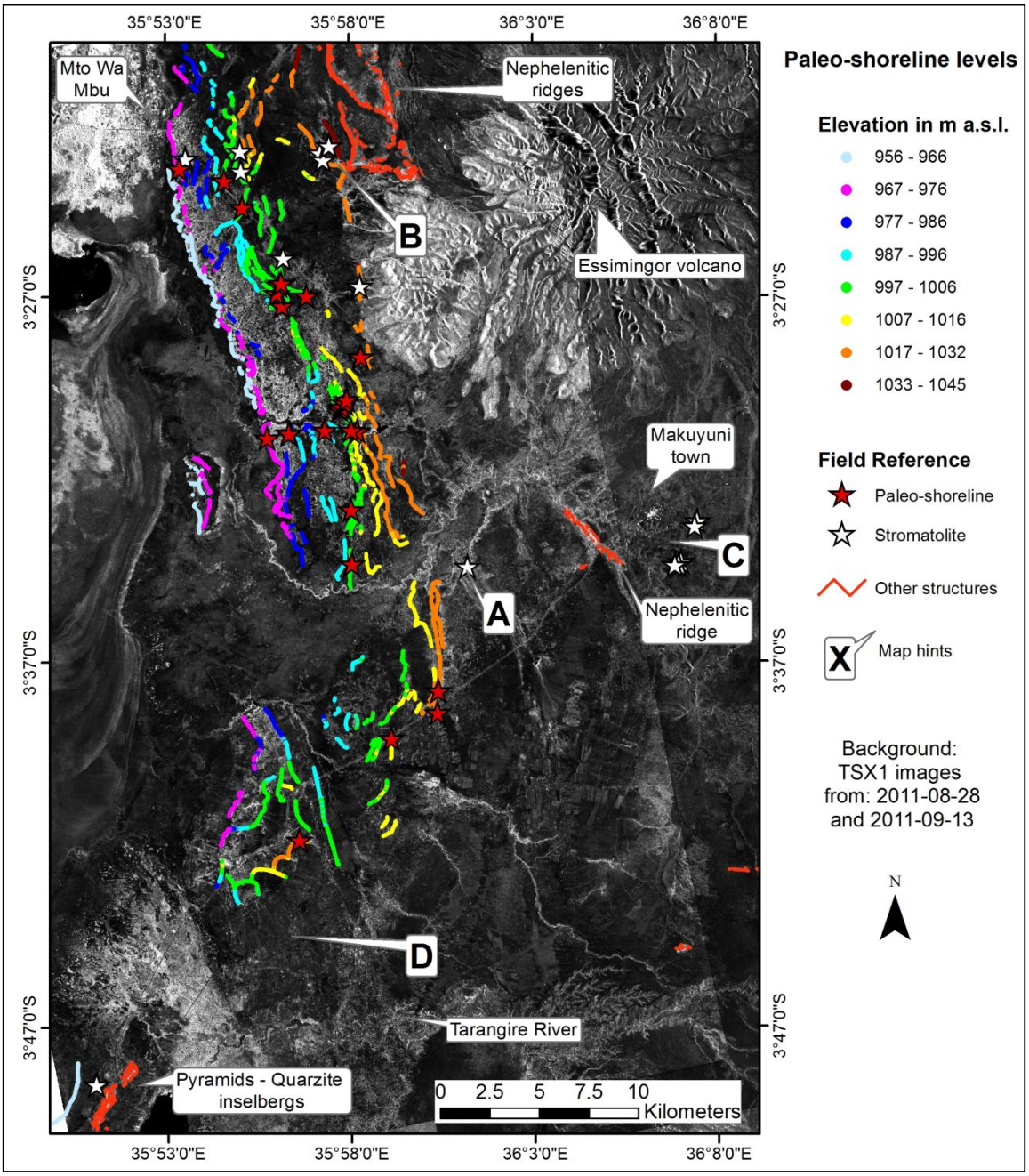

4. Results and Discussion

Different sources were used for the validation of the results. Two studies are applicable as reference from the published literature. Eight main terraces and several beaches were found and mapped up to an elevation of 1,115 m a.s.l. within the vicinity of the road leading from Makuyuni in SE direction by Keller *et al.* [17]. Four different lake levels were identified in the field but not mapped by Somi [19].

As further reference for this study, 25 paleo-shorelines and the occurrence of stromatolites (14) east of Lake Manyara were mapped with GPS points in the field during surveys in 2012 and 2013 (Figure 4).

A dense occurrence of shorelines can be seen northeast of the lake. Distinct levels of paleo-shorelines start from about 6 m to 80 m above today's lake level, some features even a few meters higher. The most frequent elevation for the occurrence of shorelines is between 1002 m and 1008 m a.s.l. (48 to 54 m above today's lake level, Figures 5 and 6). The large number of linear lacustrine features across the entire range of elevations is indicative of nearly-continuous lake level evidence by transgression and regression periods. The Makuyuni River, draining from Makuyuni into the Lake Manyara, later eroded some of the paleo-shorelines and disturbed their original distribution. The morphology of ancient shorelines is also eroded or disturbed by the Tarangire River, draining the southeastern part of the Lake Manyara Basin. The proposed method identified 24 of 25 paleo-shorelines marked by GPS points during field survey. Further, the paleolake level 2 to 6 described by Keller *et al.* [17] were delineated. The geometry of paleolake stage level 1 closest to the lake is not well enough defined for high backscatter signals. The paleolake level 7 and 8 [17] are located on elevations up to 1115 m a.s.l. and far above the lowest possible outlet into the Engaruka Basin. They coincide with the Manyara Beds, but do not agree well with findings of other studies [11,22].

No faulting for the identified shorelines can be stated, which coincides with [37–39]. Since the shorelines are in a parallel sequence and only interrupted by fluvial processes tectonic activity has not, or only marginally, affected the absolute elevations of the detected paleo-shorelines since the formation of these structures. This can be maintained at least for the shorelines in the east of the central lake and to the northeast and north of the lake. In the southeast of the lake, insufficient shorelines remain to make a corresponding statement.

Figure 5. Histogram of paleo-shoreline height level distribution. Yellow bars indicate the lake levels visualized in Figure 6.

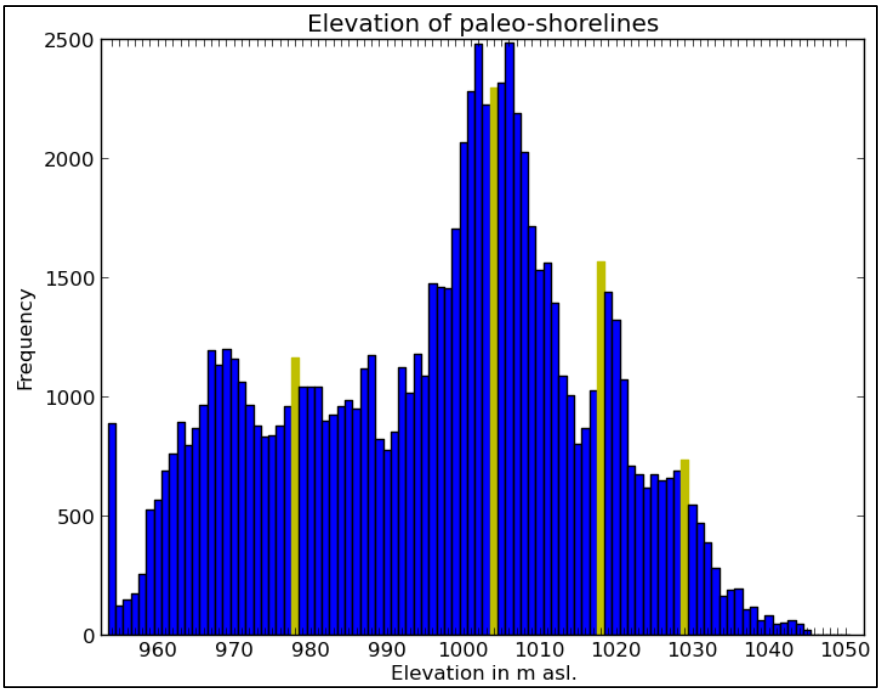

Figure 6. Different paleolake stages.

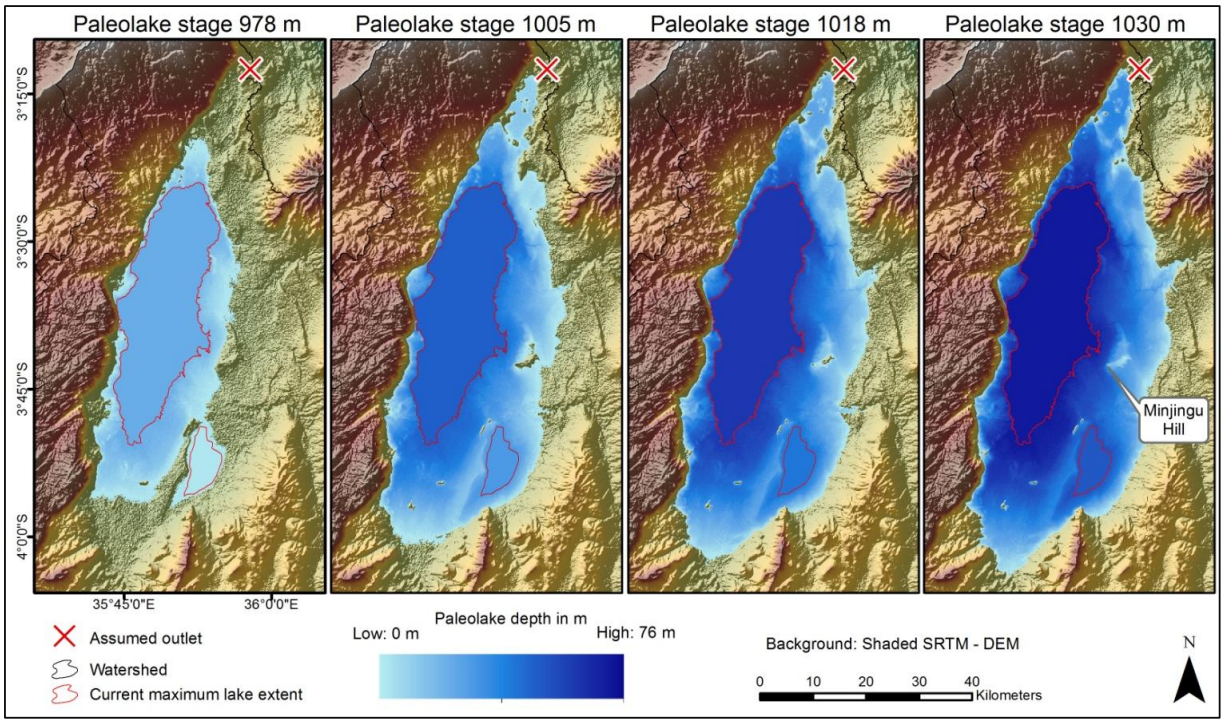

Some structures in the southeast of Lake Manyara that were mapped as smaller "beach ridges" [17] and are marked with "D" (Figure 4) could not be identified by TSX1 analysis. Because the beach ridges are not described by Keller *et al.* [17] and no field observations are available for this region we can only assume that they are too small to be detected by our analysis, or that their geometry is not well defined. Paleo-shorelines north and west of the inselbergs "Pyramids" were recognized.

Some prominent shorelines at the level of 1030 m to 1036 m a.s.l., reported by Somi [19], could not be identified by our method or during field surveys. Because their position is not described clearly and the structures are not mapped, they might be located outside the area covered by the SAR images. Alternatively, the structures might be hidden by dense trees and shrub vegetation of the Tarangire National Park so that backscatter signals fail to delineate distinct features. In addition, the PALSAR L-Band scenes could not identify these shorelines. In contrast, structures mentioned by Somi [19] close to Mto Wa Mbu and in the northeast of the Lake were clearly identified.

Linear features other than paleo-shorelines were also identified by the implemented method. These had to be reclassified using existing maps and field reference data. The structures are nephelenitic ridges north of Essimingor and west of Makuyuni, which resulted from volcanic activity, and some quartzite inselbergs southeast of Lake Manyara (Figure 4). The location marked with "A" (Figure 4) shows a section incised by the Makuyuni River, where stromatolites were found during field survey. Corresponding paleo-shorelines could not be identified in the field or by image analysis. It is likely that they belong to the older lake sediments of the Lower Manyara Beds ("C", Figure 4) close to Makuyuni, which have a radiometric age older than 0.633 Ma [11]. The Lower Manyara Beds are not the focus of this study, because they do not form distinct shorelines on the surface, because their age

exceeds the radiometric age of the paleo-shorelines, and because they have been found so far only in the surroundings of Makuyuni.

As mentioned before, we identified structures located up to 80 m above today's lake level. This is interesting because the threshold of the first possible outlet of the Manyara Basin is at about 1032 m and leads into the Engaruka and to the Natron-Magadi Basin in the north. Some authors assume that the lake level did not reach this elevation [18], others assume an even higher level above 1050 m a.s.l. [15,42], and other authors expect the maximum level of the shorelines to be around the level of the lowest possible outlet [19]. With the results from this study and the evidence of the maximum shoreline heights from field survey conducted in this study, we agree with the latter authors. The location marked with a "B" (Figure 4) illustrates the abundance of stromatolites on linear features. In this unique situation, stromatolites and oncolites are sparsely distributed on a mafic ridge and not on a well-defined shoreline. They occur four meters above the threshold for today's outflow, which can be explained by tectonic processes or an incision of the outlet from the Manyara Basin to the Engaruka Basin. By tracing these maximum lacustrine sediments to the south along the slopes of the Essimingor volcano, linear structures continue until a reference point confirms a shoreline. Directly beneath the slopes of Essimingor the paleo-shoreline might be covered by material from the talus of the volcano, like it is the case for the shorelines west of the lake at the escarpment [19]. The ridges to the east of "B" (Figure 4) are absent of lacustrine carbonate.

The histogram of the paleo-shoreline height levels (Figure 5) shows a peak at the current lake level, followed by a gap and then a steady occurrence from 960 m a.s.l. to 1040 m a.s.l. The continuous distribution of shorelines within this range indicates fluctuating lake levels. The peaks in the histogram at 970 m, 978 m, 1002 m to 1008 m, 1018 m and 1030 m depict more steady paleo-environmental conditions. For the paleolake stages marked with yellow bars in Figure 5 (24 m, 51 m, 64 m and 78 m above the current lake level) the lake extent is illustrated in Figure 6. For those paleolake levels the lake volume and the corresponding surface area were calculated (Table 2).

Table 2. Statistical evaluation of Lake Manyara paleolake stages.

Lake level	Lake Depth	Lake Volume	Surface Area
Today (954 m)	1.18 m	~0.5 km^3 *	610 km^2 (including Lake Burungi)
978 m	24 m (above today)	20.0 km^3	1152 km^2
1005 m	51 m (above today)	59.6 km^3	1757 km^2
1018 m	64 m (above today)	83.6 km^3	1932 km^2
1030 m	76 m (above today)	107.6 km^3	2062 km^2

* A bathymetric survey showed a maximum depth of 1.18 m and an average depth of 0.81 m for Lake Manyara, without Lake Burungi [23].

The lake volume and the lake surface area increase drastically with higher lake levels (Figure 6, Table 2), which is caused by the flat plain in the north, south and west of the lake. Due to the strong increase in surface, the Paleolake Manyara must have been very sensitive to climatic changes in this high temperature environment. Changes in precipitation and temperature are strongly correlated with evapotranspiration rates [17]. On one hand, this explains the amount of paleo-shorelines, and on the other hand, it suggests that Lake Manyara passed through several transgression and regression phases.

Further paleolake evidence can be confirmed for Minjingu Hill, a small inselberg five kilometers east of Lake Manyara (Figure 6). The topographic analysis shows that, even with a high stand of the lake at 1030 m (close to the height of the outlet), the hill is still not covered by water, and that very shallow waters emerge to the east of it. The hill served as a platform for cormorants which produced large quantities of guano; today, phosphate is mined in this area [17,19,60].

Overall, the detection of paleo-shorelines using the intensity information of TSX1 data was successful. The parallel orientation of the paleo-shorelines in the Lake Manyara Basin relative to the flight direction of the satellite causes a strong backscatter signal. The proposed workflow of speckle filtering to remove noise, the Canny algorithm to identify linear features, and morphological operators to extract the linear structures from the SAR images did perform well for the purpose of this study. The mapping approach is semi-automated because contextual information was necessary to remove or identify other linear features like roads, river beds and volcanic ridges. The transferability of the methodological approach is therefore limited by the availability of additional sources about other linear structures in the respective study area. Assessing the accuracy of the approach is challenging because the collection of reference points in remote areas like some parts of the Manyara Basin is difficult. Single reference points allow verifying whether a paleo-shoreline could be detected by the proposed method. To assess the completeness of the morphology of the detected paleo-shorelines, the mapping of distinct sections with multiple GPS points or kinematic measurements in the field would have been an advantage. With the field reference and literature sources [17,19], we can provide a qualitative assessment that our approach yielded good mapping results of the paleo-shorelines in the Lake Manyara Basin.

5. Conclusions

Our study shows that microwave remote sensing, image processing and topographic analysis can be combined successfully to identify and map paleo-shorelines in the Lake Manyara area, and can thereby contribute to the spatial reconstruction of paleo-environments. The endorheic Lake Manyara Basin in the eastern branch of the East African Rift System underwent different transgression and regression phases. A distinct morphologic feature of these lake fluctuations is paleo-shorelines in the form of terraces and beaches on different elevation levels across the landscape. Stromatolites of a distinct paleo-shoreline level have been radiometrically dated previously [17], leading to different conclusions about the amplitude of this fluctuations and the location of these shorelines [15,17–19,42]. In this study, we used the backscattering information of the paleo-shoreline geometry, roughness and surface cover to describe their spatial distribution. We utilized image processing methods to extract linear features and validated the results with reference data from field surveys and from literature review. In combination with a refined digital elevation model, the paleo-shoreline features served as base for the reconstruction of the paleolake stages of Lake Manyara. Some prominent paleolake levels were extracted and their spatial extent mapped (Figure 5). A maximum lake level was identified slightly above the lowest possible outlet in the north, which indicates a possible overspill into the neighboring Engaruka Basin and into the Natron-Magadi Basin in the north. The reconstructed lake level seems reasonable in the context of other research conducted in the Lake Manyara Basin. To assess the dynamics of the different transgression and regression phases and the corresponding shorelines more

detailed, additional radiometric datings are necessary. Further research is needed to help understand the emergence of the so called Lower Manyara Beds, which was not addressed in this study.

Acknowledgments

This study was financed by the Heidelberg Academy of Sciences and Humanities research center: "The Role of Culture in Early Expansions of Humans" (ROCEEH). The data used in this work were acquired as part of the activities of NASA's Science Mission Directorate, and are archived and distributed by the Goddard Earth Sciences (GES) Data and Information Services Center (DISC). We would like to thank the DLR and the German Remote Sensing Data Center (DFS) for providing the TerraSAR-X and the SRTM/X-SAR data. We acknowledge support by Deutsche Forschungsgemeinschaft and Open Access Publishing Fund of Tuebingen University.

Author Contributions

Felix Bachofer was responsible for the research design, the processing of the SAR images and the digital image analysis. All authors contributed to the collection of ground reference data during three field campaigns from 2011 to 2013. Felix Bachofer wrote the initial manuscript with significant input of Geraldine Quénéhervé and Michael Märker on the paleo-environmental context and the interpretation of the results.

Conflicts of Interest

The authors declare no conflict of interest.

References

1. Bergner, A.G.N.; Strecker, M.R.; Trauth, M.H.; Deino, A.; Gasse, F.; Blisniuk, P.; Dühnforth, M. Tectonic and climatic control on evolution of rift lakes in the Central Kenya Rift, East Africa. *Quatern. Sci. Rev.* **2009**, *28*, 2804–2816.
2. Washbourn, C.K. Lake levels and quaternary climates in the Eastern Rift valley of Kenya. *Nature* **1967**, *216*, 672–673.
3. Casanova, J. Stromatolites from the East African Rift: A synopsis. In *Phanerozoic Stromatolites II*; Bertrand-Sarfati, J., Monty, C., Eds.; Springer: Dordrecht, The Netherlands, 1994; pp. 193–226.
4. Burrough, S.L.; Thomas, D.S.G.; Bailey, R.M. Mega-lake in the Kalahari: A late Pleistocene record of the Palaeolake Makgadikgadi system. *Quatern. Sci. Rev.* **2009**, *28*, 1392–1411.
5. Olaka, L.; Odada, E.; Trauth, M.; Olago, D. The sensitivity of East African Rift lakes to climate fluctuations. *J. Paleolimnol.* **2010**, *44*, 629–644.
6. Bergner, A.G.N.; Trauth, M.H. Comparison of the hydrological and hydrochemical evolution of Lake Naivasha (Kenya) during three highstands between 175 and 60 kyr BP. *Palaeogeogr. Palaeoclimatol. Palaeoecol.* **2004**, *215*, 17–36.
7. Trauth, M.H.; Deino, A.L.; Bergner, A.G.N.; Strecker, M.R. East African climate change and orbital forcing during the last 175 kyr BP. *Earth Planet. Sci. Lett.* **2003**, *206*, 297–313.

8. Barker, P.; Gasse, F. New evidence for a reduced water balance in East Africa during the Last Glacial Maximum: Implication for model-data comparison. *Quatern. Sci. Rev.* **2003**, *22*, 823–837.
9. Schüler, L.; Hemp, A.; Zech, W.; Behling, H. Vegetation, climate and fire-dynamics in East Africa inferred from the Maundi Crater pollen record from Mt Kilimanjaro during the last glacial-interglacial cycle. *Quatern. Sci. Rev.* **2012**, *39*, 1–13.
10. Trauth, M.H.; Maslin, M.A.; Deino, A.L.; Junginger, A.; Lesoloyia, M.; Odada, E.O.; Olago, D.O.; Olaka, L.A.; Strecker, M.R.; Tiedemann, R. Human evolution in a variable environment: The amplifier lakes of Eastern Africa. *Quatern. Sci. Rev.* **2010**, *29*, 2981–2988.
11. Frost, S.R.; Schwartz, H.L.; Giemsch, L.; Morgan, L.E.; Renne, P.R.; Wildgoose, M.; Saanane, C.; Schrenk, F.; Harvati, K. Refined age estimates and Paleoanthropological investigation of the Manyara Beds, Tanzania. *J. Anthropol. Sci.* **2012**, *90*, 1–12.
12. Kaiser, T.M.; Seiffert, C.; Hertler, C.; Fiedler, L.; Schwartz, H.L.; Frost, S.R.; Giemsch, L.; Bernor, R.L.; Wolf, D.; Semprebon, G.; *et al.* Makuyuni, a new lower Palaeolithic hominid site in Tanzania. *Mitteilungen Hamburgisches Zool. Museum Inst.* **2010**, *106*, 69–110.
13. Wolf, D.; Nelson, S.V.; Schwartz, H.L.; Semprebon, G.M.; Kaiser, T.M.; Bernor, R.L. Taxonomy and paleoecology of the Pleistocene Equidae from Makuyuni, Northern Tanzania. *Palaeodiversity* **2010**, *3*, 249–269.
14. Seitsonen, O. Archaeological research in the Northern Lake Manyara Basin, Tanzania, 2003–2004. *Azania: J. Br. Inst. Eastern Afr.* **2006**, *41*, 41–67.
15. Holdship, S.A. *The Paleolimnology of Lake Manyara, Tanzania: A Diatom Analysis of a 56 m Sediment Core*; Duke University: Durham, NC, USA, 1976.
16. Barker, P.A. *Diatoms as Palaeolimnological Indicators: A Reconstruction of Late Quaternary Environments in Two East African Salt Lakes*; Loughborough University of Technology: Loughborough, UK, 1990.
17. Keller, C.M.; Hansen, C.; Alexander, C.S. Archaeology and paleoenvironments in the Manyara and Engaruka Basins, Northern Tanzania. *Geogr. Rev.* **1975**, *65*, 364–376.
18. Casanova, J.; Hillaire-Marcel, C. Chronology and paleohydrology of late Quaternary high lake levels in the Manyara Basin (Tanzania) from isotopic data (18O, 13C, 14C, ThU) on fossil stromatolites. *Quatern. Res.* **1992**, *38*, 205–226.
19. Somi, E.J. *Paleoenvironmental Changes in Central and Coastal Tanzania During the Upper Cenozoic: Magnetostratigraphy, Sedimentary Records and Shorelevel Changes*; Paleogeophysics & Geodynamics, Department of Geology and Geochemistry, University of Stockholm: Stockholm, Sweden, 1993.
20. Gaber, A.; Ghoneim, E.; Khalaf, F.; El-Baz, F. Delineation of paleolakes in the Sinai Peninsula, Egypt, using remote sensing and GIS. *J. Arid Environ.* **2009**, *73*, 127–134.
21. Elmahdy, S.I. Hydromorphological mapping and analysis for characterizing darfur paleolake, NW Sudan using remote sensing and GIS. *Int. J. Geosci.* **2012**, *2012*, 25–36.
22. Ghoneim, E.; El-Baz, F. The application of radar topographic data to mapping of a mega-paleodrainage in the Eastern Sahara. *J. Arid Environ.* **2007**, *69*, 658–675.
23. Dabbagh, A.E.; Al-Hinai, K.G.; Asif Khan, M. Detection of sand-covered geologic features in the Arabian Peninsula using SIR-C/X-SAR data. *Remote Sens. Environ.* **1997**, *59*, 375–382.

24. Schaber, G.G.; McCauley, J.F.; Breed, C.S. The use of multifrequency and polarimetric SIR-C/X-SAR data in geologic studies of Bir Safsaf, Egypt. *Remote Sens. Environ.* **1997**, *59*, 337–363.
25. Abdelsalam, M.G.; Robinson, C.; El-Baz, F.; Stern, R.J. Application of orbital imaging radar for geologic studies in arid regions: The Saharan Testimony. *Photogram. Eng. Remote Sens.* **2000**, *66*, 717–726.
26. Ghoneim, E.; El-Baz, F. DEM-optical-radar data integration for palaeohydrological mapping in the northern Darfur, Sudan: Implication for groundwater exploration. *Int. J. Remote Sens.* **2007**, *28*, 5001–5018.
27. Rahman, M.M.; Tetuko Sri Sumantyo, J.; Sadek, M.F. Microwave and optical image fusion for surface and sub-surface feature mapping in Eastern Sahara. *Int. J. Remote Sens.* **2010**, *31*, 5465–5480.
28. Ghoneim, E.; Benedetti, M.; El-Baz, F. An integrated remote sensing and GIS analysis of the Kufrah Paleoriver, Eastern Sahara. *Geomorphology* **2012**, *139–140*, 242–257.
29. Zribi, M.; Kotti, F.; Lili-Chabaane, Z.; Baghdadi, N.; Ben Issa, N.; Amri, R.; Duchemin, B.; Chehbouni, A. Soil texture estimation over a semiarid area using TerraSAR-X radar data. *IEEE Geosci. Remote Sens. Lett.* **2012**, *9*, 353–357.
30. Aubert, M.; Baghdadi, N.; Zribi, M.; Douaoui, A.; Loumagne, C.; Baup, F.; El Hajj, M.; Garrigues, S. Analysis of TerraSAR-X data sensitivity to bare soil moisture, roughness, composition and soil crust. *Remote Sens. Environ.* **2011**, *115*, 1801–1810.
31. Quackenbush, L.J. A review of techniques for extracting linear features from imagery. *Photogram. Eng. Remote Sens.* **2004**, *70*, 1383–1392.
32. Hellwich, O.; Laptev, I.; Mayer, H. Extraction of linear objects from interferometric SAR data. *Int. J. Remote Sen.* **2002**, *23*, 461–475.
33. Chanussot, J.; Mauris, G.; Lambert, P. Fuzzy fusion techniques for linear features detection in multitemporal SAR images. *IEEE Trans. Geosci. Remote Sens.* **1999**, *37*, 1292–1305.
34. Marghany, M.; Hashim, M. Developing adaptive algorithm for automatic detection of geological linear features using RADARSAT-1 SAR data. *Int. J. Phys. Sci.* **2010**, *5*, 2223–2229.
35. Marghany, M.; Sabu, Z.; Hashim, M. Mapping coastal geomorphology changes using synthetic aperture radar data. *Int. J. Phys. Sci.* **2010**, *5*, 1890–1896.
36. Marghany, M. Operational of Canny Algorithm on SAR data for modelling shoreline change. *Photogram. Fernerkundung Geoinf.* **2002**, *2*, 93–102.
37. Ring, U.; Schwartz, H.L.; Bromage, T.G.; Sanaane, C. Kinematic and sedimentological evolution of the Manyara Rift in northern Tanzania, East Africa. *Geol. Mag.* **2005**, *142*, 355–368.
38. Macheyeki, A.S.; Delvaux, D.; Batist, M.D.; Mruma, A. Fault kinematics and tectonic stress in the seismically active Manyara-Dodoma Rift segment in Central Tanzania—Implications for the East African Rift. *J. Afr. Earth Sci.* **2008**, *51*, 163–188.
39. Dawson, J.B. Neogene tectonics and volcanicity in the North Tanzania sector of the Gregory Rift Valley: Contrasts with the Kenya sector. *Tectonophysics* **1992**, *204*, 81–92.
40. Deus, D.; Gloaguen, R.; Krause, P. Water balance modeling in a semi-arid environment with limited *in situ* data using remote sensing in Lake Manyara, East African Rift, Tanzania. *Remote Sens.* **2013**, *5*, 1651–1680.

41. GES DISC (Goddard Earth Sciences (GES) Data and Information Services Center (DISC)). Available online: http://disc.sci.gsfc.nasa.gov/services (accessed on 23 December 2013).
42. Kent, P.E. A note on pleistocene deposits near lake Manyara, Tanganyika. *Geol. Mag.* **1942**, *79*, 72–77.
43. Schwartz, H.; Renne, P.R.; Morgan, L.E.; Wildgoose, M.M.; Lippert, P.C.; Frost, S.R.; Harvati, K.; Schrenk, F.; Saanane, C. Geochronology of the Manyara Beds, northern Tanzania: New tephrostratigraphy, magnetostratigraphy and 40Ar/39Ar ages. *Quatern. Geochronol.* **2012**, *7*, 48–66.
44. Uhlig, C.; Jaeger, F. *Die Ostafrikanische Bruchstufe und die angrenzenden Gebiete zwischen den Seen Magad und Lawa ja Mweri sowie dem Westfuß des Meru*; Mittler: Leipzig, Germany, 1909; p. 63.
45. Jaeger, F. *Das Hochland der Riesenkrater und die umliegenden Hochländer Deutsch-Ostafrikas; 2 Länderkundliche Beschreibung- Band 2*; Mittler: Berlin, Germany, 1913; p. 213.
46. Leakey, L.S.B. East African lakes. *Geogr. J.* **1931**, *77*, 497–508.
47. Dixit, P.C. Pleistocene lacustrine ridged oncolites from the Lake Manyara area, Tanzania, East Africa. *Sediment. Geol.* **1984**, *39*, 53–62.
48. Hillaire-Marcel, C.; Carro, O.; Casanova, J. 14C and ThU dating of Pleistocene and Holocene stromatolites from East African paleolakes. *Quatern. Res.* **1986**, *25*, 312–329.
49. Damnati, B. Sedimentology and geochemistry of lacustrine sequences of the upper Pleistocene and Holocene in intertropical area (Lake Magadi and Green Crater Lake): Paleoclimatic implications. *J. Afr. Earth Sci.* **1993**, *16*, 519–521.
50. Garcin, Y.; Junginger, A.; Melnick, D.; Olago, D.O.; Strecker, M.R.; Trauth, M.H. Late Pleistocene–Holocene rise and collapse of Lake Suguta, northern Kenya Rift. *Quatern. Sci. Rev.* **2009**, *28*, 911–925.
51. Small, D.; Miranda, N.; Meier, E. A Revised Radiometric Normalisation Standard for SAR. In Proceedings of the 2009 IEEE International on Geoscience and Remote Sensing Symposium (IGARSS), Cape Town, South Africa, 12–17 July 2009; pp. 566–569.
52. Infoterra. Radiometric Calibration of TerraSAR-X Data. Available online: http://www.astrium-geo.com/files/pmedia/public/r465_9_tsxx-itd-tn-0049-radiometric_calculations_i1.00.pdf (accessed on 23 December 2013).
53. Lee, J.S. Digital image enhancement and noise filtering by use of local statistics. *IEEE Trans. Pattern Anal. Mach. Intell.* **1980**, *2*, 165–168.
54. Jehle, M.; Perler, D.; Small, D.; Schubert, A.; Meier, E. Estimation of atmospheric path delays in TerraSAR-X data using models *vs.* measurements. *Sensors* **2008**, *8*, 8479–8491.
55. The Scikit-Image Development Team. Scikit-Image-Image Processing in Python, v0.7.2. Available online: http://scikit-image.org/ (accessed on 23 December 2013).
56. Canny, J. A Computational approach to edge detection. *IEEE Trans. Pattern Anal. Mach. Intell.* **1986**, *PAMI-8*, 679–698.
57. Gonzalez, J.H.; Bachmann, M.; Scheiber, R.; Krieger, G. Definition of ICESat selection criteria for their use as height references for TanDEM-X. *IEEE Trans. Geosci. Remote Sens.* **2010**, *48*, 2750–2757.

58. DLR SRTM X-SAR Digital Elevation Models. Status: 2012-09-28. Available online: http://eoweb.dlr.de:8080/eoweb-ng/licenseAgreements/DLR_SRTM_Readme.pdf (accessed on 23 December 2013).
59. Ludwig, R.; Schneider, P. Validation of digital elevation models from SRTM X-SAR for applications in hydrologic modeling. *ISPRS J. Photogram. Remote Sens*. **2006**, *60*, 339–358.
60. Schlüter, T.; Kohring, R. Palaeopathological fish bones from phosphorites of the Lake Manyara area, Northern Tanzania—Fossil evidence of a physiological response to survival in an extreme biocenosis. *Environ. Geochem. Health* **2002**, *24*, 131–140.

APPENDIX V: PUBLICATION P5

Comparative Analysis of Edge Detection Techniques for SAR Images.

BACHOFER, F., QUÉNÉHERVÉ, G., ZWIENER, T., MAERKER, M. & HOCHSCHILD, V., (Submitted 2015-04-27) - *Comparative Analysis of Edge Detection Techniques for SAR Images*. European Journal of Remote Sensing.

Journal: European Journal of Remote Sensing
ISSN: 2279-7254
Thomson Reuters Impact Factor 2014: 1.360
Type: Research Article.

Comparative Analysis of Edge Detection Techniques for SAR Images

Felix Bachofer [1,*], Geraldine Quénéhervé [1], Thimm Zwiener [1], Michael Maerker [2,3] and Volker Hochschild [1]

[1] Institute of Geography, University of Tuebingen, Ruemelinstr, 19-23, D-72070 Tuebingen, Germany; E-Mail: geraldine.queneherve@uni-tuebingen.de; thimm.zwiener@student.uni-tuebingen.de; volker.hochschild@uni-tuebingen.de

[2] Heidelberg Academy of Sciences and Humanities, Ruemelinstr, 19-23, D-72070 Tuebingen, Germany; E-Mail: michael.maerker@geographie.uni-tuebingen.de

[3] Earth Science Department, University of Florence, Via G. La Pira 4, I-50121 Florence, Italy

* Author to whom correspondence should be addressed; felix.bachofer@uni-tuebingen.de; Tel.: +49-7071-29-77528; Fax: +49-7071-29-5378.

Abstract: Paleo-shorelines and ancient lake terraces east of Lake Manyara in Tanzania were identified from the backscatter intensity of TerraSAR-X StripMap images. Because of their linear alignment, edge detector algorithms were applied to delineate these morphological structures from those Synthetic Aperture Radar scenes. Due to the physical properties of microwave signals, this application has proven to be a challenging task for edge detectors. This study compares the performance of different combinations of speckle reduction techniques and edge detectors in detecting linear paleo-shorelines. The Roberts, Sobel, Laplacian of Gaussian and the Canny edge detector algorithms were applied to extract and revise those linear structures. The comparison shows that the Canny edge detector is especially suitable for images with strong speckle noise. Canny achieves relatively high accuracies compared to the other operators. The stronger the filtering and speckle noise reduction, the better the performance of the other edge detection operators, compared to the Canny edge detector. The application of a wavelet transformation reduces the presence of artifacts resulting from speckle noise and emphasizes the detection of the target features.

Keywords: edge operators; SAR data; speckle noise; TerraSAR-X, wavelet transformation

Introduction

This study provides a comparison of different pre-processing and edge detection techniques. The set-up of the proposed work is a research project located in the Gregory Rift, east of Lake Manyara in northern-central Tanzania. The study area is characterized by paleo-shorelines which are related to different paleolake levels. Those linear structures appear mainly in the form of terraces and beaches. The geomorphological features and forms have been mapped only to a small extent, while some were investigated further with radiometric dating methods [Keller et al., 1975, Casanova and Hillaire-Marcel, 1992, Somi, 1993]. Optical remote sensing methods failed to delineate the above mentioned paleolake features due to spectral similarities with the surface in the vicinity. Hence, we utilized the backscatter intensity information from TerraSAR-X StripMap [Bachofer et al., 2014]. The morphological structures of shorelines and terraces east of Lake Manyara are characterized by high Synthetic Aperture Radar (SAR) backscatter values, due to their distinct geometric structure and texture (high share of gravel).

Remote sensing analysis in paleo-landscape research is a widely used and accepted method. The combination of satellite image data with digital elevation models (DEM) was applied to delineate paleolakes and paleolake related features [Ghoneim and El-Baz, 2007, Gaber et al., 2009, Elmahdy, 2012, Bachofer et al., 2014]. SAR data was used for the mapping of geological features and paleo-landscape in different studies [Dabbagh et al., 1997, Schaber et al., 1997, Abdelsalam et al., 2000]. Subsurface paleo-drainages covered by aeolian deposits could be found with remote sensing data in Egypt, Sudan and Libya [Ghoneim and El-Baz, 2007, Rahman et al., 2010, Ghoneim et al., 2012]. The detection of edges is an essential part of the extraction of linear features from images [Quackenbush, 2004] and of digital image processing in general [Gonzalez and Woods, 2010, Nixon and Aguado, 2012]. Edge detectors are also widely used to extract linear features of SAR images. Linear objects were extracted from

54 interferometric SAR data by applying a Markov Random Model and Bayesian classification
55 [Hellwich et al., 2002]. A road network could be extracted from multitemporal SAR images
56 [Chanussot et al., 1999]. Some edge detectors for SAR images consider backscatter value
57 ratios to make them more stable against speckle noise [Touzi et al., 1988, Airouche et al.,
58 2008]. Also Lee filters have been utilized to identify lineaments and coastlines from
59 RADARSAT-1 and ERS-1 SAR data [Marghany and Hashim, 2010, Marghany et al., 2010].
60 The detection of shorelines from SAR images is a frequently applied approach [Descombes et
61 al., 1996]. The Canny algorithm could indicate recent shoreline erosion from multitemporal
62 SAR images [Marghany, 2002]. Niedermeier et al. [2000] used wavelets as an active contour
63 algorithm to extract the shoreline of the German Bight. Al Fugura et al. [2011] propose a semi-
64 automated method with several steps of filtering and noise reduction, the edge enhancement
65 with a Sobel edge detector followed by a image segmentation. Another study utilizes the
66 coherence information of interferometric SAR images [Dellepiane et al., 2004].
67 The detection and delineation of landscape forms is an important element of digital image
68 processing in a geomorphological or geological context, as well as in archaeological and
69 paleo-landscape studies. SAR images yield information about the physical properties
70 (roughness and geometry) of structures and landforms. The paleo-shorelines in this case
71 example provide no clear edges like in recent shorelines, but gradual transitions. Likewise,
72 edge detection algorithms suffer from the SAR inherent effect of speckle noise and their
73 effectiveness is reduced [Touzi et al., 1988]. In this case study we compare several pre-
74 processing and filter methods combined with different edge detection techniques. The
75 intention is to provide a benchmark for the pre-processing steps of SAR images and the
76 selection of edge detection operators for applications dealing with landform detection.

77 **Study Area and Geo-Archaeological Context**

78 The endorheic Lake Manyara (954 m a.s.l.) is located in the eastern branch of the East
79 African Rift System in northern Tanzania (Fig. 1). West of the Lake Manyara Basin is a 200
80 to 600 m high escarpment, whereas in the east a west dipping monocline is adjoined. The
81 morphology of this asymmetrically shaped half graben is strongly related to Quaternary
82 volcanism and tectonic activity, which still is active [Ring et al., 2005].

83 **Figure 1 - Study area and test sites.**

84 Predominantly N-S aligned paleo-shorelines occur on the monocline east of the lake. Their
85 sizes vary from small beaches with a local relief of about 1 m to terraces which are several
86 meters high (Fig. 2). The most prominent shorelines can be found at different elevations of
87 970 m, 978 m, 1002 m to 1008 m, 1018 m and 1030 m above sea level [Bachofer et al., 2014].
88 These paleo-shorelines were formed in more humid phases during the Quaternary when the
89 lake level was higher. Some of these terraces consist of different levels which indicate
90 fluctuations of the distinct paleolake levels [Keller et al., 1975]. The terraces are covered
91 mostly with gravel sized calcrete conglomerates of up to 30 cm in diameter, which also cover
92 the scarps. The treads are often covered by densely growing shrubs and small trees. The
93 relatively flat areas between the terraces and beach ridges are mostly covered by young soils,
94 which are rich in carbonate. Stromatolites, which can be found on the shorelines and within
95 drilling cores of the lake, have been radiometrically dated [Holdship, 1976, Barker, 1990].
96 Humid periods with high lake levels could be identified for the following periods: 12,700 to
97 10,000 y BP, 22,000 y BP, 27,500 to 26,000 y BP, 27,000 to 23,000 y BP, 35,000 to 32,000 y
98 BP, 90,000 y BP, and an uncertain age of about 140,000 y BP [Hillaire-Marcel et al., 1986,
99 Casanova and Hillaire-Marcel, 1992].
100

101 **Figure 2 - (a) Distinct paleo-shoreline (Lon. 36.006°, Lat. −3.629°); (b) Shoreline section (Lon. 35.909°,**
102 **Lat. −3.396°).**

SAR Data and Processing

SAR systems illuminate a given surface and record the backscattered amplitude and the phase of the microwave signal. SAR images suffer from the speckle phenomenon which makes the interpretation and analysis difficult. It emerges as a pixel-to-pixel intensity variation. Speckle or multiplicative noise is the result of the interaction of physical properties of the ground surface and microwave signals. It is generated by the coherent addition of constructive and destructive combinations of backscatter [Lee et al., 1994, Richards, 2009]. To reduce the speckle phenomenon, multilooking and filter approaches are used with the pre-processing of the SAR data. An extensive smoothing of speckle effects leads to an information loss, a trade-off between noise reduction and information depth must therefore be determined.

SAR pre-processing

SAR sensors offer the possibility to detect and delineate distinct morphological structures. This is enabled by the relation of backscatter intensity to geometry, texture, soil moisture and surface roughness [Aubert et al., 2011, Zribi et al., 2012]. For this study we used a TerraSAR-X (TSX1) (~9.65 GHz; Single Look Complex, X-band) scene in StripMap mode. The acquisition date was 2011-09-13, 15:54 UTC (Tab 1). Soil moisture induced by precipitation leads to an increase of the dielectric constant [Aubert et al., 2011]. The resulting increase of the backscatter intensity may reduce the ability to discriminate between different landcover types. Even though no soil moisture measurements were available, the Tropical Rainfall Measurement Mission (TRMM) daily Rainfall Estimate product 3B42 (V7) shows no relevant precipitation for the preceding period [Huffman et al., 2007]. The TSX1 scenes were radiometrically calibrated to sigma naught (σ°) and normalized to correct the backscatter intensity for the predominating topography using a SRTM-X DEM and the local incident

127 angle resulting in gamma naught (γ°) [Small et al., 2009]. The resulting images were resampled
128 to 3 m ground resolution and normalized to a value range of [0, 1].

129 **Table 1 - TerraSAR-X scene.**

130 ***Multilooking***

131 Depending on the type of SAR data, there are different multilooking approaches [Lee et al.,
132 1994, Lee and Pottier, 2009]. For the TSX1 Single Look Complex (SLC) data, multilooking
133 averages the neighboring pixels in azimuth and slant range direction. Since the azimuth and the
134 slant range resolution differ, multilooking is used to create square pixels. By averaging the
135 pixels, speckle is reduced concurrently. When the number of looks is increased, the geometrical
136 resolution is degraded.

137 ***Spatial filtering***

138 For the comparison of filter methods to reduce speckle we utilized standard non-adaptive
139 and adaptive filters. The non-adaptive filters do not consider local variability in an image. The
140 median filter replaces the central pixel of a kernel with the median value of all kernel pixels,
141 while the lowpass mean filter replaces the central pixel with the mean value of the kernel
142 pixels. Adaptive filters consider statistical characteristics for the kernel extent [Gonzalez and
143 Woods, 2010]. Adaptive Lee filters assume a Gaussian distribution of the noise of the pixel in
144 a kernel. Secondly they assume a similar mean and variance of the target pixel value than for
145 the kernel values [Lee, 1980, Touzi, 2002]. The Refined Lee filter is an improvement of the
146 multiplicative Lee filter. In image areas with high variance the filter takes into account the
147 orientation of supposed edges to preserve them [Lee, 1981]. The Gamma MAP (Maximum A
148 Posteriori) filter assumes a gamma distributed cross-section and a new pixel value lying
149 between the average kernel values and the original target pixel value. The filter thereby

150 considers statistical and spatial properties of the image section [Frost et al., 1982, Lopes et al.,
151 1990]. All filters were employed on the TSX1 images with a 5 x 5 kernel.

152 **Edge Detection Operators**

153 Edge detection is based on the approach that an edge is the barrier between an object and
154 the background and additionally the boundary between overlapping objects [Dimou et al.,
155 2000]. In a grey-level picture containing homogeneous objects, an edge is the boundary
156 between two regions of different grey levels [Davis, 1975].
157 The discrimination between two regions with intensity changes provides an estimate of the
158 first-order derivative [Nixon and Aguado, 2012]. Template-based edge detection operators
159 use a small, discrete template as a model of an edge instead of using a derivative operator
160 directly [Parker, 2011]. The Roberts cross [Roberts, 1963] and Sobel [Sobel and Feldman,
161 1968] operators are such widely used examples. In the 1980s edge detection techniques were
162 improved by adding preliminary filtering steps such as smoothing (most commonly with the
163 Gaussian filter), called Laplacian of Gaussian (or Marr-Hildreth edge detector) [Marr and
164 Hildreth, 1980]. Canny followed an approach to define edges as local maxima of the
165 convolution of the image [Canny, 1986]. Wavelet transformation served as useful processing
166 step for despeckling to extract edges from images [Niedermeier et al., 2000, Gleich et al.,
167 2008].

168 ***Roberts***

169 The Roberts edge detector performs a simple 2-D spatial gradient measurement. The operator
170 uses a pair of 2 x 2 convolution kernel, one kernel is rotated by 90°. These kernels emphasize
171 edges running at 45° to the grid, one kernel for each of the two perpendicular orientations
172 [Maini and Aggarwal, 2009]:

$$\begin{matrix}1 & 0\\ 0 & -1\end{matrix} = R_x \qquad \begin{matrix}0 & 1\\ -1 & 0\end{matrix} = R_y \tag{1}$$

173 ***Sobel***

174 The Sobel operator uses 3x3 convolution masks for the detection of the gradients x and y.
175 Both of the kernels can be inverted, this provides four possible directions for measurements
176 [Nixon and Aguado, 2012].

$$\begin{matrix}1 & 0 & -1\\ 2 & 0 & -2\\ 1 & 0 & -1\end{matrix} = S_x \qquad \begin{matrix}1 & 2 & 1\\ 0 & 0 & 0\\ -1 & -2 & -1\end{matrix} = S_y \tag{2}$$

177 ***Laplacian of Gaussian (LoG)***

178 Marr and Hildreth [1980] combined their knowledge about biological vision into a
179 mathematical model. The most important points are local averaging done by smoothing the
180 image with a filter and looking for extreme values for a change in intensity (representing an
181 edge). The most commonly used smoothing filter is the Gaussian filter. The two-dimensional
182 Gaussian is the function G being convolved with the image.

$$G_\sigma(x, y) = e^{\frac{-(x^2+y^2)}{2\sigma^2}} \tag{3}$$

183 where σ is the standard deviation of the associated Gaussian probability distribution [Parker,
184 2011].

185 After the image is convolved, the Laplacian operator ∇ can be applied:

$$\nabla^2 = \frac{\delta^2}{\delta x^2} + \frac{\delta^2}{\delta y^2} \tag{4}$$

186 The Laplacian has the advantage of being invariant to rotation, therefore it responds
187 equally to changes in intensity regardless of mask direction [Gonzalez and Woods, 2010].

188 Since the order does not matter both, the Laplacian operator and the Gaussian filter, can be
189 combined into the Laplacian of Gaussian (LoG):

$$\nabla^2 G_\sigma = \left(\frac{r^2 - 2\sigma^2}{\sigma^4}\right) e^{\left(\frac{-r}{2\sigma^2}\right)} \quad \text{where } r = \sqrt{x^2 + y^2} \text{ [Parker, 2011].} \tag{5}$$

190 ***Canny edge detection***

191 Canny [Canny, 1986] followed an approach to improve current methods by defining three
192 performance criteria: i) the signal-to-noise ratio should be as large as possible, ii) the distance
193 between the calculated edge pixels and the edge should be as small as possible and iii) the
194 edge detector should not identify multiple edge pixels when there is one single edge. The
195 author defined a filter f that performs best for all three criteria. An efficient approximation for
196 those criteria is the first derivative of a Gaussian function.

197 The Gaussian has the form:

$$G(x) = e^{-\frac{x^2}{2\sigma^2}} \tag{6}$$

198 The derivative with respect to x is therefore:

$$G'(x) = \left(-\frac{x}{\sigma^2}\right) e^{-\left(\frac{x^2}{2\sigma^2}\right)} \tag{7}$$

199 In two dimensions, a Gaussian is given by:

$$G(x, y) = \sigma^2 e^{-\left(\frac{x^2 + y^2}{2\sigma^2}\right)} \tag{8}$$

200 Furthermore, G has derivatives in both the x and y directions. The approximation of
201 Canny's optimal filter for edge detection is G', and so by convolving the input image with G',
202 an image E that has enhanced edges will be obtained [Parker, 2011]. The next step is a
203 nonmaximum suppression, which suppresses all values alongside the magnitude of gradients.
204 Hysteresis thresholding is applied to exclude weak edges which are not connected to strong
205 edges, by tracking the edges by a lower and an upper threshold [Canny, 1986, McIlhagga,
206 2011].

Discrete Wavelet Transformation

The wavelet transformation developed as an advancement of the Fourier transformation in signal processing. The transformation is based on small waves (wavelets), which can have a varying frequency and are more sensitive to local variations [Mallat, 1989, Gonzalez and Woods, 2010]. They allow the decomposing of complex image information into elementary forms and the reconstruction of them again. The Discrete Wavelet Transformation (DWT), Wavelet ψ(x) and scaling φ(x) are coefficients of the function $f(x) \in L^2(\mathbf{R})$. The DWT coefficients for a sequence of numbers $f(n)$ are defined as:

$$W_\varphi(j_0,k) = \frac{1}{\sqrt{M}} \sum_n f(n) \varphi_{j_0,k}(n) \tag{9}$$

$$W_\psi(j,k) = \frac{1}{\sqrt{M}} \sum_n f(n) \psi_{j,k}(n) \quad \text{for } j \geq j_0 \tag{10}$$

The applied function results in four sub images: the low pass approximation (LL), the low pass (rows) and high pass (columns) (vertical edge details - LH), the high pass (row) and low pass (column) (horizontal edge details - HL) and high pass filtering (diagonal edge details - HH) (Fig. 3). The reconstruction of the DWT coefficients can be achieved by:

$$f(n) = \frac{1}{M} \sum_k W_\varphi(j_0,k) \varphi_{j_0,k}(n) + \frac{1}{\sqrt{M}} \sum_{j=j_0}^{\infty} \sum_k W_\psi(j,k) \psi_{j,k}(n) \tag{11}$$

Figure 3 - One scale DWT for "test site 2" (pre-processing: multilooking 4 / median filter 5x5 kernel).

A comparison of values along a profile and a source image and the reconstructed DWT, considering three levels of decomposition, shows distinct edges where high intensities occur (Fig. 4). As the operator, we used the Haar function, which is discussed in detail by Strömberg [1981] and Beylkin et al. [1991].

Figure 4 - Comparison of a value profile (test site 2) between source image (pre-processing: multilooking 4 / median filter 5x5 kernel) and 3-level DWT on a 520 m transect.

226 ***Experimental set-up***

227 A different number of looks and/or one of the spatial filters were applied to the TSX-1
228 subsets (see Fig. 1; Area 1 to 4). The proposed edge detectors were then utilized to determine
229 linear structures/edges in the pre-processed images. The results were compared with ground
230 reference information which was collected by GPS tracks in the four study areas during field
231 campaigns between 2010 and 2014 (Fig. 1). The number of edge pixels, which were identified
232 correctly, was set into relation with wrongly identified edges in each subset. To allow the
233 comparability of the achieved accuracies between the four test sites, the number of correctly
234 identified pixels was normalized with the total number of pixels for each test site.
235 All edge detectors need at least one parameter to define a threshold, which declares a
236 change in pixel values as an edge or a value which defines an accompanied filter. Since the
237 selection of these values is crucial for a comparison we applied an automated search from the
238 upper and lower bounds of the value range, which was iteratively refined. For each study area
239 an individual minimum number of edges to be detected were defined based on expert
240 knowledge to assure an adequate representation of the paleo-shorelines. The Sobel and Canny
241 Operator were applied to the reconstructed DWT in order to examine if DWT emphasizes the
242 detection of edges of such continuous landforms.

243 **Results and Discussion**

244 Different combinations of speckle reduction methods and edge detection algorithms were
245 processed and compared with the corresponding field reference for each test site. The
246 diagrams from figure 5 illustrate the accuracies for all four study areas. Table 2 shows
247 detailed results for a selection of processing set-ups for “study area 2”. Similar trends are
248 recognizable in all test sites. The Canny filter outperforms all other edge detectors, with most
249 of the pre-processing datasets, for all test sites. The results indicate that this advantage of the

Canny operator is mainly achieved with a low grade pre-processing images. The first-derivative edge detectors achieve 3-6 % lower accuracies than the Canny operator for the methods with "1 look" and "2 looks" (Table 2, ID numbers 1 to 6). The LoG achieves lower accuracies than the other edge detectors, especially for images with a high number of looks. This is mainly because the Gaussian filter is highly affected by low gradients, which are produced with high speckle noise reduction.

Figure 5 - Diagrams of the edge detection accuracy for the four test sites. The number on the x-axis stands for the multilooking/filter combination (see Table 2).

Table 2 - Weighted accuracy in percent of edge detection methods for "test site 2". T = threshold for edge detection; S = sigma value; LH = lower hysteresis; UH = upper hysteresis; LA = laplacian alpha; k = kernel size.

The performance of the Canny filter converges, with an increasing number of looks, with the accuracies of the other operators. A strong reduction in speckle noise and filtering first-order derivates produced relative high accuracies compared to the Canny operator. Since the Canny edge detector and the LoG operator apply a filter before detecting edges, they perform relatively well with images which have a low number of looks and a relatively high share of speckle noise. This advantage declines with a further reduction of speckle noise by multilooking and spatial filtering. A balanced speckle reduction leads therewith to a significant improvement in the edge detection accuracy. For "4 looks", "8 looks", "10 looks" and "12 looks" (ID numbers 9 to 16) Roberts and Sobel filters perform equally well or even outperform the results of the Canny operator in certain cases.

For median filtered images, higher accuracies were achieved (ID numbers 3, 6, 11 and 14). The pre-processing chain which applied a number of "2 looks" or "4 looks" and a median filter could achieve in average the highest accuracies for all test sites and for all edge

operators (ID numbers 6 and 11). Furthermore, the application of DWT leads to an improvement in the edge detection performance with up to 5 % higher accuracies.

For “test site 1” and “test site 2”, low accuracies can be found while pre-processing with “8 looks” and Lee filtering (ID number 13). Low accuracy results for “test site 4” were produced from pre-processing with “8 looks” (ID number 12), and other pre-processing chains, where only multilooking was applied (Fig. 5 & 6). This results from a strong smoothing effect (Lee filter), which causes the borders of the shorelines to exceed the field reference and thereby significantly reduce the calculated accuracy. The same filtering yields a positive effect in “test site 4” (ID number 13, excluding LoG), whilst the images, with only multilooking and no further filtering, remain very noisy and are resulting into low accuracies (ID number 12).

Figure 6 - Multilooking and filtering for “test site 1” (images: a, b, c with an extent of 1546 m x 1102 m) and for “test site 4” (images d, e, f with an extent of 3718 m x 1590 m)

The visual interpretation of the results for “test site 2” indicates that the Canny filter delineates the paleo-shorelines exceptionally well (Fig. 7 d, k, l). While both the Sobel and the LoG operators result in many single segments, the Canny operator delivers coherent edges. First-order derivatives generally produce thicker edges in an image whereas second-order derivatives show a stronger response to thin lines and noise. The DWT reduces the number of artifacts and amplifies the target structures significantly.

Figure 7 - Speckle reduction and edge detection for “study area 2”. The extent of the image is 2400 m x 1800 m. a), d) and g) represent different pre-processing examples.

Conclusions

In conclusion, the study has demonstrated that by using edge detectors, morphological features in SAR images can be detected with high accuracies. We compared different speckle reduction techniques in combination with different edge detectors, striving to detect paleo-

300 shorelines in a TSX1 SAR image. The case study determined that the performance of the
301 proposed pre-processing techniques and edge detectors lead to different accuracies. The
302 Canny edge detector is especially suitable for images exhibiting a high speckle noise. The
303 combination of DWT and the Canny operator yields the highest accuracies and provides
304 stable results with different pre-processing steps. First-derivative edge operators have proven
305 to perform well when applied to speckle reduced images. Median filtering proved to be an
306 advantageous pre-processing step.

307 We are inclined to state that the derived values for thresholds of the operators and the
308 lower and upper hysteresis of the canny operator are dependent on the land cover, soil
309 moisture, and morphological structure of the target features, as well as the wavelength and the
310 calibration of the SAR sensor. Nevertheless, the general trend in the results can be transferred
311 to other edge detection issues and serve as a benchmark.

312 **Acknowledgments**

313 This study was financed by the Heidelberg Academy of Sciences and Humanities research
314 center: “The Role of Culture in Early Expansions of Humans” (ROCEEH). We would like to
315 thank the DLR and the German Remote Sensing Data Center (DFS) for providing the
316 TerraSAR-X and the SRTM/X-SAR data. We acknowledge support by Deutsche
317 Forschungsgemeinschaft and Open Access Publishing Fund of Tuebingen University.

318 **References**

319 Abdelsalam, M. G., Robinson, C., El-Baz, F. & Stern, R. J., 2000 - *Application of Orbital*
320 *Imaging Radar for Geologic Studies in Arid Regions: The Saharan Testimony*.
321 Photogrammetric Engineering & Remote Sensing 66 (6): 717-726.
322 Airouche, M., Zelmat, M. & Kidouche, M., 2008 - *Statistical Edge Detectors Applied to SAR*
323 *Images* International Journal of Computers Communications & Control 3 144-149.
324 Al Fugura, A. k., Billa, L. & Pradhan, B., 2011 - *Semi-automated procedures for shoreline*
325 *extraction using single RADARSAT-1 SAR image*. Estuarine, Coastal and Shelf Science
326 95 (4): 395-400. doi: 10.1016/j.ecss.2011.10.009.
327 Aubert, M., Baghdadi, N., Zribi, M., Douaoui, A., Loumagne, C., Baup, F., El Hajj, M. &
328 Garrigues, S., 2011 - *Analysis of TerraSAR-X data sensitivity to bare soil moisture,*

329 *roughness, composition and soil crust*. Remote Sensing of Environment 115 (8): 1801-
330 1810. doi: 10.1016/j.rse.2011.02.021.
331 Bachofer, F., Quénéhervé, G. & Märker, M., 2014 - *The Delineation of Paleo-Shorelines in the*
332 *Lake Manyara Basin Using TerraSAR-X Data*. Remote Sensing 6 (3): 2195-2212.
333 Barker, P. A., 1990 - *Diatoms as palaeolimnological indicators: A reconstruction of Late*
334 *Quaternary environments in two East African salt lakes.* Loughborough University of
335 Technology, Doctor of Philosophy.
336 Beylkin, G., Coifman, R. & Rokhlin, V., 1991 - *Fast wavelet transforms and numerical*
337 *algorithms I*. Communications on Pure and Applied Mathematics 44 (2): 141-183. doi:
338 10.1002/cpa.3160440202.
339 Canny, J., 1986 - *A Computational Approach to Edge Detection*. Pattern Analysis and Machine
340 Intelligence, IEEE Transactions on PAMI-8 (6): 679-698. doi:
341 10.1109/tpami.1986.4767851.
342 Casanova, J. & Hillaire-Marcel, C., 1992 - *Chronology and paleohydrology of late Quaternary*
343 *high lake levels in the Manyara basin (Tanzania) from isotopic data (18O, 13C, 14C,*
344 *ThU) on fossil stromatolites*. Quaternary Research 38 (2): 205-226. doi: 10.1016/0033-
345 5894(92)90057-p.
346 Chanussot, J., Mauris, G. & Lambert, P., 1999 - *Fuzzy fusion techniques for linear features*
347 *detection in multitemporal SAR images*. Geoscience and Remote Sensing, IEEE
348 Transactions on 37 (3): 1292-1305. doi: 10.1109/36.763290.
349 Dabbagh, A. E., Al-Hinai, K. G. & Asif Khan, M., 1997 - *Detection of sand-covered geologic*
350 *features in the Arabian Peninsula using SIR-C/X-SAR data*. Remote Sensing of
351 Environment 59 (2): 375-382. doi: Doi: 10.1016/s0034-4257(96)00160-5.
352 Davis, L. S., 1975 - *A survey of edge detection techniques*. Computer Graphics and Image
353 Processing 4 248-270. doi: 10.1016/0146-664X(75)90012-X.
354 Dellepiane, S., De Laurentiis, R. & Giordano, F., 2004 - *Coastline extraction from SAR images*
355 *and a method for the evaluation of the coastline precision*. Pattern Recognition Letters
356 25 (13): 1461-1470. doi: 10.1016/j.patrec.2004.05.022.
357 Descombes, X., Moctezuma, M., Maître, H. & Rudant, J.-P., 1996 - *Coastline detection by a*
358 *Markovian segmentation on SAR images*. Signal Processing 55 (1): 123-132. doi:
359 10.1016/S0165-1684(96)00125-9.
360 Dimou, A., Uzunoglou, N., Frangos, P., Jäger, G. & Benz, U., 2000 - *Linear features' detection*
361 *in SAR images using Fuzzy Edge Detector*. In proceeding of: SBOT 2000, 49.1 - 49.12,
362 Samos/Greece.
363 Elmahdy, S. I., 2012 - *Hydromorphological Mapping and Analysis for Characterizing Darfur*
364 *Paleolake, NW Sudan Using Remote Sensing and GIS*. International Journal of
365 Geosciences 2012 (3): 25-36. doi: 10.4236/ijg.2012.31004.
366 Frost, V. S., Stiles, J. A., Shanmugan, K. S. & Holtzman, J., 1982 - *A Model for Radar Images*
367 *and Its Application to Adaptive Digital Filtering of Multiplicative Noise*. Pattern
368 Analysis and Machine Intelligence, IEEE Transactions on PAMI-4 (2): 157-166. doi:
369 10.1109/TPAMI.1982.4767223.
370 Gaber, A., Ghoneim, E., Khalaf, F. & El-Baz, F., 2009 - *Delineation of paleolakes in the Sinai*
371 *Peninsula, Egypt, using remote sensing and GIS*. Journal of Arid Environments 73 (1):
372 127-134. doi: 10.1016/j.jaridenv.2008.08.007.
373 Ghoneim, E., Benedetti, M. & El-Baz, F., 2012 - *An integrated remote sensing and GIS analysis*
374 *of the Kufrah Paleoriver, Eastern Sahara*. Geomorphology 139–140 (0): 242-257. doi:
375 10.1016/j.geomorph.2011.10.025.
376 Ghoneim, E. & El-Baz, F., 2007 - *The application of radar topographic data to mapping of a*
377 *mega-paleodrainage in the Eastern Sahara*. Journal of Arid Environments 69 (4): 658-
378 675. doi: 10.1016/j.jaridenv.2006.11.018.

379 Ghoneim, E. & El-Baz, F., 2007 - *DEM-optical-radar data integration for*
380 *palaeohydrological mapping in the northern Darfur, Sudan: implication for*
381 *groundwater exploration*. International Journal of Remote Sensing 28 (22): 5001-5018.
382 doi: 10.1080/01431160701266818.
383 Gleich, D., Kseneman, M. & Datcu, M., 2008 - *Despeckling of TerraSAR-X data using second*
384 *generation wavelets*. ESA-EUSC 2008: Image Information Mining: pursuing
385 automation of geospatial intelligence for environment and security, Frascati (Italy).
386 Gonzalez, R. C. & Woods, R. E., 2010 - *Digital image processing*. 3rd, Prentice Hall, Upper
387 Saddle River, N.J.
388 Hellwich, O., Laptev, I. & Mayer, H., 2002 - *Extraction of linear objects from interferometric*
389 *SAR data*. International Journal of Remote Sensing 23 (3): 461-475. doi:
390 10.1080/01431160110046750.
391 Hillaire-Marcel, C., Carro, O. & Casanova, J., 1986 - *14C and ThU dating of Pleistocene and*
392 *Holocene stromatolites from East African paleolakes*. Quaternary Research 25 (3): 312-
393 329. doi: 10.1016/0033-5894(86)90004-9.
394 Holdship, S. A., 1976 - *The paleolimnology of Lake Manyara, Tanzania : a diatom analysis of*
395 *a 56 meter sediment core: a diatom analysis of a 56 meter sediment core.* Duke
396 University, Dissertation/Thesis.
397 Huffman, G. J., Adler, R. F., Bolvin, D. T., Gu, G. J., Nelkin, E. J., Bowman, K. P., Hong, Y.,
398 Stocker, E. F. & Wolff, D. B., 2007 - *The TRMM multisatellite precipitation analysis*
399 *(TMPA): Quasi-global, multiyear, combined-sensor precipitation estimates at fine*
400 *scales*. Journal of Hydrometeorology 8 (1): 38-55. doi: Doi 10.1175/Jhm560.1.
401 Keller, C. M., Hansen, C. & Alexander, C. S., 1975 - *Archaeology and Paleoenvironments in*
402 *the Manyara and Engaruka Basins, Northern Tanzania*. Geographical Review 65 (3):
403 364-376.
404 Lee, J.-S., 1981 - *Refined filtering of image noise using local statistics*. Computer Graphics and
405 Image Processing 15 (4): 380-389. doi: 10.1016/S0146-664X(81)80018-4.
406 Lee, J.-S. & Pottier, E., 2009 - *Polarimetric radar imaging : from basics to applications*. CRC
407 Press, Boca Raton, Fla. [u.a.].
408 Lee, J. S., 1980 - *Digital image enhancement and noise filtering by use of local statistics*. IEEE
409 Trans Pattern Anal Mach Intell 2 (2): 165-168.
410 doi: 10.1109/TPAMI.1980.4766994.
411 Lee, J. S., Jurkevich, L., Dewaele, P., Wambacq, P. & Oosterlinck, A., 1994 - *Speckle filtering*
412 *of synthetic aperture radar images: A review*. Remote Sensing Reviews 8 (4): 313-340.
413 doi: 10.1080/02757259409532206.
414 Lopes, A., Nezry, E., Touzi, R. & Laur, H., 1990 - *Maximum A Posteriori Speckle Filtering*
415 *And First Order Texture Models In Sar Images.* Geoscience and Remote Sensing
416 Symposium, 1990. IGARSS '90. 'Remote Sensing Science for the Nineties'., 10th
417 Annual International, 2409-2412.
418 Maini, R. & Aggarwal, H., 2009 - *Study and Comparison of Various Image Edge Detection*
419 *Techniques*. International Journal of Image Processing (IJIP) 3 (1): 1-11. doi:
420 Mallat, S. G., 1989 - *A theory for multiresolution signal decomposition: the wavelet*
421 *representation*. Pattern Analysis and Machine Intelligence, IEEE Transactions on 11
422 (7): 674-693. doi: 10.1109/34.192463.
423 Marghany, M., 2002 - *Operational of Canny Algorithm on SAR data for modelling shoreline*
424 *change*. Photogrammetrie, Fernerkundung, Geoinformation (PFG) 2 93-102. doi:
425 Marghany, M. & Hashim, M., 2010 - *Developing adaptive algorithm for automatic detection*
426 *of geological linear features using RADARSAT-1 SAR data*. International Journal of
427 Physical Sciences 5 2223-2229.

428 Marghany, M., Sabu, Z. & Hashim, M., 2010 - *Mapping coastal geomorphology changes*
429 *using synthetic aperture radar data*. International Journal of Physical Sciences 5 (12):
430 1890-1896.
431 Marr, D. & Hildreth, E., 1980 - *Theory of Edge Detection*. Proceedings of the Royal Society of
432 London. Series B. Biological Sciences 207 (1167): 187-217. doi:
433 10.1098/rspb.1980.0020.
434 McIlhagga, W., 2011 - *The Canny Edge Detector Revisited*. International Journal of
435 Computer Vision 91 (3): 251-261. doi: 10.1007/s11263-010-0392-0.
436 Niedermeier, A., Romaneessen, E. & Lehner, S., 2000 - *Detection of coastlines in SAR images*
437 *using wavelet methods*. Geoscience and Remote Sensing, IEEE Transactions
438 on 38 (5): 2270-2281. doi: 10.1109/36.868884.
439 Nixon, M. S. & Aguado, A. S., 2012 - *Feature extraction & image processing for computer*
440 *vision*. 3rd, Academic Press, Oxford.
441 Parker, J. R., 2011 - *Algorithms for image processing and computer vision*. 2nd, Wiley
442 Computer Pub., New York.
443 Quackenbush, L. J., 2004 - *A Review of Techniques for Extracting Linear Features from*
444 *Imagery*. Photogrammetric Engineering & Remote Sensing 70 (12): 1383–1392. doi:
445 Rahman, M. M., Tetuko Sri Sumantyo, J. & Sadek, M. F., 2010 - *Microwave and optical image*
446 *fusion for surface and sub-surface feature mapping in Eastern Sahara*.
447 International Journal of Remote Sensing 31 (20): 5465 - 5480. doi:
448 10.1080/01431160903302999.
449 Richards, J. A., 2009 - *Remote sensing with imaging radar*. Springer, Heidelberg ; New York.
450 Ring, U., Schwartz, H. L., Bromage, T. G. & Sanaane, C., 2005 - *Kinematic and*
451 *sedimentological evolution of the Manyara Rift in northern Tanzania, East Africa*.
452 Geological Magazine 142 (4): 355-368. doi: 10.1017/s0016756805000841.
453 Roberts, L. G., 1963 - *Machine perception of three-dimensional solids. Massachusetts Institute*
454 *of Technology. Dept. of Electrical Engineering,* Massachusetts Institute of
455 Technology, Ph.D.
456 Schaber, G. G., McCauley, J. F. & Breed, C. S., 1997 - *The use of multifrequency and*
457 *polarimetric SIR-C/X-SAR data in geologic studies of Bir Safsaf, Egypt*. Remote
458 Sensing of Environment 59 (2): 337-363. doi: 10.1016/s0034-4257(96)00143-5.
459 Small, D., Miranda, N. & Meier, E., 2009 - *A revised radiometric normalisation standard for*
460 *SAR*. Geoscience and Remote Sensing Symposium,2009 IEEE International,IGARSS
461 2009, 4, IV-566-IV-569.
462 Sobel, I. & Feldman, G., 1968 - *"A 3x3 Isotropic Gradient Operator for Image Processing*.
463 presented at a talk at the Stanford Artificial Project,
464 Somi, E. J., 1993 - *Paleoenvironmental Changes in Central and Coastal Tanzania During the*
465 *Upper Cenozoic: Magnetostratigraphy, Sedimentary Records and Shorelevel*
466 *Changes. Department of Geology and Geochemistry,* Paleogeophysics &
467 Geodynamics, Department of Geology and Geochemistry , University of Stockholm,
468 Doctoral.
469 Strömberg, J., 1981 - *A modified Haar system and higher order spline systems on R as*
470 *unconditional bases for Hardy spaces*. Conference in Harmonic Analysis in Honor of
471 Antoni Zygmund II, 475-493, Belmont, California, USA.
472 Touzi, R., 2002 - *A review of speckle filtering in the context of estimation theory*. Geoscience
473 and Remote Sensing, IEEE Transactions on 40 (11): 2392-2404. doi:
474 10.1109/TGRS.2002.803727.
475 Touzi, R., Lopes, A. & Bousquet, P., 1988 - *A statistical and geometrical edge detector for*
476 *SAR images*. Geoscience and Remote Sensing, IEEE Transactions on 26 (6): 764-773.
477 doi: 10.1109/36.7708.

Zribi, M., Kotti, F., Lili-Chabaane, Z., Baghdadi, N., Ben Issa, N., Amri, R., Duchemin, B. & Chehbouni, A., 2012 - *Soil Texture Estimation Over a Semiarid Area Using TerraSAR-X Radar Data*. Geoscience and Remote Sensing Letters, IEEE 9 (3): 353-357. doi: 10.1109/lgrs.2011.2168379.

Figure 1 - Study area and test sites.

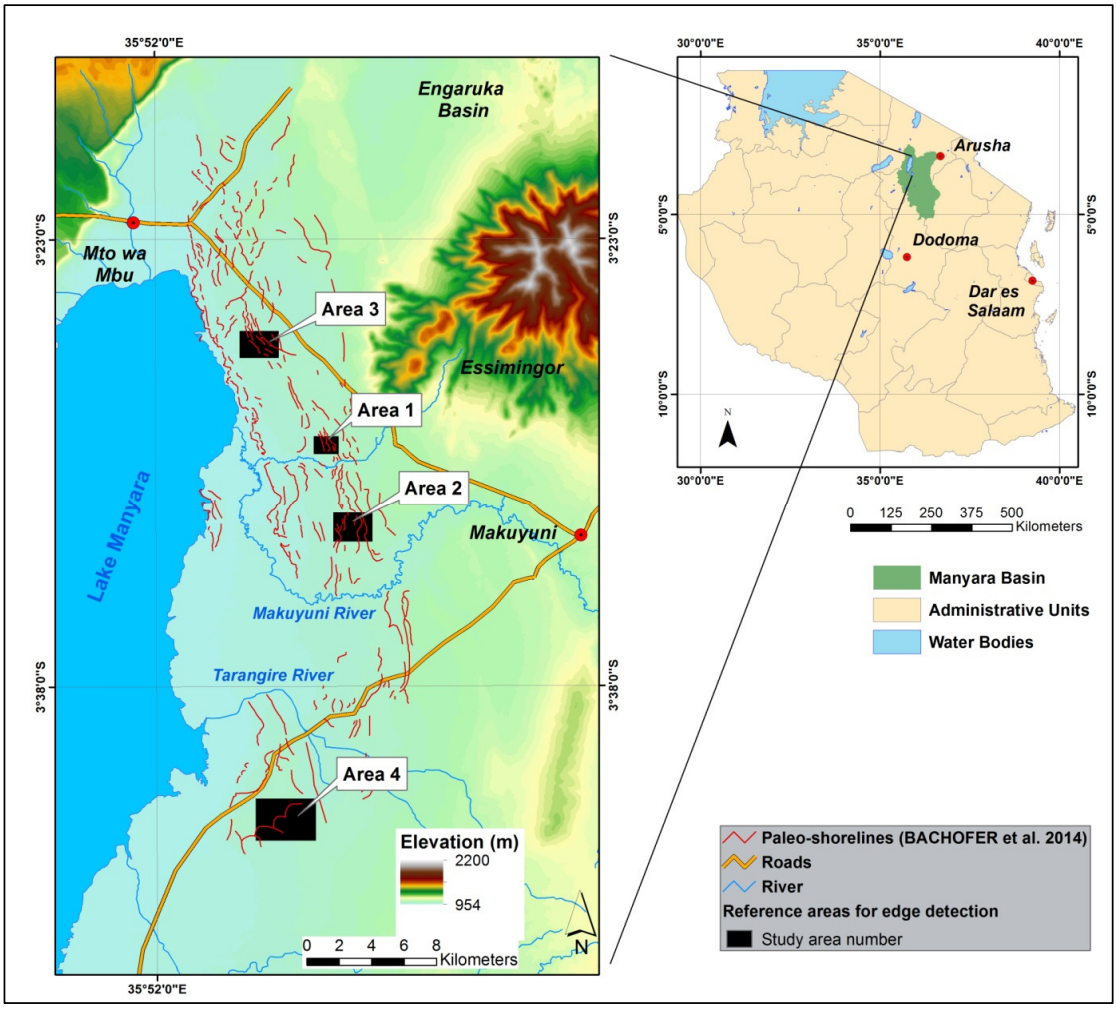

Figure 2 - (a) Distinct paleo-shoreline (Lon. 36.006°, Lat. −3.629°); (b) Shoreline section (Lon. 35.909°, Lat. −3.396°).

Table 1 - TerraSAR-X scene.

Sensor	Mode	Date	Time (UTC)	Orbit	Incident Angle	Polarization
TerraSAR-X	StripMap	2011-09-13	15:54:39	Ascending	44.4°	HH

500 **Figure 3 - One scale DWT for "test site 2" (pre-processing: multilooking 4 / median filter**
501 **5x5 kernel).**

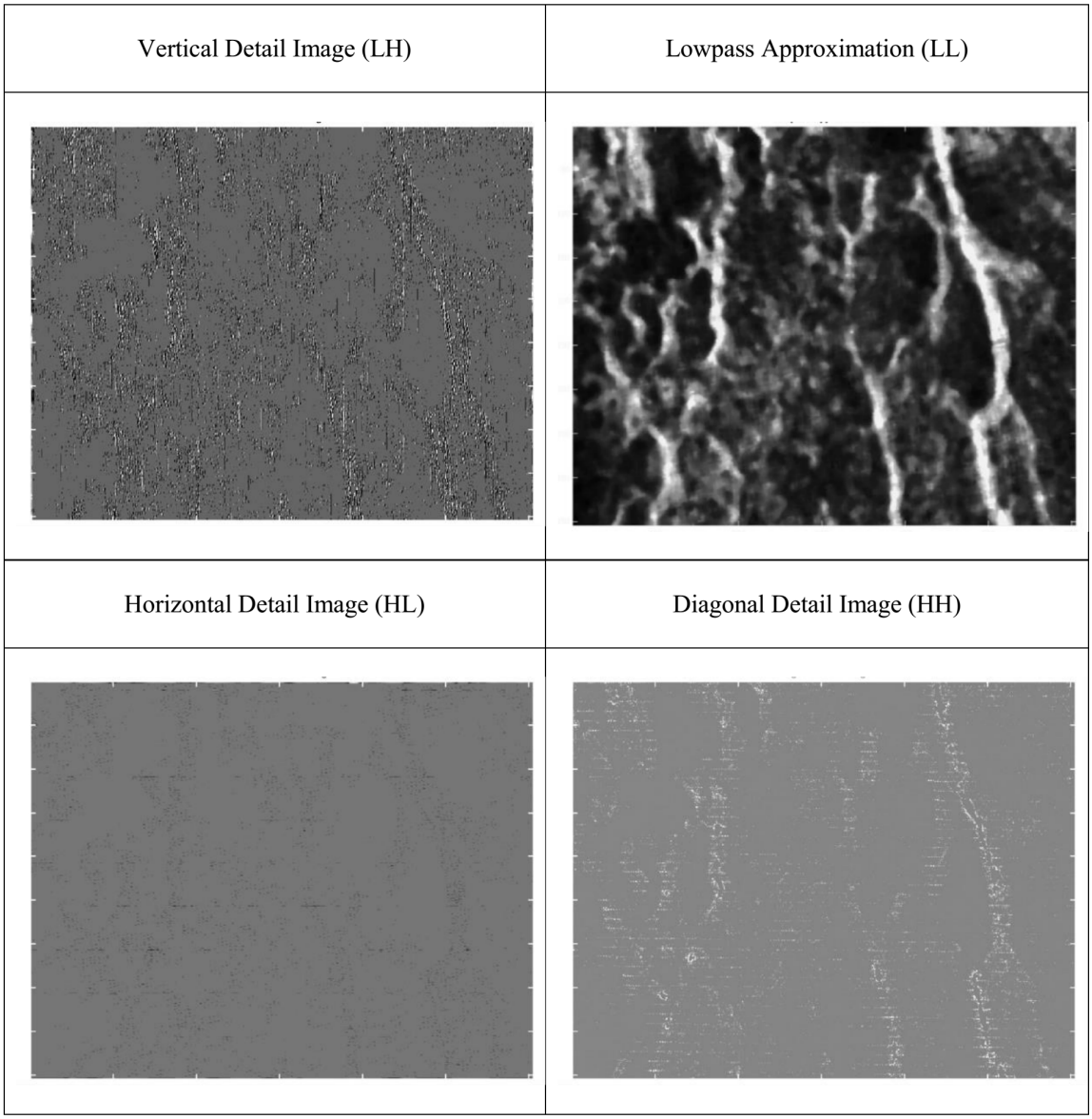

502

503

504

505

506 **Figure 4 - Comparison of a value profile (test site 2) between source image (pre-**
507 **processing: multilooking 4 / median filter 5x5 kernel) and 3-level DWT on a 520 m**
508 **transect.**

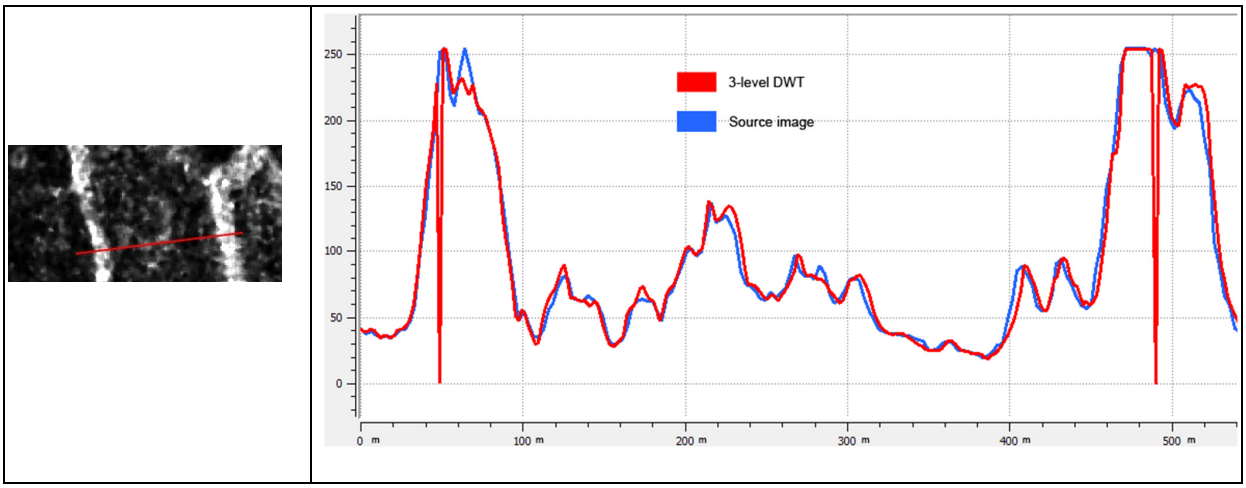

509

510

511

512

513

514

515

516

517

518

519

520 **Figure 5 - Diagrams of the edge detection accuracy for the four test sites. The number on the x-**
521 **axis stands for the multilooking/filter combination (see Table 2).**

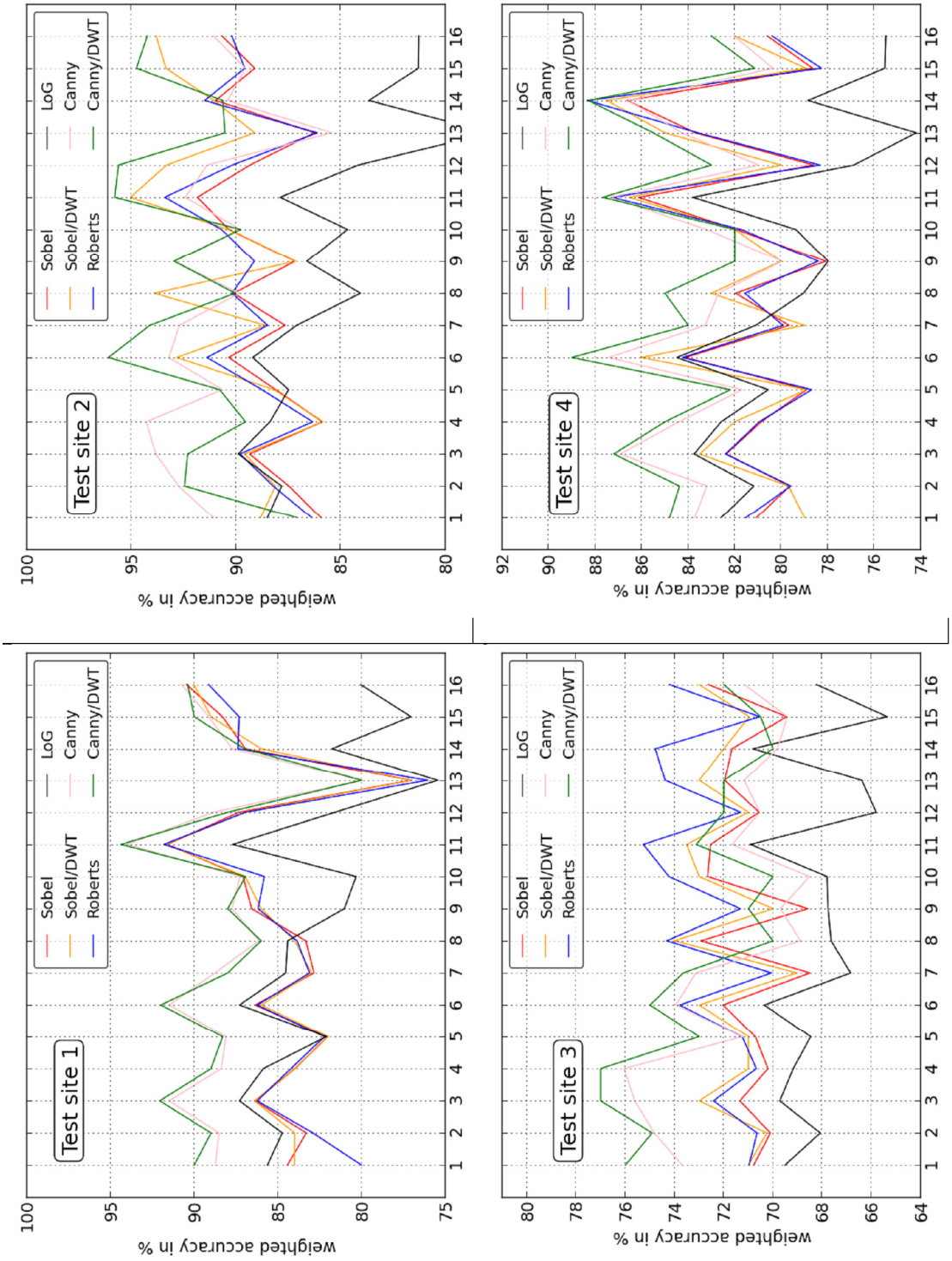

522

523 **Table 2 - Weighted accuracy in percent of edge detection methods for "test site 2". T =**
524 **threshold for edge detection; S = sigma value; LH = lower hysteresis; UH = upper**
525 **hysteresis; LA = laplacian alpha; k = kernel size.**

ID / Looks / Filter	Roberts	Sobel	DWT / Sobel	LoG	Canny	DWT / Canny
(1) 1 look / no filter	86.4 % T: 0.348	85.9 % T: 0.325	88.8 % T: 0.039	88.5 % T: 0.027 S: 2	91.1 % LH/UH: 0.16 / 0.758 S: 1.5	95.0 % LH/UH: 0.152 / 0.757 S: 1.5
(2) 1 look / Lee filter (k = 5)	88.2 % T: 0.151	87.5 % T: 0.166	88.1 % T: 0.171	87.8 % T: 0.02 S: 1.8	92.7 % LH/UH: 0.112 / 0.669 S: 0.1	93.8 % LH/UH: 0.135 / 0.664 S: 0.1
(3) 1 look / median filter (k = 5)	89.8 % T: 0.175	89.4 % T: 0.183	89.6 % T: 0.186	88.4 % T: 0.02 S: 2	93.8 % LH/UH: 0.09 / 0.713 S: 0.1	94.8 % LH/UH: 0.099 / 0.706 S: 0.1
(4) 2 looks / no filter	86.3 % T: 0.22	85.9 % T: 0.239	85.8 % T: 0.261	88.4 % T: 0.026 S: 2	94.3 % LH/UH: 0.139 / 0.821 S: 0.5	94.1 % LH/UH: 0.166 / 0.815 S: 0.5
(5) 2 looks / Lee filter (k = 5)	88.8 % T: 0.068	88.1 % T: 0.081	88.2 % T: 0.081	87.5 % T: 0.011 S: 1.6	90.7 % LH/UH: 0.092 / 0.319 S: 0.5	90.8 % LH/UH: 0.086 / 0.318 S: 0.5
(6) 2 looks / median filter (k = 5)	91.4 % T: 0.074	90.4 % T: 0.085	92.8 % T: 0.093	89.2 % T:0.012 S: 1.6	93.2 % LH/UH: 0.136 / 0.475 S: 0.1	96.1 % LH/UH: 0.049 / 0.296 S: 0.1
(7) 4 looks / no filter	88.5 % T: 0.114	87.7 % T: 0.128	88.6 % T: 0.133	87.1 % T: 0.013 S: 2.2	92.7 % LH/UH: 0.084 / 0.586 S: 0.1	94.1 % LH/UH: 0.08 / 0.481 S: 0.1

526

(8) 4 looks / Lee filter (k = 5)	90.2 % T: 0.031	90.1 % T: 0.037	93.9 % T: 0.045	84.1 % T: 0.005 S: 1.2	89.8 % LH/UH: 0.072 / 0.131 S: 0.1	94.4 % LH/UH: 0.108 / 0.125 S: 1.0
(9) 4 looks / refined Lee filter	89.1 % T: 0.071	87.1 % T: 0.078	87.2 % T: 0.078	86.6 % T: 0.011 S: 1.8	92.9 % LH/UH: 0.015 / 0.378 S: 0.5	93.0 % LH/UH: 0.03 / 0.377 S: 0.5
(10) 4 looks / gamma filter	90.7 % T: 0.032	90.4 % T: 0.039	90.4 % T: 0.039	90.7 % T: 0.006 S: 1.2	89.8 % LH/UH: 0.072 / 0.097 S: 0.1	89.7 % LH/UH: 0.057 / 0.105 S: 0.1
(11) 4 looks / median filter (k = 5)	93.4 % T: 0.035	91.9 % T: 0.04	95.1 % T: 0.047	87.9 % T: 0.004 S: 1.6	92.4 % LH/UH: 0.14 / 0.289 S: 0.1	95.8 % LH/UH: 0.088 / 0.189 S: 1.5
(12) 8 looks / no filter	90.2 % T: 0.047	89.3 % T: 0.056	93.3 % T: 0.065	84.1 % T: 0.004 S: 1.8	91.4 % LH/UH: 0.139 / 0.321 S: 0.1	95.6 % LH/UH: 0.089 / 0.235 S: 1
(13) 8 looks / Lee filter (k = 5)	86.1 % T: 0.018	86.3 % T: 0.023	86.1 % T: 0.026	77.8 % T: 0.001 S: 2	85.4 % LH/UH: 0.137 / 0.163 S: 0.1	90.5 % LH/UH: 0.095 / 0.24 S: 1
(14) 8 looks / median filter (k = 5)	91.5 % T: 0.022	90.9 % T: 0.026	91.1 % T: 0.026	83.7 % T: 0.001 S: 2	90.4 % LH/UH: 0.087 / 0.26 S: 0.1	90.6 % LH/UH: 0.11 / 0.258 S: 0.1
(15) 10 looks / no filter	89.6 % T: 0.038	89.1 % T: 0.047	93.4 % T: 0.054	81.3 % T: 0.002 S: 2	89.6 % LH/UH: 0.126 / 0.305 S: 0.1	94.8 % LH/UH: 0.08 / 0.17 S: 1
(16) 12 looks / no filter	90.2 % T: 0.032	90.7 % T: 0.04	93.8 % T: 0.047	81.3 % T: 0.028 S: 1	91.1 % LH/UH: 0.223 / 0.297 S: 1.5	94.2 % LH/UH: 0.063 / 0.153 S: 1.5

527

528 **Figure 6 - Multilooking and filtering for "test site 1" (images: a, b, c with an extent of 1546 m x**

529 **1102 m) and for "test site 4" (images d, e, f with an extent of 3718 m x 1590 m)**

a) 1 look / no filter	b) 8 looks / no filter	c) 8 looks / Lee filter
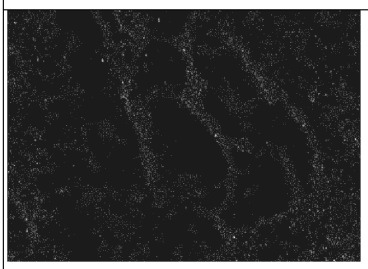	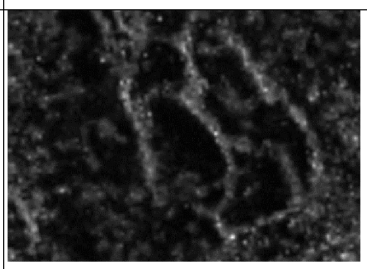	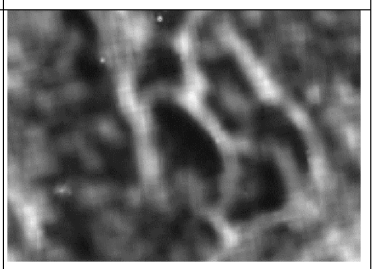
d) 1 look / no filter	e) 8 looks / no filter	f) 8 looks / Lee filter
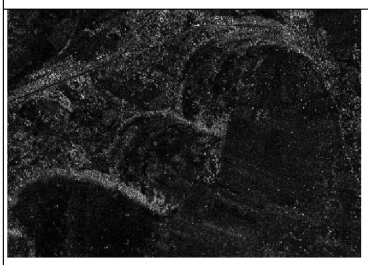	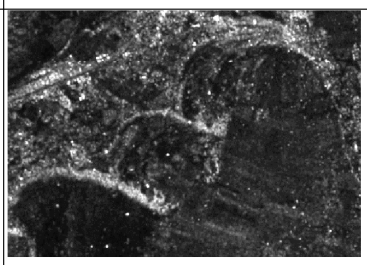	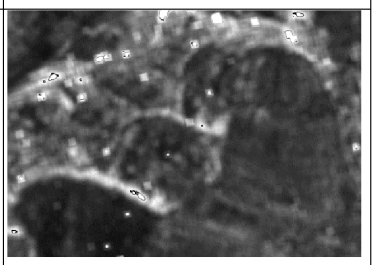

530

531

532

533

534

535

536

537

538

539 **Figure 7 - Speckle reduction and edge detection for "study area 2". The extent of the image is**

540 **2400 m x 1800 m. a), d) and g) represent different pre-processing examples.**

a) 1 look / no filter	b) Canny applied to (a)	c) Field reference
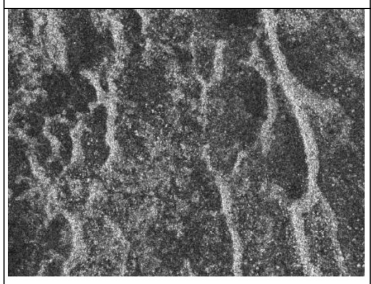	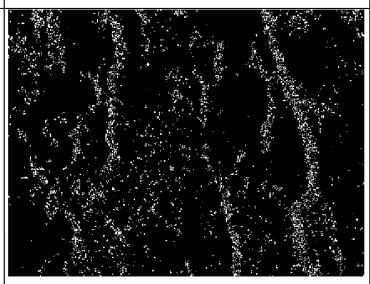	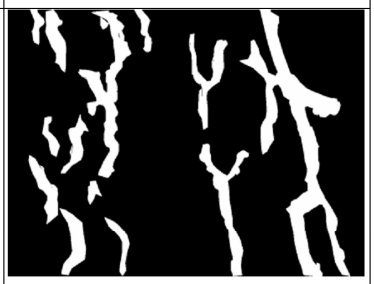
d) 8 looks / Lee filter	e) Sobel applied to (d)	f) Canny applied to (d)
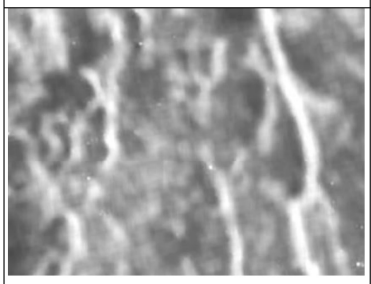	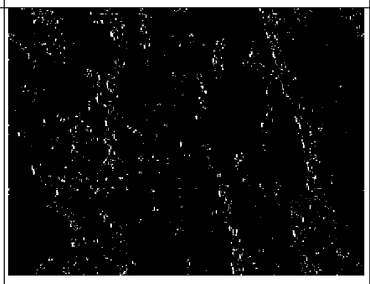	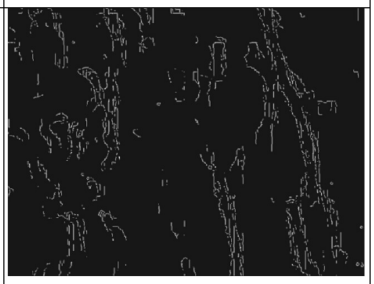
g) 4 looks / Median filter	h) Sobel applied to (g)	i) DWT/Sobel appl. to (g)
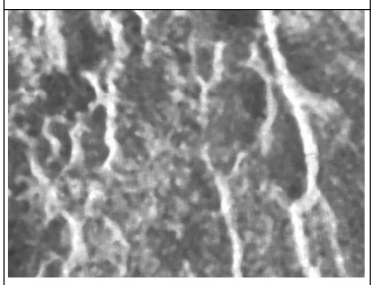	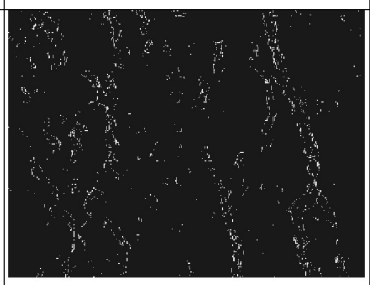	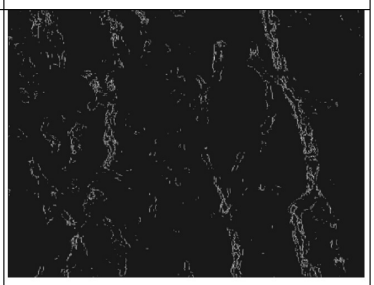
j) LoG applied to (g)	k) Canny applied to (g)	l) DWT/Canny appl. to (g)
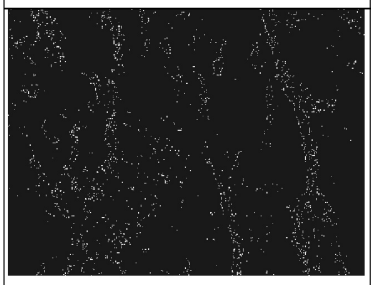	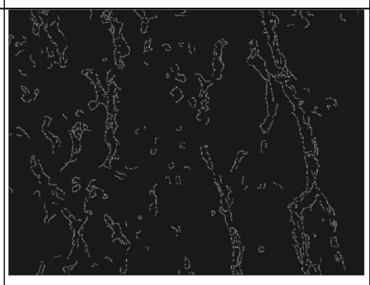	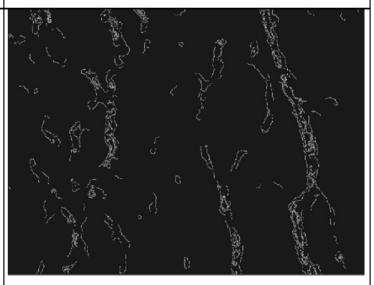

541

542

APPENDIX VI: PUBLICATION P6

A simple DEM assessment procedure for gully system analysis in the Lake Manyara area, northern Tanzania.

MAERKER, M., QUÉNÉHERVÉ, G., BACHOFER, F. & MORI, S., 2015 - *A simple DEM assessment procedure for gully system analysis in the Lake Manyara area, northern Tanzania.* Natural Hazards: 1-19 (doi: 10.1007/s11069-015-1855-y).

Paper History

The publication was developed on the basis of joint field work and the Bachelor of Science Thesis of Simone Mori "Valutazione di Modelli digitali per l'analisi di sistemi gully nella zona del lago Manyara, nord Tanzania" (in Italian) at the University of Florence, Italy in 2011. Michael Märker supervised this thesis. Data of the thesis was re-analysed and re-interpreted for the publication.

Journal: Natural Hazards
ISSN: 0921-030X
Thomson Reuters Impact Factor 2014: 1.719
Type: Research Article.

Nat Hazards
DOI 10.1007/s11069-015-1855-y

ORIGINAL PAPER

A simple DEM assessment procedure for gully system analysis in the Lake Manyara area, northern Tanzania

Michael Maerker[1,2] · Geraldine Quénéhervé[3] · Felix Bachofer[3] · Simone Mori[4]

Received: 30 August 2014 / Accepted: 30 May 2015

Abstract Gully erosion is a major threat concerning landscape degradation in large areas along the northern Tanzanian Rift valley. It is the dominant erosion process producing large parts of the sediments that are effectively conducted into the river network. The study area is located in the Lake Manyara—Makuyuni River catchment, Arusha, northern Tanzania. During fieldwork, we measured topographic data of eight gully systems close to Makuyuni Town. The main focus of this study is to assess gully erosion dynamics using improved DEMs with original resolutions of 30 and 20 m, respectively. We assessed terrain characteristics to extract information on environmental drivers. To improve the DEM, we integrated information deduced from satellite images as well as from acquired GPS field data. Topographic indices such as Stream Power Index or Transport Capacity Index were derived from the re-interpolated DEM. To evaluate gully evolution, we assessed also the longitudinal slope profiles. Finally, the gully evolution phases of each gully were classified according to the concept proposed by Kosov et al. (Eksperimental'naya geomorfologiya, vol 3. Moscow University, Moskva, pp 113–140, 1978). The re-interpolated DEMs revealed a positive response especially for the more developed gullies. We show that the extraction of information on this spatial process scale based on "low-resolution" data is feasible with little additional fieldwork and image interpretation. In fact, areas identified as having a greater risk of gully erosion have been confirmed by observations and surveys carried out in the field.

Keywords Soil erosion · Gully erosion · GIS · DEM interpolation · Terrain analysis · Tanzania

✉ Michael Maerker
mmaerker@unifi.it; michael.maerker@ggi.uni-tuebingen.de

[1] Heidelberg Academy of Sciences and Humanities, Rümelinstr. 19-23, 72070 Tübingen, Germany

[2] Department of Earth Sciences, University of Florence, Via La Pira 4, 50121 Florence, Italy

[3] Institute of Geography, Tübingen University, Rümelinstr. 19-23, 72070 Tübingen, Germany

[4] Laboratory of Geo-Information Science and Remote Sensing, Wageningen University, Droevendaalsesteeg 3, 6708 Wageningen, The Netherlands

1 Introduction

The semiarid landscape of the northern Tanzanian Rift is highly sensitive to climate and socio-economic changes. Particularly, along the eastern flanks of the East African Rift half-graben system within the Lake Manyara basin, fertile soils are potentially threatened by soil erosion processes. Particularly gully erosion processes are very effectively destroying entire areas where a suitable and sustainable land management is not implemented (Vrieling et al. 2006; Mwanukuzi 2011). Furthermore, the rift valley is still a very active tectonic area influencing and triggering hydrological and geomorphological processes (Dawson 1997). The study area is also subject to a specific precipitation pattern with long dry periods and intensive rains during the wet seasons. Climatic conditions varied a lot over the last thousands of years, documented by intense fluctuating levels of the Gregory rift lakes and different levels of corresponding fluvial terraces (Trauth et al. 2003; Bergner et al. 2009; Trauth et al. 2009). Generally, gully erosion processes indicate active geomorphic areas where hydraulic settings and sediment dynamics of the terrain are strongly modified. Gullies efficiently concentrate surface runoff, and they transport huge amounts of sediments rapidly down to the river networks (Capra 2013; Shellberg et al. 2013; Rengers and Tucker 2014). Gullies in this area expose archaeological and paleontological finds dated to 78–630 ka BP (Ring et al. 2005; Schwartz et al. 2012). The "off-site damages" of gully erosion processes are related to the transported sediments that are mainly affecting water quality and are causing reservoir sedimentation (Flügel et al. 2003; Sidorchuk et al. 2003). Consequently, a detailed assessment of gullying processes yields valuable information on the landscape and landscape functions such as sediment load, water quality, landscape stability, soil- and groundwater storage as well as soil fertility and soil depth (Sidorchuk 2006; Hancock and Evans 2010).

However, for areas affected by gully erosion processes in Africa and elsewhere, a proper assessment of process dynamics is related to the availability of suitable data and spatial information derived by remote sensing. This is mainly due to the fact that most of those areas are not accessible for comprehensive fieldwork (missing permits; dangerous areas because of conflicts, diseases, etc.). Additionally, analyses are mostly conducted with low financial budgets, even though some remotely sensed data are freely available and can be purchased by the research community; high-resolution data is still cost intensive. Therefore, it is often necessary to find a compromise between the cost and the quality of the data. Consequently, in some studies freely available data such as Shuttle Radar Topographic Mission (SRTM) digital elevation models (DEM) derived from X- or C-band or the Advanced Spaceborne Thermal Emission and Reflection Radiometer (ASTER) GDEM are used in the assessment of erosion processes and feature detection because of their almost global coverage (Brooks et al. 2009; El Haj Tahir et al. 2010). Often these DEMs are the only valuable elevation information in remote areas where no high-quality topographic maps are available. The medium resolution of these DEMs with 30 m is in most of the cases not adequate for assessing erosion processes that have a spatial resolution of less than 10 m like rill or gully features. Consequently, the question remains, whether and how the quality of these models can be enhanced to be able to evaluate gully erosion processes?

The aim of this study is to investigate the potential improvement of freely available data and to develop a simple methodology allowing a proper assessment of soil erosion, especially gully erosion processes, for data-scarce areas. We will explore additional data sources providing topographic information like GoogleEarth™ images in order to enhance

the spatial accuracy and resolution of the datasets. We will test the approach in the Lake Manyara area in northern Tanzania to decipher landscape characteristics and evolutionary phases. Since we are mainly interested in revealing the landscape potential for erosion processes, we primarily concentrate on the triggering topography. Therefore, we consider for this screening approach soils, substrates, vegetation and climate as homogeneous.

2 Materials and methods

2.1 Study area

The Lake Manyara basin is located in an asymmetrically shaped half-graben situated in the eastern branch of the East African Rift System with a 200–600 m high escarpment along the western shoulder and with the Ngorongoro crater as highest elevation (2960 m). The eastern shoulder of the rift is lower in elevation and consists of tectonic blocks that are dipping toward the west. The northeastern part of the catchment area is dominated by the Essimingor volcano (2154 m). Tectonic settings and climatological conditions formed the Lake Manyara catchment in northern Tanzania as an endorheic basin. The Lake Manyara

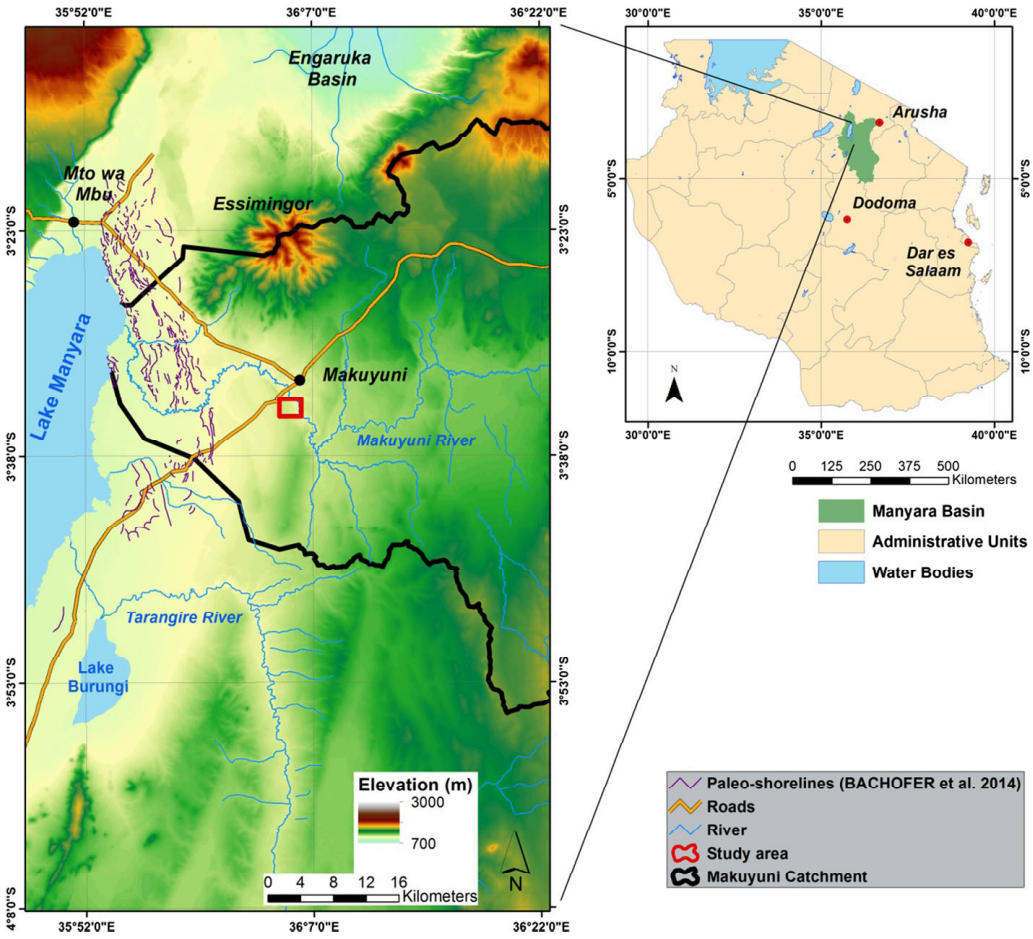

Fig. 1 The regional setting of the Lake Manyara and the study area

(954 m a.s.l.) is a shallow soda lake with a maximum depth of 1.18 m (Deus et al. 2013). Remains of a paleolake Manyara can be found, especially in the eastern part of the basin. Paleoshorelines indicate paleolake levels up to 80 m above today's lake level, which is also the lowest possible outlet point into the northern Engaruka and Lake Natron basins (Keller et al. 1975; Bachofer et al. 2014). Radiocarbon-dated stromatolites (Th/U series) indicate a maximum age of about 140 ka BP (Casanova and Hillaire-Marcel 1992). Today's Lake Manyara is mainly fed with seasonal drainages of the Tarangire and Makuyuni rivers from the east and by some springs at the base of the escarpment in the west. The Makuyuni River catchment east of Lake Manyara is characterized by a bimodal precipitation pattern with an average annual rainfall of about 700 mm that results in a sparse semiarid vegetation cover, dominated by bushed grasslands (Bachofer et al. 2014). The land use consists mainly in pastures and rain-fed agriculture. The study area, located south of the Makuyuni River and east of the road Arusha–Dodoma, is characterized by different fluvial terrace systems related to the lake-level fluctuations in the past (Fig. 1). Fine fluvial deposits formed the substrates and the soils developed on top of them. A paleolake margin is also identified in the study area consisting of tephra deposits with a radiocarbon date of 630 ka BP (Schwartz et al. 2012). These tephra deposits form a distinct escarpment in turn representing harder substrates than the surrounding weathered soil material or outcropping pedogen carbonatic concretions. The underlying geology is characterized by crystalline rocks and basaltic dyke systems (Frost et al. 2012).

2.2 Assessment procedure

The objective of this study is to enhance existing global elevation data with additional topographic information that is available, e.g., via GoogleEarth. Many studies already used this information directly or indirectly to assess soil erosion processes (Costanzo et al. 2012; Conoscenti et al. 2013; Frankl et al. 2013; Zakerinejad and Maerker 2014). However, the data can also be utilized to improve DEM quality and thus may allow a proper erosion process assessment based on these DEMs. The general approach we follow in this study consists in the succeeding steps:

1. GPS tracking of the gully drainage networks and gully profile recording in the study area.
2. Identification and digitalization of gully features and drainage networks from high resolution, freely accessible GoogleEarth images, Google (2012).
3. Preprocessing of available ASTER GDEM, SPOT DEM and SRTM-X DEM (noise and artifact filtering and fill sink procedures).
4. Re-interpolation of ASTER GDEM, SPOT and SRTM-X DEMs at higher resolution taking into account digitized streamlines and GPS-measured ground control points within the gully networks.
5. Assessment of gully erosion processes by detailed Geographic Information System-based (GIS) terrain analysis.
6. Determination of gully development phases according to a gully evolution model.

In the following chapters, we describe in detail the procedure to enhance DEM resolution and quality and the data utilized in the approach. The data sources used in this research can be divided in two categories: remotely sensed and other digital information as well as field acquired data.

2.3 Digital data sources

The remote sensing data consist of DEMs and high-resolution satellite images (Table 1). For gully and drainage network detection, we utilized GoogleEarth, which provides free access to satellite images with high resolution. Regarding the study area, GoogleEarth made two images available: Ikonos-2 (2005) with a resolution of 1 m and GeoEye-1 (2010) with 0.5 m resolution. As a reference, we used a commercial WorldView-2 scene acquired 2010-10-15.

We compared three available DEMs in order to find the most suitable one for our methodological approach:

1. The NASA Shuttle Radar Topography Mission (SRTM) DEM (DLR 2012). In February 2000, a series of synthetic aperture radar (SAR) images was taken by a space shuttle with the aim to build a high-resolution topographic database of the entire world. The result is a DEM with 90 m resolution (3 arcsec, acquired in C-band) and one with 30 m resolution (1 arcsec, acquired in X-band). The major advantage of radar techniques and in particular of the resulting SRTM-X DEM is that microwaves are capable to penetrate clouds and to some degree also the vegetation cover. Even though the SRTM-X DEM offers no global coverage, it covers the study area completely.
2. The Advanced Spaceborne Thermal Emission and Reflection Radiometer (ASTER) Global DEM (GDEM, version 2) is generated using nadir-viewing and backward-viewing bands of the medium resolute ASTER sensor (ASTER GDEM Validation Team 2011). The resulting DEM has a resolution of 30 m at the Equator. The vertical and horizontal accuracy is about 30 m (Nelson et al. 2009).
3. Satellite Pour l'observation De La Terre (SPOT) DEM. The abbreviation SPOT refers to a series of French optical earth observation satellites. The DEM is derived from stereo-pair images of forward- and backward-facing sensors of the SPOT-5 satellite and has a spatial resolution of 20 m. The SPOT DEM is not freely available and does not have a global coverage so far. The DEMs have a vertical accuracy of at least 10 m and a horizontal accuracy of at least 15 m at a confidence level of 90 % (Nelson et al. 2009).

2.4 Fieldwork

Field data were achieved during September/October 2011 southwest of Makuyuni village (Fig. 2). Within the study area, we selected eight gullies (A–H) that are representative for

Table 1 List of DEMs and satellite images used

Dataset name	Resolution	Information
DEM SRTM-X	30 m	NASA SRTM-X DEM 1 arcsec
ASTER GDEM	30 m	ASTER GDEM
DEM SPOT	20 m	Compiled with 4 pairs of satellite images (01/01/2006; 30/07/2004; 23/01/2005; and 27/06/2006)
Ikonos-2	1 m (0.82 m nadir)	Image from Ikonos-2 satellite, available through GoogleEarth™, date 12/09/2005
GeoEye-1	0.5 m (nadir)	Image from GeoEye-1, satellite available through GoogleEarth™, date 25/01/2010
WorldView-2	0.5 m (0.46 m nadir)	15/10/2010

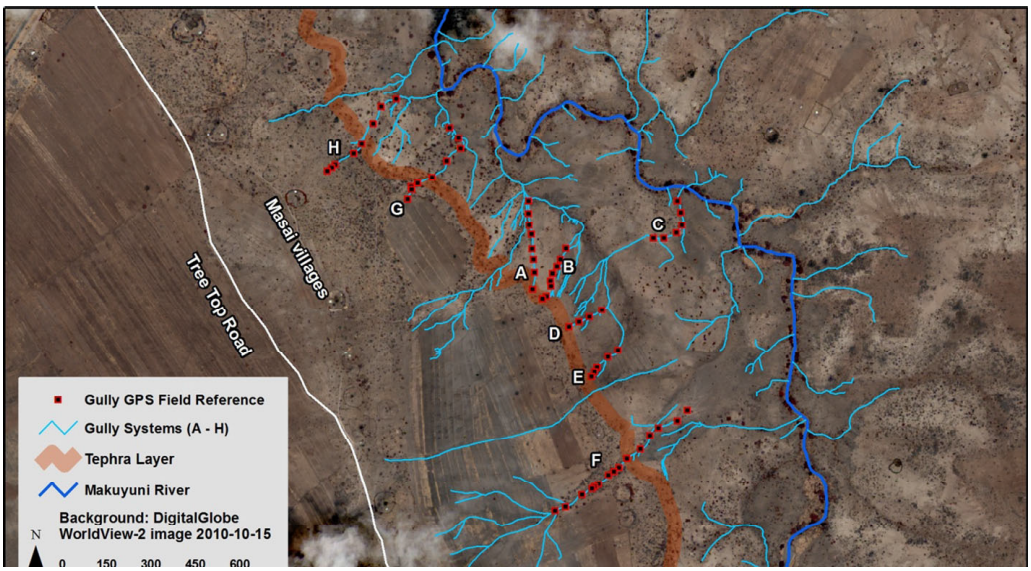

Fig. 2 Digitized gully drainage lines and recorded GPS thalweg points for gully systems *A–H*

this part of the basin and that are used as reference for the terrain analysis. Using Garmin handheld GPS devices, we measured *x*- and *y*-coordinates, moving along the gully from upstream (gully head) to downstream (gully mouth) along the thalwegs, reaching the Makuyuni river channel (Fig. 2). The accuracy of the GPS measurements for *x*- and *y*-coordinates is less than 1 m. For each GPS *x*-, *y*-point, we also performed a classical cross-sectional measurement, registering the exact gully depth and width using a measuring tape and stick (Table 2). These data, especially the depth values, were utilized in the DEM interpolation (see Sect. 3.1). We also took geo-tagged photographs of gully profiles at the recorded GPS points to document general features such as soil skeleton, structure and color of the substrates. Moreover, we performed a finger test to estimate the soil texture. This information is important for the interpretation of gully dynamics after the GIS analyses were conducted.

2.5 Gully drainage detection

Digitizing streamlines by manual photograph-interpretation techniques allows the operator to remove obstructions of vegetation cover and/or delineate flow paths of small-to-medium

Table 2 Figures and averaged values of the sampled gullies A to H

Gully	A	B	C	D	E	F	G	H
Length (m)	298.4	199.3	200.3	128.7	132.5	589.1	364.9	355.1
Average depth (cm)	183.3	96.9	165.8	72	53	174.6	116.4	109.6
Max depth (cm)	270	200	350	102.5	71	373	195	200
Min depth (cm)	50	30	10	33	30	13	28	35
Average width (m)	6.1	2.6	13.6	9.8	11.2	8.8	6.2	7.3
Max width (m)	11.02	5	25.2	14.5	22.5	17.3	15	23.6
Min width (m)	2.5	1.1	0.8	7.1	5.7	2.7	2.4	2.1

scale erosion processes such as gullies. Combined vector elevation information like elevation points, contour lines and streamlines often outperform raster approaches, especially in low-relief areas where moderate elevation errors in remotely sensed data can effectively preclude an accurate determination of the surface shape and drainage lines (Garbrecht and Starks 1995; Wilson and Gallant 2000). Not many interpolation techniques utilize drainage networks or thalwegs without elevation values, but particularly the algorithm developed by Hutchinson (1989) uses drainage lines to improve DEM interpolation.

The GeoEye-1 and the Ikonos-2 satellite images were acquired during the dry season, minimizing the vegetation cover and showing very clear paths of gullies and the river network of the Makuyuni River (Fig. 2). The high resolution of 0.5 m of the GeoEye-1 image allows for an accurate and detailed identification of drainage lines. On the other hand, due to its coarser resolution, the Ikonos-2 image permits only to digitize the more developed gullies that were mainly corresponding to the ones sampled in the field. This drainage lines are an integral part in our study for the DEM improvement and interpolation described in the following chapter.

3 GIS analyses

3.1 DEM interpolation

The ASTER GDEM, SRTM-X and SPOT DEMs were filtered using a simple 3 × 3 average filter in order to remove noise and to loose as less topographic information as possible. Subsequently, the raster data were transformed in point-type vector data attributing the elevation information to each centroid of the raster cells. We calculated the gully depths from the cross-sectional information at the *x*- and *y*-GPS points. The depth was then subtracted from the surrounding raster grid cells in order to estimate the absolute elevation of the gully bottom at the GPS points. We added these points to the raster centroid dataset to generate the point elevation dataset. We digitized the Makuyuni river fluvial network and the visible gullies based on the satellite images (Fig. 2) to provide a linear vector-type thalweg shapefile.

To create an improved DEM for a proper terrain analysis, the different datasets containing absolute (elevation point dataset) or relative elevation information (thalwegs or drainage networks dataset) were again interpolated. This interpolation was conducted using the ANUDEM algorithm developed by Hutchinson (Hutchinson 1986, 1989). This algorithm is an interpolation method specifically designed for the creation of hydrological correct DEMs (Reuter et al. 2009; Arun 2013). The interpolation algorithm is based on thin-plate splines and produces a surface that incorporates ridgelines and stream networks in order to represent as much as possible a natural drainage surface (Reuter et al. 2009). The drainage enforcement option, part of the ANUDEM method, attempts to remove all sink points in the fitted grid (Hutchinson 1989). Removing erroneous (spurious) sinks guarantee a hydrological correct network where water flows from the watershed divides to the respective catchment outlet (Tarboton et al. 1991). A spurious sink is often an erratic feature that does not correspond with actual features of the terrain. These sinks have to be removed to allow accurate hydrologic modeling (Nelson et al. 2009). Hence, the drainage enforcement algorithm significantly increase the accuracy of DEMs interpolated from sparse, but well chosen, surface-specific elevation data (Hutchinson 1989). To interpolate the SPOT DEM, we used the drainage lines digitized on the GeoEye-1 image (0.5 m

Table 3 DEM interpolation scheme

SPOT	SRTM-X	GPS data	Drainage lines	Drainage enforce (on/off)	10 m interpolated DEM
×		×	×	On	SPOT ENF10
×		×	×	Off	SPOT B10
	×	×	×	On	SRTM ENF10
	×	×	×	Off	SRTM B10

ground resolution), and to interpolate the SRTM-X DEM, we utilized the ones digitized on the Ikonos-2 image (1 m ground resolution). The difference between both derived drainage lines is small even though there is a difference in resolution. The main drainage pattern is reproduced well with both datasets, which subsequently are validated by field reference and the WorldView-2 image (0.5 m ground resolution). With the ANUDEM-based method, we interpolated four new elevation models with 10 m resolution based on SRTM-X with 30 m resolution and SPOT with 10 m resolution (Table 3). The ASTER GDEM was not taken into consideration after a first validation because of its low spatial resolution and obvious artifacts resulting from shadowing effects and savanna vegetation. A qualitative assessment was done with a hillshade DEM, checking minimum and maximum values. Moreover, we evaluated visually the differences between the original DEMs and hydrological correct DEMs.

3.2 Terrain analysis

3.2.1 Flow direction

The physics of a purely gravity-driven flow dictates that water always takes the steepest downhill path, such that flow lines cross contour lines at a right angle (Gruber and Peckham 2009). Due to the nature of this study, we took into account two flow direction algorithms: D8 and D∞. The D8 method is the simplest flow direction algorithm: from each cell, all flow is passed to the neighbor with the steepest downslope gradient resulting in 8 possible drainage directions. It can model convergence (several cells draining into one), but not divergence (one cell draining into several cells) (Gruber and Peckham 2009). In the case of ambiguous flow directions, for example if two cells have the same minimum downslope, an arbitrary decision is made. This simple method is often used to extract river networks and is integrated in many GIS packages. D∞ is based on representing flow direction as a single angle taken as the steepest downward slope on the eight triangular facets centered at each grid point. The upslope area is then calculated by proportioning the flow between two downslope pixels according to how close the flow direction is to the direct angle to the downslope pixel (Tarboton 1997). This procedure offers improvements over prior procedures that have restricted a flow to only eight possible directions.

3.2.2 Flow accumulation

The contributing area, also known as basin area, upslope area or flow accumulation, is a planar area and describes the spatial extent of a collecting area over which water from rainfall, snowfall, etc. can be aggregated (Gruber and Peckham 2009). The total contributing area (TCA) is a definite area where values of every raster cell represent the total

number of cells that flows into it, while the specific contributing area (SCA) refers to an area per unit of contour length (SCA = TCA/w).

3.2.3 Potential linear erosion processes

The Stream Power Index (SPI) (Moore et al. 1988) was used to identify and describe potential linear erosion processes such as rills and gullies along slopes based on slope and contributing area (D'Agostino and Vianello 2005). The SPI measures erosive power of flowing water based on the assumption that discharge is proportional to the specific contributing area A_s and flow velocity proportional to the slope gradient (tan β) (Wilson and Gallant 2000). As specific contributing area and slope steepness increase, the amount of water contributed by upslope areas and the velocity of water flow increase, hence stream power and potential erosion increase (Gruber and Peckham 2009). The stream power index SPI is defined as (Wilson and Gallant 2000):

$$\mathrm{SPI} = A_s \cdot \tan\beta \tag{1}$$

3.2.4 Sediment transport

To describe areal or sheet erosion processes, the sediment transport capacity parameter was developed to describe how and where sediments are transported and deposited by the flow. We used the Transport Capacity Index (TCI) (also called LS factor or RUSLE 3D index) (Wischmeier and Smith 1978; Renard et al. 1997). TCI is the 3D equivalent to the Universal Soil Loss Equation (USLE) slope length and steepness factor (LS Factor). TCI substitutes the slope length as proxy for water volume with the contributing area (Desmet and Govers 1996). The modified equation to compute the TCI is (Wilson and Gallant 2000):

$$LS_{(r)} = (m+1) \cdot \left[\frac{A_{(r)}}{22.13}\right]^m \cdot \left[\frac{\sin\beta_{(r)}}{0.09}\right]^n \tag{2}$$

where $A_{(r)}$ is the upslope contributing area (in m^2); $\beta_{(r)}$ is the maximum slope angle (in degrees); and n and m are parameters dependent on the flow. The number values 22.13 m (length) and 0.09 (9 % slope) representing the standard USLE plots.

3.2.5 Flow path profile

Longitudinal profiles are very useful to trace flow path profiles along gully systems and drainage lines. These profiles can be correlated with field measurements and study area morphologies in order to identify and validate fluvial terraces, areas with higher slopes and the spatial distribution of soil characteristics like soil texture. They can furthermore help to explain erosion processes.

3.3 Gully development and evolution

According to gully morphometric characteristics such as gully length, gully depth, gully catchment area and gully volume, we are able to attribute specific gully evolution phases according to Kosov et al. (1978). The authors divided the gully lifetime in a dynamic phase covering just the first 5 % of the gully's lifetime and a static phase covering the remaining

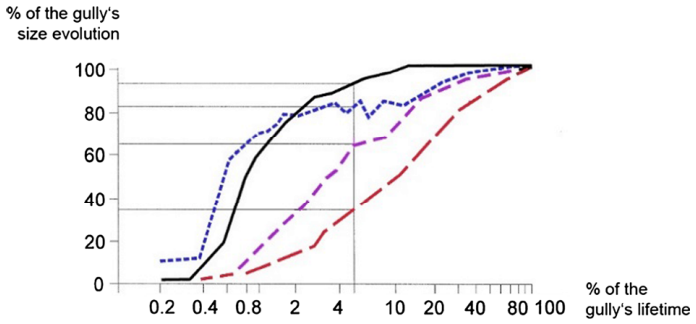

Fig. 3 Gully evolution phases according to gully morphometric characteristics (from Sidorchuk 1999, after Kosov et al. 1978)

95 % of the gully's lifetime. As illustrated in Fig. 3, the dynamic phase is characterized by (1) a gully length up to 90 % of the entire length development, (2) a gully depth that reaches up to 80 % of its final depth, (3) a gully catchment or contributing area of less than 60 % of the entire contributing area and (4) less than 45 % of the final gully volume. The formula used for the classification of dynamic and static gully phases is:

$$\text{ratio}\,\% = \frac{\text{AH} - \text{TCA}}{\text{TCA}}$$

where AH is the contributing area at gully head (m^2), and TCA is the total contributing area at the downstream situated gully mouth (m^2). In this study, we utilized the gully area to divide between dynamic and stable gully evolution phases. A ratio greater then 60 % indicate static gully systems, and ratios below 60 % reveal dynamic systems.

4 Results and discussion

4.1 DEM comparison

Comparing the original DEMs with the interpolated DEMs, we observed a much higher detail and precision for the study of gully erosion for the interpolated DEMs. The enhanced resolution in the interpolated DEMs is the effect of adding crucial information into the interpolation process. Particularly, small-scale erosion processes cannot be derived from the original DEMs because their resolution is too coarse and they do not allow extrapolating information that has a process scale of about 5–10 m. As illustrated in Fig. 4, the interpolated DEMs show more detail and hence allow an assessment of higher spatial erosion process details.

The incorporation of thalwegs and drainage lines as local relative elevation minima provides more realistic and hydrological correct elevation models. We used field measured *x*-/*y*-GPS points and depth information we derived from the cross sections as input in the ANUDEM procedure to increase the elevation accuracy particularly along the gully drainage lines. The models with an enforced drainage system generally show better results than the ones without the enforced drainage option set during the interpolation procedure.

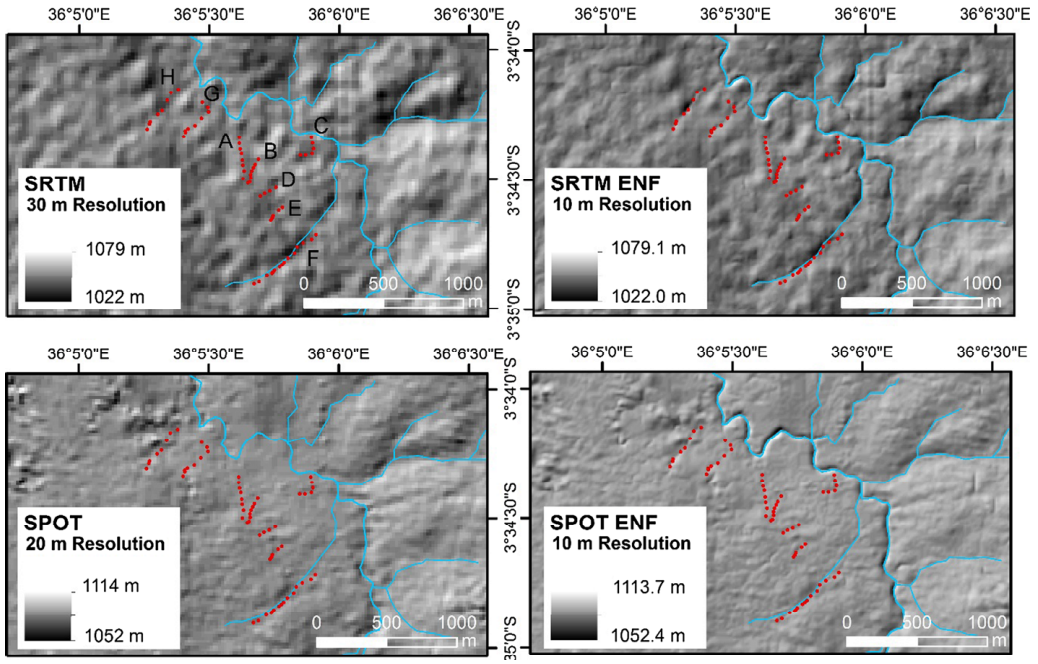

Fig. 4 Comparison between original SRTM-X and SPOT data and their accordingly interpolated DEMs, all shown with underlying hillshade. *Blue lines* are river channels and *red points* the gully thalweg ground truth locations

Hence, in the following we concentrate on the enforced drainage DEMs. Generally, adding digitized drainage lines into raster datasets results in a correction of the drainage networks, especially in areas with very smooth or flat terrain and unclear drainage pattern. The drainage lines were identified and digitized on dry-season high-resolution satellite images GeoEye-1 (0.5 m resolution) and Ikonos-2 (1 m resolution). Due to the low vegetation cover and the high resolution of the satellite images, the delineated drainage network used in the interpolation is very reliable and reflects the real-world situation. The satellite images used to process the SPOT DEM were taken during the long dry season and the short dry season, when the vegetation cover is at its minimum. Therefore, the elevation values of these DEMs are only marginally influenced by the vegetation. To remove the noise generated by big trees like baobab (*Adansonia digitata*), the SPOT DEM has been filtered to smooth these spatial discontinuities. Finally, the use of an interpolation algorithm to generate hydrological correct models like ANUDEM, allowed creating DEMs that are suitable to make terrain analysis for the interpretation of erosion processes such as gullies. The use of different interpolation methods (Kriging, IDW, natural neighbor) results in DEMs that are particularly less suitable for the erosion process assessments (Reuter et al. 2007; Hu et al. 2014).

The main problem with ASTER GDEM data is that the vegetation cover is included in the height information of the cells, due to the stereoscopic methodology of optical image pairs. The surface elevation including vegetation might be useful in some kind of studies, but not for hydro-erosive terrain analyses where the actual ground surface topography is needed. The ASTER GDEM scene for the study area shows a lot of noise and artifacts due to vegetation cover and shadowing effects, especially along the Makuyuni River main

channel and for baobabs located in the study area. The dataset also has a lower resolution compared to the SPOT DEM. Consequently, it was excluded from the analysis because its resolution is not suitable to detect gully processes.

The new interpolation of the original SPOT DEM with 20 m pixel size, to a resolution of 10 m pixel size, means that we divide the original cell into four cells, each with 100 m^2. Theoretically, the information obtained seem to be more accurate. However, we can observe directly from Fig. 5a, b that the surface of the SRTM ENF10 is less homogenous and coarser than the SPOT ENF10, even if the SAR sensor can pass through vegetation. Consequently, we yield a better performance, especially for the terrain analysis, with the SPOT ENF10 DEM because the surface is more regular, reflecting better the real terrain surface.

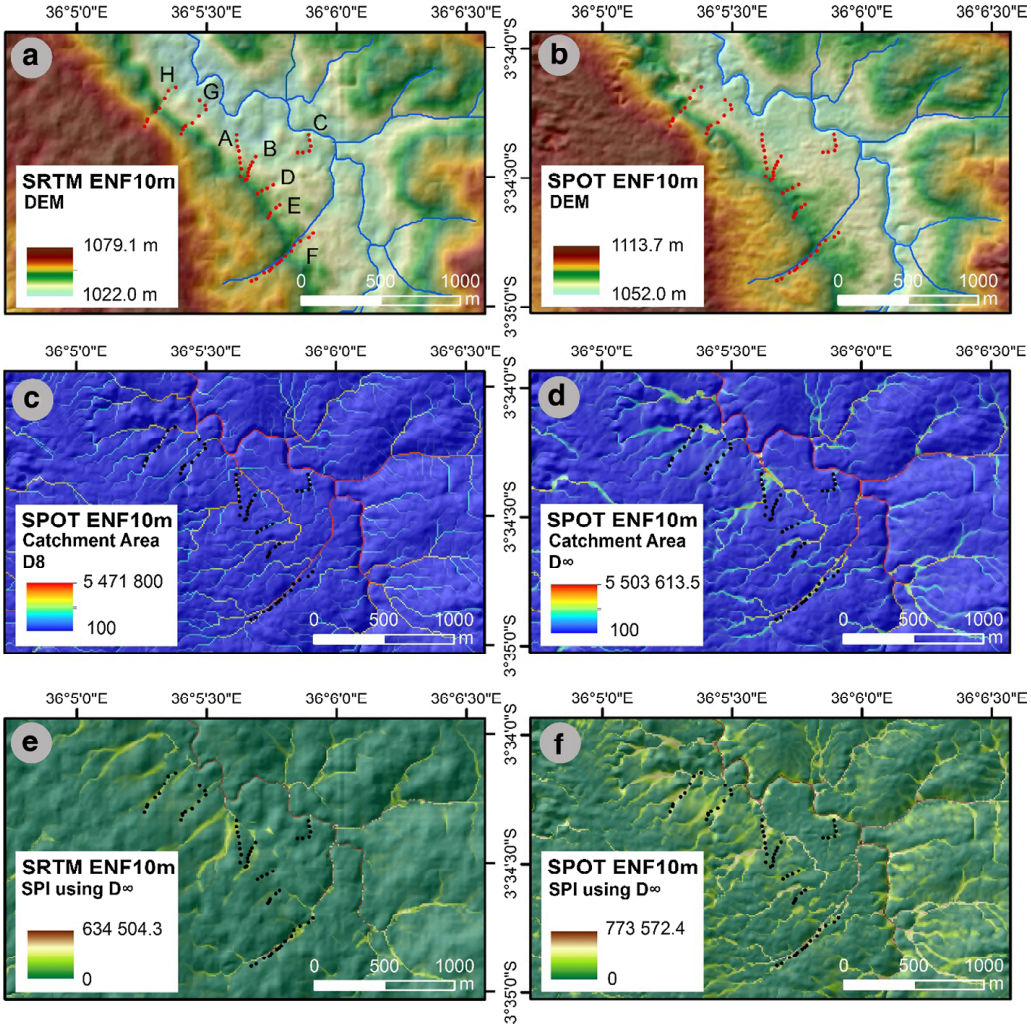

Fig. 5 GIS-based analyses of the different DEMs with underlying hillshade. **a** SRTM-X ENF10, **b** SPOT ENF10, **c** catchment area calculated with D8 from SPOT ENF10, **d** catchment area calculated with D∞ from SPOT ENF10, **e** SPI calculated with D∞ from SRTM-X ENF10, **f** SPI calculated with D∞ from SPOT ENF10

4.2 Terrain analysis

The Stream Power Index (SPI) as a tool to identify linear erosion processes like gullies, is very powerful even when using DEMs with a resolution that is actually lower than the scale of the erosion processes. Moreover, we derive also the Transport Capacity Index (TCI) to understand and identify the more areal erosion like sheet erosion processes.

The flow accumulation generated with D∞ flow accumulation algorithm from the DEM SPOT ENF10 can identify basically all the reference gullies even though there are some uncertainties in the drainage pattern of gully A, especially in the upper part (Fig. 5d). The same conclusions can be drawn for the flow accumulation generated with the D8 algorithm. Nonetheless, D8 is less conform with a real situation because all the water contained in a cell is moved to another cell; consequently water flows are always converging although in reality water can flow in different directions such as in flat or convex areas (Fig. 5c).

The SPI calculated on the DEM SRTM ENF10 identifies successfully the gullies B, C, F, G and H, with some uncertainty in the area around the gully head and the mouth of gully A (see Fig. 5e, f). The gullies E and D can be identified with the SPI values. However, they are not represented by very high SPI values such as the other gullies due to the smaller catchment area and divergent drainage pattern. This is probably caused by a very low depth of the gully systems; hence, it is difficult to interpolate these areas accurately. According to the field measurement, gully D has an average depth of 72 cm and a maximum of 102.5 cm, which is lower than all the other gullies. Gully C on the lower Makuyuni River terrace was also identified by both SRTM ENF10 and SPOT ENF10. The model SPOT ENF10 generally shows a higher accuracy in identifying the gully systems. Where SPI values are medium or high (red to gray color), the energy available for erosion processes is high. Hence, where the index is low (bright green color), the energy is lower. The SPI values of the SPOT ENF10 (Fig. 5f) are high for gullies B, F and H and for lower parts of gully A; are medium for gullies C and G; and are low for gullies D, E and the upstream half of gully A. The same values can be generally observed in the SRTM ENF10 DEM, but with a greater uncertainty (Fig. 5e).

The SPI values show that sites of more intensive gully incision are located in zones with high slope gradient, thus higher surface runoff velocities and/or larger contributing areas and hence larger flow volumes. This correlation of SPI and slope is confirmed also by the longitudinal profiles. Moreover, three zones with high SPI values can be identified: a first one is localized on the banks or lower terraces of the Makuyuni River related to retrogressive erosion and easily erodible fluvial materials, a second one on the escarpment of the second river terrace where all gullies pass through, and a third one on the escarpment next to the Tree Tops road plateau. These three zones have been also identified in the field by a visual evaluation (Figs. 2, 6).

The central zone of the study area, characterized by high SPI and slope values (see Fig. 6 for slope degree values), is dominated by a tephra layer that was dated to 633 ka BP (Schwartz et al. 2012). In this area, most of the gully head cuts are located. The high slope angles of this escarpment increase surface runoff speed. During the rainy season, the surface runoff gets concentrated and hence rills and gullies develop and sediments are eroded and transported downstream to the river. The Transport Capacity Index (TCI) or LS Factor takes into account the specific catchment area and slope degree highlighting the spatial distribution of material transport and deposition. The areas with higher slope gradient identified by the SPI are also the ones where there is more material transport by surface runoff (Fig. 5e, f; yellow to brown colors). The greater the erosional energy,

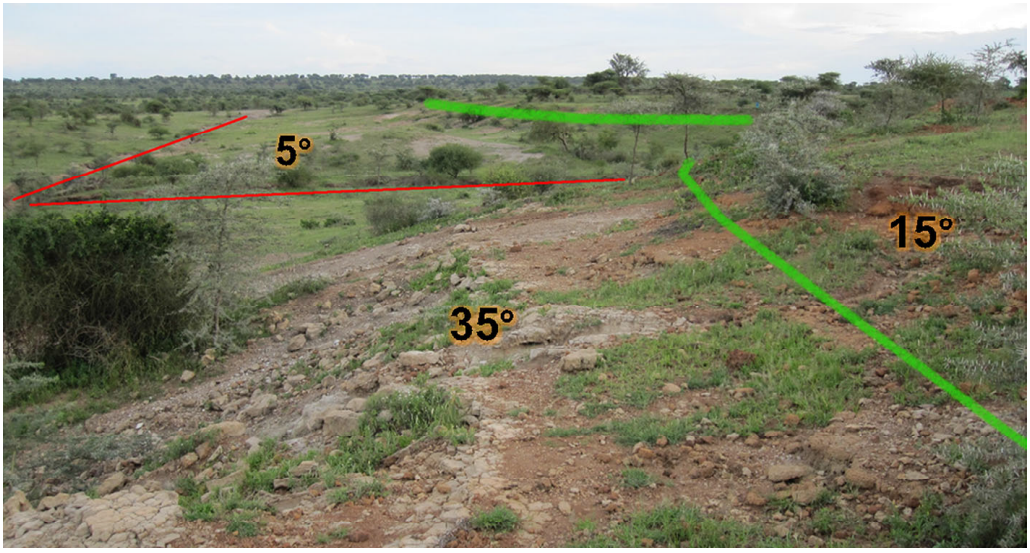

Fig. 6 Second escarpment close to Tree Top road. In *red* are gullies *A* and *B*, and in *green* the tephra outcrops. The fluvial terrace above has a slope of 15° whereas the Tephra escarpment 35° and the lower fluvial terrace a slope of 5°

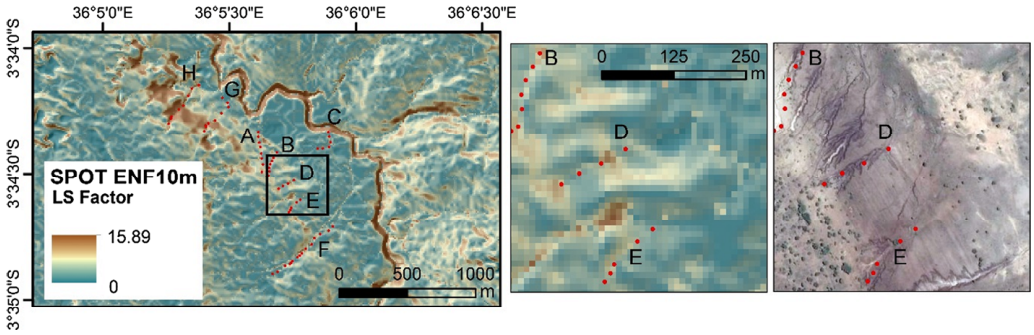

Fig. 7 TCI or LS Factor calculated with D∞ on SPOT ENF10 (*left*); close up of the LS factor for gullies *B*, *D* and *E* (*middle*) as well as a close up underlied by GeoEye-1 data (*right*)

coupled with an increasing soil particle detachment, the more material has to be transported in the water flow. TCI zones showing no transport and thus material deposition and accumulation occur where the transport capacities diminish (shown in blue green colors, Fig. 7 left and middle). For example we identified depositional areas at the downstream parts of gullies B, D and E (zoomed area in Fig. 7 middle and right).

4.3 Gully development and evolution

In order to validate the SPI values in the field, we plotted the SPI values of gully H against the distance from the gully head downstream to the Makuyuni River, shown in Fig. 8. In this figure, a few SPI peaks were identified. The first increase is marked as T and corresponds to the head of the gully where the outcropping tephra layer is located. The peak T_2 is further downstream, where the water starts to concentrate flowing inside the gully itself.

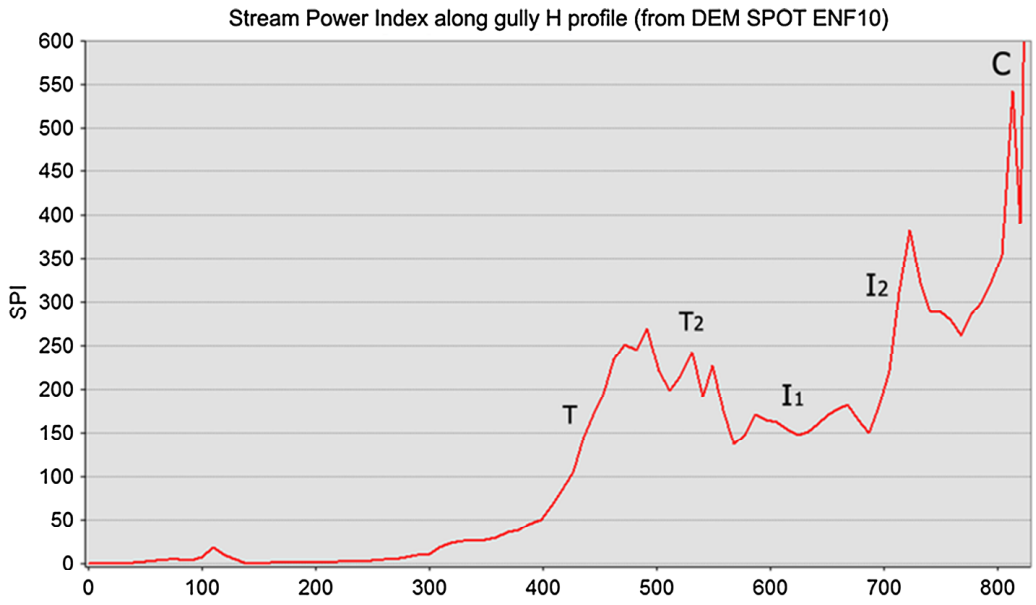

Fig. 8 SPI along the gully H longitudinal profile, from DEM SPOT ENF10

Table 4 Gully phase classification according to the Sidorchuk model

Gully	AH (m^2)	TCA (m^2)	AH – TCA (m^2)	(AH − TCA)/TCA	%	Phase
A	1408	592,435	591,027	0.99762	99.76	Static
B	1196	592,435	591,239	0.99798	99.80	Static
C	153,086	173,053	19,967	0.11538	11.54	Dynamic
D	1161	172,760	171,599	0.99328	99.33	Static
E	1061	172,760	171,699	0.99386	99.39	Static
F	266,877	555,278	288,401	0.51938	51.94	Dynamic
G	1497	382,423	380,926	0.99609	99.61	Static
H	19,196	382,422	363,226	0.94980	94.98	Static

In this area during dry season, there is almost no vegetation, indicating intensive erosion dynamics. Moreover, the SPI values decrease in the area of I_1 (Fig. 5e, f), where the gully depth decreases and gullies almost disappear (lower river terrace). Subsequently, at peak I_2 the gully area increases abruptly due to another tributary gully system that flows into gully H (Fig. 5e, f). The zone C is located close to the Makuyuni River where the material is transported to and deposited.

To asses the evolution stage of the gullies, we applied a methodology based on Kosov et al. (1978). We identified two phases: (1) a static phase that corresponds to 95 % of gully's lifespan and (2) the dynamic developing phase covering the first 5 % of gully lifetime. The model was successfully applied in various studies to classify gully dynamics (e.g., Sidorchuk et al. 2003). We calculated the contributing area at the head cut (AH) and the total contributing area downstream (TCA) for all eight gullies, using the D∞-based catchment area derived from the SPOT ENF10, and the results are shown in Table 4.

The classification shows that most of the gullies are in the static phase. Only gullies C and F show a dynamic pattern. The stable gullies do not significantly grow anymore in their area, and therefore, they are supposed to be quite old systems. The contributing area at the upstream of gully C shows very high values due to many gullies flowing into gully C at this location. Hence, this gully seems to be still in a dynamic phase. Gully F is also classified as dynamic; however, the model did not take into account the sedimentation/aggregation along the lower reach of this gully.

The longitudinal profiles show the elevation of the gully beds and adjacent slopes along the gully channel, from upstream to downstream. We made longitudinal profiles for all the gullies. Figure 9 illustrates the profile for gully F showing the two river terraces between 400–800 and 1200–1600 m flow length and the two escarpment zones with steeper slopes at 100–400 and 900–1100 m flow length. The comparison of the gully longitudinal profile (red line) with a profile in the not eroded area located on the undisturbed surface next to the gully (gully shoulder: blue line), demonstrates that the eroded areas are located where the slope is higher and/or where soil material is easily erodible (bigger vertical distance between red and blue line). The latter is confirmed by the substrate analysis in the field. The upper part consists of shallow soils on steeper slopes that are eroded further down exposing carbonatic concretions. Between 400 and 900 m flow length, the soil depth is increasing again. Soils mainly consist in erodible vertisols. Deepest incisions are localized in the area of the tephra outcrops that protect the underlying paleosols and paleolake deposits (900–1000 m flow length). At a distance between 1100 and 1400 m flow length, the gully bed elevation is higher than the surrounding areas indicating deposition and accumulation of transported sediments. This area is also highlighted for gullies B, D and E (see Fig. 7). Particularly, the lower fluvial terrace of the Makuyuni river at 1065–1070 m elevation a.s.l. is composed of fine erodible vertic fluvial deposits. The fluvial terraces are related to raising and lowering phases of a Paleolake Manyara.

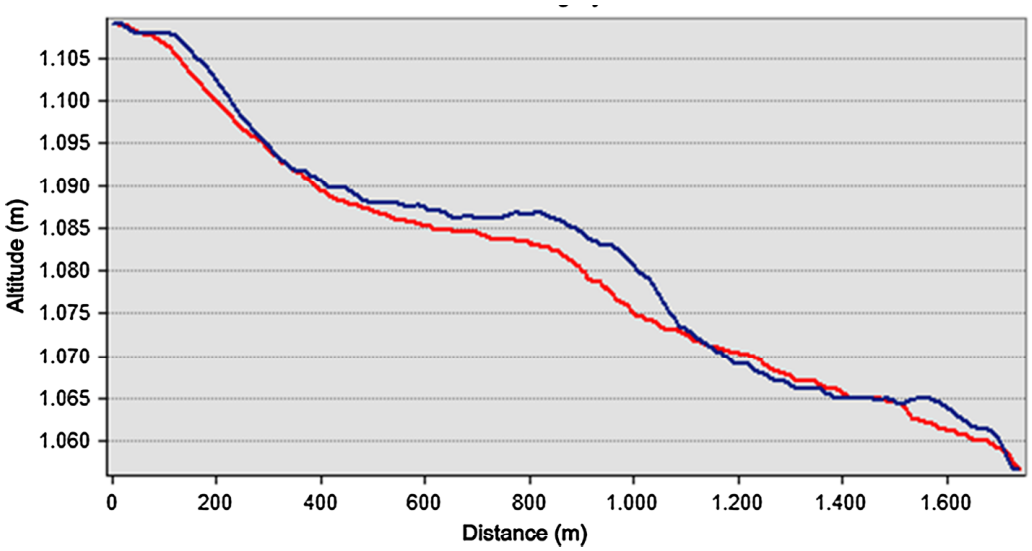

Fig. 9 Longitudinal profile of gully F. In *red gully thalweg* elevation and in *blue gully shoulder* elevation

5 Conclusions

Additional topographic information such as (1) measured *x*-/*y*-GPS gully points, (2) gully depth derived using cross-sectional measurements and (3) gully drainage networks digitized from GeoEye-1 and Ikonos-2 are used to re-interpolate DEMs yielding a higher topographic resolution than the source DEM based on SPOT and SRTM-X data. Generally, the re-interpolated SPOT DEM provides the best results in terms of spatial accuracy, low noise and artifacts. Even though SRTM-X is a SAR-based DEM with low influence of vegetation, the noise in the resulting DEMs was higher than in the SPOT-based DEM. The lowest performance was obtained by the ASTER GDEM due to the fact that ASTER scenes are strongly influenced by the vegetation cover and have a lower spatial resolution compared to the SPOT DEM. Best results for the interpolation of the DEMs were obtained by applying the hydrological forcing option of the ANUDEM algorithm "Topo to Raster." This algorithm guarantees a hydrological correct DEM without sinks. The assessment of the gully erosion processes was subsequently conducted with the best-performing DEM, namely the SPOT ENF10 DEM.

The terrain analysis is mainly based on topographic indices related to slope degree and catchment area. For the latter, we applied the D8 and D∞ algorithms. Generally, the D∞ yield better results and is closer to reality. The calculation of the topographic indices like SPI and TCI finally showed that specific gully features such as head cuts, catchment areas and erosion/deposition zones can be assessed with the improved SPOT ENF10 DEM. The derived results of SPI and LS Factor were also validated in the field confirming the high accuracy and reliability of the improved DEM. The investigated gully systems seem to be very old and belonging to the static gully phase according to Kosov et al. (1978). This is also confirmed by archeological and paleontological evidence in the area.

Additional topographic information can be derived by fieldwork (GPS points and gully cross sections) and GoogleEarth mapping of thalweg systems at high spatial accuracy. This information incorporated in a DEM artificially increases the spatial resolution. The derived DEMs show a good performance in terms of the hydrological and geomorphological process dynamics, which were assessed by terrain analysis. The presented approach is a simple low-cost methodology for gully assessment.

Acknowledgments This study was financed by the The Role of Culture in Early Expansions of Humans (ROCEEH) Research Centre of the Heidelberg Academy of Sciences and Humanities, Germany. We thank the Tanzania Commission for Science and Technology (COSTECH) for their research permission. We would also like to thank the DLR and the German Remote Sensing Data Center (DFS) for providing the SRTM/X-SAR data. ASTER GDEM is a product of the Ministry of Economy, Trade, and Industry (METI) of Japan and the United States National Aeronautics and Space Administration (NASA). The SPOT DEM was acquired from the ISIS Programme, Centre National d'Etudes Spatiales (CNES, France). Finally, we also would like to thank the EU IRSES Project (PIRSES-GA-2012-318969) for support of researcher exchange.

References

Arun PV (2013) A comparative analysis of different DEM interpolation methods. Geod Cartogr 39(4):171–177. doi:10.3846/20296991.2013.859821

ASTER GDEM Validation Team (2011) ASTER global digital elevation model: version 2. Summary of validation results. https://igskmncnwb001.cr.usgs.gov/aster/GDEM/Summary_GDEM2_validation_report_final.pdf. Accessed 5 April 2014

Bachofer F, Quénéhervé G, Märker M (2014) The delineation of paleo-shorelines in the Lake Manyara basin using TerraSAR-X data. Remote Sens 6(3):2195–2212. doi:10.3390/rs6032195

Bergner AGN, Strecker MR, Trauth MH, Deino AL, Gasse F, Blisniuk P, Dühnforth M (2009) Tectonic and climatic control on evolution of rift lakes in the Central Kenya Rift, East Africa. Quat Sci Rev 28(25–26):2804–2816

Brooks AP, Shellberg J, Knight J, Spencer J (2009) Alluvial gully erosion: an example from the Mitchell fluvial megafan, Queensland, Australia. Earth Surf Proc Landforms 34(14):1951–1969. doi:10.1002/esp.1883

Capra A (2013) Ephemeral gully and gully erosion in cultivated land: a review. In: Lannon EC (ed) Drainage basins and catchment management: classification, modelling, and environmental assessment. Nova Science, Hauppauge, pp 109–141

Casanova J, Hillaire-Marcel C (1992) Chronology and paleohydrology of late quaternary high lake levels in the Manyara basin (Tanzania) from isotopic data (18O, 13C, 14C, Th/U) on fossil stromatolites. Quat Res 38(2):205–226. doi:10.1016/0033-5894(92)90057-P

Conoscenti C, Agnesi V, Angileri S, Cappadonia C, Rotigliano E, Märker M (2013) A GIS-based approach for gully erosion susceptibility modelling: a test in Sicily, Italy. Environ Earth Sci 70(3):1–17. doi:10.1007/s12665-012-2205-y

Costanzo D, Cappadonia C, Conoscenti C, Rotigliano E (2012) Exporting a Google Earth™ aided earth-flow susceptibility model: a test in central Sicily. Nat Hazards 61(1):103–114. doi:10.1007/s11069-011-9870-0

D'Agostino V, Vianello A (2005) Identificazione morfodinamica del reticolo idrografico: integrazione fra rilievi di campo e tecniche GIS. Quaderni di Idronomia Montana 24:271–290 **(in Italian)**

Dawson JB (1997) Neogene; recent rifting and volcanism in northern Tanzania; relevance for comparisons between the Gardar Province and the East African Rift valley. Mineral Mag 61(4):543–548

Desmet PJJ, Govers G (1996) A GIS procedure for automatically calculating the USLE LS factor on topographically complex landscape units. J Soil Water Conserv 51(5):427–433

Deus D, Gloaguen R, Krause P (2013) Water balance modeling in a semi-arid environment with limited in situ data using remote sensing in Lake Manyara, East African Rift, Tanzania. Remote Sens 5(4):1651–1680

DLR (2012) SRTM X-SAR digital elevation models: status: 2012-09-28. http://eoweb.dlr.de:8080/eoweb-ng/licenseAgreements/DLR_SRTM_Readme.pdf. Accessed 23 December 2013

El Haj Tahir M, Kääb A, Xu C-Y (2010) Identification and mapping of soil erosion areas in the Blue Nile, Eastern Sudan using multispectral ASTER and MODIS satellite data and the SRTM elevation model. Hydrol Earth Syst Sci 14(7):1167–1178. doi:10.5194/hess-14-1167-2010

Flügel W-A, Märker M, Moretti S, Rodolfi G, Sidorchuk A (2003) Integrating geographical information systems, remote sensing, ground truthing and modelling approaches for regional erosion classification of semi-arid catchments in South Africa. Hydrol Process 17(5):929–942. doi:10.1002/hyp.1171

Frankl A, Poesen J, Haile M, Deckers J, Nyssen J (2013) Quantifying long-term changes in gully networks and volumes in dryland environments: the case of Northern Ethiopia. Geomorphology 201:254–263. doi:10.1016/j.geomorph.2013.06.025

Frost SR, Schwartz HL, Giemsch L, Morgan LE, Renne PR, Wildgoose MM, Sanaane C, Schrenk F, Harvati K (2012) Refined age estimates and Paleoanthropological investigations of the Manyara Beds, Tanzania. JASs 90:151–169

Garbrecht J, Starks P (1995) Note on the use of USGS level 1 7.5-minute DEM coverages for landscape drainage analyses. Photogramm Eng Remote Sens 61(5):519–522

Google (2012) http://www.google.com/intl/en-US/help/terms_maps.html. Accessed 20 February 2014

Gruber S, Peckham SD (2009) Land-surface parameters and objects in hydrology. In: Hengl T, Reuter HI (eds) Geomorphometry: concepts, software, applications. Developments in soil science, vol 33. Elsevier, Amsterdam, pp 171–194

Hancock GR, Evans KG (2010) Gully, channel and hillslope erosion. An assessment for a traditionally managed catchment. Earth Surf Proc Landforms 35(12):1468–1479. doi:10.1002/esp.2043

Hu J, Tan Q, Wang H, Xu X (2014) Accuracy assessment of DEM interpolation algorithms in different landform regions. J Basic Sci Eng 1(1):139–149

Hutchinson MF (1986) Algorithm 642: a fast procedure for calculating minimum cross-validation cubic smoothing splines. ACM Trans Math Softw 12(2):150–153. doi:10.1145/6497.214322

Hutchinson MF (1989) A new procedure for gridding elevation and stream line data with automatic removal of spurious pits. J Hydrol 106(3–4):211–232. doi:10.1016/0022-1694(89)90073-5

Keller CM, Hansen C, Alexander CS (1975) Archaeology and Paleoenvironments in the Manyara and Engaruka Basins, Northern Tanzania. Geogr Rev 65(3):364–376

Kosov BF, Nikol'skaya II, Zorina Y (1978) Eksperimental'nyye issledovaniya ovragoobrazovaniya. In: Makkaveev NI (ed) Eksperimental'naya geomorfologiya, vol 3. Moscow University, Moskva, pp 113–140 (**in Russian**)

Moore ID, Burch GJ, Mackenzie DH (1988) Topographic effects on the distribution of surface soil water and the location of ephemeral gullies. Trans Am Soc Agric Eng 31(4):1098–1107

Mwanukuzi PK (2011) Impact of non-livelihood-based land management on land resources: the case of upland watersheds in Uporoto Mountains, South West Tanzania. Geogr J 177(1):27–34. doi:10.1111/j.1475-4959.2010.00362.x

Nelson A, Reuter HI, Gessler PE (2009) DEM production methods and sources. In: Hengl T, Reuter HI (eds) Geomorphometry: concepts, software, applications. Developments in soil science, vol 33. Elsevier, Amsterdam, pp 65–85

Renard KG, Foster GR, Weesies GA, McCool DK, Yoder DC (1997) Predicting soil erosion by water: a guide to conservation planning with the Revised Universal Soil Loss Equation (RUSLE). Agriculture Handbook, Washington

Rengers FK, Tucker GE (2014) Analysis and modeling of gully headcut dynamics, North American high plains. J Geophys Res Earth Surf 119(5):983–1003. doi:10.1002/2013JF002962

Reuter HI, Nelson A, Jarvis A (2007) An evaluation of void-filling interpolation methods for SRTM data. IJGIS 21(9):983–1008. doi:10.1080/13658810601169899

Reuter HI, Hengl T, Gessler PE, Soille P (2009) Preparation of DEM for geomorphometric analysis. In: Hengl T, Reuter HI (eds) Geomorphometry: concepts, software, applications. Developments in soil science, vol 33. Elsevier, Amsterdam, pp 87–120

Ring U, Schwartz HL, Bromage TG, Sanaane C (2005) Kinematic and sedimentological evolution of the Manyara Rift in northern Tanzania, East Africa. Geol Mag 142(4):355–368. doi:10.1017/s0016756805000841

Schwartz HL, Renne PR, Morgan LE, Wildgoose MM, Lippert PC, Frost SR, Harvati K, Schrenk F, Sanaane C (2012) Geochronology of the Manyara Beds, northern Tanzania: new tephrostratigraphy, magnetostratigraphy and $^{40}Ar/^{39}Ar$ ages. Quat Geochronol 7:48–66. doi:10.1016/j.quageo.2011.09.002

Shellberg JG, Brooks AP, Rose CW (2013) Sediment production and yield from an alluvial gully in northern Queensland, Australia. Earth Surf Proc Landforms 38(15):1765–1778. doi:10.1002/esp.3414

Sidorchuk A (1999) Dynamic and static models of gully erosion. CATENA 37(3–4):401–414. doi:10.1016/S0341-8162(99)00029-6

Sidorchuk A (2006) Stages in gully evolution and self-organized criticality. Earth Surf Proc Landforms 31(11):1329–1344. doi:10.1002/esp.1334

Sidorchuk A, Märker M, Moretti S, Rodolfi G (2003) Gully erosion modelling and landscape response in the Mbuluzi River catchment of Swaziland. CATENA 50(2–4):507–525

Tarboton DG (1997) A new method for the determination of flow directions and upslope areas in grid digital elevation models. Water Resour Res 33(2):309–319. doi:10.1029/96WR03137

Tarboton DG, Bras RL, Rodriguez-Iturbe I (1991) On the extraction of channel networks from digital elevation data. Hydrol Process 5(1):81–100. doi:10.1002/hyp.3360050107

Trauth MH, Deino AL, Bergner AGN, Strecker MR (2003) East African climate change and orbital forcing during the last 175 kyr BP Earth Planet. Sci Lett 206(3–4):297–313

Trauth MH, Larrasoaña JC, Mudelsee M (2009) Trends, rhythms and events in Plio-Pleistocene African climate. Quat Sci Rev 28(5–6):399–411

Vrieling A, Sterk G, Vigiak O (2006) Spatial evaluation of soil erosion risk in the West Usambara Mountains, Tanzania. Land Degrad Dev 17(3):301–319. doi:10.1002/ldr.711

Wilson JP, Gallant JC (eds) (2000) Terrain analysis: principles and applications. Wiley, New York

Wischmeier WH, Smith DD (1978) Predicting rainfall erosion losses—a guide to conservation planning, vol 537. Agriculture Handbook, Washington

Zakerinejad R, Maerker M (2014) Prediction of gully erosion susceptibilities using detailed terrain analysis and maximum entropy modeling: a case study in the Mazayejan plain, southwest Iran. Geogr Fis Dinam Quat 37(1):67–76

APPENDIX VII: PUBLICATION P7

Modelling the Spatial Distribution of Archaeological Sites in the Makuyuni Region, Tanzania.

MÄRKER, M., BACHOFER, F., QUÉNÉHERVÉ, G., HERTLER, C., SAANANE, C., GIEMSCH, L. & THIEMAYER, H., 2013 - *Modelling the Spatial Distribution of Archaeological Sites in the Makuyuni Region, Tanzania.* CAA'2010 Fusion of Cultures. Proceedings of the 38th Annual Conference on Computer Applications and Quantitative Methods in Archaeology, BAR International Series 2494, 523-529, Granada, Spain.

Correction of content:

Chapter 3.1 "Input Data Preparation":

> "Moreover, we exploited spectral satellite data from the ASTER platform in the visible channel (3 bands) and near infrared channel (1 band), as well as in the short wave infrared channel (5 bands)."

The sentence has to be replaced with:

> "Moreover, we exploited multispectral satellite data of the ASTER sensor in the visible and near-infrared spectral region (3 bands), as well as in the short-wave infrared spectral region (6 bands)."

ISBN-10: 1407311085
Thomson Reuters Impact Factor 2014: -
Type: Conference Proceedings.

Proceedings of the 38th Annual Conference on Computer Applications and Quantitative Methods in Archaeology, CAA2010
F. Contreras, M. Farjas and F.J. Melero (eds.)

Modelling the Spatial Distribution of Archaeological Sites in the Makuyuni Region, Tanzania

Märker, M.[1], Bachofer, F.[2], Quénéhervé, G.[1], Hertler, C.[1], Saanane, C.[3], Giemsch, L.[4], Thiemeyer, H.[5]

[1] Heidelberg Academy of Sciences and Humanities
[2] University of Tübingen
[3] University of Dar es Salaam
[4] LVR-State Museum Bonn
[5] University of Frankfurt, Germany
michael.maerker@geographie.uni-tuebingen.de

In this study we focus on archaeological sites in the area of Lake Manyara and the Makuyuni river basin in Northern Tanzania. This region is known for fossil finds and artefacts. In order to analyze the spatial distribution of potential find locations we applied a methodology based on statistical mechanics. This method is able to handle presence-only datasets such as the Archaeological find locations we have collected in literature and by own field work over the last years. For the modeling we utilized environmental information such as 30m SRTM DEM and vegetation information as well as ASTER multispectral data as predictor variables. The results reveal potential areas where further fossil sites may be located. These sites with high probability values will be preferentially screened during the next field stage.

Keywords: Spatial modelling, Maxent, Tanzania.

1. Introduction

Tanzania is well known for ancient specimens of early hominids that were found, for example, in Olduvai Gorge (LEAKEY, 1979) or Laetoli (LEAKEY, 1986). These sites have been intensively studied in the past and are still a focus of many research teams dealing with early human evolution. The geographic centre of this study lies within the rift valley zone around the eastern margins of Lake Manyara and along the Makuyuni River. The Paleontological deposits in the vicinity of the locality of Makuyuni have been subjected to analyses conducted by (JÄGER, 1913), (RECK, 1921) and (RECK and KOHL-LARSEN, 1936). The Pleistocene sequences in the valley of the Makuyuni River were discovered early on by Louis and Mary Leakey, and were later examined by Kent in 1935 (KENT, 1941; 1942). Keller and colleagues collected Pleistocene faunal material, Acheulean and MSA lithics, and published several stratigraphic sections (KELLER *et al*., 1975). Renewed investigation of the geology, paleontology, and archaeology of the Lake Manyara Beds was conducted in 1994 and 1995 by a team led by F. Schrenk and T.G. Bromage (SCHRENK *et al*., 1995; KAISER *et al*., 1995; KAISER, 2000; SAANANEe, 2004; RING *et al*., 2005). In 2008 the area was again surveyed by F. Schrenk, C. Saanane and K. Harvati (SCHRENK *et al*., 2008). We conducted a two-week field season from July through August 2009 in the vicinity of Makuyuni Village, Monduli District, Arusha Region to detect further sites and collect additional information about the topography, vegetation, geology and the soils. Moreover we validated multispectral satellite information such as LANDSAT- and ASTER data.

Previous studies showed that two fossil bearing layers of different age occur in the area, namely the Lower and Upper Manyara Beds. Correlations with the sequence in Olduvai indicate Lower and Middle Pleistocene ages for the Upper Manyara Beds (RING *et al*., 2005). The large number of find locations of specimens of fossil vertebrates and artifacts detected during our own field campaign in 2009 was the reason for a more in depth analysis of the spatial distribution of these sites in relation to present day environmental characteristics and processes. Therefore we developed an integrative spatial modeling concept using GIS, Remote Sensing, and sophisticated statistical methodologies. The approach takes into account a variety of data such as topographic data, spectral satellite information, field observations, and stratigraphic characteristics.

This paper discusses the methodology and results of the spatial modeling of archaeological sites and gives an outlook on future work.

2. Study Area

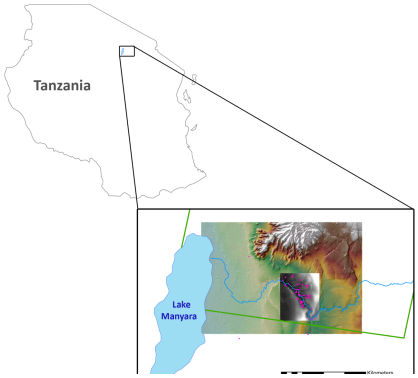

Figure 1: *Location of Study area, showing Lake Manyara and Makuyuni River as well as the find locations (red). The green frame shows the extent of the ASTER spectral data.*

The Study area is located in the Northern part of Tanzania (Fig. 1). The study area is situated along the southern end of the Gregory Rift, part of the East African Rift System (EARS). It covers the Eastern parts of lake Manyara and the lower part of the Makuyuni River Basin. Lake Manyara is extending NNE-SSW, has a surface of about 480 km², and an elevation of 960 m asl. The study area is extensively covered by late Proterozoic metasediments, Neogene volcanic material, and Plio-Pleistocene and Holocene lake beds (VAIDYANADHAN *et al*., 1993). The Lower and Upper Manyara beds are made up of grey silty ash clays and marls with horizons of chert nodules and calcareous algal concretions. Interbeded are sandstones, pebbly limestones, conglomerates and occasional tuffs. Those lake beds occur either as low flat-topped hills or as long ridges (SCHULTZ, 1967; VAIDYANADHAN *et al.,* 1993).

3. Materials and Methods

3.1. Input Data Preparation

The input data consists of topographic data, spectral satellite information, field observations, and stratigraphic characteristics. For the Makuyuni - Lake Manyara area an SRTM DEM with a resolution of 25 m x 25 m was chosen. The SRTM DEM was preprocessed using a simple filter to reduce the artefacts caused by vegetation and inherent noise. Thereafter the DEM was hydrologically corrected using the algorithm of Planchon and Darboux (2001). Subsequently, the corrected DEM was utilized to derived topographic indices with the SAGA GIS software (OLAYA and CONRAD, 2008). The dataset applied in the modelling consists of 22 continuously distributed parameters: i) topographic wetness index (BEVEN and KIRKEBY, 1979), ii) stream power index (MOORE *et al*., 1991), iii) transport capacity index (MOORE *et al*., 1997), iv) slope after Horn (1981), v) aspect, vi-viii) curvature (plan, profile, combined), ix) relief elevation above thalweg (OLAYA and CONRAD, 2008), x) upward flow length after Tarboton (1997), (xi) NDVI from ASTER, xii-xxi) single ASTER channels 1-9 and xxii a principal component analysis of ASTER channels 1-9. The target variable consist in sites with archaeological evidence such as fossils or artefacts. These sites have been measured with DGPS and transformed in a point vector type information. Totally 99 sites were identified that were used in the modelling.

The topographic indices characterize erosion transport and deposition processes, as well as climatic and geologic variations in the landscape, thus they not only describe the immediate vicinity of a specific location, but also a wider territorial context. Moreover, we exploited spectral satellite data from the ASTER platform in the visible channel (3 bands) and near infrared channel (1 band), as well as in the short wave infrared channel (5 bands). We used the single bands and derivatives of them as predictor variable. The Normal Differentiated Vegetation Index (NDVI) and a principal component analysis describe specific environmental characteristics like vegetation density and spatially homogeneous spectral entities. Figure 3 shows relevant predictor variables characterizing the study area such as DEM, slope, TWI and NDVI. The predictor variables were stacked and resampled to match with the DEM resolution of 25 m. The predictive variables such as the DEM and its derivatives as well as the satellite information were converted in a tabular matrix. The target variable containing the information about the archaeological find locations was added to this table. Subsequently the resulting matrix was then further processed with a sophisticated statistical approach.

3.2. Modeling and Prediction

Recently, predictive modeling techniques, such as generalized linear models (GLM), generalized additive models (GAM), classification tree analysis (CTA), neural networks (ANN), and multiple adaptive regression splines (MARS) have been applied in various disciplines from geomorphology, and ecology to medicine and social sciences (e.g. MIHKA and HJORT, 2005). However, normally, these methods need presence and absence data of the respective target variable to be able to generate a model. In our case we have only archaeological find locations whereas areas void of fossils are not mapped. Consequently, a suitable method is needed that is able to handle presence-only datasets.

In this study we utilized the Maxent approach developed by (PHILLIPS *et al*., 2006). Maxent is a general-purpose method for making predictions or inferences from incomplete information. Its origins lie in statistical mechanics (JAYNES, 1957).

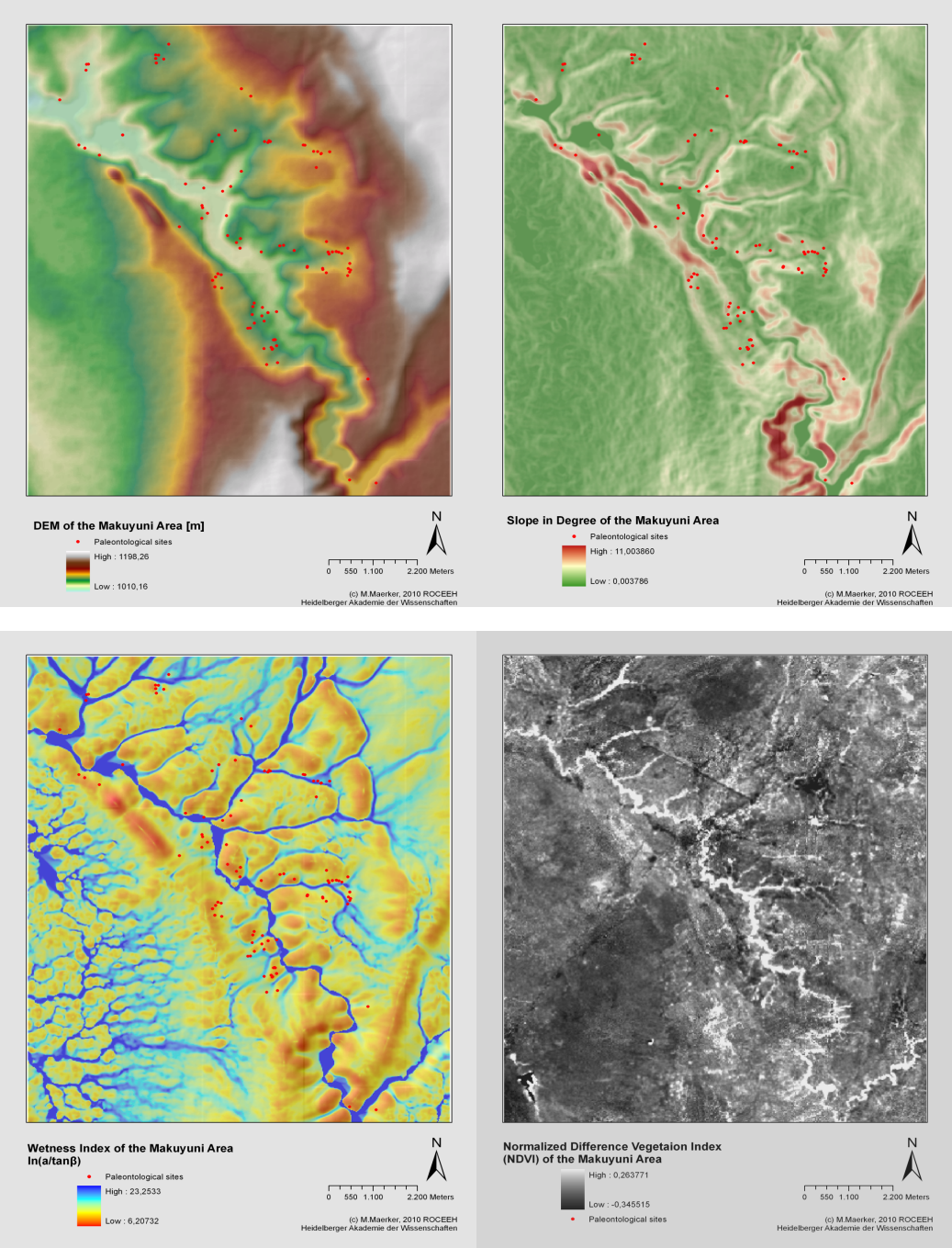

Figure 2: *Selected predictor variables: above left: DEM; above right: slope; Below left: TWI, below right: NDVI.*

The idea of Maxent is to estimate a target probability distribution by finding the probability distribution of maximum entropy (i.e., that is most spread out, or closest to uniform), subject to a set of constraints that represent our incomplete information about the target distribution. The information available about the target distribution often presents itself as a set of real-valued variables, called "features", and the constraints are that the expected value of each feature should match its empirical average (PHILLIPS *et al.*, 2006). When Maxent is applied to presence-only species distribution modeling, the pixels of the study area make up the space on which the Maxent probability distribution is defined, pixels with known species occurrence records constitute the sample points, and the features are terrain variables derived from the SRTM DEM and spectral ASTER information and functions thereof. The advantages of Maxent can be summarized as follows: (1) It requires only presence data, together with environmental information for the whole study area. (2) It can utilize both continuous and categorical data, and can incorporate interactions between different variables. (3)

Efficient deterministic algorithms have been developed that are guaranteed to converge to the optimal (maximum entropy) probability distribution. (4) The Maxent probability distribution has a concise mathematical definition, and is therefore, is amenable to analysis. For further model information we refer to (PHILLIPS *et al.,* 2006).

The model was applied to predict the potential spatial distribution of archaeological sites of the entire area of 120 km2 in a spatially explicit way. Therefore, the model was applied to the entire data set given all explanatory variables for the entire area. In the last step, the resulting tabulated data, i.e. the predicted probabilities for the archaeological sites - or to be more precise: the predicted probabilities of each pixel to be an archaeological site - were post-processed to produce probability maps with GIS. In order to evaluate the models' predictive performance besides classification

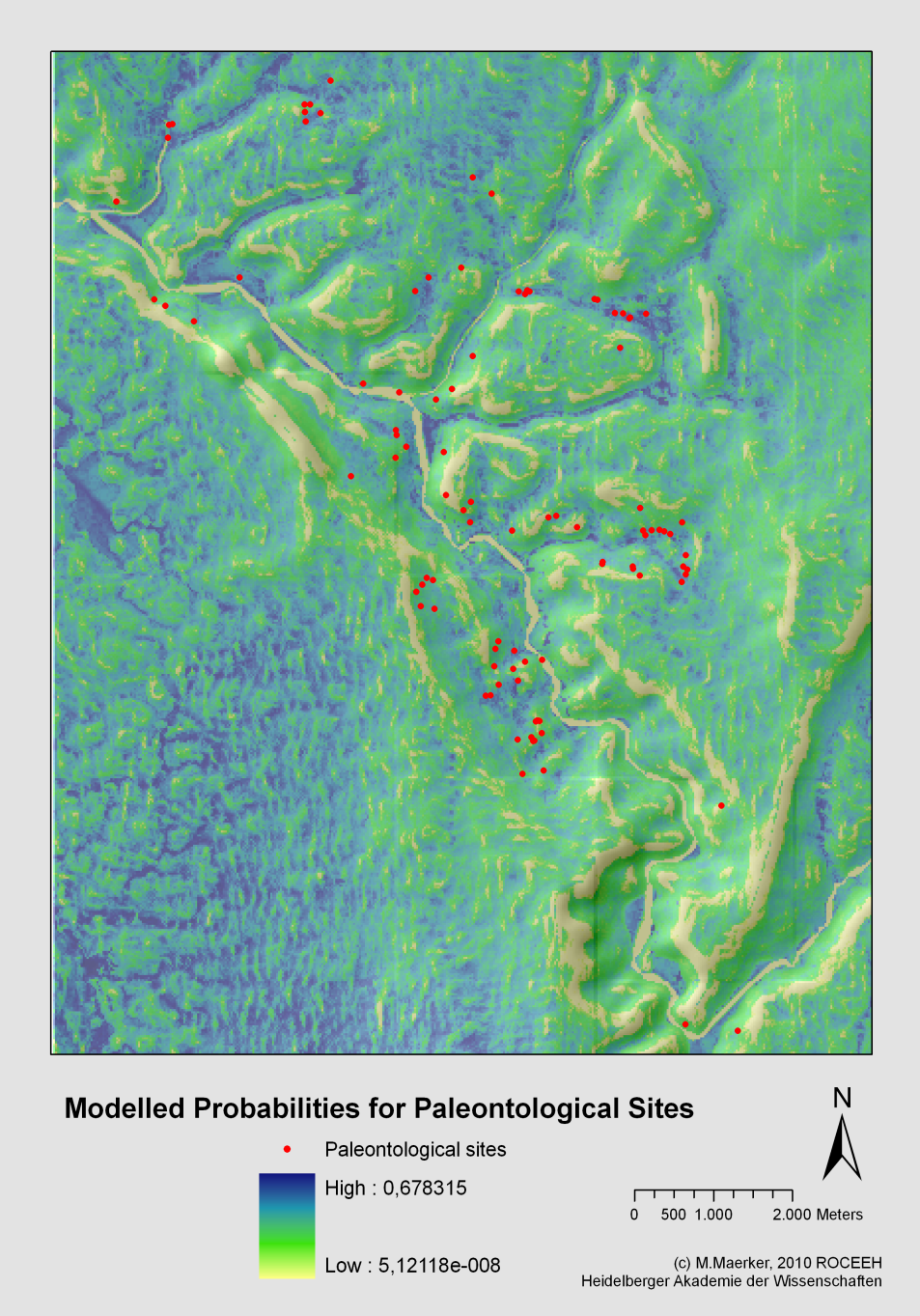

Figure 3: *Modelled probabilities for Archaeological sites in the Makuyuni area. In red fossil sites.*

matrices, we calculated the Receiver Operating Characteristics (ROC) curves. In a ROC curve the true positive rate (Sensitivity) is plotted over the false positive rate (1-Specificity) for all possible cut-off points (SWETS, 1988). Each point on the ROC plot represents a sensitivity/specificity pair corresponding to a particular decision threshold. A perfect discrimination between positives and negatives has a ROC plot that passes through the upper left corner (100% sensitivity, 100% specificity), so that the area under the ROC curve, AUC, is 1 (cf. REINEKING and SCHRÖDER, 2006). According to HOSMER and LEMESHOW (2000), AUC-values exceeding 0.7/ 0.8/ 0.9 indicate acceptable/ excellent/ outstanding predictions. For improving model interpretation, we calculated predictor variable importance, ranking all predictors due to their contribution to the final model.

4. Results and Discussion

As shown in Figure 2 the spatial distribution of the archaeological sites is related to specific characteristics of the predictor variables such as the elevation (DEM), slope, TWI or NDVI. A certain distance to the river network, a certain elevation range and eroded areas without vegetation (NDVI) seem to be intuitively detectable criteria for the archeological site distribution. However, a proper analysis of the entire set of predictor variables is only feasible with more sophisticated approaches such as Maxent.

In the first simulations, in total 99 points (archaeological sites), are used to determine the Maxent distribution (background points and presence points).

The model results obtained with the Maxent approach show an area under curve value (AUC) for the train dataset of 0,642. The variable importance can be summarized as follows: i) catchment area (47,5%), ii) curvature (28,3%), iii) profile curvature (16,1%), iv) NDVI (4,7%), v) TWI (1,2 %), vi) slope (1%), and vii) ASTER 3rd band (0,2%).

The AUC value of 0.64 for the train data set can be interpreted as an acceptable performance for the small number of train data (N= 99). However, model performance may be enhanced in the future using: i) additional topographic information form differential GPS to calibrate and validate the DEM, and ii) further archaeological sites that are surveyed in the next years.

The variable importance that results from the model run illustrates that the variables describing the hydrological characteristics of the test area are most important. Especially the catchment area yields information about the potential amount of surface runoff, and thus about transport capacities. The curvature is an index that describes the accumulation or distribution of water on the one hand, as well as the acceleration or deceleration of surface runoff (profile curvature). The importance of the hydrological relevant indices triggering surface runoff might also be an indicator for the transport of artefacts and fossils towards the toeslopes. This hypothesis is currently under investigation.

As observed in the field most of the sites are found at the boundary of Upper and Lower Manyara Beds. They are found at a certain distance and altitude from the present day river network. This indicates that fossils and artifacts are mainly found in the vicinity of the former lake shore or toeslope positions, characterized by the boundary between Upper and Lower Manyara Beds. Moreover, the spectral information in ASTER band 2 and 3 (green & red light; NDVI) describes surface color characteristics. Especially the differences between the Upper and Lower Upper Manyara Beds and their surroundings are very distinctive.

Figure 3 shows the resulting spatial distribution of the modeled occurrence probabilities for archaeological sites. In dark blue the areas that have the highest probabilities. The highest probabilities are related to lower areas where runoff concentrates. Since the Maxent model also takes into account tectonic activities (altitudeabove stream channel), paleosurfaces can be detected showing a much more complex topography as the present day digital elevation model does. Figure 4 illustrates the topographic index altitude above the stream channel network. Here topographic structure become visible that are hidden in the present day DEM. However, also in this iondex, a close relation between the topographic position and archaeological sites are

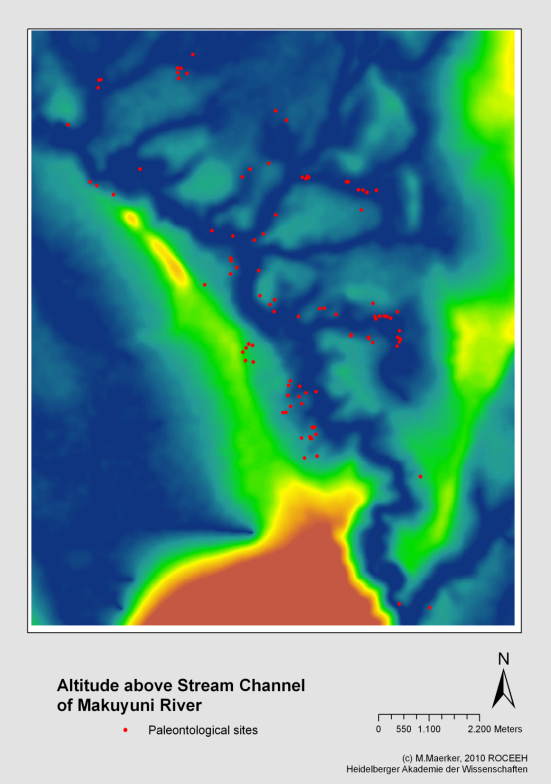

Figure 4: *Altitude above stream channel of the lower Makuyuni River Basin. In red archaeological sites.*

clearly visible. However, in the South-western part of the area, different lithological characteristics may influence the simulation. In this area no sites were discovered yet.

The results presented in Figure 3 reveal potential areas where further fossil sites may be located. These sites with high probability values will be preferentially screened during the next field stage in March 2011. Moreover, the study contributes substantially in the preparation of the next field campaign.

Conclusions

The study presents a first attempt to detect the occurrence of archaeological sites in relation to physigraphic information. However, the study also tells a lot about the processes that might be related to the sites where fossiles and artifacts are found. We especially identified topographic characteristics that describe surface runoff and associated transport processes. Thus, besides the fact that archaeological sites are located in the vicinity of the former lake boundary (Upper- Lower Manyara Beds boundary), may be these fossils might have also been transported and accumulated at the former erosion basis. This hypothesis is part of a following research project characterizing the present day hydrological dynamics and to reconstruct Paleo-process dynamics.

Acknowledgements

We would like to thank the Heidelberg Academy of Sciences and Humanities for funding and supporting this research. Data presented here will be stored and held available in the ROAD-database of the Research Unit "The role of culture in early expansions of humans" funded by the Heidelberg Academy of Sciences and Humanities (Germany). The ROAD server is located at Tuebingen University. For further information on database and research unit please consult www.roceeh.net.

References

BEVEN, K.J., KIRKBY, M.J., 1979. A physically-based variable contributing area model of basin hydrology. *Hydrological Science Bulletin* 24, 43-69.

HORN, B.K.P., 1981. Hillshading and the reflectance map. *Proceedings of the IEEE*, 69(1).

JÄGER, F., 1913. Das Hochland der Riesenkrater und die umliegenden Hochländer Deutsch-Ostafrikas. Ergebnisse einer amtlichen Forschungsreise ins abflußlose Gebiet des nördlichen Deutsch-Ostafrika 1906/07. *Mitteilungen aus den Deutschen Schutzgebieten. Ergänzungsheft*, 4; Berlin. - [1911] u. Ergänzungsheft, 8; Berlin.

JAYNES, E.T., 1957. *Information theory and statistical mechanics*. Phys. Rev. 106, 620–630.

KAISER, T., 1996. *Die Taphonomie plio-pleistozäner Hominidenfundstellen Ostafrikas mit besonderer Berücksichtigung der Säugetierfaunen des Laetoli- und Lake Manyara-Gebietes in Nordtansania.* Ph.D. Dissertation, Technische Hochschule Darmstadt.

KAISER, T.M., 2000. Die Taphonomie plio-pleistozäner Hominidenfundstellen Ostafrikas mit besonderer Berücksichtigung der Säugetierfaunen des Laetoli- und Lake Manyara-Gebietes in Nordtansania. *Archäologische Informationen* 23: 139-142.

KAISER, T.M., Bromage, T.G., Schrenk, F., 1995. Hominid Corridor Research Project update: New Pliocene fossil localities at Lake Manyara and putative oldest Early Stone Age occurrences at Laetoli (Upper Ndolanya Beds), northern Tanzania. *Journal of Human Evol.* 28: 117-120.

KAISER, T.M., BROMAGE, T.G., SCHRENK, F., 1995. Hominid Corridor Research Project update: New Pliocene fossil localities at Lake Manyara and putative oldest Early Stone Age occurrences at Laetoli (Upper Ndolanya Beds), northern Tanzania. *Journal of Human Evol.* 28: 117-120.

KELLER, C.M., HANSEN, C., ALEXANDER, C.S., 1975. Archaeology and paleoenvironments in the Manyara and Engaruka Basins, Northern Tanzania. *Geographical Review* 65:365-376.

KENT, P.E., 1941. The recent history and pleistocene deposits of the plateau North of Lake Eyasi, Tanganyika. *Geological Magazine* 78: 173-184.

KENT, P.E., 1942. A Note on Pleistocene Deposits Near Lake Manyara, Tanganyika. *Geological Mag*. 79:72-77.

LEAKEY, M., 1979. *Olduvai Gorge: My Search for Early Man.* William Collins Sons & Co. Ltd., London.

LEAKEY, M. (ED.), 1986. *Laetoli: A Pliocene site in Northern Tanzania*. Clarendon Press, Oxford Science Publications.

MISKA, L., HJORT, J., 2005. Evaluation of current statistical approaches for predictive geomorphological mapping. *Geomorphology* 67, 299–315.

MOORE, I.D., GARSON, R.B., LADSON, A.R., 1991. Digital terrain modelling: a review of hydrological, geomorphological and biological applications. *Hydrological Processes*, 5, 3-30.

MOORE, I.D., GARSON, R.B., LADSON, A.R., 1997. Digital terrain modelling: a review of hydrological, geomorphological and biological applications. Soil *Science Society of America Journal*, 57, 443-452.

PHILLIPS, S.J., ANDERSON , R.P. SCHAPIRE, R.E., 2006. Maximum entropy modeling of species geographic distributions. *Ecological Modelling*, 190:231-259, 2006.

PLANCHON, O., DARBOUX, F. 2001. A fast, simple and versatile algorithm to fill the depressions of digital elevation models. *Catena* 46: 159-176.

OLAYA, V., CONRAD, O., 2008. Geomorphometry in SAGA. In: Hengl, T., Reuter, H.I. (Eds.), Geomorphometry: Concepts, Software,Applications. Elsevier, Amsterdam, pp. 293–308.

RECK, H., 1921. Eine neue diluviale Säugetierfundstelle am Minjonjo in Deutsch-Ostafrika. - Sitzungsberichte der Gesellschaft Naturforschender Freunde, 1-3: 25-36.

RECK, H., KOHL-LARSEN, L., 1936. Erster Überblick über die jungdiluvialen Tier- und Menschenfunde Dr. Kohl-Larsens im nordöstlichen Teil des Njarasa-Grabens (Ostafrika) und die geologischen Verhältnisse des Fundgebietes. - *Geologische Rundschau*, 27(5): 400-441; Stuttgart.

REINEKING B., SCHROEDER, B., 2006. Constrain to perform: regularization of habitat models. *Ecol Model* 193, 675-690.

RING, U., SCHWARTZ, H.L., BROMAGE, T.G., SAANANE, C., 2005. Kinematic and sedimentological evolution of the Manyara Rift in northern Tanzania, East Africa. *Geological Magazine* v. 142:355-368.

SAANANE, C., 2004. *Taphonomy and Palaeoecology of Laetoli as well as Makuyuni, Arusha Region in Northern Tanzania*. PhD Dissertation, Fachbereich Biologie, JWG Universität Frankfurt.

SCHRENK, F., BROMAGE, T. G., KAISER, T., SEIFFERT, C., HARVATI, K., FROST, S.R., SCHWARTZ, H.L. SZALAY, F. S., RING. U., 1995. Geology and Paleontology of the Arusha Region. Field report to the Director of Antiquities, Tanzania, 15 p., unpublished.

SCHRENK, F., SAANANE, C. B., FROST, S., HARVATI, K., SCHWARTZ, H., GIEMSCH, L., 2008. Paleoanthropological Field Research of Lake Manyara Beds, Makuyuni, Arusha. Field report to the Director of Antiquities, Tanzania, 11 p., unpublished.

SCHULTZ, J. 1967. Mbulu Distrikt (nördliches Tanzania): eine naturräumliche Erhebung unter besonderer Berücksichtigung der Vegetation: 242 S.

SWETS, J.A., 1988. Measuring the accuracy of diagnostic systems. *Science* 240, 1285-1293.

TARBOTON, D.G., 1997. A new method for the determination of flow directions and contributing areas in grid Digital Elevation Models. *Water Resources Research*, 33(2), 309-319.

VAIDYANADHAN, R., DIXIT, P.C., SCHLÜTER, T., 1993. Geomorphology and Sedimentology of Lake Manyara environs, Tanzania, East Africa. Documenta Naturae 77: 41-62.

APPENDIX VIII: PRECIPITATION IN THE STUDY AREA 2000 - 2014

Dataset Origin:

Tropical Rainfall Measurement Mission Project (TRMM); Dataset title: Daily TRMM and Other Satellites Precipitation Product (3B42 V6 derived); Dataset Publisher: Goddard Space Flight Center Distributed Active Archive Center (GSFC DAAC); Analysis & Compilation: Felix Bachofer, University of Tuebingen.

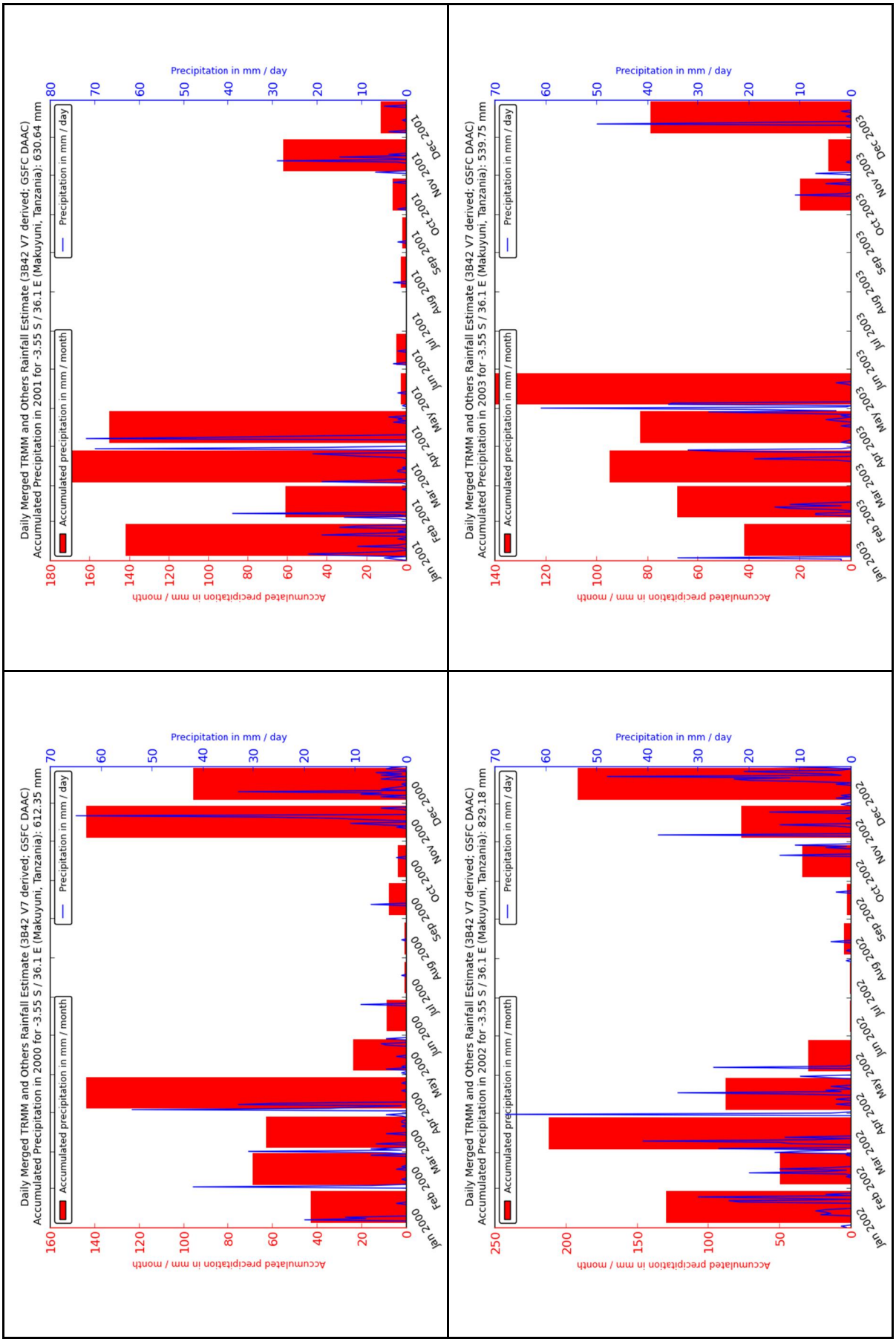

Dataset Originator: Tropical Rainfall Measurement Mission Project (TRMM); Dataset title: Daily TRMM and Other Satellites Precipitation Product (3B42 V7 derived); Dataset Publisher: Goddard Space Flight Center Distributed Active Archive Center (GSFC DAAC); Analysis & Compilation: Felix Bachofer, University of Tuebingen

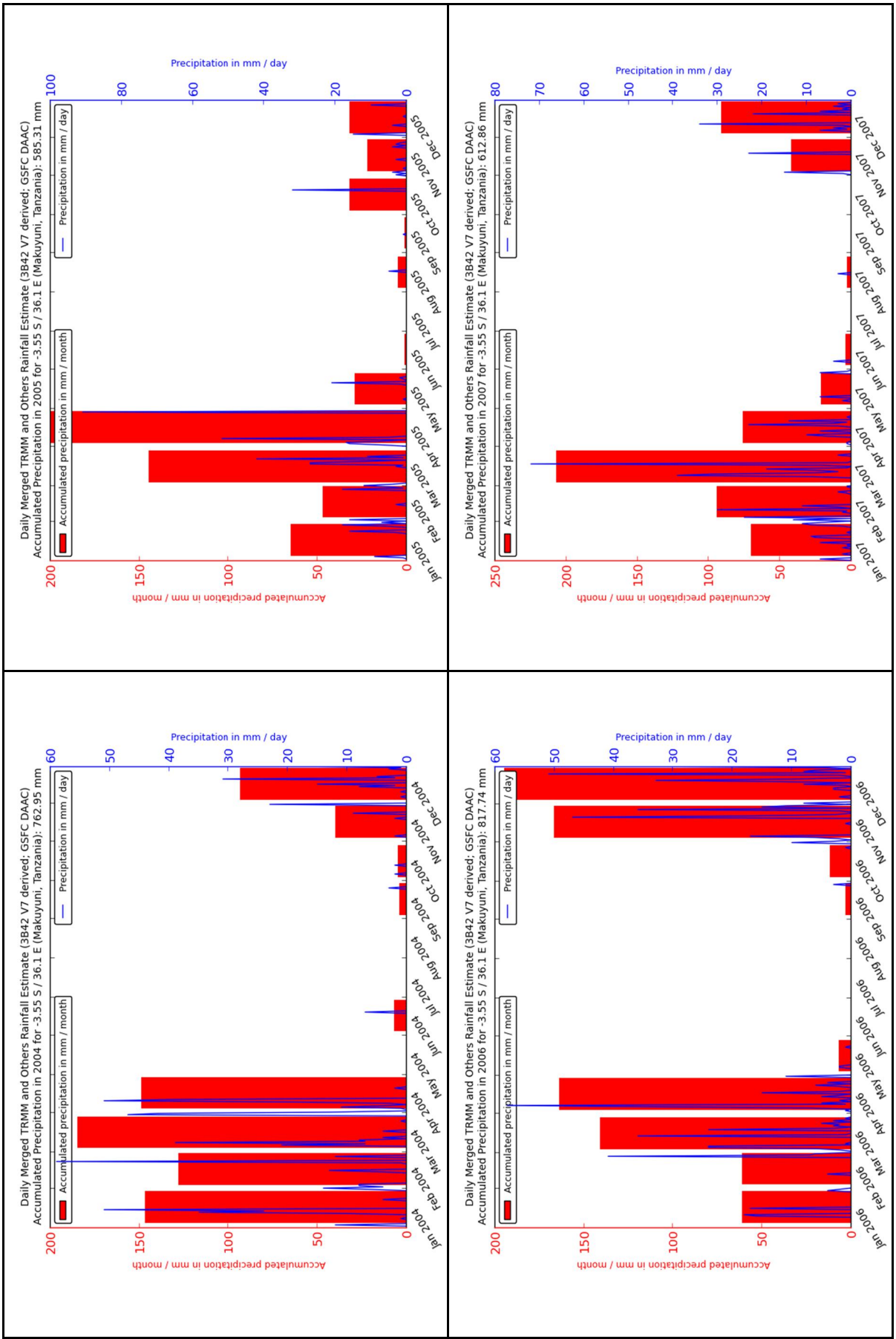

Dataset Originator: Tropical Rainfall Measurement Mission Project (TRMM); Dataset title: Daily TRMM and Other Satellites Precipitation Product (3B42 V7 derived); Dataset Publisher: Goddard Space Flight Center Distributed Active Archive Center (GSFC DAAC); Analysis & Compilation: Felix Bachofer, University of Tuebingen

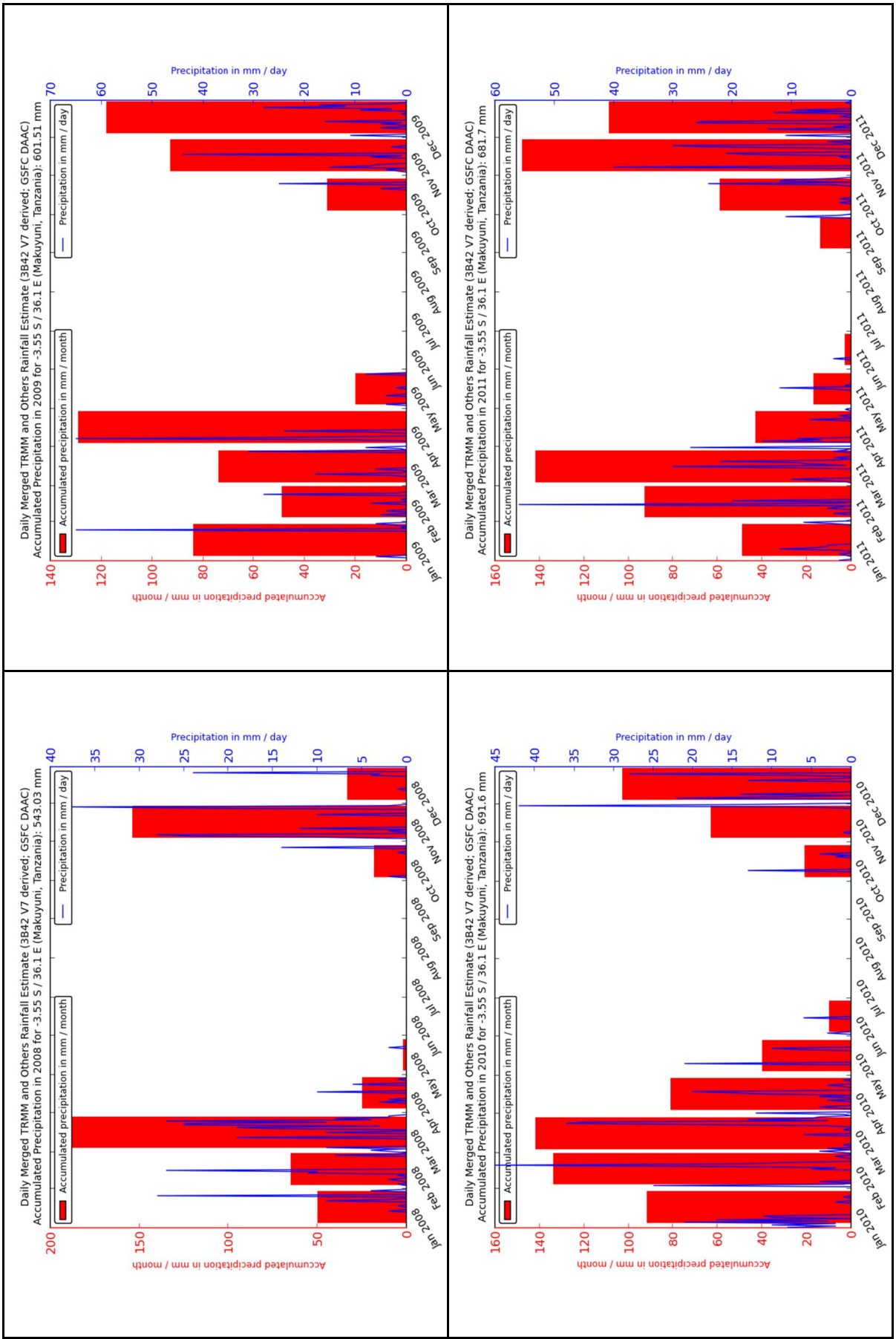

Dataset Originator: Tropical Rainfall Measurement Mission Project (TRMM); Dataset title: Daily TRMM and Other Satellites Precipitation Product (3B42 V7 derived); Dataset Publisher: Goddard Space Flight Center Distributed Active Archive Center (GSFC DAAC); Analysis & Compilation: Felix Bachofer, University of Tuebingen

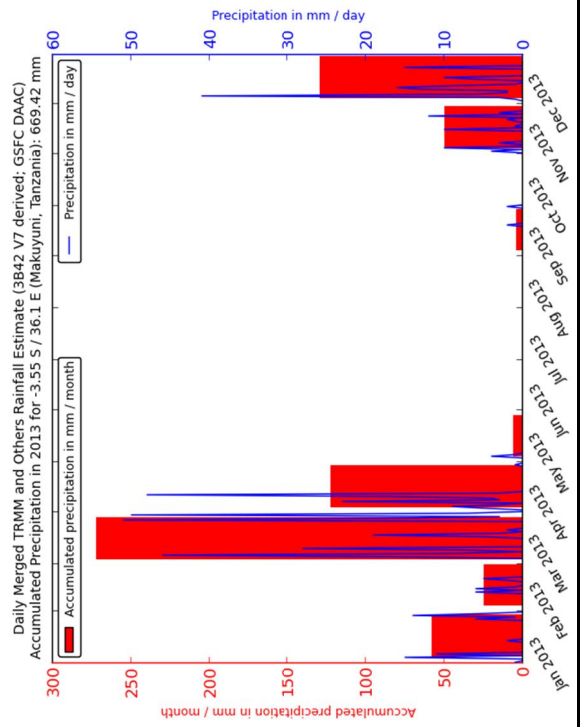

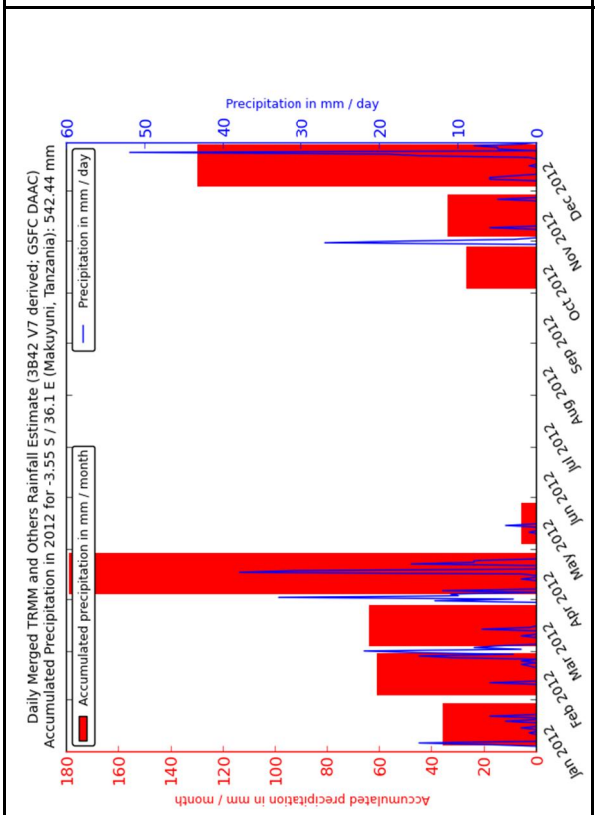

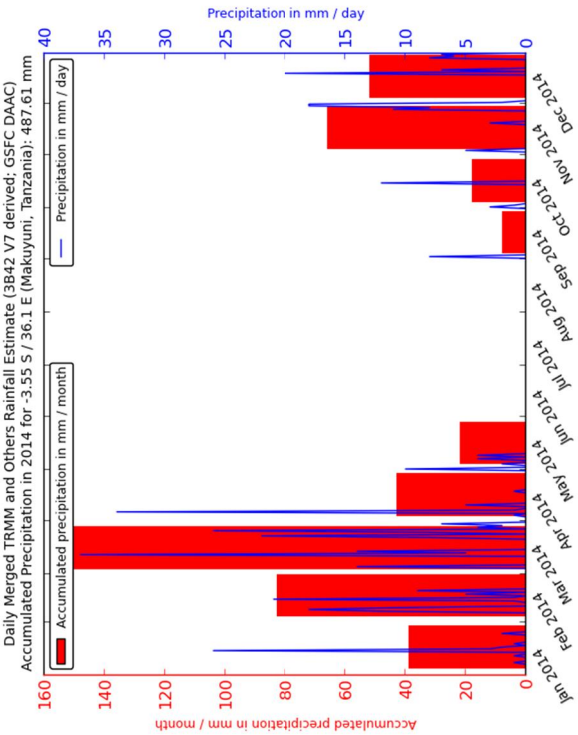

Dataset Originator: Tropical Rainfall Measurement Mission Project (TRMM); Dataset title: Daily TRMM and Other Satellites Precipitation Product (3B42 V7 derived); Dataset Publisher: Goddard Space Flight Center Distributed Active Archive Center (GSFC DAAC); Analysis & Compilation: Felix Bachofer, University of Tuebingen

APPENDIX IX: LABORATORY ANALYSIS OF THE SOIL SAMPLES

The laboratory analysis was conducted by:

Laboratorio Regionale Analisi Terreni e Produzioni Vegetali di Sarzana. Dipartimento Agricoltura, Sport, Turismo e Cultura, Regione Liguria. Loc. Pallodola c/o Mercato Ortofrutticolo, 19038 - Sarzana (SP).

Coordinates UTM 37S (WGS84)		Laboratory analysis														
X	Y	Coarse sand (0.5 – 2 mm) in g / kg	Fine / Medium sand (0.05 – 0.5 mm) in g / kg	Silt (0.002 – 0.05 mm) in g / kg	Clay (< 0.002 mm) in g / kg	Calcium (Ca) in g / kg	Organic carbon (C_{org}) in g / kg	Iron (Fe) in mg / kg	Manganese (Mn) in mg / kg	Aluminium (Al) in mg / kg	Calcium cation (Ca^{2+}) in meq / 100 g	Magnesium cation (Mg^{2+}) In meq / 100 g	Sodium cation (Na^{+}) in meq / 100 g	Potassium cation (K^{+}) in meq / 100 g	Chlorides (Cl) in mg / kg	Water soluble sulfate (SO_4) in mmol / kg
179661	9604743	388	367	188	57	89	1.2	3.55	4.88	0.23	4.44	1.01	2.08	0.6	22.3	8.1
179542	9604603	361	357	210	72	30	12.1	4.84	26.07	0.23	14.75	2.62	0.59	1.38	46.2	38.3
179349	9604581	253	494	232	21	78	6.7	3.32	14.2	0.44	12.44	3.5	1.06	0.93	19.8	12.3
179349	9605262	625	209	100	66	2	8	4.14	46.4	0.33	2.17	0.77	0.22	1.55	43.8	19.3
178361	9605928	96	281	469	154	17	3.2	6.71	27.12	0.13	21.39	6.1	39.9	0.93	8	5
178441	9606308	70	303	368	259	172	1.4	6.83	1.33	0.06	7.44	12.26	13.91	1.84	232	6.2
175583	9605807	193	226	275	306	48	13.9	9.95	28.16	0.11	29.56	2.96	1.55	1.18	13.5	14.7
177225	9601709	246	128	325	301	7	17	8.66	46.1	0.21	11.67	4.15	0.14	2.66	7.3	7.3
175466	9601215	161	139	305	395	49	13.8	6.29	13.38	0.12	35.47	6.97	0.43	1.43	25.6	7.9
175635	9603894	393	286	129	192	4	15	5.1	29.9	0.19	6.01	2.24	0.11	1.51	7.2	5.7
171132	9600034	59	284	429	228	98	45.6	4.88	12.73	0.12	30.89	8.11	1.54	1.03	8.9	8.6
150080	9578227	31	262	584	123	164	13.7	3.76	26.5	0.06	28.84	7.38	5.85	2.72	302	448.8
145395	9581035	27	281	449	243	169	10.3	12.97	38.92	0.13	6.69	1.38	33.39	0.98	821	312.1
149070	9578627	18	78	640	264	392	9	5.74	5.45	0.49	3.77	0.06	135.41	1.62	2295	7229
165397	9602795	247	362	330	61	173	1.7	2.32	9.97	0.39	5.79	0.84	2.42	0.51	813	520.8
174893	9605036	404	307	198	91	7	7	6.95	29.52	0.2	4.91	1.79	0.4	1.01	15.5	8.7
176582	9601979	363	152	258	227	19	17.8	6.88	32.5	0.2	10.72	2.84	0.13	2.17	4.3	4.6
175751	9601310	516	189	199	96	3	16.8	5.59	35.94	0.21	7.31	2.27	0.33	1.62	8.6	6.1
174295	9601151	96	109	482	313	57	10.5	8.73	19.3	0.16	32.6	7.24	2.37	1.19	8.7	6.5
173191	9601711	127	268	497	108	77	21.3	8.94	29.46	0.27	22.61	6.7	0.39	2.17	52	18
171410	9600056	104	134	264	498	331	0.8	7.49	1.14	0.05	1.76	0.62	30.9	1.71	43.9	86

Coordinates UTM 37S (WGS84)		Laboratory analysis														
X	Y	Coarse sand (0.5 – 2 mm) in g / kg	Fine / Medium sand (0.05 – 0.5 mm) in g / kg	Silt (0.002 – 0.05 mm) in g / kg	Clay (< 0.002 mm) in g / kg	Calcium (Ca) in g / kg	Organic carbon (C_{org}) in g / kg	Iron (Fe) in mg / kg	Manganese (Mn) in mg / kg	Aluminium (Al) in mg / kg	Calcium cation (Ca^{2+}) in meq / 100 g	Magnesium cation (Mg^{2+}) In meq / 100 g	Sodium cation (Na^{+}) in meq / 100 g	Potassium cation (K^{+}) in meq / 100 g	Chlorides (Cl) in mg / kg	Water soluble sulfate (SO_4) in mmol / kg
167844	9598093	105	299	438	158	42	23.3	6.55	34.2	0.19	24.41	7.4	0.43	2.71	148.5	78
171100	9605816	48	201	498	253	15	16.8	10.53	34.16	0.25	17.9	7.65	0.16	2.27	12.2	11.4
174423	9606347	90	150	258	502	23	17.8	25.77	68.81	0.2	21.66	10.12	0.29	2.62	3.7	4.3
160377	9635240	111	400	381	108	61	15.5	4.65	18.01	0.22	21.15	3.18	0.18	3.48	8.8	6.7
163147	9651054	228	467	222	83	43	12.1	4.76	14.51	0.48	12.58	2.29	0.16	3.58	21.9	12.4
166921	9655849	146	632	178	44	15	2.3	3.11	6.56	0.84	9.31	1.89	0.11	2.82	4.6	9.4
157388	9625452	320	356	271	53	84	9.7	2.13	11.07	0.22	8.69	1.09	0.14	2.16	29.6	14.8
162943	9626362	142	324	372	162	23	32.2	7.32	28.6	0.56	23.67	3.69	0.1	2.02	11.8	4.2
167025	9614400	41	272	299	388	27	13.9	27.03	83.26	0.74	14.84	5.42	0.12	2.26	24.8	13.5
170689	9610569	19	217	454	310	11	18.7	13.58	78.39	0.3	14.62	7.63	0.1	2.97	10.4	5.7
174460	9609075	56	231	584	129	5	24.5	12.21	44.06	0.36	26.54	5.36	0.17	2.81	22.5	10.2
184191	9600032	117	317	325	241	23	12.1	10.51	90.5	0.34	13.91	4.29	0.12	2.61	10.4	10.1
177844	9597147	415	225	130	230	23	8.4	6.13	50.07	0.26	4.76	1.32	0.1	1.67	6.8	6.7
179537	9606842	116	247	475	162	2	9.8	9.17	20.14	0.22	22.46	3.7	6.1	1.08	7.2	7.8
161882	9625723	15	155	423	407	23	19.9	13.17	62.36	0.24	26.28	8.58	0.15	0.03	15.3	12.2

APPENDIX X: STROMATOLITE SAMPLES

Stromatolites found in situ on paleo-shorelines and in the Lower Manyara Beds (most probably ex situ) (Fig. 6). A selection, based on the spatial distribution and elevation, has been sent to the Max Planck Institute for Evolutionary Anthropology for Uranium-series dating (U/Th) dating.

Coordinates UTM 37S (WGS84)					
X	**Y**	**Elevation a.s.l. (EGM96) in m**	**Sample number**	**Send in for U/Th series dating**	**Comment**
150144.9	9578318.5	980.6	S1		
162991.5	9607355.1	1008.1	S3, S4, S5	S3	
162989.5	9611372.3	1016.5	S6, S7, S8	S6	
161661.4	9611376.9	1002.3	S9, S10		
159903.1	9611220.3	998.7	S11		
158748.2	9610977.9	983.5	S12, S13	S12	
154309.8	9624566.1	988.6	S14	S14	
167391.0	9598229.6	1034.9	S20		
169031.6	9602932.7	1058.5	S21		Found in the Lower Manyara Beds - Ex situ.
159510.1	9617656.5	1003.9	Sx1		
159567.1	9620061.1	1001.8	Sx2		
161422.5	9625385.1	1042.4	Sx3	Sx3	
161560.0	9625029.5	1045.8	Sx4		
181442.2	9604619.3	1134.2	Sx5		Found in the Lower Manyara Beds - Ex situ.
180349.5	9606559.6	1094.3	Sy1	Sy1	Found in the Lower Manyara Beds - Ex situ.

APPENDIX XI: CONTRIBUTIONS

Data

- One publication of this thesis includes a SPOT DEM © CNES ISIS program (2011), distribution Spot Image S.A.
- WorldView-2 Image (21-02-2011) courtesy of the DigitalGlobe Foundation.
- ASTER multispectral scene: USGS, and Japan ASTER Program (2012), ASTER scene AST_L1B_00308232006080708, 1B, USGS, Sioux Falls, 23-08-2006. The ASTER L1B data were obtained through the online Data Pool at the NASA Land Processes Distributed Active Archive Center (LP DAAC), USGS/Earth Resources Observation and Science (EROS) Center, Sioux Falls, South Dakota, USA.
- ASTER GDEM is a product of the Ministry of Economy, Trade, and Industry (METI) of Japan and the United States National Aeronautics and Space Administration (NASA). These data are distributed by the Land Processes Distributed Active Archive Center (LP DAAC), located at USGS/EROS, Sioux Falls, SD. http://lpdaac.usgs.gov.
- The National Aeronautics and Space Administration (NASA) SRTM (v.3) DEM data distributed by the Land Processes Distributed Active Archive Center (LP DAAC), located at USGS/EROS, Sioux Falls, SD. http://lpdaac.usgs.gov.
- I would like to thank the National Aeronautics and Space Research Centre of the Federal Republic of Germany (DLR) and the German Remote Sensing Data Center (DFS) for providing the TerraSAR-X and the SRTM/X-SAR data.
- ENVISAT ASAR Data provided by European Space Agency (ESA); ESA Project ID-10022.
- ALOS PALSAR Data provided by European Space Agency (ESA). ALOS PALSAR © TPMO 2014; ESA Project ID-10022.

Figures

- Fig. 4 contains material, which is reprinted from Tectonophysics, 204 (1–2), Dawson, J. B, *Neogene tectonics and volcanicity in the North Tanzania sector of the Gregory Rift Valley: contrasts with the Kenya sector*, p. 83-86, Copyright (1992), with permission from Elsevier. The copyright remains with Elsevier.
- Fig. 5 contains material, which is reprinted from Tectonophysics, 448 (1–4), Le Gall, B., Nonnotte, P., Rolet, J., Benoit, M., Guillou, H., Mousseau-Nonnotte, M., Albaric, J. & Deverchère, J., 2008 - *Rift propagation at craton margin.: Distribution of faulting and volcanism in the North Tanzanian Divergence (East Africa) during Neogene times*, p. 1-19, Copyright (2008), with permission from Elsevier. The copyright remains with Elsevier.
- Fig. 7 is a reprint from *Ring, U., Schwartz, H. L., Bromage, T. G. & Sanaane, C., 2005 - Kinematic and sedimentological evolution of the Manyara Rift in northern Tanzania, East Africa. Geological Magazine, Vol: 142 (4): 355-368* reproduced by permission of Cambridge University Press (28.07.2015). The copyright remains with Cambridge University Press.
- Fig. 12 is a full reprint from *Lillesand, T. M., Kiefer, R. W. & Chipman, J. W., 2015 - Remote sensing and image interpretation. 7, Wiley, New York*, which was permitted by John Wiley & Sons Ltd (15.08.2015). Copyright © 2015 John Wiley & Sons, Inc. All rights reserved.